AD_____

Award Number: W81XWH-11-1-0178

TITLE: Systematic Analysis of the Functional Relevance of Nuclear Structure and Mechanics in Breast Cancer Progression

PRINCIPAL INVESTIGATOR: Jan Lammerding

CONTRACTING ORGANIZATION: Cornell University
ITHACA, , NY 14850

REPORT DATE: July2014

TYPE OF REPORT: Final Report

PREPARED FOR: U.S. Army Medical Research and Materiel Command
Fort Detrick, Maryland 21702-5012

DISTRIBUTION STATEMENT: Approved for Public Release;
Distribution Unlimited

The views, opinions and/or findings contained in this report are those of the author(s) and should not be construed as an official Department of the Army position, policy or decision unless so designated by other documentation.

REPORT DOCUMENTATION PAGE

Form Approved
OMB No. 0704-0188

Public reporting burden for this collection of information is estimated to average 1 hour per response, including the time for reviewing instructions, searching existing data sources, gathering and maintaining the data needed, and completing and reviewing this collection of information. Send comments regarding this burden estimate or any other aspect of this collection of information, including suggestions for reducing this burden to Department of Defense, Washington Headquarters Services, Directorate for Information Operations and Reports (0704-0188), 1215 Jefferson Davis Highway, Suite 1204, Arlington, VA 22202-4302. Respondents should be aware that notwithstanding any other provision of law, no person shall be subject to any penalty for failing to comply with a collection of information if it does not display a currently valid OMB control number. **PLEASE DO NOT RETURN YOUR FORM TO THE ABOVE ADDRESS.**

1. REPORT DATE	2. REPORT TYPE	3. DATES COVERED
July2014	Final	11 JUL 2011 - 30 JUN 2014

4. TITLE AND SUBTITLE
Systematic Analysis of the Functional Relevance of Nuclear Structure and Mechanics in Breast Cancer Progression

5a. CONTRACT NUMBER

5b. GRANT NUMBER
W81XWH-11-1-0178

5c. PROGRAM ELEMENT NUMBER

6. AUTHOR(S)
Jan Lammerding

E-Mail: jan.lammerding@cornell.edu

5d. PROJECT NUMBER

5e. TASK NUMBER

5f. WORK UNIT NUMBER

7. PERFORMING ORGANIZATION NAME(S) AND ADDRESS(ES)
Cornell University,
Ithaca, NY 14853

8. PERFORMING ORGANIZATION REPORT NUMBER

9. SPONSORING / MONITORING AGENCY NAME(S) AND ADDRESS(ES)
U.S. Army Medical Research and Materiel Command
Fort Detrick, Maryland 21702-5012

10. SPONSOR/MONITOR'S ACRONYM(S)

11. SPONSOR/MONITOR'S REPORT NUMBER(S)

12. DISTRIBUTION / AVAILABILITY STATEMENT
Approved for Public Release; Distribution Unlimited

13. SUPPLEMENTARY NOTES

14. ABSTRACT

Abnormal nuclear shape and structure has long been recognized as a characteristic feature of cancer cells, but the underlying molecular basis and functional consequences have remained elusive. It is now emerging that many breast cancer cells have reduced expression of lamins A/C, which negatively correlates with disease-free survival. To investigate the consequences of altered lamin expression in more detail, we modulated the expression of lamins in a panel of breast cancer cells. By developing and using novel microfluidic devices that mimic the conditions encountered during perfusion through capillaries or migration through interstitial spaces, we demonstrated that nuclear deformability, governed by levels of lamins A/C, constitutes a rate-limiting factor in the ability of cells to pass through openings smaller than the nucleus. Furthermore, we found that metastatic cells can dynamically adjust their nuclear envelope composition during migration through confining 3-D environments, facilitating transit through narrow constrictions. Interestingly, cells with reduced levels of lamins A/C were more prone to repetitive nuclear rupture, which could result in increased DNA damage and chromosomal rearrangements. Loss of lamins A/C also disturbed MKL1/SRF signaling. Our findings could provide novel diagnostic and prognostic markers for the treatment of cancer patients; ultimately, a better understanding of the molecular mechanisms underlying the ability of breast cancer cells to dynamically alter their nuclear envelope composition may lead to the identification of new therapeutic targets.

15. SUBJECT TERMS
Lamins, MCF10A, MDA-MB-231, nuclear stiffness, nuclear shape, cell migration

16. SECURITY CLASSIFICATION OF:			17. LIMITATION OF ABSTRACT	18. NUMBER OF PAGES	19a. NAME OF RESPONSIBLE PERSON
a. REPORT	b. ABSTRACT	c. THIS PAGE			USAMRMC
U	U	U	UU	153	19b. TELEPHONE NUMBER *(include area code)*

Table of Contents

Page

INTRODUCTION

The central hypothesis of this proposal was that changes in the expression of nuclear envelope proteins such as lamins or lamin B receptor (LBR) may contribute to the characteristic irregular morphology of cancer cell nuclei and directly modulate cellular functions relevant to cancer progression. Nuclear lamins, particularly lamins A and C, are important determinants of nuclear shape and stiffness.[1-3] At the same time, these proteins also interact with various transcription factors, thereby affecting important signaling pathways.[1, 4] The purpose of this study was to conduct a systematic analysis of the functional consequences of changes in the expression of lamins (A, B1, B2, and C) and lamin B receptor on nuclear morphology and stiffness, as well as the functional consequences of such changes on cell migration through confined spaces (where more deformable nuclei may facilitate enhanced passage), proliferation, and other cancer related functions. In addition, we proposed to conduct an analysis of samples derived from breast cancer patients and orthotopic mouse models of the disease to assess changes in the expression of nuclear envelope proteins in breast cancer samples.

BODY

Due to the move of the PI from Brigham and Women's Hospital to Cornell University in 2011 and the associated delays in the transfer of this award to the new institution, and the setting up of the new the laboratory at Cornell, we had requested a no-cost extension to 7/31/2014 that was granted on 3/7/2013. Consequently, this report covers the period from July 1, 2011 to July 31, 2014. Despite the official end of the project this summer, we are committed to continuing our research on this topic. And while the primary hypothesis of altered lamin and LBR expression in breast cancer patients has now been confirmed by us and others,[5-7] many open questions remain into the molecular mechanisms by which changes in nuclear envelope protein expression can contribute to cancer progression. Particularly the results outlined in Tasks 3 and 6 hold the promise for revealing additional insights into the role of lamins A/C in breast cancer cells.

***Task 1:* Acquire a panel of cell lines and patient-derived samples representing various stages of breast cancer progression from benign to metastatic.**

For our in vitro studies, we focused our initial efforts on a subset of cell lines to optimize experimental techniques. We started by analyzing the following cell lines: MCF10A (normal mammary epithelial cells), MDA-MB-231 (metastatic breast cancer cells), and MCF7 (non-metastatic breast cancer cells). We successfully modified these cell lines to either overexpress lamins (A, B1, B2, C) and LBR or to stably knockdown the expression of these nuclear envelope proteins. In addition, we obtained am additional panel of ~10 breast cancer cell lines which we have modified to fluorescently label the cell nucleus for use in our cell migration studies (Task 3). Since two recent studies confirming our hypothesis of altered lamin levels in breast cancer patients were recently published,[5, 6] including one showing a significant correlation between loss of lamins A/C expression and reduced disease-free survival,[6] and we also confirmed these results in primary breast cancer patient tissue samples (see below), we dedicated most of our efforts to investigate the underlying cellular mechanism, rather than characterizing a large panel of cancer cell lines as initially proposed. We have primarily focused on functional results obtained with the MDA-MB-231 cell line in which we modulated expression of lamins, as we believe that it represents the most relevant model for aggressive breast cancer. Nonetheless, as I recently joined the Cornell University Center on the Microenvironment and Metastasis that is part of the National Cancer Institute Physical Science in Oncology (PSOC) initiative, we are continuing to collaborate with other laboratories at Cornell University and Weill Cornell Medical College to confirm our findings in additional breast cancer cell lines and clinical samples. In

particular, we established a collaboration with Dr. Linda Vahdat at Weill Cornell Medical College, who has provided us with paraffin embedded tissue sections to assess expression levels of nuclear envelope proteins by immunofluorescence and immunohistochemistry. Results from these samples are presented under the section for Task 4.

***Task 2:* Modulate nuclear shape and stiffness in a panel of well characterized breast cancer cells and non-tumorigenic controls by stable, ectopic expression of lamins A, B1, B2, C, a dominant negative lamin A mutant, or lamin B receptor (LBR).**

We created a panel of cell lines derived from MCF10A and MDA-MB-231 cells in which we selectively overexpressed lamin A, lamin B1, lamin B2, lamin C, or LBR with a custom-designed retroviral construct followed by fluorescence activated cell sorting to obtain physiological expression levels.[8] In addition, we created a corresponding panel of cell lines in which we reduced expression of lamins A/C, lamin B1, lamin B2, and LBR by shRNA mediated knockdown. Changes in protein levels were confirmed by Western blot analysis (Fig. 1). As we experienced that even in these stably modified cells lamin expression can revert back over time, presumably due to strong selection pressure, we also created clonal populations of the modified cells, which are more resistant to population drift. In addition, we have been repeating some of the functional experiments with transient siRNA mediated knockdown to confirm results obtained with the stably modified cells.

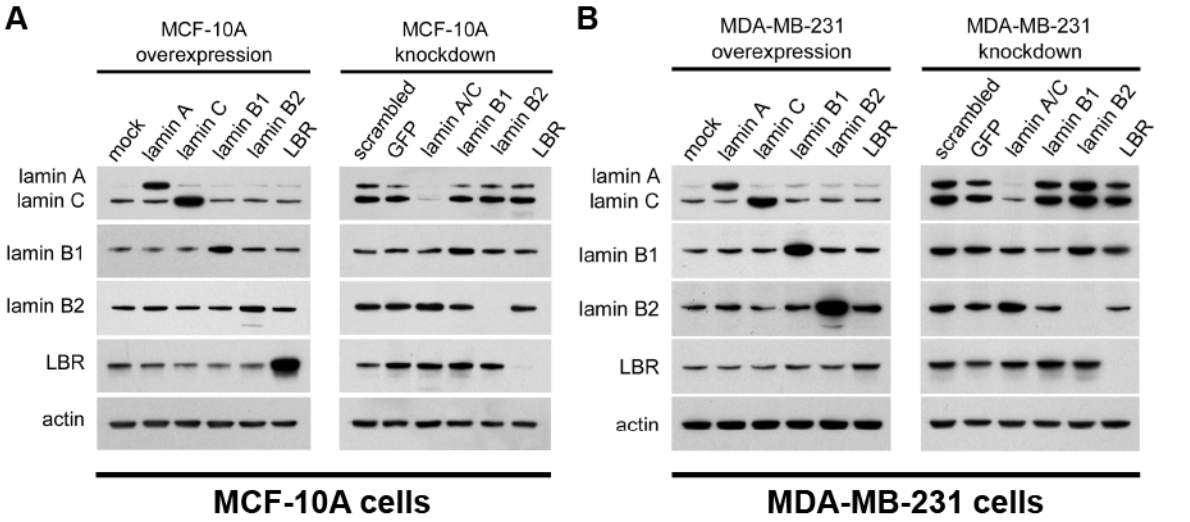

Figure 1. Western analysis of cells modified to express different levels of nuclear envelope proteins. Overexpression was achieved with the bicistronic retroviral constructs and subsequent fluorescence activated cell sorting (FACS). Knockdown of specific nuclear envelop proteins was achieved by shRNA lentiviral constructs and subsequent selection. (A) Results for MCF10A normal breast epithelial cells. (B) Results for MDA-MB-231 breast cancer cells.

We next evaluated the effect of changes in protein expression on nuclear morphology (Fig. 2). We found that most modifications had relatively minor effects on nuclear shape. However, overexpression of LBR resulted in nuclei with severe lobulations (Fig. 2), whereas overexpression of lamin A resulted in rounder nuclei. These results were confirmed by quantitative analysis of nuclear 'roundness' using the Contour Index (CI), defined as

$$CI = 4\pi \times (\textit{nuclear cross-sectional area}) / (\textit{nuclear periphery})^2$$

The *CI* reaches a maximum of 1 for perfectly circular nuclei and decreases with increasingly irregular nuclear shape. Knockdown of lamins A/C and of lamin B2 resulted in more irregularly shaped nuclei, indicated by a decrease in the corresponding *CI* (Figs. 2 & 3). In contrast, overexpression of lamin A resulted in rounder nuclei with an increased *CI*. Overexpression of LBR caused severe lobulation of nuclei in MCF10A cells, resembling those of cancer cells (Fig. 2).

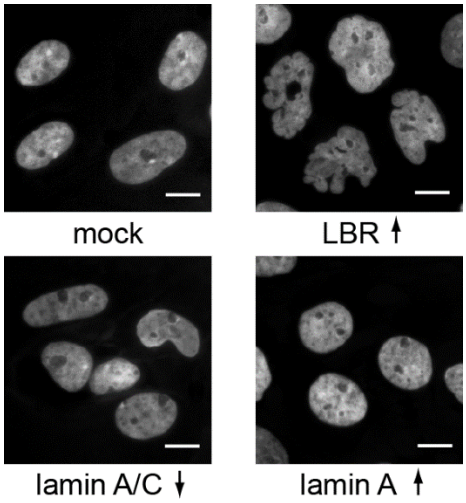

Figure 2. Examples of altered nuclear morphology in MCF10A cells with altered expression of lamin A/C or LBR, revealing increased nuclear lobulation in cells with reduced expression of lamin A/C or increased expression of LBR. Cells overexpressing lamin A have rounder nuclei.

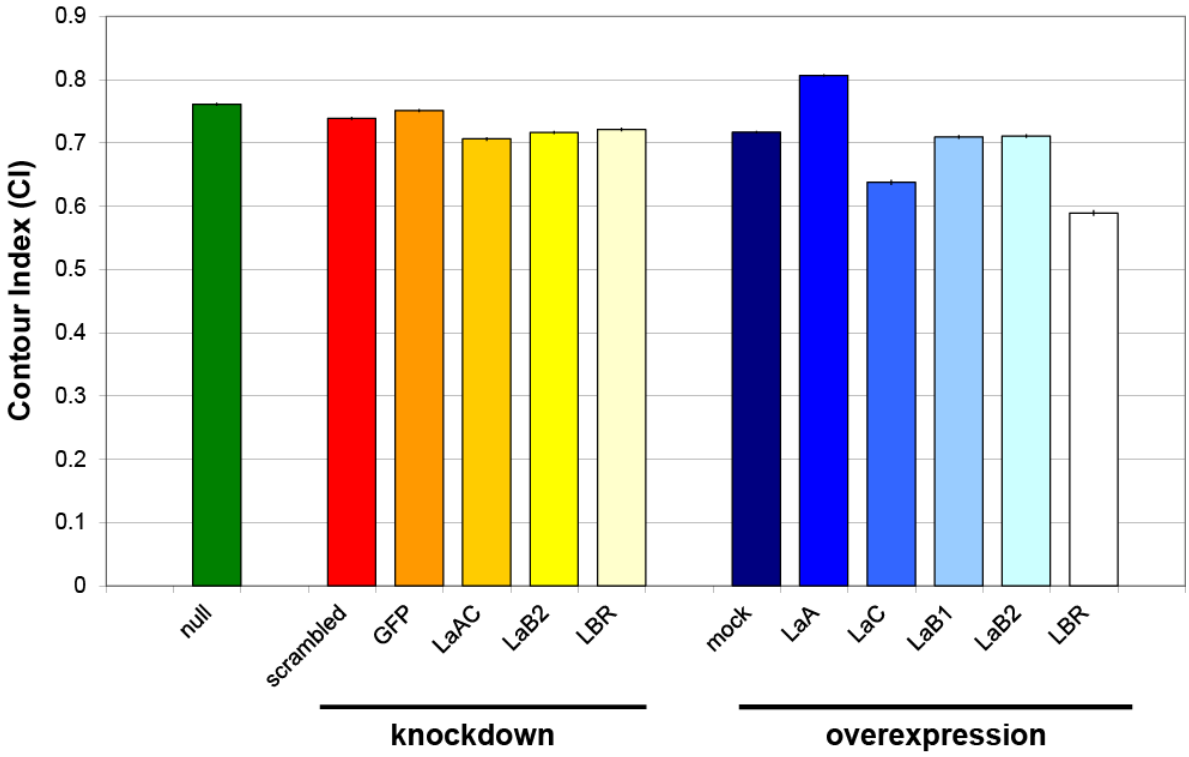

Figure 3. Quantitative analysis of nuclear shape in MCF10A cells with altered expression of nuclear envelope proteins. Data based on ~500 to 1000 cells per cell lines. Null, non-modified controls.

To assess the effect of altered nuclear envelope protein expression on nuclear deformability, we subjected the panel of modified MCF10A cells to substrate strain experiments and measured the resulting nuclear deformations. The normalized nuclear strain, defined as the induced nuclear strain divided by the applied substrate strain, can serve as a direct indicator for nuclear stiffness.[3, 9] Lower normalized nuclear strain values indicate stiffer nuclei, while higher values, corresponding to larger nuclear deformations, indicate softer nuclei. In our experiments, we found that increased expression of lamin A significantly increased nuclear stiffness, while reduced expression of lamins A/C dramatically decreased nuclear stiffness (Fig. 4). The effects of changes in the expression of other nuclear envelope proteins were less dramatic, but still significant, particularly for overexpression of lamin C, lamin B1, and LBR, which reduced nuclear stiffness.

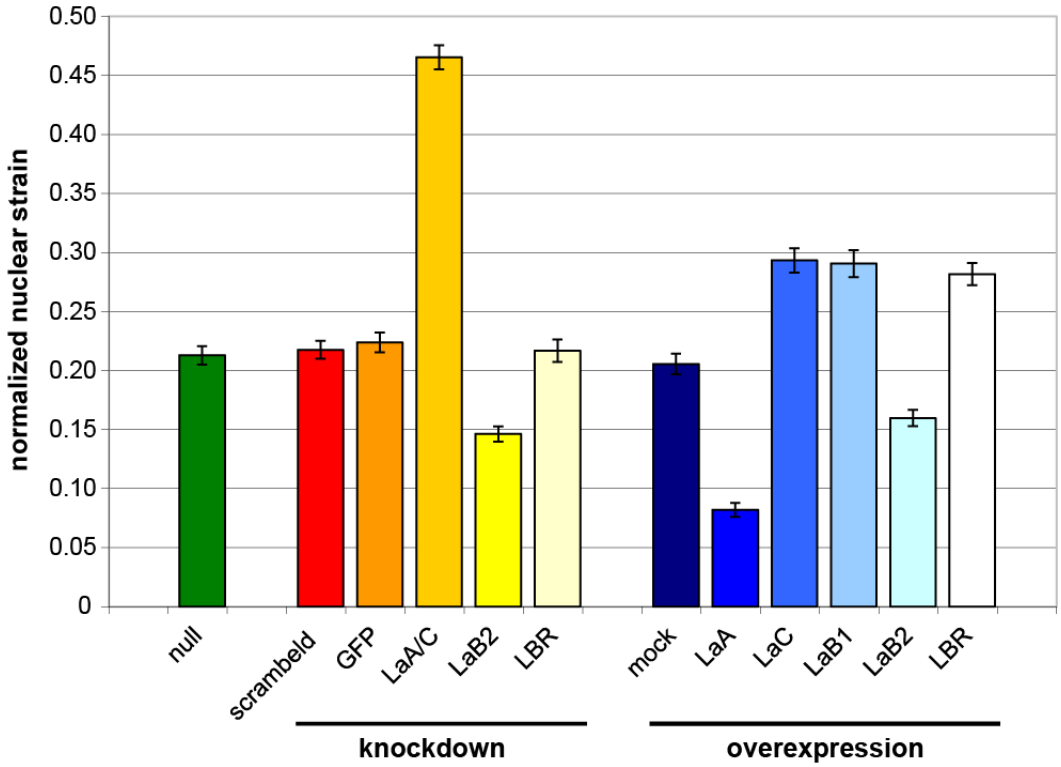

Figure 4. Effect of altered expression of nuclear envelope proteins on nuclear deformability. Lower normalized nuclear strain values indicate stiffer, less deformable nuclei, while higher values indicate softer nuclei.

Due to the reduced adhesion of MCF7 and MDA-MB-231 cells, these cells could not be subjected to sufficient substrate strain without detaching from the silicone membrane. To overcome this problem, we recently developed a micropipette aspiration set-up that we already successfully validated for lamin A/C-deficient and wild-type mouse embryo fibroblasts[10] and that we are currently applying to a panel of cancer cells to measure their nuclear stiffness. In addition, we are collaborating with the group of Peter Friedl and Katarina Wolf at the Radboud University Nijmegen Medical Centre to measure nuclear deformability using atomic force microscopy (AFM). These experiments have already yielded encouraging results (data not shown). To provide a more generalizable tool to measure nuclear stiffness in a large number of cancer cells independent of their adhesive properties, we also developed a novel experimental system in which suspended cells are perfused through a microfluidic device with constrictions smaller than the size of the nucleus while imaging the transit of the cell through the constrictions

with a high speed camera on a microscope (Fig. 5).[11] The nuclear deformability can be inferred from the measured transit time. Our results (see Task 3 for more details) from these experiments confirm that breast cancer cells with reduced levels of lamin A/C have increased nuclear deformability. We recently further improved the design of the microfluidic device (Fig. 6), along with the custom-written image processing algorithm, enabling us to assess nuclear mechanics in hundreds of cells per minute,[10, 11] i.e., with vastly higher throughput then existing substrate strain and micropipette aspiration assays. We are currently in the process of further optimizing the design and validating it in a larger panel of cancer and normal control cells. In the long term, we are confident that our microfluidic device can be used to rapidly characterize large populations of (cancer) cells and even identify small subpopulations from heterogeneous samples, which could ultimately aid in the diagnosis and prognosis of cancer samples, for example, by assessing the fraction of highly deformable metastatic cells.

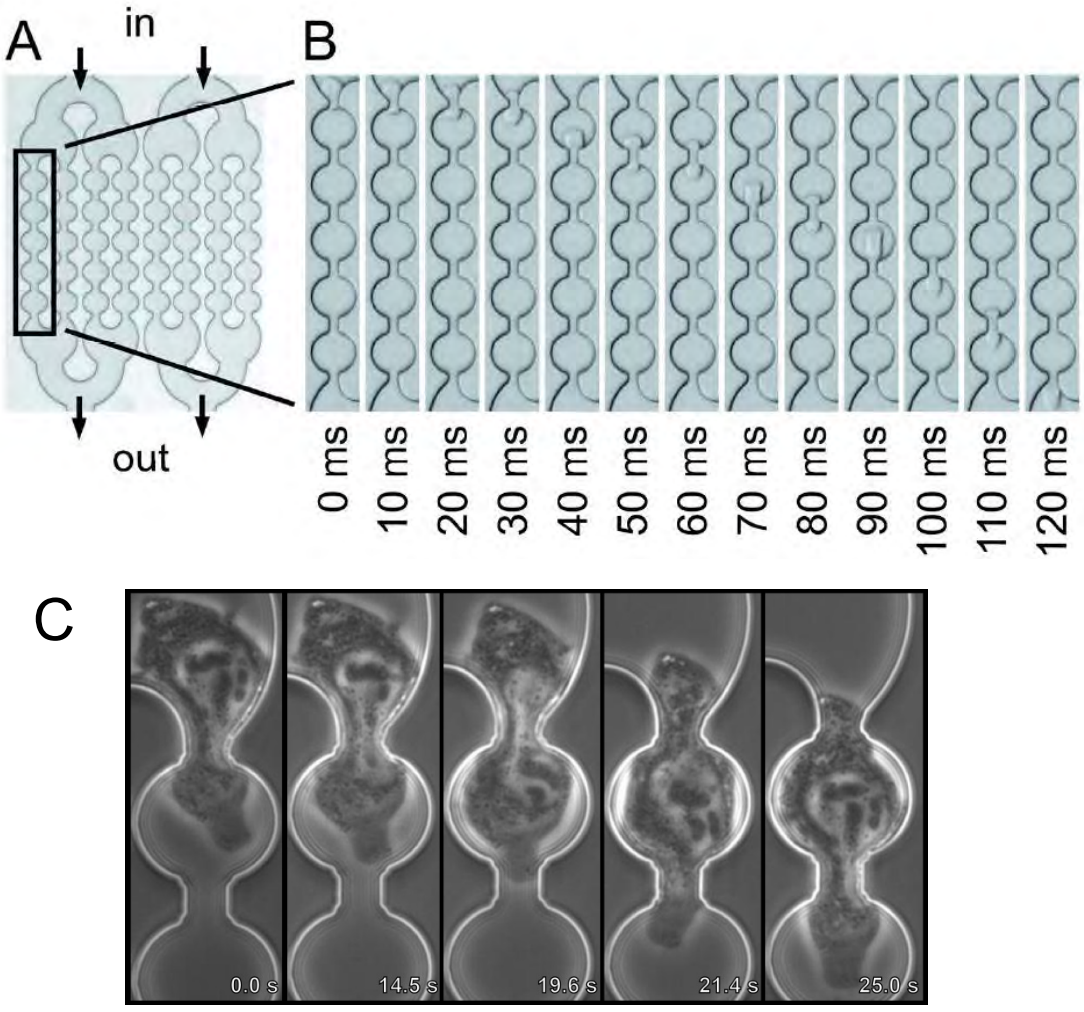

Figure 5: Microfluidic device to study nuclear deformability. (A) Image of 8 parallel constriction channels in bright field mode. Constrictions are 8 µm in width. Cells are perfused from the top and exit the channels at the bottom as indicated by the arrows. (B) Time-series of a cell passing through a channel with 5µm-wide constriction at a pressure of 10 psi, acquired at 100 frames per second. The limiting step for the cell to travel through the channels is the deformation time to pass the first constriction. Subsequent constrictions are traversed substantially faster. (C) Close-up of perfusion of MDA-MB-231 cells through microfluidic constriction, revealing substantial nuclear deformation as the cell passes through the 5 x 10 μm^2 pore.

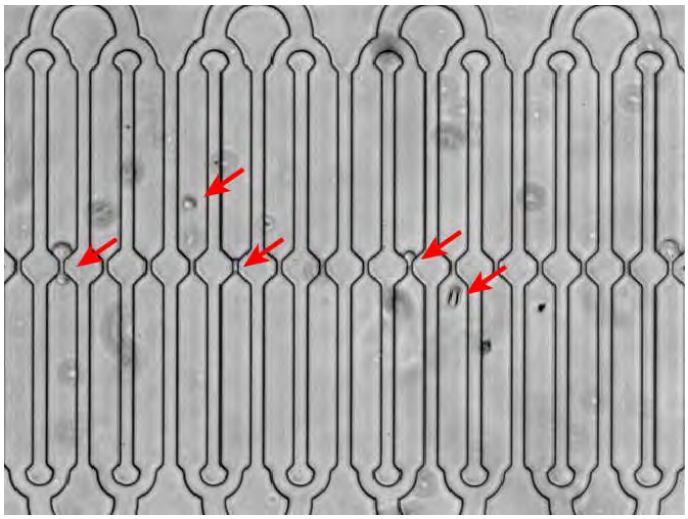

Figure 6. Latest version of the microfluidic perfusion device to rapidly measure nuclear deformability of cancer cells. Red arrows indicate MDA-MB-231 breast cancer cells at various stages of transit through an array of parallel constriction channels. The single constriction and the long and wide sections preceding and following the constriction facilitate automated measurements of cell size and transit time using a custom-written MATLAB algorithm.

***Task 3:* Investigate whether changes in nuclear shape or stiffness can alter invasion, migration, or perfusion through narrow channels in the newly created panel of cell lines.**

In the first set of experiments, we evaluated whether changes in the expression of lamins A/C, which are the primary determinants of nuclear stiffness[2] (see also Fig. 4) enhanced the ability of cells to flow through narrow constrictions when driven by a pressure gradient. We validated our device with lamin A/C-deficient (*Lmna*$^{-/-}$) and wild-type mouse embryo fibroblasts, which we had previously characterized by substrate strain analysis.[2, 3] These experiments, published earlier this year, showed that lamin A/C-deficient cells pass significantly faster through 5 μm constrictions than cells from wild-type littermates.[10] When investigating the panel of MDA-MB-231 cells in which we had modulated the levels of lamins A/C to correspond to the changes seen in patient samples (see Task 4), we similarly found that cells with reduced expression of lamins A/C were able to pass through the 5 μm constrictions significantly faster than comparably sized cells with normal levels of lamins A and C (mock controls), likely due to their increased nuclear deformability. Nonetheless, as the cell size varied within and between the various populations and it was recently shown that the transit time of cells through narrow constriction exponentially increases with cell size,[12] we also plotted the regression curves for MDA-MB-231 cells with reduced levels of lamin A/C and mock controls (Fig. 7). These plots revealed a substantial downward shift of the regression line for the MDA-MB-231 cells, indicating faster transit times for a given cell size. Taken together with the irregular nuclear shape and increased nuclear deformability observed in the cells with reduced levels of lamin A/C, our findings indicate that loss of lamins A/C results in reduced nuclear stiffness, which promotes the transit of cells through constrictions smaller than the size of the nucleus during perfusion. These results could have direct implication on the spreading of metastatic cells through the vascular system, were the capillaries, particularly in the lung, may act as a physical filter for the distribution of cancer cells, and increased nuclear deformability in cancer cells with reduced levels of lamin A/C could allow cells to pass this filter and metastasize to other organs. We are currently in the process of preparing follow up studies to test this hypothesis in a mouse model.

Our data further illustrate the power of our new microfluidic device to rapidly measure nuclear mechanics in large numbers of cancer cells. We have already initiated additional experiments to characterize a larger panel of cancer cells and healthy controls with this experimental system to

determine whether nuclear deformability correlates with metastatic potential and cancer aggressiveness.

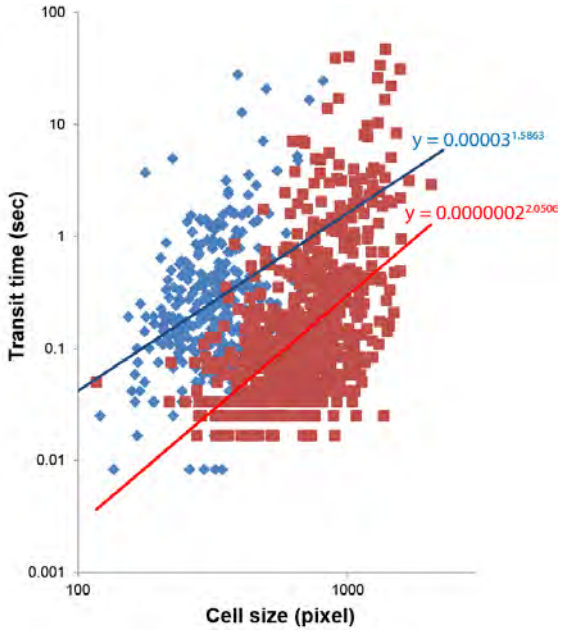

Figure 7. Transit times during perfusion of MDA-MB-231 cells with stably reduced levels of lamin A/C (red) and mock controls (blue) through 5μm constrictions plotted as a function of cell size (log-log plot). Red and blue lines represent the least-squares regression fit for each of the cell populations, revealing that lamin A/C-deficient cells (red) with their more deformable nuclei can pass through the narrow constrictions faster than wild-type cells.

The above experiments assessed the role of (passive) nuclear mechanics during the rapid transit of cells through narrow pores during perfusion, i.e., cells in suspension driven through the pores by a pressure gradient. To study the effect of altered lamin expression and changes in nuclear deformability on the ability of cells to migrate through narrow constrictions, which occurs on much slower time scales (minutes and hours for migration studies *vs*. seconds and milliseconds during perfusion experiments), we developed a novel microfluidic device with precisely engineered constrictions ranging from 2 to 15 μm in size and induced cells to migrate through the constrictions along a chemotactic gradient across the channels. We monitored passage of cells through these constrictions at high spatial and temporal resolution and measured transit time, migration speed, and transmigration probability (Fig. 8). We first validated the devices using human and mouse embryo fibroblasts expressing different levels of lamins A/C. In these cells, we found that reduced expression of lamins A/C, which results in increased nuclear deformability, enhances the ability of cells to pass through narrow constrictions.[10] While the different cell lines displayed only small differences in migration speed in 15 μm wide channels, cells expressing normal levels of lamin A/C took longer and longer when the constriction size was reduced to 5, 3, and 2 μm (Fig. 9). In contrast, lamin A/C-deficient fibroblasts moved through the smallest constrictions just as fast as through the larger constrictions, indicating that their more malleable nuclei no longer presented a rate-limiting obstacle. Cells with 50% reduced levels of lamin A/C (*Lmna*$^{+/-}$ MEFs) displayed an intermediate phenotype. Our just published results are consistent with a recent report by the Friedl lab, which observed that nuclear deformability poses a rate-limiting factor during migration of cells through dense collagen matrices,[13] and findings by the Discher group (University of Pennsylvania) that lung cancer cells with reduced levels of lamins A/C were more efficient at migrating through small pores.[14] A manuscript with the detailed characterization of our new microfluidic device is

currently in preparation and will be submitted to *Lab on a Chip* in August 2014. Using our device in a collaboration with the Egelhoff group (Cleveland Clinic), we were able to show that breast cancer cells require non-muscle myosin IIb to move the large and relative stiff nucleus through the narrow constrictions, and that inhibition or knockdown of myosin IIb significantly increased the time cells took to pass through constrictions smaller than the size of the nucleus. The resulting manuscript received very encouraging reviews from the *Journal of Cell Biology* and is under revision for resubmission).

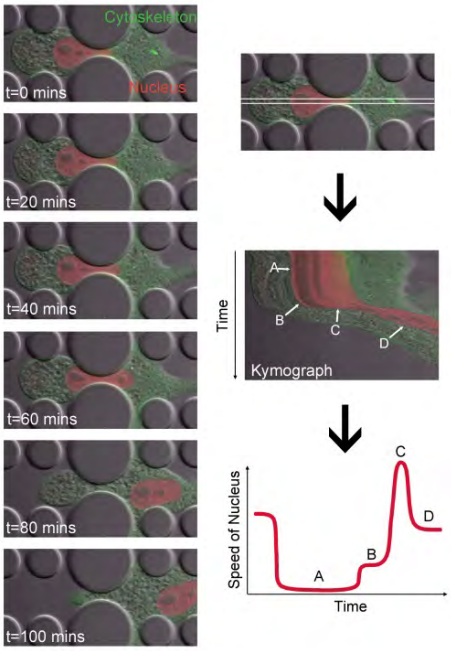

Figure 8. Representative example of a cell with fluorescently labeled cytoplasm (green) and nucleus (red) migrating across a 3 µm constriction along a chemotactic gradient. (Left) Series of frames from time-lapse microscopy acquired over a range of 100 minutes. (Right) Detailed analysis of nuclear movement using a kymographs, i.e., plotting the fluorescence intensity profile along a fixed line (thin white rectangle) over time. The resulting kymograph (right, center) shows how the nucleus initially stalls at the constriction (A), then slowly advances (B) before suddenly slipping through the constrictions once it has sufficiently advanced (C). Once the nucleus has passed the constriction, the cell and nucleus resume their normal migration (D).

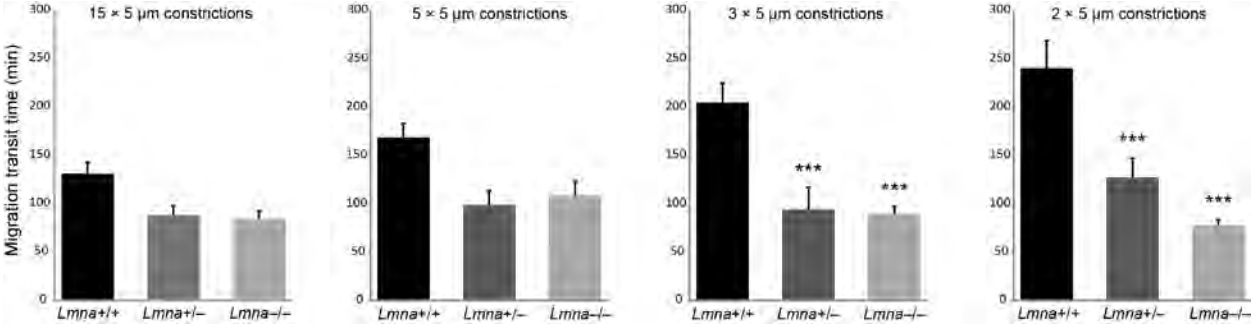

Figure 9. Time required for mouse embryo fibroblasts with different levels of lamins A/C to migrate through microscopic constirictions of different sizes. Transit times for wild-type cells (Lmna+/+) increase significantly with decreasing constriction size. In contrast, transit times for lamin A/C-deficient (Lmna–/– cells) are shorter and independent of the constriction size.

At the same time, our investigation of breast cancer cells migrating through the narrow constrictions produced some unexpected results. While the perfusion studies confirmed that knockdown of lamins A/C in MDA-MB-231 cells resulted in more deformable nuclei and faster perfusion times than control cells with normal levels of lamins A/C, surprisingly, cells with reduced levels of lamins A/C were no faster in migrating across the narrow constrictions than controls with normal lamin A/C levels (Fig. 10). Additional studies confirmed this result by showing that similar numbers of cells had crossed the length of the constriction channels after 48 hours for both lamin A/C knockdown and mock control cells (data not shown).

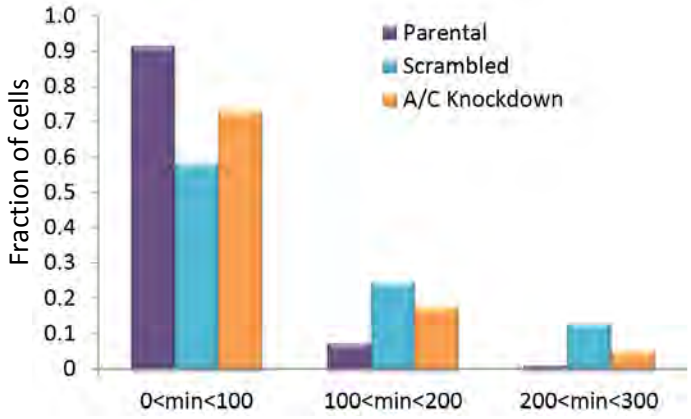

Figure 10. Histogram of migration transit times for MDA-MB-231 breast cancer cells with reduced levels of lamin A/C (A/C knockdown) and cells with normal levels of lamin A/C (non-modified parental cells and non-target controls). The cells with reduced levels of lamin A/C were no faster to transit the 2 x 5 μm^2 constrictions than the control cells.

Given that we and other groups had recently shown in different cell lines (mouse embryo fibroblasts, neutrophils, fibrosarcoma cells, lung cancer cells) that lower lamin A/C levels corresponded to increased migration efficiency through small constrictions,[10, 14, 15] we decided to investigated nuclear events during migration of breast cancer cells in more detail. Immunofluorescence staining of mock and non-modified cells in the devices revealed that lamins A/C levels and/or organization were dynamically regulated in these cells, with a decrease in fluorescence labeling for lamin A/C within the constriction channels, and an increase upon exiting the channels (Fig. 11). In contrast, levels of lamin B were not substantially altered during migration, confirming that the observed changes in nuclear envelope composition were specific to lamin A/C. These unexpected findings may explain the similar migration capability of lamin A/C knockdown and mock controls, as the latter cells' ability to temporarily reduce lamin A/C levels inside the channels effectively minimizes the difference in nuclear envelope composition with the knockdown cells. We are currently in the process of investigating the molecular mechanisms of the observed dynamic changes in lamin A/C levels during the migration, which could result from increased solubility of lamin A/C caused by phosphorylation, altered gene expression mediated by nuclear mechanosensing,[16] or by proteasomal degradation.

Of note, in addition to changes in nuclear envelope composition, we observed repetitive transient nuclear rupture during the migration through narrow constrictions, as visualized by NLS-copGFP escaping into the cytoplasm, then re-entering the nucleus after restoration of nuclear membrane integrity (Fig. 12). Importantly, lamins A/C knockdown cells had a significantly higher rate of nuclear rupture incidents than control cells (17% for lamin A/C knockdown cells *vs*. 2% for non-target controls), and nuclear rupture incidence increased in all cells when the device height was reduced from 5 µm to 3 µm. We have already presented these

results at a number of scientific conferences in 2013 and 2014 and are currently preparing a manuscript for publication. We will continue to investigate the molecular mechanism by which breast cancer cells manage to dynamically adjust their nuclear envelope composition and thereby overcome the normally rate-limiting factor of nuclear stiffness when migrating through dense 3-D environments. In addition, we are planning on following up on the finding of repetitive nuclear rupture in breast cancer cells during 3-D migration, particularly in cells with reduced levels of lamins A/C, as the repetitive nuclear damage may result in DNA damage and rearrangements that could further promote cancer progression.

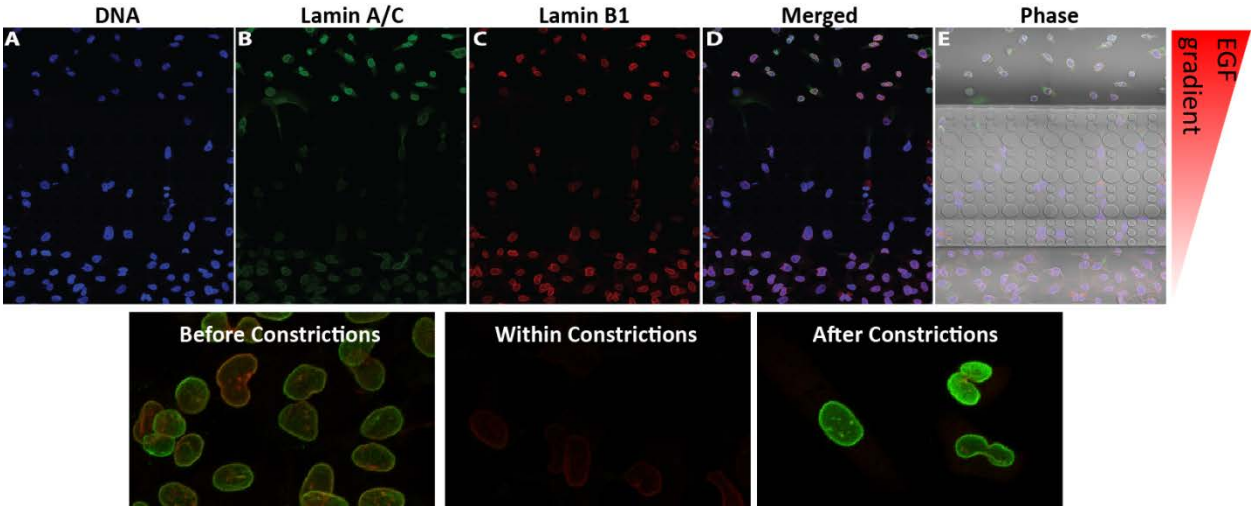

Figure 11. Breast cancer cells dynamically modify their nuclear envelope organization during migration through narrow constrictions. MDA-MB-231 cells were seeded into 5 µm tall PDMS channels with an EGF gradient to induce cell migration. After 48 hours, cells were stained for lamin A/C (green), lamin B (red), and DNA (blue). Cells had decreased lamin A/C levels while crossing the constrictions and increased lamin A/C levels upon exit from the constrictions. Levels of B-type lamins remained unchanged throughout crossing and after exit. This indicates a possible dynamic regulation of lamin A/C that is activated by environmental constraints and may promote cell invasion.

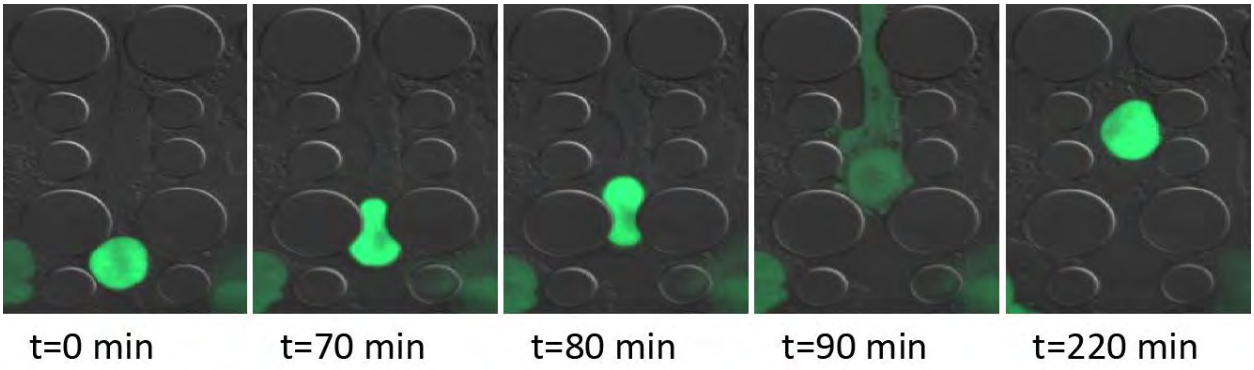

Figure 12. Nuclear rupture in breast cancer cells during migration through narrow constriction. MDA-MB-231 cells expressing an NLS-GFP fluorescent fusion protein were seeded into 5 µm tall PDMS channels with an EGF gradient to induce cell migration. Escape of the fluorescent protein from the nucleus indicates (temporary) loss of nuclear membrane integrity (left). Many cells displayed repeated nuclear rupture during migration through the narrow constrictions, particularly in cells with reduced levels of lamins A/C.

***Task 4:* Quantify expression levels of lamins and LBR in breast cancer cell lines, patient-derived breast cancer cells/tissue sections and determine correlation with disease progression from benign to more aggressive/metastatic phenotypes.**

We analyzed expression of lamins and LBR in MCF10A, MDA-MB-231, and MCF7 cells, as well as in a panel of other breast cancer cell lines. However, given the heterogeneous distribution of lamin A/C levels in several of the breast cancer cell lines,[5] our findings of dynamic changes in lamin A/C levels in the breast cancer cells, and three recently published reports confirming our hypothesis of altered levels of lamins and LBR in breast cancer patients,[5-7] we decided to focus our attention more on patient-derived tumor samples. Analyzing lamin A/C expression in patient-derived tissues samples provided by Linda Vahdat (Weill Cornell Medical College, New York, NY), we observed highly heterogeneous staining for lamin A/C in many of the cancer tissues and complete loss of lamins A/C in a subset of breast cancer cells (Fig. 13), similar to recently reported findings.[5] We are currently planning *in vivo* experiments on mouse models to test whether this subpopulation of cells is particularly aggressive and responsible for cancer metastasis.

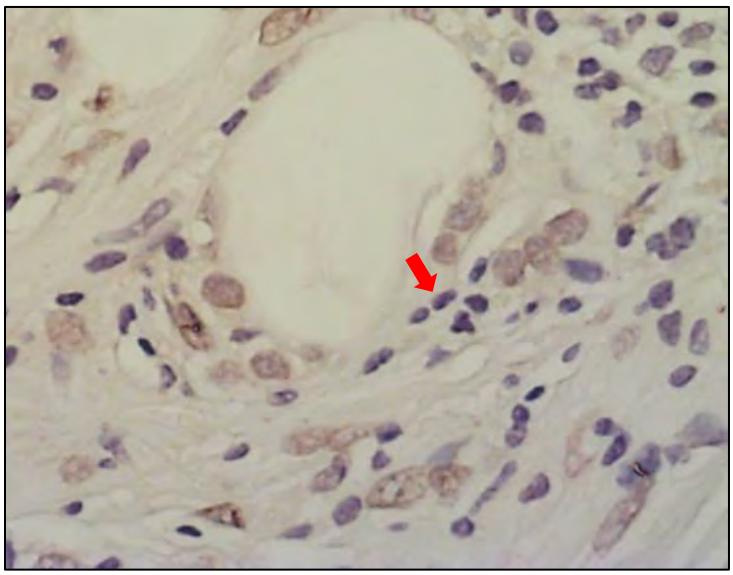

Figure 13. Human breast cancer tissue section stained with H&E (blue) and anti-lamin A/C (brown) revealing heterogeneous staining of cancer cell nuclei for lamin A/C, including some cells completely lacking lamin A/C expression (red arrow, nuclei appearing blue). Our hypothesis of altered lamin expression in breast cancer progression is further supported by a study published in the *Chinese Journal of Cancer* that described that lamins A/C are absent in almost 40% of human breast cancer tissues and that even in lamin A/C-positive cancers, expression of lamin A/C is heterogeneous or marked by altered intracellular distribution in the tumor cells,[5] and another recent report that found that breast cancer tissue has increased expression of lamin B1 compared to normal tissue.[7]

Interestingly, one sample from a triple negative breast cancer showed very abnormal levels of lamin A/C (Fig. 14). According to the oncologist, this patent had had one of the most aggressive breast cancers she had ever seen. We are currently acquiring additional patient samples to see whether we can uncover a correlation between lamin expression levels and disease progression/aggressiveness., particularly in light of a recent report that showed a significant correlation between altered lamins A/C expression and reduced disease-free survival.[6] Further analysis with a larger panel of samples may help to elucidate whether altered lamin expression can serve as a useful diagnostic and prognostic marker in breast cancer.

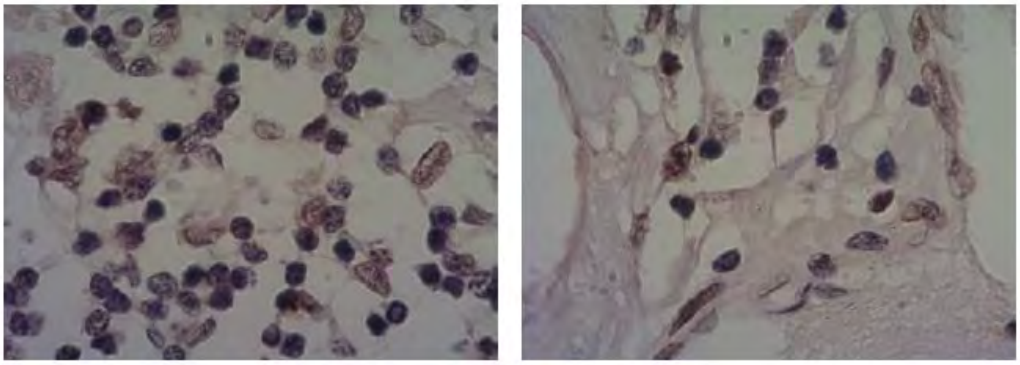

Figure 14. Altered and highly heterogeneous expression of lamin A/C in a patient with particularly aggressive triple negative breast cancer.

Task 5: **Investigate whether changes in the expression of lamins or LBR could modulate biophysical cell functions such as invasion, migration, and perfusion through narrow channels.**

The outcomes of this task are described under Task 3, as we used modulation of expression of lamins A/C to modify nuclear stiffness. Our data revealed that reduced expression of lamin A/C enhances the ability of (cancer) cells to flow through narrow constrictions during perfusion. At the same time, we uncovered surprising differences in the behavior of breast cancer cells from that of other cells (fibroblasts, fibrosarcome cells, neutrophils, lung cancer cells) when cells were induced to migrate through narrow constrictions, as highly metastatic breast cancer cells (MDA-MB-231 and MDA-MD-468) were able to dynamically change their nuclear envelope composition to facilitate migration through narrow constrictions (Fig. 11). In addition, we found that reduced levels of lamins A/C, as observed in a subset of patient breast cancer tissue, results in increased nuclear fragility and repetitive nuclear rupture during migration through narrow spaces, which could result in increasing DNA damage in those cells.

Task 6: **Investigate whether changes in the expression of lamins or LBR could modulate non-biophysical cell functions such as proliferation or epithelial-to-mesenchymal transition in the newly created panel of cell lines.**

We recently identified a remarkable and surprising effect of loss of lamin A/C on the intracellular localization and activity of the transcriptional coactivator megakaryoblastic leukaemia-1 (MKL1).[17] We found that while in normal cells MKL1 translocates from the cytoplasm to the nucleus in response to serum or mechanical stimulation, in lamin A/C-deficient and lamin A/C-depleted cells, MKL1 mostly remains in the cytoplasm (Fig. 15). This defect was caused by altered actin dynamics in the lamin A/C-deficient cells, as nuclear import and export of MKL1 are dependent on its interaction with monomeric G-actin. The altered actin dynamics were a result of the actin-polymerizing function of emerin, which is lost from the nuclear envelope in lamin A/C-deficient cells. As a consequence of disturbed actin dynamics and impaired nuclear translocation of MKL1, lamin A/C-deficient cells had reduced expression of MKL1/SRF target genes, which include actin, actin-binding proteins, vinculin, and serum response factor (SRF). These results were recently published in *Nature*.[17] While some of our findings were originally obtained in the context of cardiac disease caused by lamin A/C mutations, they are also highly relevant to cancer progression, as recent publication suggest a strong link between MKL1 activity and metastatic processes, including epithelial-to-mesenchymal transition (EMT) and cell invasion and migration,[18] including in MDA-MB-231 cells.[19] We have already begun to follow up

on these findings to examine MKL1 signaling in MDA-MB-231 cells with altered expression of lamins A/C and to evaluate the effect of altered lamin expression on EMT.

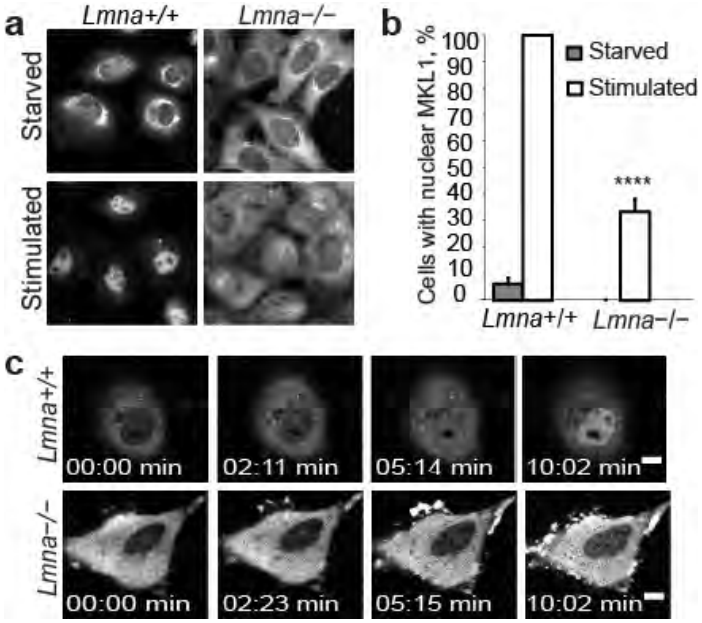

Figure 15. Impaired nuclear translocation of MKL1 in lamin A/C-deficient cells. (a) Lamin A/C-deficient (*Lmna*$^{-/-}$) cells had a lower fraction of nuclear MKL1 after serum stimulation than wild-type (*Lmna*$^{+/+}$) cells, based on MKL1 immunofluorescence. Scale bar, 10 μm. (b) Quantitative analysis of cells with positive nuclear MKL1 staining in response to serum stimulation ($N \approx 50$ per cell line). (c) Time-lapse sequences of cells expressing MKL1-GFP stimulated with serum, revealing impaired nuclear translocation of MKL1 in the lamin A/C-deficient cells. Scale bar, 10 μm.

In addition to these intriguing findings, we are following up on the question whether increased nuclear fragility can result in higher rates of DNA damage in breast cancer cells with reduced levels of lamin A/C. In preliminary experiments obtained during the last few weeks of this project, we observed that MDA-MB-231 cells with reduced levels of lamin A/C have substantially increased levels of γ-H2AX, a marker of double stranded DNA breaks. We are now investigating these results in more detail.

KEY RESEARCH ACCOMPLISHMENTS

- We confirmed that breast cancer tissue samples have altered (and highly heterogeneous) expression of lamins and LBR.
- We generated a cell panel with systematic variation in the expression of the nuclear envelope proteins lamin A, lamin B1, lamin B2, lamin C, and lamin B receptor (LBR) by shRNA mediated knockdown or ectopic expression, mimicking expression levels seen in patient tissue samples.
- We developed a novel microfluidic device to study nuclear deformability during perfusion of cells through precisely defined constriction channels, providing higher-throughput measurements of nuclear mechanics than traditional methods such as micropipette aspiration, substrate strain application, or atomic force microscopy.
- We designed a novel microfluidic system to visualize cancer cells migrating through precisely defined constrictions at high spatial and temporal resolution, representing a significant advance over traditional Boyden chambers or transwell migration assays.
- We characterized the effect of changes in nuclear envelope composition on nuclear shape and deformability – increased expression of lamin A causes the most severe increase in nuclear stiffness; decreased expression of lamins A/C results in the most severe decrease in nuclear stiffness
- We demonstrated that reduced levels of lamins A/C results in faster transit of cells through narrow constrictions, which might have important implications during perfusion of cancer cells through the circulatory system or proteolysis-independent migration through interstitial spaces.
- We identified a unique and unexpected feature of highly metastatic breast cancer cells, which are capable of dynamically adjusting their nuclear envelope composition as they migrate through 3-D environments and narrow constrictions. These adaptive changes may facilitate the migration of the metastatic cells through dense tissue and microenvironments.
- We identified increased rates of (transient) nuclear rupture in breast cancer cells with reduced levels of lamins A/C migrating through narrow constrictions, including extrusion of DNA from the nucleus, which could result in DNA damage and chromosomal rearrangements that could further promote cancer progression.
- We identified a novel connection between the nuclear envelope proteins lamin A/C and emerin and the transcriptional co-activator MKL1, which fails to properly localize to the nucleus in lamin A/C-deficient cells, resulting in reduced MKL1/SRF activity. As MKL1 is involved in several metastatic processes, these findings could have important implications in cancer progression.

REPORTABLE OUTCOMES

Manuscripts

We published the following manuscripts acknowledging funding from this project. Please see appendix for copies of the most relevant articles. Four additional manuscripts are currently in preparation or under review/revision.

1. Davidson PM, Denais C, Bakshi MC, **Lammerding J**. (2014). Nuclear deformability constitutes a rate-limiting step during cell migration in 3-D environments. *Cell and Molecular Bioengineering*. Published online June 20, 2014.
2. Davidson PM, **Lammerding J**. (2014). Broken nuclei – lamins, nuclear mechanics and disease. *Trends in Cell Biology*. 2014. 24(4):247-256
3. Denais C, **Lammerding J**. (2014). Nuclear mechanics in cancer. In: E.C. Schirmer and J.I. de las Heras, editors. Cancer Biology and the Nuclear Envelope, *Advances in Experimental Medicine and Biology*. 2014. 773: 435-470. DOI 10.1007/978-1-4899-8032-8_20
4. Ho CY, Jaalouk DE, **Lammerding J**. (2013). Novel insights into the disease etiology of laminopathies. *Rare Diseases*. Published online Nov. 6, 2013
5. Isermann P, **Lammerding J**. (2013). Nuclear Mechanics and Mechanotransduction in Health and Disease. *Curr Biol*. 2013. 23(24): R1113-R1121
6. Ho CY, Jaalouk DE, Vartiainen MK, **Lammerding J**. (2013). Lamin A/C and emerin regulate MKL1/SRF activity by modulating actin dynamics. *Nature*. 497(7450):507-11
7. Zwerger M, Jaalouk DE, Lombardi ML, Isermann P, Mauermann M, Dialynas G, Herrmann H, Wallrath LL, **Lammerding J**. (2013). Myopathic lamin mutations impair nuclear stability in cells and tissue and disrupt nucleo-cytoskeletal coupling. *Hum Mol Gen*. 2013. 22(12):2335-49
8. Rowat A, Jaalouk DJ, Zwerger M, Ung WL, Eydelnant IA, Olins D, Olins A, Herrmann H, Weitz DA, **Lammerding J**. (2013) Nuclear envelope composition determines the ability of neutrophil-type cells to passage through micron-scale constrictions. *J Biol Chem*. 288(12):8610-8618
9. Isermann P, Davidson PM, Sliz JD, Lammerding J. (2012). Assays to measure nuclear mechanics in interphase cells. *Curr Protoc Cell Biol*. 56:22.16.1- 22.16.21
10. Ho CY, **Lammerding J**. (2012). Lamins at a Glance. *J Cell Sci*. 125 (9): 2087-2093.

Conferences/Seminars/Meetings

Work performed as part of this project has been presented at the following meetings/invited seminars:

1. Breast cancer cells alter nuclear envelope composition to aid migration through narrow constrictions. Gilbert R, Denais C, Krause M, Wolf K, Lammerding J. Platform presentation based on submitted abstract. Biomedical Engineering Society (BMES) 2014 Annual Meeting. San Antonio, Texas (October 22-25, 2014)
2. Nuclear Deformability Constitutes a Rate-limiting Step During Cell Migration in 3-D Environments. Davidson P, Denais C, Bakshi M, Lammerding J. Platform presentation based on submitted abstract. Biomedical Engineering Society (BMES) 2014 Annual Meeting. San Antonio, Texas (October 22-25, 2014)

3. The role of lamin A/C and Nuclear Mechanics in Breast Cancer Cell Migration. Denais C, Gilbert R, Wolf K, Lammerding J. Invited presentation (and poster) based on submitted abstract. Gordon Research Conference on Intermediate Filaments. Mount Snow, West Dover, VT (June 18, 2014)
4. The nucleus under stress - mechanosensing by lamins, emerin, and nuclear actin. Invited presentation. Gordon Research Conference on Intermediate Filaments. Mount Snow, West Dover, VT (June 18, 2014)
5. The nuclear envelope proteins lamin A/C govern nuclear deformability and cell migration in confined 3-D environments. Invited presentation. International Workshop on Multiscale Mechanobiology (IWMM). Hong Kong (May 16, 2014)
6. Squish and Squeeze – Nuclear Biomechanics and Mechanotransduction in Health and Disease. Invited seminar. Department of Biomedical Engineering, Yale University (May 1, 2014)
7. Nuclear lamins – their contribution to cellular mechanics and mechanotransduction in health and disease. Invited seminar. Cardiovascular Science Conference Series. University of California San Diego, CA (Mar. 14, 2014)
8. Squish and squeeze – nuclear biomechanics in health and disease. Invited seminar. Condensed Matter and Biological Physics Seminar Series. Department of Physics, Syracuse University. Syracuse, NY (Feb. 28, 2014)
9. Squish and squeeze – nuclear biomechanics and mechanotransduction in health and disease. Invited seminar. BME Colloquium Series. Department of Biomedical Engineering, University of Rochester. Rochester, NY (Feb. 25, 2014)
10. Getting to the nucleus of it – Lamins, nuclear mechanics, and mechanotransduction. Invited speaker. Biomedical Engineering Society (BMES) – Cell and Molecular Bioengineering (CMBE) Special Interest Group 2014 Annual Meeting. San Diego, CA (Jan. 11, 2014)
11. Designing a microfluidic device to study the deformability of cancer cells. Lopez G, Davidson PM, Denais C, Lammerding J. Poster presentation based on submitted abstract. 2013 Annual Biomedical Research Conference for Minority Students (ABRCMS). Nashville, TN (Nov. 16, 2013)
12. Squish and squeeze – nuclear biomechanics in health and disease. Invited seminar. Cornell Institute for Biology Teachers Return-to-Campus workshop. Cornell University, Ithaca, NY (Oct. 26, 2013)
13. Squish and squeeze – nuclear biomechanics in health and disease. Invited seminar. Biophysics Colloquium seminar series at Cornell University, Ithaca, NY (Oct. 23, 2013)
14. Role of cellular mechanics during cell migration in 3-D environments. Invited platform presentation. Biomedical Engineering Society (BMES) Annual Meeting. Seattle, WA (Sept. 26, 2013)
15. Loss of lamin B2 expression enhances 3D migration in HT1080 fibrosarcoma. Jonnalagadda US, Denais CM, Krause M, Wolf K, and Lammerding J. Invited platform presentation selected from submitted abstracts. Biomedical Engineering Society (BMES) Annual Meeting. Seattle, WA (Sept. 26, 2013)
16. Lamins modulate nuclear deformability and transit through narrow constrictions of cancer cells. Denais CM, Jonnalagadda US, Zwerger M, Krause M, Wolf K, Vahdat L,

and Lammerding J. Invited platform presentation selected from submitted abstracts. Biomedical Engineering Society (BMES) Annual Meeting. Seattle, WA (Sept. 26, 2013)

17. Nuclear lamins – their contribution to cellular mechanics and mechanotransduction in health and disease. Seminar Series. Department of Molecular Biology and Genetics at Cornell University, Ithaca, NY (Sept. 20, 2013)
18. Squish and Squeeze – the Role of Cellular Biomechanics in Human Diseases. Invited seminar for the BME 5875 –Frontiers in Biomedical Research for Teachers course. Cornell University, Ithaca, NY (Aug. 9, 2013)
19. Nuclear mechanics and mechanotransduction in health and disease. PhD Symposium of the International PhD Program Molecular Mechanisms of Cell Signaling "Cells don't play dice"; University of Vienna and Medical University of Vienna; Vienna, Austria. June 2013.
20. Nuclear Lamins – their contribution to cellular mechanics and human disease. Invited seminar. Cellular & Molecular Medicine Seminar Series at the Cleveland Clinic; Cincinnati, OH. May 2013
21. Nuclear lamins – their role in nuclear mechanics and mechanotransduction in physiology and disease. Invited seminar. University of Pennsylvania – Institute for Medicine and Engineering (IME); Philadelphia, PA. April 2013.
22. Nuclear lamins govern nuclear deformability and modulate the ability of cells to transit through narrow constrictions during migration and perfusion. Invited keynote talk. ASME 2nd Global Congress on NanoEngineering for Medicine & Biology; Boston, MA. February 2013.
23. Significance of the mechanical properties of the cell nucleus in cell migration and transit through narrow constrictions. Invited speaker. Physics of Cancer 2012 Symposium at the University of Leipzig, Germany. November 2012
24. Exploring nuclear deformability as a rate-limiting factor in cancer cell migration. Selected for a platform presentation at the 2012 Annual Meeting of the Biomedical Engineering Society (BMES) in Atlanta, GA. October 2012
25. Intracellular Mechanics and Mechanosensing in Physiology and Disease. Invited seminar at the College of Engineering, Montana State University, Bozeman, MT in April 2012.

Cell lines

We created the following cell lines:

- MDA-MB-231 cells overexpressing either lamin A, lamin B1, lamin B2, lamin C or lamin B receptor (LBR), including unsorted cells and cells sorted for medium or high levels of overexpression
- MDA-MB-231 with reduced expression of either lamins A/C, lamin B1, lamin B2, or LBR, including heterogeneous and clonal populations
- MCF10A cells overexpressing either lamin A, lamin B1, lamin B2, lamin C or LBR
- MCF10A with reduced expression of either lamins A/C, lamin B1, lamin B2, or LBR
- All of the above cell lines, as well as MDA-MB-468 cells, are also available with fluorescently labeled nuclei, either by expression of NLS-GFP or fluorescently labeled histones.
- We also created similarly modified cell lines of non-breast cancer cells lines (fibroblasts, fibrosarcoma cells) for comparison to identify effects specific to breast cancer cells.

Microfluidic migration and perfusion devices
We designed and generated novel microfluidic devices that enable visualizing cancer cells migrating or being perfused through precisely defined constrictions at high spatial and temporal resolution. We have already disseminated some of these devices to collaborating laboratories at the Cleveland Clinic and will continue to make them available to interested groups. We are currently finalizing a manuscript for submission to *Lab on a Chip* characterizing the device in more detail. The cell perfusion device for rapid measurements of nuclear deformability has already been published (Isermann et al. *Curr Prot Cell Biol* 2012).

Personnel supported through this award
The following personnel received pay from the research effort of this project.

- Jan Lammerding, Assistant Professor, Cornell University
- Celine Denais, Postdoctoral Fellow, Lammerding Lab
- Patricia Davidson, Postdoctoral Fellow, Lammerding Lab
- Philipp Isermann, Visiting Scientist, Lammerding Lab
- Josiah Sliz, Student Employee/Temporary Staff, Lammerding Lab

Funding
Experimental methods developed for the work on this project contributed to generating preliminary data for a project that was rewarded with a National Science Foundation Career Award to Jan Lammerding. The work proposed in the NSF Career Award is aimed at addressing the molecular mechanisms by which normal (i.e., non-cancerous) cells overcome the resistance of the large and stiff nucleus when migrating through narrow constrictions.

We are currently exploring additional funding opportunities to continue the research funded by this DoD Idea Award, with a particular focus on investigating how breast cancer cells—unlike several other cells—can dynamically adjust their nuclear envelope composition to facilitate passage through narrow constrictions and dense tissues, and to test whether the increased rates of nuclear rupture, caused by the increased nuclear fragility of cancer cells with low levels of lamin A/C, can lead to DNA damage and chromosomal rearrangements, which could further promote cancer progression.

CONCLUSIONS

The premise of this proposal was to test whether breast cancer cells and tissue have disturbed expression of the nuclear envelope proteins lamin and LBR, which could explain the often abnormal nuclear morphology of breast cancer cells and also directly contribute to altered function of cancer cells relevant to metastatic processes. Recent publications by other laboratories and our own work have now confirmed that expression of lamins and LBR is indeed altered in many breast cancer cells and further suggest that lower levels of lamins A/C correlate with reduced disease free survival.[5-7]

Based on these results, we generated a panel of cells lines with systematic modulation of the expression levels of lamins and LBR, which enabled us to rigorously study the functional effects of disturbed expression of nuclear envelope proteins seen in breast cancer tissues. In addition, we developed novel microfluidic devices to study the biomechanical aspects of altered nuclear envelope protein expression on the ability of cells to pass through narrow constrictions, mimicking conditions encountered during perfusion through the capillary system or migration through the interstitial space.

Using these tools, we were able to identify that nuclear deformability, which is governed by the levels of lamins A/C, constitutes a rate-limiting factor in the ability of cells to pass through pores and openings smaller than the nuclear size, which is highly relevant to the distribution of cancer cells through basement membranes, interstitial space, and small capillaries during cancer metastasis. Importantly, we identified a unique feature of highly metastatic cancer cells, as these cells—unlike fibroblasts and some other cancer cells investigated for comparison—were able to dynamically adjust their nuclear envelope composition during migration through confining 3-D environments by reducing the levels of lamins A/C at the nuclear envelope. These changes are predicted to make the nucleus more deformable and facilitate transit through narrow constrictions. At the same time, we observed that cells with reduced levels of lamins A/C were more prone to repetitive transient nuclear rupture during migration through narrow constriction, which could result in increased DNA damage and chromosomal rearrangements that could further promote cancer progression. In addition, we described for the first time that cells lacking lamins A/C have disturbed nuclear localization and activity of the MKL1/SRF pathway, which is highly relevant to EMT and cell migration.

Taken together, our findings could have important clinical implications for breast cancer. Analysis of expression levels of nuclear envelope proteins could be used in the diagnosis and particularly the prognosis of breast cancers, where a high fraction of cells with softer nuclei could indicate higher risk to the patient. Such prognostic approaches would be particularly powerful when applied to the analysis of circulating tumor cells, as it may help identify particularly aggressive subpopulations of tumor cells. We continue to follow up on our findings reported here to investigate whether the subset of breast cancer cells lacking lamins A/C are particularly responsible for metastatic spreading and to better understand the molecular mechanisms underlying the ability of breast cancer cells to dynamically alter their nuclear envelope composition, which may ultimate lead to the identification of new therapeutic targets.

REFERENCES

1. Ho, C.Y. and J. Lammerding, *Lamins at a glance.* J Cell Sci, 2012. **125**(Pt 9): p. 2087-93.
2. Lammerding, J., L.G. Fong, J.Y. Ji, K. Reue, C.L. Stewart, S.G. Young, and R.T. Lee, *Lamins A and C but not lamin B1 regulate nuclear mechanics.* J Biol Chem, 2006. **281**(35): p. 25768-80.
3. Lammerding, J., P.C. Schulze, T. Takahashi, S. Kozlov, T. Sullivan, R.D. Kamm, C.L. Stewart, and R.T. Lee, *Lamin A/C deficiency causes defective nuclear mechanics and mechanotransduction.* J Clin Invest, 2004. **113**(3): p. 370-8.
4. Schreiber, K.H. and B.K. Kennedy, *When lamins go bad: nuclear structure and disease.* Cell, 2013. **152**(6): p. 1365-75.
5. Capo-chichi, C.D., K.Q. Cai, J. Smedberg, P. Ganjei-Azar, A.K. Godwin, and X.X. Xu, *Loss of A-type lamin expression compromises nuclear envelope integrity in breast cancer.* Chin J Cancer, 2011. **30**(6): p. 415-25.
6. Wazir, U., M.H. Ahmed, J.M. Bridger, A. Harvey, W.G. Jiang, A.K. Sharma, and K. Mokbel, *The clinicopathological significance of lamin A/C, lamin B1 and lamin B receptor mRNA expression in human breast cancer.* Cell Mol Biol Lett, 2013. **18**(4): p. 595-611.
7. Davalieva, K., S. Kiprijanovska, C. Broussard, G. Petrusevska, and G.D. Efremov, *Proteomic analysis of infiltrating ductal carcinoma tissues by coupled 2-D DIGE/MS/MS analysis.* Mol Biol (Mosk), 2012. **46**(3): p. 469-80.
8. Zwerger, M., D.E. Jaalouk, M.L. Lombardi, P. Isermann, M. Mauermann, G. Dialynas, H. Herrmann, L.L. Wallrath, and J. Lammerding, *Myopathic lamin mutations impair nuclear stability in cells and tissue and disrupt nucleo-cytoskeletal coupling.* Hum Mol Genet, 2013. **22**(12): p. 2335-49.
9. Caille, N., Y. Tardy, and J.J. Meister, *Assessment of strain field in endothelial cells subjected to uniaxial deformation of their substrate.* Ann Biomed Eng, 1998. **26**(3): p. 409-16.
10. Davidson, P.M., C. Denais, M.C. Bakshi, and J. Lammerding, *Nuclear deformability constitutes a rate-limiting step during cell migration in 3-D environments.* Cell Mol Bioeng, 2014.
11. Isermann, P., P.M. Davidson, J.D. Sliz, and J. Lammerding, *Assays to measure nuclear mechanics in interphase cells.* Curr Protoc Cell Biol, 2012. **Chapter 22**: p. Unit22 16.
12. Byun, S., S. Son, D. Amodei, N. Cermak, J. Shaw, J.H. Kang, V.C. Hecht, M.M. Winslow, T. Jacks, P. Mallick, and S.R. Manalis, *Characterizing deformability and surface friction of cancer cells.* Proc Natl Acad Sci U S A, 2013. **110**(19): p. 7580-5.
13. Wolf, K., M. Te Lindert, M. Krause, S. Alexander, J. Te Riet, A.L. Willis, R.M. Hoffman, C.G. Figdor, S.J. Weiss, and P. Friedl, *Physical limits of cell migration: Control by ECM space and nuclear deformation and tuning by proteolysis and traction force.* J Cell Biol, 2013. **201**(7): p. 1069-84.
14. Harada, T., J. Swift, J. Irianto, J.W. Shin, K.R. Spinler, A. Athirasala, R. Diegmiller, P.C. Dingal, I.L. Ivanovska, and D.E. Discher, *Nuclear lamin stiffness is a barrier to 3D migration, but softness can limit survival.* J Cell Biol, 2014. **204**(5): p. 669-82.
15. Rowat, A.C., D.E. Jaalouk, M. Zwerger, W.L. Ung, I.A. Eydelnant, D.E. Olins, A.L. Olins, H. Herrmann, D.A. Weitz, and J. Lammerding, *Nuclear envelope composition determines the ability of neutrophil-type cells to passage through micron-scale constrictions.* J Biol Chem, 2013. **288**(12): p. 8610-8.
16. Swift, J., I.L. Ivanovska, A. Buxboim, T. Harada, P.C. Dingal, J. Pinter, J.D. Pajerowski, K.R. Spinler, J.W. Shin, M. Tewari, F. Rehfeldt, D.W. Speicher, and D.E. Discher, *Nuclear lamin-A scales with tissue stiffness and enhances matrix-directed differentiation.* Science, 2013. **341**(6149): p. 1240104.

17. Ho, C.Y., D.E. Jaalouk, M.K. Vartiainen, and J. Lammerding, *Lamin A/C and emerin regulate MKL1-SRF activity by modulating actin dynamics.* Nature, 2013. **497**(7450): p. 507-11.
18. Scharenberg, M.A., R. Chiquet-Ehrismann, and M.B. Asparuhova, *Megakaryoblastic leukemia protein-1 (MKL1): Increasing evidence for an involvement in cancer progression and metastasis.* Int J Biochem Cell Biol, 2010. **42**(12): p. 1911-4.
19. Medjkane, S., C. Perez-Sanchez, C. Gaggioli, E. Sahai, and R. Treisman, *Myocardin-related transcription factors and SRF are required for cytoskeletal dynamics and experimental metastasis.* Nat Cell Biol, 2009. **11**(3): p. 257-68.

APPENDICES

Electronic copies (PDFs) of 8 published manuscripts most relevant to this research project are included on the following pages. All of the articles acknowledged funding through the DoD Idea Award.

SUPPORTING DATA

None – all figures are included in the text above

Cellular and Molecular Bioengineering (© 2014)
DOI: 10.1007/s12195-014-0342-y

BMES BIOMEDICAL ENGINEERING SOCIETY™
www.bmes.org

Nuclear Deformability Constitutes a Rate-Limiting Step During Cell Migration in 3-D Environments

PATRICIA M. DAVIDSON, CELINE DENAIS, MAYA C. BAKSHI, and JAN LAMMERDING

Department of Biomedical Engineering, Weill Institute for Cell and Molecular Biology, Cornell University, Ithaca, NY 14853, USA

(*Received 17 February 2014; accepted 12 June 2014*)

Associate Editor David Schaffer oversaw the review of this article.

Abstract—Cell motility plays a critical role in many physiological and pathological settings, ranging from wound healing to cancer metastasis. While cell migration on 2-dimensional (2-D) substrates has been studied for decades, the physical challenges cells face when moving in 3-D environments are only now emerging. In particular, the cell nucleus, which occupies a large fraction of the cell volume and is normally substantially stiffer than the surrounding cytoplasm, may impose a major obstacle when cells encounter narrow constrictions in the interstitial space, the extracellular matrix, or small capillaries. Using novel microfluidic devices that allow observation of cells moving through precisely defined geometries at high spatial and temporal resolution, we determined nuclear deformability as a critical factor in the cells' ability to pass through constrictions smaller than the size of the nucleus. Furthermore, we found that cells with reduced levels of the nuclear envelope proteins lamins A/C, which are the main determinants of nuclear stiffness, passed significantly faster through narrow constrictions during active migration and passive perfusion. Given recent reports that many human cancers have altered lamin expression, our findings suggest a novel biophysical mechanism by which changes in nuclear structure and composition may promote cancer cell invasion and metastasis.

Keywords—Lamin, Nucleus, Mechanics, Cancer, Microfluidics, Microstructures, Metastasis, Invasion, Nuclear envelope.

ABBREVIATIONS

2-D	Two-dimensional
3-D	Three-dimensional
ANOVA	Analysis of variance
BSA	Bovine serum albumin
DMEM	Dulbecco Modified Eagle Medium
FBS	Fetal bovine serum
GFP	Green fluorescent protein
LINC	Linker of nucleoskeleton and cytoskeleton
MEF	Mouse embryonic fibroblast
MMP	Matrix metalloproteinase
PBS	Phosphate buffered saline

Address correspondence to Jan Lammerding, Cornell University, Weill Hall, Room 235, Ithaca, NY 14853, USA. Electronic mail: jan.lammerding@cornell.edu

This paper is part of the 2014 Young Innovators Issue.

Dr. Jan Lammerding is an Assistant Professor in the Department of Biomedical Engineering and the Weill Institute for Cell and Molecular Biology at Cornell University. He received a Bachelor of Engineering degree from the Thayer School of Engineering at Dartmouth College, a *Diplom Ingenieur* degree in Mechanical Engineering from the University of Technology Aachen, Germany, and a Ph.D. in Biological Engineering from the Massachusetts Institute of Technology (MIT). Before joining Cornell University, Dr. Lammerding served as a faculty member at Harvard Medical School/Brigham and Women's Hospital (BWH) while also teaching in the Department of Biological Engineering at MIT. At Cornell, the Lammerding laboratory is developing novel experimental techniques to investigate the interplay between cellular mechanics and function, with a particular emphasis on the cell nucleus and its response to mechanical forces. Dr. Lammerding has won several prestigious awards, including a National Science Foundation CAREER Award, an American Heart Association Scientist Development Grant, and the BWH Department of Medicine Young Investigator Award. Dr. Lammerding has published over 40 peer-reviewed articles, including in *Nature* and *PNAS*. His research is supported by grants from the National Institutes of Health, the National Science Foundation, the Department of Defense Breast Cancer Research Program, the American Heart Association, and the Progeria Research Foundation.

© 2014 Biomedical Engineering Society

Published online: 20 June 2014

PDGF Platelet derived growth factor
PDMS Polydimethylsiloxane

INTRODUCTION

The ability of cells to move within their environment is crucial for numerous physiological and pathological processes. During development, cell migration contributes to shaping the growing embryo and to forming nascent tissues; in mature organisms, immune cells are mobilized from the blood stream to enter sites of infection, and migration of epithelial cells and fibroblasts is vital for proper wound healing and tissue repair. In cancer metastasis, cell migration drives the invasion of tumor cells into the surrounding tissue and the dissemination to other organs. The fact that cancer metastasis, rather than the primary tumor, is responsible for up to 90% of all cancer deaths[4] has been one of the primary motivators to study cell migration.

Traditionally, research on cell migration has involved observing cells moving on flat, two-dimensional (2-D) substrates, owing primarily to the convenience in sample preparation and the ability to image cells at high spatial and temporal resolution. These studies have resulted in tremendous insights into the intricate processes occurring during cell migration, particularly at focal adhesions and the actin cytoskeleton. Nonetheless, research carried out over the past decade indicates that cell migration in 3-D environments, as is the case in most physiological processes inside the human body, can substantially deviate from migration on 2-D substrates.[1,11,12,20,31] Much of this work has focused on specific changes in cell morphology (e.g., spreading, cytoplasmic organization, *etc.*) or migration mode (e.g., amoeboid vs. mesenchymal migration) when comparing cells in 2-D vs. 3-D environments.[11,12] However, one additional and particularly important difference is that in 3-D migration, cells have to overcome the confinement of the surrounding extracellular matrix and other cells.[1,13,20] In many cases, the openings in the cell's 3-D environment can be as small as 2–30 μm in diameter,[36,43] i.e., substantially smaller than the cell diameter. Under these conditions, cells have two options: (1) to degrade/modify their environment to create sufficient space, for example, by secretion of matrix metalloproteinases (MMPs); or (2) to deform to fit through the available space. In the latter option, the deformability of the cell becomes an important factor in the ability of cells to pass through 3-D environments.

The cytoplasm is very flexible and can undergo large deformations; in addition, the cytoskeleton can actively remodel to take up the available space, allowing it to penetrate openings as small as 1 μm.[44] The cell nucleus, on the other hand, is 2- to 10-times stiffer than the surrounding cytoplasm and occupies a large fraction of the cellular volume[7]; with a typical diameter of 3–10 μm, the nucleus is larger than many of the pores encountered in the extracellular environment, so that cell movement through such constrictions requires substantial nuclear deformations.[13,14,39,44] Importantly, a recent study by Wolf and colleagues suggests that nuclear deformability constitutes a rate-limiting factor during non-proteolytic migration of cells through 3-D collagen matrices.[44] As nuclear deformability is directly dependent on the expression of the nuclear envelope proteins lamins A and C,[24,25] we analyzed the effect of lamin expression on the ability of cells to transit constrictions smaller than the nuclear diameter during migration in 3-D environments or perfusion through microfluidic devices with precisely controlled constrictions. We found that mouse embryonic fibroblasts (MEFs) partially ($Lmna^{+/-}$) or completely ($Lmna^{-/-}$) lacking lamins A/C, for which we had previously demonstrated increased nuclear deformability,[24,25] passed significantly faster through the narrow constrictions than wild-type ($Lmna^{+/+}$) controls.

MATERIALS AND METHODS

Cell Culture

MEFs from mice with homozygous ($Lmna^{-/-}$) or heterozygous ($Lmna^{+/-}$) deletion of the *Lmna* gene encoding lamins A/C, along with wild-type littermate controls ($Lmna^{+/+}$), were generously provided by Dr. Colin Stewart.[37] Human SV40 virus-transformed skin fibroblasts (GM00637J), originally obtained from Coriell Cell Repositories, were stably modified with a tetracycline-regulated (Tet-off) GFP-lamin A construct[15] provided by Dr. Tom Glover and maintained as described previously.[41] NIH 3T3 fibroblasts were modified with mCherry–Histone-4 and GFP-LifeAct to allow visualization of nuclear position and F-actin distribution. All cells were maintained in Dulbecco Modified Eagle Medium (DMEM) supplemented with 10% fetal bovine serum (FBS), penicillin and streptomycin. Medium for live cell imaging was further supplemented with 25 mM HEPES buffer.

Device Fabrication

The migration devices were fabricated at the Cornell NanoScale Science and Technology Facility (CNF) using standard lithography techniques. The perfusion devices were modeled on a design by the Fletcher laboratory[32] and described previously.[21,33] In brief, the design consists of 10 μm tall microfluidic channels that bifurcate multiple times and lead to 5 μm-wide

constriction channels. A wide bypass channel is included to assure maintenance of uniform pressure drop across the constriction channels even if some channels are blocked.

The migration devices contain features of two different heights, produced from a mold composed of two layers: one 5 μm tall layer to form the constrictions channels, and a second, 250 μm tall layer to create cell collection areas directly before the constrictions (in which cells are seeded) and behind the constrictions (in which cells that have passed the constriction can gather). The constriction channels are made of a series of round pillars, with three narrow openings in a row, measuring 5, 3, and 2 μm in width, respectively (Fig. 1a). We created two variations of the migration devices; one of which consisted entirely of channels with narrow constrictions, the other additionally including regularly spaced 15 μm wide passages that were used to study cell migration in the 5 μm tall channels without substantial nuclear deformation. Large reservoirs on either side of the constrictions that can be filled with media were used to establish a chemotactic gradient across the device.

Molds of the devices were fabricated from SU-8 photoresist. Briefly, a silicon wafer was baked at 200 °C for half an hour, then SU-8 was spun onto the wafer to obtain a 5 μm thick layer. To study the migration of cells along a chemotactic gradient in less confined conditions, we also created a variation of the migration device in which the channels had a height of 15 μm, but were otherwise identical. Wafers were baked at 60 °C for 10 min, cooled, and UV exposed using the first mask. Wafers were then baked briefly at 95 °C, cooled, and the unexposed SU-8 was dissolved in SU-8 developer. After development, the wafers were baked again at 200 °C for half an hour, then SU-8 was spun on the wafers to obtain the 250 μm thick layer. The wafers were then baked at 50 °C for 24 h, exposed using the second mask, and baked at 95 °C for 10 min. After cooling down, the wafers were developed, the heights of the structures were measured on a profilometer and the wafers were coated with (1*H*,1*H*,2*H*,2*H*-perfluorooctyl)trichlorosilane to facilitate detachment during replica production. Replicas of the SU-8 molds were produced using polydimethylsiloxane (PDMS). The two components of Sylgard 184 (Dow Corning) were mixed in the 1:10 ratio recommended by the manufacturer, the mixture was degassed to eliminate bubbles and poured over the wafer in a plastic petri dish. This assembly was then baked at 65 °C for 2 h. The resulting PDMS replica was carefully peeled away from the SU-8 structures and individual migration devices were cut out and placed on packing tape to prevent dust from accumulating on the clean surface. Inlets for cells were punched using 1.2 mm biopsy punches, and reservoirs for medium were created using 5 mm biopsy punches (Harris).

Microfluidic devices were assembled by bonding the PDMS replicas to glass slides. Glass slides were incubated in 0.2 M HCl overnight, rinsed with deionized water, isopropanol and water again, then dried off with filtered air. Both the glass slides and the PDMS replicas were exposed to an oxygen plasma for 5 min and the PDMS was then placed on the glass slides, which sealed instantly. The newly formed microfluidic devices were baked at 95 °C on a hot plate for 5 min, doused and perfused with 70% ethanol to sterilize, followed by sterile water.

Validation of Gradient Formation in Migration Devices

Migration devices were passivated with 30 mg/mL BSA in PBS at 4 °C overnight to reduce absorption of fluorescently labeled dextran to the PDMS surface. Prior to imaging, the BSA solution was replaced with PBS on the side the cells are loaded on and Texas Red-labeled 70-kDa dextran (Molecular Probes) dissolved at 10 mg/mL in PBS (Invitrogen) on the other side, mimicking the conditions for the migration experiments with a PDGF gradient. The devices were then covered with a glass coverslip to minimize evaporation, placed on the heated microscope stage or in a temperature controlled incubator and imaged at defined time-points for up to 24 h. Line profiles of the fluorescence intensity were obtained using Zen light software (Zeiss) and the average profiles from at least three different measurements at each time point were used to determine the time course and stability of the gradient formation reported in Fig. 1. As the PDGF used for the migration experiments has a lower molecular weight (~25 kDa) than the fluorescently labeled dextran, it is expected that the PDGF gradient forms even faster than the data presented in Fig. 1.

Cell Perfusion Experiments

Experiments to measure passive nuclear deformability were performed as described previously.[21] In brief, prior to the experiments, the microfluidic channels were treated with BSA (20 mg/mL in PBS) for 30 min to reduce cell adhesion. Cells suspended in PBS with 20 mg/mL bovine serum albumin (BSA) at a final concentration of 3×10^6 cells/mL were passed through a cell strainer and transferred into Exmire Microsyringes mounted on a microdialysis pump (CMA Microdialysis). A second syringe loaded with PBS + 20 mg/mL BSA was used to prime and occasionally flush the devices. Cells were perfused through

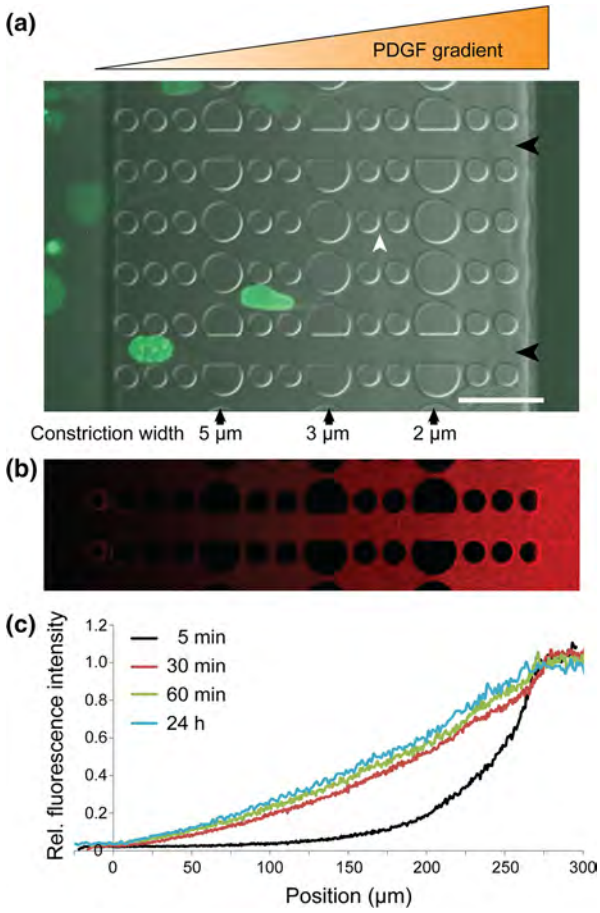

FIGURE 1. Overview of the microfluidic migration device. (a) Cells are seeded in a 250 μm tall chamber of the device (far left), which is separated from the other chamber (far right) by 5 μm tall constriction channels consisting of PDMS pillars. Larger pillars create a series of 5, 3, and 2 μm wide constrictions (black arrows). In the direction perpendicular to the gradient, 2 μm wide spacings between pillars (white arrowhead) allow the gradient to form uniformly even when cells are inside the constriction channels. Channels with wider spacing (15 μm, black arrowheads) are provided to assess the cell migration speed without nuclear confinement. Shown here are human skin fibroblasts expressing GFP-lamin A migrating through a device towards a PDGF chemotactic gradient. Scale bar: 50 μm. (b) Gradient formation of fluorescently labeled (Texas Red) 70 kD dextran after 24 h. (c) Fluorescence intensity across the migration device during gradient formation with 70 kD fluorescent dextran, demonstrating that the gradient forms quickly (within 30 min) and is stable over 24 h.

the microfluidic device at a rate of 2.0 μL/min and imaged at 20× magnification with a MegaPlus 310T CCD camera (Roper Scientific) at 30 frames/s. Perfusion transit times through the 5 μm constrictions were determined from recorded 60–90 s long videos as described previously.[32] Separate aliquots of the cell suspensions were imaged at 10× magnification with a Roper CoolSNAP HQ and cell sizes were determined using ImageJ software. All cells used for the perfusion experiments had a similar size distribution.

Micropipette Aspiration

Experiments to measure nuclear stiffness were carried out following previously established protocols.[8,34] Micropipettes were pulled from glass capillary tubing (Sutter Instrument; 1 mm outer diameter; 0.5 mm inner diameter) with a Flaming/Brown Micropipette Puller (Model P-97, Sutter Instrument). Micropipettes were then cut to have an opening with an inner diameter of 4.0–5.5 μm. Subsequently, micropipettes were fire-polished and shaped using a Micro Forge (MF-900, Narishige). Micropipettes were immersed in PBS with 20 mg/mL BSA for 1 h to minimize cell adhesion and backfilled with PBS. Cells incubated with Hoechst 33342 for 10 min at 37 °C were suspended in DMEM + 10% FBS and placed in a microscope mounted glass-bottom culture dish. Individual cells in suspension were carefully positioned at the mouth of the micropipette using a negative aspiration pressure of ΔP = 10 mm H_2O. Subsequently, the aspiration pressure was increased to ΔP = 75.5 mm H_2O with a valve system developed in house, resulting in partial aspiration of the cell nucleus. Aspiration continued until an equilibrium position was reached and the nucleus stopped further advancing into the micropipette (typically less than 15 s). For a given aspiration pressure, the nuclear elasticity inversely scales with the ratio of the aspirated nuclear length, L_P, and the micropipette diameter, D (Fig. 3).[8] Cells in which the nucleus was positioned away from the micropipette were excluded from the analysis. Cell viability during the experiments was monitored using propidium iodide in the medium.

Cell Migration Through Microfluidic Constrictions

Cells for migration experiments were suspended in DMEM containing 10% FBS at a final concentration of 5×10^6 cells/mL. The migration devices were incubated with 0.2 mg/mL fibronectin (Millipore) in phosphate buffered saline (PBS) for at least 2 h at 37 °C. The fibronectin-coated devices were then filled with fresh medium and aliquots of 20000 cells were added to each device (4 μL of 5×10^6 cells/mL). Live cell imaging experiments were carried out 24 h after seeding cells into the devices. Immediately prior to imaging, the medium in both wells of the device was replaced with phenol red-free medium containing 25 mM HEPES (Gibco); for experiments using a chemotactic gradient, the well towards which the cells were migrating additionally contained 200 ng/mL PDGF as a chemoattractant. After medium replacement, glass coverslips were added to the top of the devices to limit evaporation, and the devices were placed in a temperature-controlled chamber on a Zeiss LSM 700 confocal microscope (AxioObserver) equipped with a CCD camera (CoolSNAP EZ, Photometrics)

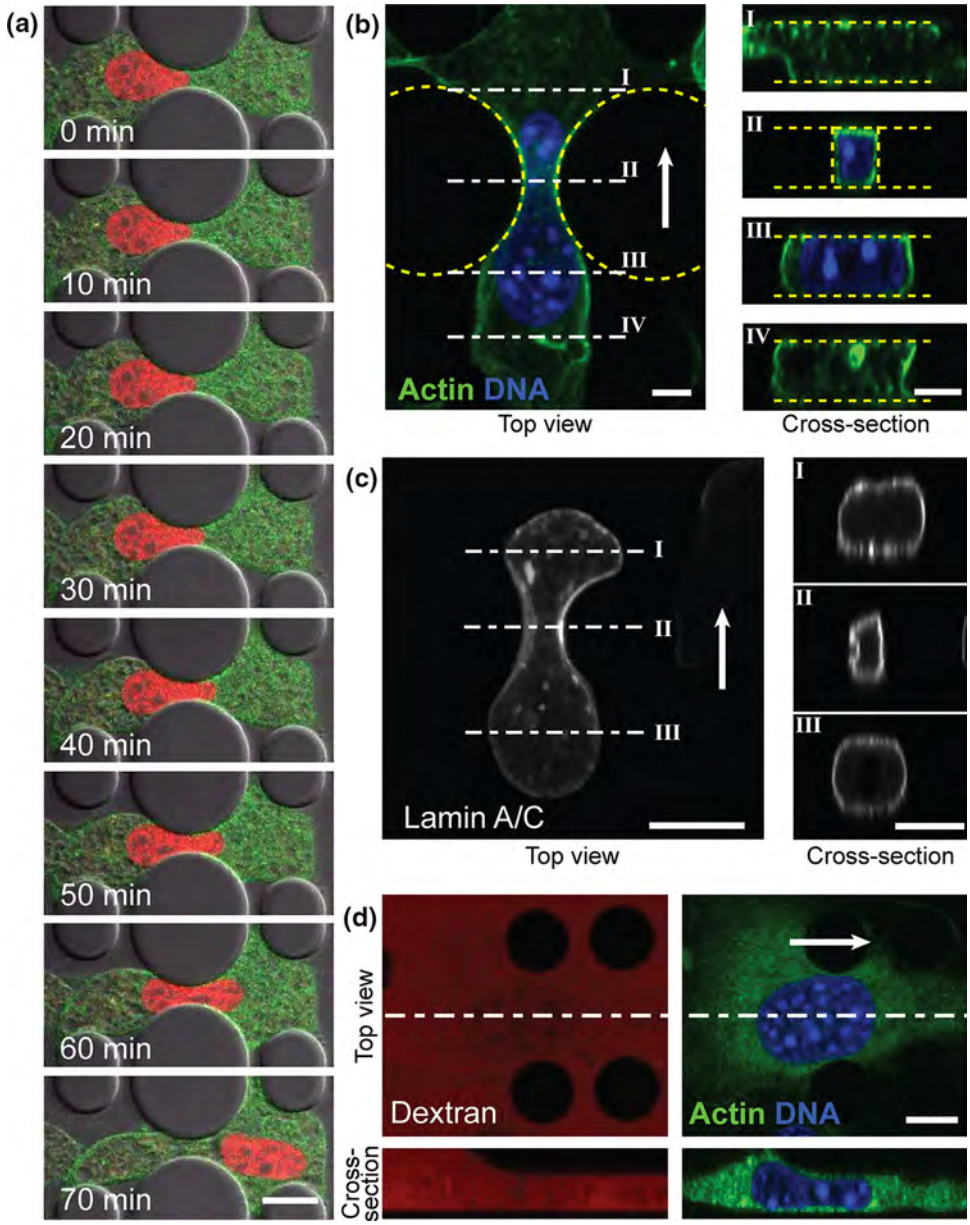

FIGURE 2. Nuclear deformation during migration through narrow constrictions. (a) Time-lapse image sequence of NIH 3T3 cells expressing fluorescently tagged Histone-4 (red) and actin (green) migrating through a 3 μm wide constriction, revealing substantial nuclear deformation. Scale bar: 20 μm. (b) Top-view and cross-sections of a confocal 3-D reconstruction of a cell migrating through a 3 μm-wide constriction, stained for DNA (blue) and F-actin (green). The cross-sections (right) demonstrate that the cell takes up the entire height of the device and that the nucleus fills out the constriction. Scale bar: 5 μm. White arrow denotes direction of migration. (c) Confocal 3-D reconstruction of a cell expressing GFP-lamin A migrating through a 2 μm-wide constriction. The cross-section through the constriction (II) suggests compression and buckling of the nuclear lamina inside the constriction. Scale bar: 5 μm. (d) Confocal top- and side-view of a single cell entering the 5 μm tall constriction channel inside the migration device. The channels were filled with fluorescently labeled dextran (red; left images) and cells were stained for DNA (blue) and expressed fluorescent actin (green). As the cell enters the 5 μm tall channel, the cell and nuclear height adjusts to the available height of the channel (compare bottom left and right images). Scale bar: 10 μm.

and a motorized stage (Zeiss). Time-lapse images were recorded every 2 or 10 min for 8–14 h total. Image sequences used for the analysis of cell migration were acquired with a 20× objective in widefield/phase contrast mode. Fluorescence images were acquired in confocal mode with a 63× objective.

For the 48 h migration studies, we quantified the number of cells successfully passing through the constriction channels using devices that did not contain the wider 15 μm channels. Cells were seeded in the devices; after 24 h, the medium was replaced with imaging medium; the media in the reservoir on the

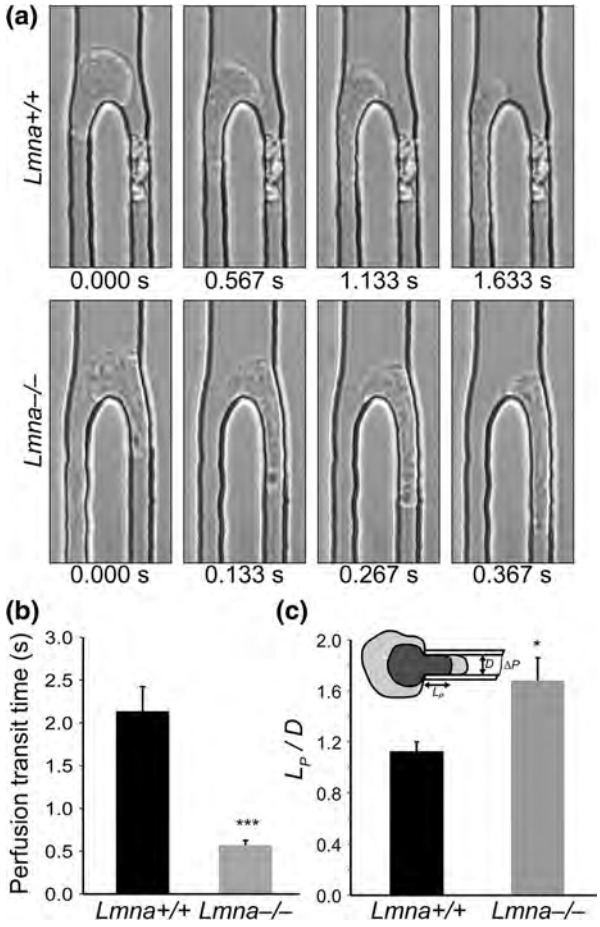

FIGURE 3. Lamin A/C-deficient cells have more deformable nuclei. (a) Representative images from high-speed time-lapse videos of cells being perfused through 5 μm wide microfluidic constriction channels, revealing that wild-type cells (*Lmna*$^{+/+}$) take substantially longer to enter and move through the constriction channel than lamin A/C-deficient (*Lmna*$^{-/-}$) cells. (b) Perfusion transit times through 5 μm constriction channels in the perfusion experiments. $N = 167$ cells for *Lmna*$^{+/+}$, 236 for *Lmna*$^{-/-}$; ***, $p < 0.0001$. (c) Micropipette aspiration measurements on wild-type and lamin A/C-deficient cells, demonstrating that lamin A/C-deficient cells have more deformable nuclei. The nuclear elasticity is inversely proportional to the ratio of the aspirated nuclear length, L_P, and the micropipette diameter, D. $N = 17$ cells for *Lmna*$^{+/+}$, 18 for *Lmna*$^{-/-}$; *, $p = 0.0105$.

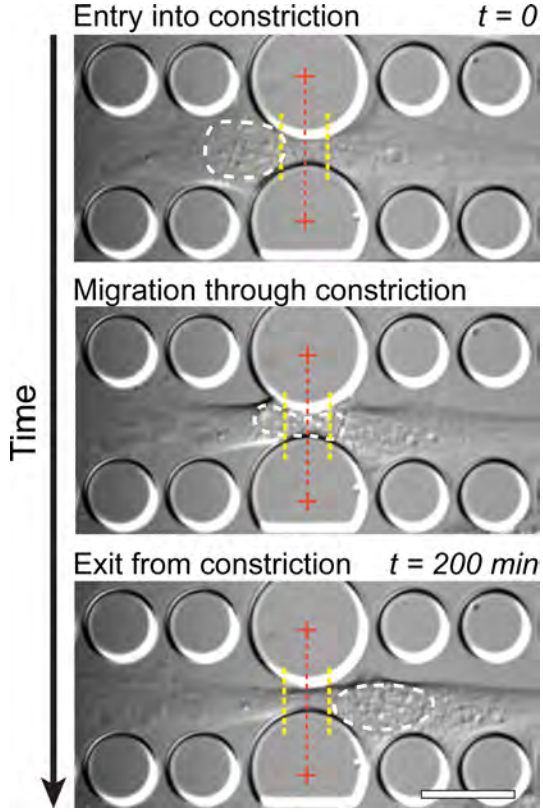

FIGURE 4. Experimental approach to quantify the migration transit times of the nucleus through the narrow constrictions. Time-lapse image sequences were used to measure the amount of time between when the cell nucleus enters and exits the constriction. In this example, a *Lmna*$^{+/+}$ MEF is shown. Entry into the constriction is defined as the time point at which the cell nucleus crosses a threshold (left yellow dotted line) located 5 μm in front of the constriction center; the nucleus is defined as having exited the constriction when the back of the nucleus crosses a threshold 5 μm past the center of the constriction (right yellow dotted line). The white dashed line indicates the outline of the nucleus for demonstration purposes. The center of the constriction is marked with a red dashed line. See Supplemental Data for representative time-lapse microscopy sequences of *Lmna*$^{+/+}$, *Lmna*$^{+/-}$ and *Lmna*$^{-/-}$ cells. Scale bar: 20 μm.

other side of the constrictions was additionally supplemented with 200 ng/mL PDGF. Images were taken then and 24 h later on an inverted microscope (Zeiss AxioObserver) with a 10× objective and a CCD camera (CoolSNAP EZ). The number of cells that had successfully passed through the constrictions was determined from these images. The proliferation rates of the different cell lines were measured by passaging the cells every 48 h five-times in a row, counting the cells and each time re-seeding 1×10^6 cells in a T75 flask. The average fold-change over a 48 h period was then determined from the cell counts and used to normalize the number of cells that had migrated through the constrictions.

Analysis of Cell Migration Through Microfluidic Devices

Time-lapse image sequences were collated into movies and corrected for drift in the x–y plane using a custom-written MATLAB algorithm. In most cases, the cells analyzed only went through one constriction within the time frame of the experiment and the data points presented here thus represent different cells. Movies of individual cells traveling through constrictions were cropped and the Manual Tracking plugin in ImageJ was used to track the position of the front and

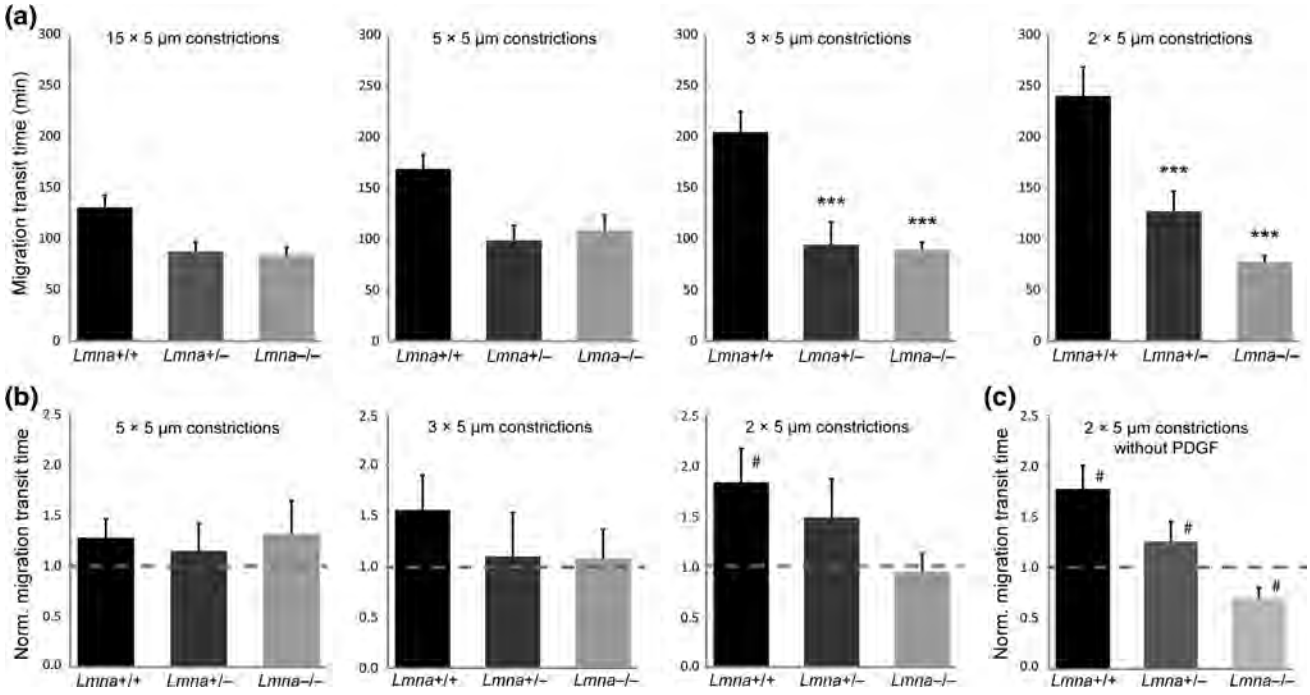

FIGURE 5. Reduced lamin A/C levels facilitate migration through narrow constrictions. (a) Migration transit times for *Lmna*$^{+/+}$, *Lmna*$^{+/-}$ and *Lmna*$^{-/-}$ cells migrating through constrictions 15, 5, 3, or 2 μm wide and 5 μm tall. Wild-type (*Lmna*$^{+/+}$) cells take significantly longer to pass through the 2 × 5 and 3 × 5 μm^2 constrictions than cells with reduced lamin A/C levels. For wild-type cells, but not *Lmna*$^{+/-}$ and *Lmna*$^{-/-}$ cells, migration transit times were negatively correlated with constriction size ($p < 0.01$). N = 24–41 cells per genotype, constriction; ***, $p < 0.001$ compared to *Lmna*$^{+/+}$ cells. (b) Migration transit times through narrow constrictions normalized to the corresponding migration transit times through 15 μm-wide channels, which are larger than the nucleus. Wild-type cells have impaired migration efficiency through the smallest constrictions, indicated by increased normalized migration transit times, while cells with reduced levels of lamins A/C maintain comparable migration transit times for all constriction sizes. N = 24–41 cells per genotype, constriction; #, $p < 0.05$ compared to migration transit times through 15 μm channels. (c) Migration transit times through 2 × 5 μm^2 constrictions normalized to the 15 μm channels without the presence of a chemoattractant gradient; #, $p < 0.05$ compared to migration transit times through 15 μm channels.

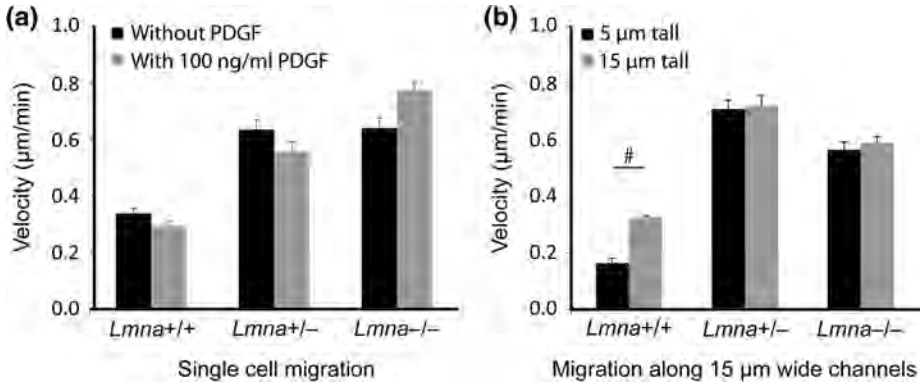

FIGURE 6. Cell migration velocity in unconfined conditions. (a) Single cell migration analysis of MEFs migrating on 2-D fibronectin-coated glass substrates, indicating that wild-type (*Lmna*$^{+/+}$) MEFs migrate slower than *Lmna*$^{+/-}$ and *Lmna*$^{-/-}$ cells. PDGF stimulation had no significant effect on migration velocity. (b) Migration velocity in the direction of a chemoattractant (PDGF) gradient in 15 μm wide channels with heights of 5 μm (3-D migration) or 15 μm (2.5-D migration). Consistent with the 2-D migration experiments, wild-type cells moved more slowly than the lamin A/C-deficient cells; unlike the lamin A/C-deficient cells, wild-type cells had impeded migration speeds in the 5 μm tall channels compared to the 15 μm tall channels, indicating a possible effect of partial nuclear compression (Fig. 2d).

the back of the nucleus as it was passing through the constrictions. The migration transit time of a cell through a constriction was defined as the time between when the front of the cell crossed an imaginary line 5 μm in front of the constriction center and when the back of the nucleus passed a corresponding line 5 μm

behind the constriction center (see dotted lines in Fig. 4). A similar analysis was performed on cells in the 15 μm wide channels to obtain values of the migration transit time of cells under non-constrained conditions. In addition, we measured the size and circularity of nuclei inside the 5 μm tall channels (but outside the narrow constrictions) using a custom-written MATLAB script.

Single Cell Migration Experiments and Analysis

Single cell migration assays were performed using small chambers built by punching 1 cm diameter holes into PDMS slabs approximately 5 mm thick and bonding these slabs onto glass slides to obtain multiple wells. The size of the glass slides was such that six wells could fit on one glass slide, allowing observation of the three cell types, with and without PDGF, during the same experiment. Before experiments, the wells were sterilized with 70% ethanol and incubated with 0.2 mg/mL fibronectin (Millipore) in PBS at 37 °C for at least 2 h. Cells were passaged, seeded at 100 cells/well, and allowed to adhere for at least 6 h prior to the start of experiments. Immediately before imaging, the medium on the cells was replaced with phenol red-free medium containing 25 mM HEPES (Gibco). Half of the wells also contained 100 ng/mL PDGF; the concentration was chosen to be half-maximal concentration in the chemotactic gradient, thereby matching the average PDGF concentration inside the constriction channels. After replacing the medium, a glass slide was placed over the wells to limit evaporation; the PDMS assembly was then placed in a temperature-controlled chamber on a Zeiss LSM 700 confocal microscope (AxioObserver) equipped with a CCD camera (CoolSNAP EZ, Photometrics) and a motorized stage (Zeiss). Time-lapse images were recorded every 10 min for 8–14 h total. Image sequences used for the analysis of cell migration were acquired with a 20× objective in widefield/phase contrast mode. Following the experiment, the position of the cells was tracked using the Manual Tracking plugin in ImageJ, and the average velocities were obtained. Cells that divided or were in contact with other cells were discarded from the analysis.

Statistical Analysis

Experiments were performed at least three independent times. Statistical analysis was performed with PRISM 3.0 software (GraphPad) and SAS v 9.13 (SAS Institute 2003). Data representing two groups were compared by unpaired Student's *t* test with Welch's

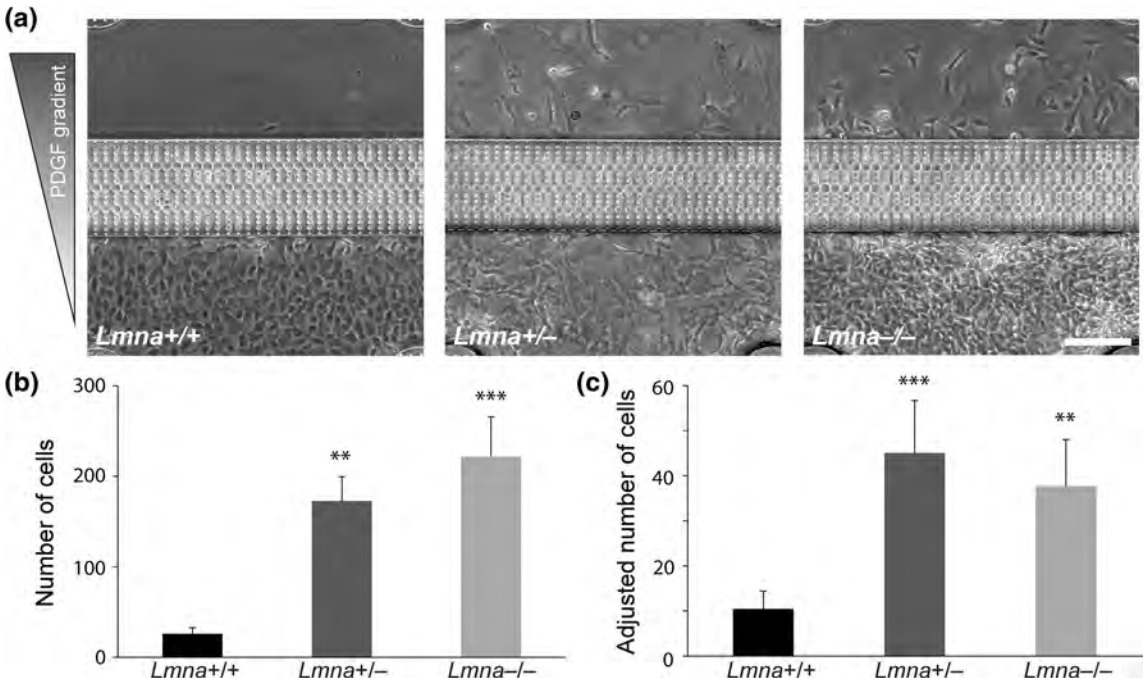

FIGURE 7. Cells with reduced levels of lamin A/C migrate through narrow constrictions more efficiently. (a) Representative images of migration devices after 48 h of migration, revealing increased numbers of *Lmna*$^{+/-}$ and *Lmna*$^{-/-}$ cells that have passed through the constrictions. (b) Quantitative analysis of cell numbers that have passed through the channels after 48 h. Cells with a reduced expression of lamins A/C had significantly larger numbers than wild-type cells. (c) Cell numbers were adjusted for the different proliferation rates between cell lines. The adjusted data confirmed that cells with reduced levels of lamins A/C were more efficient at migrating through the narrow constrictions. $N = 8$ (from three independent experiments); **, $p < 0.01$, ***, $p < 0.001$, compared to *Lmna*$^{+/+}$ cells. Scale bar: 200 μm.

correction to allow for different variances. For samples that did not follow a Gaussian distribution (perfusion transit times), data were compared with the non-parametric Mann–Whitney test. Data representing three groups (migration and perfusion transit times and cell number studies; Figs. 4, 5 and 7) were compared using an omnibus *F*-test and Tukey–Kramer multiple-means-analysis. Statistical correlation between constriction size and migration transit time for each cell line was analyzed using the Pearson test (Fig. 5). The data in the cell number study (Fig. 7) were transformed using a $\log(x + 1)$ transformation prior to analysis to better meet the assumptions of variance of the ANOVA. Data are expressed as arithmetic mean ± SEM. For all experiments, a two-tailed *p*-value of less than 0.05 was considered significant.

RESULTS

Nuclear Deformation During Migration in Confined 3-D Environments

It is now well established that cell motility in 3-D environments can substantially deviate from cell migration on flat substrates.[11,31] Recent reports further suggest that the deformability of the cell, and particularly the nucleus, may present a rate-limiting factor in 3-D migration.[13,18,44] However, most current strategies to study cell migration in 3-D environments are limited in their ability to quantitatively assess the effect of the physical environment on single cells: collagen matrices used for 3-D cell migration contain randomly distributed pores of variable size[44] and the dense collagen network can make high resolution imaging challenging; transwell migration assays and Boyden chambers, on the other hand, have precisely defined pore sizes but do not allow real-time imaging of the cells traveling through the narrow constrictions at high resolution. We have therefore designed a novel microfluidic device in which cells migrate along a chemotactic gradient through well-defined constrictions (Fig. 1). The device is composed of an array of 5 μm tall channels containing a series of increasingly narrower constrictions measuring 5, 3 and 2 μm in width, respectively. Small lateral openings (Fig. 1a, white arrowhead) between the channels assure a uniform chemotactic gradient across the constrictions and nutrient supply to the cells, while intermittent 15 μm wide channels (Fig. 1a, black arrowhead) serve as controls to account for inherent differences in migration speed. By imaging the fluorescence intensity distribution of Texas Red-labeled dextran, we confirmed that gradients formed rapidly (<30 min) within the device and remained stable over the time-course of the experiments (Figs. 1b and 1c). Using this device, we obtained high resolution time-lapse sequences of fibroblasts moving along a PDGF gradient through the constrictions, revealing substantial nuclear deformations as the cells squeezed through the constrictions (Figs. 2a, 2b, 2c, and 2d), including deformation of the nuclear lamina (Fig. 2c). In some cases, what appeared like buckling of the nuclear lamina was observed in cells expressing GFP-lamin A (Fig. 2c), possibly due to the presumably more rigid nuclear lamina in these cells. Importantly, the cells took up the entire height of the channels and adhered to both the top and the bottom of the fibronectin-coated channels (Fig. 2b), indicating that the device presents a true 3-D environment to the cell. Furthermore, the height of the channels (5 μm) was sufficient to confine the nucleus, as evidenced by the reduction in nuclear height as cells entered the channels (Fig. 2d).

Cells with Lower Lamin A/C Expression have More Deformable Nuclei

Given the large nuclear deformations required to pass through the narrow constrictions in our microfluidic channels and observed during non-proteolytic cell migration in dense collagen matrices,[44] we hypothesized that cells with more deformable nuclei may be able to transit faster through constrictions that are smaller than the nuclear diameter. The deformability of the nucleus is primarily governed by the chromatin and the mechanical properties of the nuclear envelope.[7] In particular, the nuclear envelope proteins lamins A/C are one of the major determinants of nuclear deformability, and MEFs from lamin A/C-deficient mice ($Lmna^{-/-}$) have substantially softer nuclei than cells from wild-type littermates ($Lmna^{+/+}$), with heterozygous cells ($Lmna^{+/-}$) displaying an intermediate phenotype.[24] As the $Lmna^{+/+}$, $Lmna^{+/-}$ and $Lmna^{-/-}$ MEFs have been well characterized in terms of their nuclear mechanics[24,25] and their migration on 2-D substrates,[10,17,26,28] we focused our subsequent studies on these cells. To confirm the increased nuclear deformability of the lamin A/C-deficient cells during passage through narrow constrictions, we perfused cells through microfluidic channels with constrictions smaller than the size of the nucleus (Fig. 3a). The lamin A/C-deficient cells passed through the constrictions significantly faster than wild-type controls (Figs. 3a and 3b), indicating that they had softer nuclei that required less time (and energy) to deform. We further confirmed the increased nuclear deformability of the lamin A/C-deficient cells using nuclear micropipette aspiration assays (Fig. 3c), consistent with previous results of cells with reduced levels of lamins A/C.[22,30,38]

Cells with Lower Lamin A/C Levels Migrate Faster Through Narrow Constrictions

To test whether reduced levels of lamins A/C and the associated increased nuclear deformability could improve the ability of cells to migrate through confined environments, we measured the migration transit time (Fig. 4) of $Lmna^{+/+}$, $Lmna^{+/-}$ and $Lmna^{-/-}$ MEFs cells migrating through precisely defined constrictions of 5 μm height and 5, 3, or 2 μm width (see Fig. 1). The cells with reduced lamin A/C levels ($Lmna^{+/-}$ and $Lmna^{-/-}$) had significantly shorter migration transit times through the 3 and 2 μm wide constrictions than the wild-type cells (Fig. 5a; see also Supplemental Data for representative videos); the difference between the $Lmna^{+/-}$ and $Lmna^{-/-}$ cells was not statistically significant. In the 5 μm wide constrictions, the cells with lower lamin A/C levels displayed a trend towards faster migration transit times, but the difference between the cell lines was not quite statistically significant ($p = 0.057$).

To account for inherent differences in the migration speeds between the three cell lines in unconfined conditions (Figs. 6a and 6b), we normalized migration transit times through the various constrictions by the corresponding migration transit times in the 15 μm-wide channels for each cell line. This normalization allows for a more general comparison of the effect of small constrictions on the migration behavior of the different cell lines. A normalized migration transit time larger than '1' indicates that cells from a given cell line take longer to migrate through a given constriction than the same cells would take to pass through a large channel that does not require nuclear deformation. For the 5 μm-wide constrictions, all three cell lines had normalized migration transit times close to '1', indicating that this constriction size had no significant effect on cell migration (Fig. 5b, left graph). However, when further reducing the constriction size, this resulted in progressively increasing normalized migration transit times for the wild-type cells, particularly in the 2 μm-wide constrictions (Fig. 5b, right graph). These data suggest that in wild-type cells, nuclear deformability becomes rate-limiting when passing through openings substantially smaller than the nucleus. In contrast, for cells with reduced levels of lamins A/C, restricting the constriction size down to as small as $2 \times 5\ \mu m^2$ had no effect on the migration transit time. In fact, for these cells the migration transit times through the narrow constrictions were indistinguishable from those for the 15 μm-wide channels, i.e., the normalized migration transit time remained close to '1' (Fig. 5b, right graph), suggesting that the nuclei of these cells do not significantly resist deformation in the constriction sizes tested.

Effect of Lamin Expression on Cell Migration is Independent of PDGF-Gradient

To test whether the results depend on the specific chemotactic gradient used here (i.e., PDGF), we also performed experiments on cells migrating through the constriction channels without a chemotactic gradient. We found that the experimental observation remained the same: the $Lmna^{+/+}$ cells took significantly longer to pass through the narrow ($2 \times 5\ \mu m^2$) constrictions than the 15 μm-wide constrictions ($p < 0.001$), and the $Lmna^{+/+}$ cells had significantly increased normalized migration transit times through the $2 \times 5\ \mu m$[1] constrictions compared to $Lmna^{-/-}$ cells (Fig. 5c). Just as in the experiments with the PDGF gradient, $Lmna^{+/-}$ cells displayed an intermediate phenotype between the $Lmna^{+/+}$ and the $Lmna^{-/-}$ cells. Taken together, these results suggest that differences in lamin A/C expression and the associated changes in nuclear deformability, rather than differential responses to the chemotactic gradient, are responsible for the different abilities to pass through constrictions smaller than the nuclear diameter.

We conducted additional assays in which cells were induced to migrate through the constrictions in the absence or presence of a chemotactic gradient while being maintained in a cell culture incubator. For these experiments, we used devices without the 15 μm-wide channels to ensure that all cells had migrated through the narrow constriction channels. After 48 h, significantly more $Lmna^{+/-}$ and $Lmna^{-/-}$ cells had passed through the constrictions than wild-type cells (Figs. 7a and 7b), confirming the results obtained in the time-lapse microscopy studies. However, we observed that lamin A/C-deficient cells proliferate faster than wild-type cells (doubling times were 0.68, 1.0, and 1.6 days for the $Lmna^{-/-}$, $Lmna^{+/-}$, and $Lmna^{+/+}$ cells, respectively), which could affect the number of cells on both sides of the constriction after 48 h despite identical initial seeding densities. We therefore also compared migration efficiency after normalizing the cell numbers to the proliferation rate for each cell line. Importantly, even after accounting for the different proliferation rates, cells with reduced levels of lamins A/C had significantly higher migration efficiencies through the narrow constrictions than wild-type cells, while differences between $Lmna^{+/-}$, and $Lmna^{-/-}$ cells were not statistically significant (Fig. 7c). Experiments performed without a PDGF gradient produced similar findings (data not shown). Taken together, these data demonstrate that cells with reduced levels of lamins A/C, which have more deformable nuclei, are significantly more efficient at migrating through constrictions smaller than the size of the nucleus.

DISCUSSION

Using novel microfluidic migration devices that enable imaging of nuclear deformation during cell passage through tight constrictions in 3-D environments, we found that reduced levels of lamins A/C result in enhanced transit efficiency during passive perfusion and active cell migration. These results provide further support for an important role of nuclear mechanics in 3-D cell migration and indicate that changes in nuclear envelope composition, which often affect nuclear deformability, can have important implications in the ability of cells to move through dense tissues or other confined spaces. Cells embedded in dense collagen matrices show severe nuclear deformations when MMP activity is inhibited, and reducing the pore size between collagen fibers to less than $\approx 6\ \mu m^2$ (or about 1/10 of the cross-sectional area of the unconfined nucleus) causes stalled cell migration and nuclei forming long protrusions as they unsuccessfully attempt to pass through the constriction.[44] Similarly, breast cancer cells moving through microfluidic PDMS channels have significantly decreased rates of migration when the channel size is reduced below 8 μm $\times$ 5 μm,[14] and osteosarcoma cell migration is impaired when channel width is reduced below 20 μm.[39]

In our experiments, we did not observe permanent arrest of cell migration, even in the $2 \times 5\ \mu m^2$ constrictions; however, when using migration channels with similar design but a channel height of only 3 μm, migration efficiency was substantially lower than in the 5 μm tall constriction channels, particularly for the wild-type cells (data not shown). Importantly, even though the cells in our experiments had not reached the 'nuclear deformation limit' beyond which 3-D cell migration stalls,[44] nuclear deformability had nonetheless a strong effect on migration efficiency through constrictions smaller than the unconfined nuclear diameter. In wild-type cells, migration transit times negatively correlated with a decrease in constriction size ($p < 0.01$), and migration through $2 \times 5\ \mu m^2$-sized constrictions was significantly slower than through the $15 \times 5\ \mu m^2$-sized reference channels. In contrast, cells with reduced levels of lamins A/C, which have more deformable nuclei,[24,25] needed less time to pass through the narrow constrictions than wild-type cells; furthermore, their migration transit times were independent of the size of the constriction, at least down to the $2 \times 5\ \mu m^2$-sized constrictions used in our experiments.

To further compare the migration behavior of cells in 2-D and 3-D environments, we also performed single cell migration experiments on 2-D glass substrates. In these experiments, wild-type cells were significantly slower than lamin-A/C deficient cells (Fig. 6), suggesting some inherent cell line-to-cell line variation and prompting us to use normalized migration transit times for further analysis to account for differences in migration speed in unconfined conditions. In addition, we also used migration devices with 15 μm tall channels to assess the migration speeds under the influence of a chemotactic gradient in 2.5-D, i.e., cells adhering to the side-walls and bottom or top, but not the top and bottom simultaneously. Similar to the results of the 2-D experiments, the wild-type cells migrated more slowly than the lamin A/C-deficient cells. Interestingly, while we observed similar migration speeds between 2.5-D and 3-D migration for the lamin A/C-deficient cells (Fig. 6b), the wild-type cells had lower migration velocities in the 5 μm tall channels (3-D migration) compared to the 15 μm tall channels (2.5-D migration), suggesting that wild-type cells already resist nuclear compression when reducing the available height down to 5 μm (see Fig. 2d), impairing their migration. Thus, normalizing the migration transit times with the (faster) transit times through the 15 μm wide sections in the 15 μm tall channels, rather than the (slower) times for the 5 μm tall channels as done in the current analysis, would result in even greater differences between the wild-type and lamin A/C-deficient cells.

As PDGF is a known effector of lamin A/C phosphorylation,[9] and lamin A/C can conversely affect several signaling pathways involved in cell migration,[19] we performed additional experiments to assess the effect of the PDGF chemoattractant on cell migration in wild-type and lamin A/C-deficient cells in more detail. Wild-type cells, but not lamin A/C-deficient cells, responded to the PDGF gradient by increasing their migration speed through the constriction channels compared to cells migrating without a PDGF gradient. However, this effect was independent of the constriction size (data not shown); hence, the PDGF gradient had little effect on the normalized migration transit times (compare Figs. 5b and 5c). Importantly, migration transit times for wild-type cells were always significantly longer than corresponding transit times for lamin A/C-deficient cells, regardless of the absence or presence of a PDGF gradient. Thus, the rate-limiting role of nuclear deformability in 3-D migration through narrow constrictions, governed by levels of lamins A/C, was independent of the chemoattractant used in the experiments.

Furthermore, the improved migration efficiency of the lamin A/C-deficient cells during 3-D migration through narrow constrictions could not be explained by differences in nuclear size, as the cells with reduced lamin A/C levels had larger nuclei than the control cells, with nuclear cross-sectional areas of 330 ± 10, 320 ± 10, and $210 \pm 10\ \mu m^2$ for $Lmna^{-/-}$, $Lmna^{+/-}$

and *Lmna*$^{+/+}$ MEFs, respectively. In fact, the larger nuclear size of the *Lmna*$^{-/-}$ and *Lmna*$^{+/-}$ cells would be expected to impair cell migration through narrow constrictions, pointing to an even greater effect of lamin A/C levels on cell motility. Further support for the importance of nuclear lamins and nuclear deformability on 3-D cell migration comes from a recent study in which cells expressing progerin, a lamin A mutant that results in more rigid nuclei,[6,40] had difficulties passing between microposts positioned 6 μm apart, but showed no difference in unconfined migration.[2] Similarly, ectopic overexpression of lamin A dramatically reduced the ability of neutrophil-like cells to pass through narrow constrictions during passive perfusion or active migration.[33] Importantly, neutrophils normally have highly lobulated nuclei and downregulate lamins A/C and other nuclear envelope proteins during granulopoiesis while upregulating expression of lamin B receptor[29]; it has long been speculated that this change in nuclear envelope composition and the associated changes in nuclear shape and stiffness enhance the ability of neutrophils to migrate through microscopic openings between endothelial cells during extravasation and promote mobility in tissues during infection.[13,33] Developmentally or environmentally regulated changes in lamin A/C expression have also been postulated to contribute to enhanced nuclear deformability in stem cells and may contribute to the correct trafficking of hematopoietic stem cells.[35,38]

Interestingly, even though *Lmna*$^{+/-}$ cells have only 50% reduced levels of lamins A/C and their nuclear deformability falls between that of *Lmna*$^{-/-}$ and wild-type cells, the ability of *Lmna*$^{+/-}$ cells to migrate through narrow constrictions was virtually indistinguishable from that of *Lmna*$^{-/-}$ cells (Figs. 5 and 7). One possible reason is that lamins A/C form an extended part of the LINC (Linker of nucleoskeleton and cytoskeleton) complex.[5,16] Consequently, complete loss of lamins A/C will not only increase nuclear deformability, which should enhance migration efficiency, but can also disrupt force transmission between the nucleus and the cytoskeleton, which could negatively affect cell migration.[18] Consistent with this idea, recent studies found that complete loss of lamins A/C or LINC complex disruption impairs the physical coupling between the actin cytoskeleton and nucleus, resulting in impaired cell polarization and migration on 2-D substrates[10,17,26–28] and in 3-D collagen matrices.[23] Cells with reduced (but not absent) levels of lamins A/C, such as the *Lmna*$^{+/-}$ MEFs, may thus benefit from the increased nuclear deformability caused by reduced lamin A/C expression while retaining near-normal nucleo-cytoskeletal coupling.

In conclusion, the role of lamins A/C in contributing to nuclear stiffness has important implications in determining the ability of cells to pass through narrow constrictions during 3-D migration or perfusion through narrow capillaries. These properties are not only relevant in various physiological processes, but are also attracting increasing interest in the study of cancer metastasis, as altered expression of lamins has been reported in a variety of human cancers (reviewed in Ho and Lammerding[19]). Breast cancer tumor cells, for example, often have reduced expression of lamins A/C,[3,42] and loss of lamins A/C negatively correlates with disease-free survival.[42] The increased nuclear deformability associated with reduced lamin A/C levels may promote invasion of metastatic cancer cells into surrounding tissues and spreading through the vascular and lymphatic system, thereby constituting a substantial risk factor on top of gene-regulatory changes linked to altered lamin expression.[19] Thus, an improved understanding of the multifaceted function of lamins has the potential to uncover novel therapeutic targets in cancer metastasis and diseases caused by mutations in nuclear envelope proteins.

ELECTRONIC SUPPLEMENTARY MATERIAL

The online version of this article (doi: 10.1007/s12195-014-0342-y) contains supplementary material, which is available to authorized users.

ACKNOWLEDGMENTS

The authors thank Philipp Isermann for providing plasmids (GFP-LifeAct, mCherry–Histone-4), advice, and some MATLAB image analysis scripts; Drs. Colin Stewart and Tom Glover for providing cells and reagents; Dr. Amy Rowat for design and fabrication of some of the perfusion devices; Dr. Sarah Jandricic for help with statistical analysis; Kathy Zhang and Ileana D'Aloisio for quantification of cell migration assays; and Rachel Gilbert for helpful discussions. This work was performed in part at the Cornell NanoScale Facility, a member of the National Nanotechnology Infrastructure Network, which is supported by the National Science Foundation (Grant ECCS-0335765). This work was supported by National Institutes of Health awards [R01 NS059348 and R01 HL082792]; the Department of Defense Breast Cancer Idea Award [BC102152]; a National Science Foundation CAREER award to Lammerding J [CBET-1254846]; and a Pilot Project Award by the Cornell Center on the Microenvironment & Metastasis through Award Number U54CA143876 from the National Cancer Institute. The content of this article is solely the responsibility of

the authors and does not necessarily represent the official views of the National Cancer Institute or the National Institutes of Health.

CONFLICTS OF INTEREST

Patricia M. Davidson, Celine Denais, Maya C. Bakshi, and Jan Lammerding declare that they have no conflicts of interest.

ETHICAL STANDARDS

No human studies were carried out by the authors for this article. No animal studies were carried out by the authors for this article.

REFERENCES

[1]Balzer, E. M., Z. Tong, C. D. Paul, W. C. Hung, K. M. Stroka, A. E. Boggs, S. S. Martin, and K. Konstantopoulos. Physical confinement alters tumor cell adhesion and migration phenotypes. *FASEB J.* 26(10):4045–4056, 2012.

[2]Booth-Gauthier, E. A., V. Du, M. Ghibaudo, A. D. Rape, K. N. Dahl, and B. Ladoux. Hutchinson–Gilford progeria syndrome alters nuclear shape and reduces cell motility in three dimensional model substrates. *Integr. Biol. (Camb.)* 5(3):569–577, 2013.

[3]Capo-chichi, C. D., K. Q. Cai, J. Smedberg, P. Ganjei-Azar, A. K. Godwin, and X. X. Xu. Loss of A-type lamin expression compromises nuclear envelope integrity in breast cancer. *Chin. J. Cancer* 30(6):415–425, 2011.

[4]Chaffer, C. L., and R. A. Weinberg. A perspective on cancer cell metastasis. *Science* 331(6024):1559–1564, 2011.

[5]Crisp, M., Q. Liu, K. Roux, J. B. Rattner, C. Shanahan, B. Burke, P. D. Stahl, and D. Hodzic. Coupling of the nucleus and cytoplasm: role of the LINC complex. *J. Cell Biol.* 172(1):41–53, 2006.

[6]Dahl, K. N., P. Scaffidi, M. F. Islam, A. G. Yodh, K. L. Wilson, and T. Misteli. Distinct structural and mechanical properties of the nuclear lamina in Hutchinson–Gilford progeria syndrome. *Proc. Natl. Acad. Sci. USA* 103(27):10271–10276, 2006.

[7]Davidson, P. M., and J. Lammerding. Broken nuclei—lamins, nuclear mechanics, and disease. *Trends Cell Biol.* 24(4):247–256, 2014.

[8]Deguchi, S., K. Maeda, T. Ohashi, and M. Sato. Flow-induced hardening of endothelial nucleus as an intracellular stress-bearing organelle. *J. Biomech.* 38(9):1751–1759, 2005.

[9]Fields, A. P., G. Tyler, A. S. Kraft, and W. S. May. Role of nuclear protein kinase C in the mitogenic response to platelet-derived growth factor. *J. Cell Sci.* 96(Pt 1):107–114, 1990.

[10]Folker, E. S., C. Ostlund, G. W. Luxton, H. J. Worman, and G. G. Gundersen. Lamin A variants that cause striated muscle disease are defective in anchoring transmembrane actin-associated nuclear lines for nuclear movement. *Proc. Natl. Acad. Sci. USA* 108(1):131–136, 2011.

[11]Friedl, P., E. Sahai, S. Weiss, and K. M. Yamada. New dimensions in cell migration. *Nat. Rev. Mol. Cell Biol.* 13(11):743–747, 2012.

[12]Friedl, P., and K. Wolf. Plasticity of cell migration: a multiscale tuning model. *J. Cell Biol.* 188(1):11–19, 2010.

[13]Friedl, P., K. Wolf, and J. Lammerding. Nuclear mechanics during cell migration. *Curr. Opin. Cell Biol.* 23(1):55–64, 2011.

[14]Fu, Y., L. K. Chin, T. Bourouina, A. Q. Liu, and A. M. VanDongen. Nuclear deformation during breast cancer cell transmigration. *Lab Chip* 12(19):3774–3778, 2012.

[15]Glynn, M. W., and T. W. Glover. Incomplete processing of mutant lamin A in Hutchinson–Gilford progeria leads to nuclear abnormalities, which are reversed by farnesyltransferase inhibition. *Hum. Mol. Genet.* 14(20):2959–2969, 2005.

[16]Gundersen, G. G., and H. J. Worman. Nuclear positioning. *Cell* 152(6):1376–1389, 2013.

[17]Hale, C. M., A. L. Shrestha, S. B. Khatau, P. J. Stewart-Hutchinson, L. Hernandez, C. L. Stewart, D. Hodzic, and D. Wirtz. Dysfunctional connections between the nucleus and the actin and microtubule networks in laminopathic models. *Biophys. J.* 95(11):5462–5475, 2008.

[18]Harada, T., J. Swift, J. Irianto, J. W. Shin, K. R. Spinler, A. Athirasala, R. Diegmiller, P. C. Dingal, I. L. Ivanovska, and D. E. Discher. Nuclear lamin stiffness is a barrier to 3D migration, but softness can limit survival. *J. Cell Biol.* 204(5):669–682, 2014.

[19]Ho, C. Y., and J. Lammerding. Lamins at a glance. *J. Cell Sci.* 125(Pt 9):2087–2093, 2012.

[20]Hung, W. C., S. H. Chen, C. D. Paul, K. M. Stroka, Y. C. Lo, J. T. Yang, and K. Konstantopoulos. Distinct signaling mechanisms regulate migration in unconfined vs. confined spaces. *J. Cell Biol.* 202(5):807–824, 2013.

[21]Isermann, P., P. M. Davidson, J. D. Sliz, and J. Lammerding. Assays to measure nuclear mechanics in interphase cells. *Curr. Protoc. Cell Biol.* Chapter 22:Unit22.16, 2012. doi:10.1002/0471143030.cb2216s56.

[22]Ivanovska, I., J. Swift, T. Harada, J. D. Pajerowski, and D. E. Discher. Physical plasticity of the nucleus and its manipulation. *Methods Cell Biol.* 98:207–220, 2010.

[23]Khatau, S. B., R. J. Bloom, S. Bajpai, D. Razafsky, S. Zang, A. Giri, P. H. Wu, J. Marchand, A. Celedon, C. M. Hale, S. X. Sun, D. Hodzic, and D. Wirtz. The distinct roles of the nucleus and nucleus-cytoskeleton connections in three-dimensional cell migration. *Sci. Rep.* 2:488, 2012.

[24]Lammerding, J., L. G. Fong, J. Y. Ji, K. Reue, C. L. Stewart, S. G. Young, and R. T. Lee. Lamins A and C but not lamin B1 regulate nuclear mechanics. *J. Biol. Chem.* 281(35):25768–25780, 2006.

[25]Lammerding, J., P. C. Schulze, T. Takahashi, S. Kozlov, T. Sullivan, R. D. Kamm, C. L. Stewart, and R. T. Lee. Lamin A/C deficiency causes defective nuclear mechanics and mechanotransduction. *J. Clin. Investig.* 113(3):370–378, 2004.

[26]Lee, J. S., C. M. Hale, P. Panorchan, S. B. Khatau, J. P. George, Y. Tseng, C. L. Stewart, D. Hodzic, and D. Wirtz. Nuclear lamin A/C deficiency induces defects in cell mechanics, polarization, and migration. *Biophys. J.* 93(7):2542–2552, 2007.

[27]Lombardi, M. L., D. E. Jaalouk, C. M. Shanahan, B. Burke, K. J. Roux, and J. Lammerding. The interaction between nesprins and sun proteins at the nuclear envelope is critical for force transmission between the nucleus and cytoskeleton. *J. Biol. Chem.* 286(30):26743–26753, 2011.

[28]Luxton, G. W., E. R. Gomes, E. S. Folker, E. Vintinner, and G. G. Gundersen. Linear arrays of nuclear envelope proteins harness retrograde actin flow for nuclear movement. *Science* 329(5994):956–959, 2010.

[29]Olins, A. L., T. V. Hoang, M. Zwerger, H. Herrmann, H. Zentgraf, A. A. Noegel, I. Karakesisoglou, D. Hodzic, and D. E. Olins. The LINC-less granulocyte nucleus. *Eur. J. Cell Biol.* 88(4):203–214, 2009.

[30]Pajerowski, J. D., K. N. Dahl, F. L. Zhong, P. J. Sammak, and D. E. Discher. Physical plasticity of the nucleus in stem cell differentiation. *Proc. Natl. Acad. Sci. USA* 104(40):15619–15624, 2007.

[31]Petrie, R. J., and K. M. Yamada. At the leading edge of three-dimensional cell migration. *J. Cell Sci.* 125(Pt 24):5917–5926, 2012.

[32]Rosenbluth, M. J., W. A. Lam, and D. A. Fletcher. Analyzing cell mechanics in hematologic diseases with microfluidic biophysical flow cytometry. *Lab Chip* 8(7):1062–1070, 2008.

[33]Rowat, A. C., D. E. Jaalouk, M. Zwerger, W. L. Ung, I. A. Eydelnant, D. E. Olins, A. L. Olins, H. Herrmann, D. A. Weitz, and J. Lammerding. Nuclear envelope composition determines the ability of neutrophil-type cells to passage through micron-scale constrictions. *J. Biol. Chem.* 288(12):8610–8618, 2013.

[34]Shao, J. Y., and J. Xu. A modified micropipette aspiration technique and its application to tether formation from human neutrophils. *J. Biomech. Eng.* 124(4):388–396, 2002.

[35]Shin, J. W., K. R. Spinler, J. Swift, J. A. Chasis, N. Mohandas, and D. E. Discher. Lamins regulate cell trafficking and lineage maturation of adult human hematopoietic cells. *Proc. Natl. Acad. Sci. USA* 110(47):18892–18897, 2013.

[36]Stoitzner, P., K. Pfaller, H. Stossel, and N. Romani. A close-up view of migrating Langerhans cells in the skin. *J. Investig. Dermatol.* 118(1):117–125, 2002.

[37]Sullivan, T., D. Escalante-Alcalde, H. Bhatt, M. Anver, N. Bhat, K. Nagashima, C. L. Stewart, and B. Burke. Loss of A-type lamin expression compromises nuclear envelope integrity leading to muscular dystrophy. *J. Cell Biol.* 147(5):913–920, 1999.

[38]Swift, J., I. L. Ivanovska, A. Buxboim, T. Harada, P. C. Dingal, J. Pinter, J. D. Pajerowski, K. R. Spinler, J. W. Shin, M. Tewari, F. Rehfeldt, D. W. Speicher, and D. E. Discher. Nuclear lamin-A scales with tissue stiffness and enhances matrix-directed differentiation. *Science* 341(6149):1240104, 2013.

[39]Tong, Z., E. M. Balzer, M. R. Dallas, W. C. Hung, K. J. Stebe, and K. Konstantopoulos. Chemotaxis of cell populations through confined spaces at single-cell resolution. *PLoS ONE* 7(1):e29211, 2012.

[40]Verstraeten, V. L., J. Y. Ji, K. S. Cummings, R. T. Lee, and J. Lammerding. Increased mechanosensitivity and nuclear stiffness in Hutchinson–Gilford progeria cells: effects of farnesyltransferase inhibitors. *Aging Cell* 7(3):383–393, 2008.

[41]Verstraeten, V. L., L. A. Peckham, M. Olive, B. C. Capell, F. S. Collins, E. G. Nabel, S. G. Young, L. G. Fong, and J. Lammerding. Protein farnesylation inhibitors cause donut-shaped cell nuclei attributable to a centrosome separation defect. *Proc. Natl. Acad. Sci. USA* 108(12):4997–5002, 2011.

[42]Wazir, U., M. H. Ahmed, J. M. Bridger, A. Harvey, W. G. Jiang, A. K. Sharma, and K. Mokbel. The clinicopathological significance of lamin A/C, lamin B1 and lamin B receptor mRNA expression in human breast cancer. *Cell. Mol. Biol. Lett.* 18(4):595–611, 2013.

[43]Weigelin, B., G.-J. Bakker, and P. Friedl. Intravital third harmonic generation microscopy of collective melanoma cell invasion. Principles of interface guidance and microvesicle dynamics. *IntraVital* 1(1):32–43, 2012.

[44]Wolf, K., M. Te Lindert, M. Krause, S. Alexander, J. Te Riet, A. L. Willis, R. M. Hoffman, C. G. Figdor, S. J. Weiss, and P. Friedl. Physical limits of cell migration: control by ECM space and nuclear deformation and tuning by proteolysis and traction force. *J. Cell Biol.* 201(7):1069–1084, 2013.

Nuclear Mechanics in Cancer

Celine Denais and Jan Lammerding

Abstract Despite decades of research, cancer metastasis remains an incompletely understood process that is as complex as it is devastating. In recent years, there has been an increasing push to investigate the biomechanical aspects of tumorigenesis, complementing the research on genetic and biochemical changes. In contrast to the high genetic variability encountered in cancer cells, almost all metastatic cells are subject to the same physical constraints as they leave the primary tumor, invade surrounding tissues, transit through the circulatory system, and finally infiltrate new tissues. Advances in live cell imaging and other biophysical techniques, including measurements of subcellular mechanics, have yielded stunning new insights into the physics of cancer cells. While much of this research has been focused on the mechanics of the cytoskeleton and the cellular microenvironment, it is now emerging that the mechanical properties of the cell nucleus and its connection to the cytoskeleton may play a major role in cancer metastasis, as deformation of the large and stiff nucleus presents a substantial obstacle during the passage through the dense interstitial space and narrow capillaries. Here, we present an overview of the molecular components that govern the mechanical properties of the nucleus, and we

C. Denais
Department of Biomedical Engineering, Weill Institute for Cell and Molecular Biology, Cornell University, Ithaca, NY 14853, USA
e-mail: cmd326@cornell.edu

J. Lammerding (✉)
Department of Biomedical Engineering, Weill Institute for Cell and Molecular Biology, Cornell University, Ithaca, NY 14853, USA

Department of Biomedical Engineering, Weill Institute for Cell and Molecular Biology, Cornell University, Weill Hall, Room 235, Ithaca, NY 14853, USA
e-mail: jan.lammerding@cornell.edu

E.C. Schirmer and J.I. de las Heras (eds.), *Cancer Biology and the Nuclear Envelope*, Advances in Experimental Medicine and Biology 773, DOI 10.1007/978-1-4899-8032-8_20,
© Springer Science+Business Media New York 2014

discuss how changes in nuclear structure and composition observed in many cancers can modulate nuclear mechanics and promote metastatic processes. Improved insights into this interplay between nuclear mechanics and metastatic progression may have powerful implications in cancer diagnostics and therapy and may reveal novel therapeutic targets for pharmacological inhibition of cancer cell invasion.

Keywords Cytoskeleton • LINC complex • Mechanotransduction • Mechanical stability • Nuclear lamina

Abbreviations

ER	Endoplasmic reticulum
KASH	Klarsicht, ANC-1, Syne Homology
LAPs	Lamina-associated polypeptides
LBR	Lamin B receptor
LINC	*L*inker of *N*ucleoskeleton and *C*ytoskeleton
NPC	Nuclear pore complex

Introduction

The cell nucleus was the first organelle discovered in the seventeenth century. In the oldest preserved depictions of the nucleus, Antonie van Leeuwenhoek described a central "clear area" in salmon blood cells that is now commonly acknowledged as the nucleus [1]. A more detailed description of the nucleus was subsequently provided by the botanist Robert Brown, who first articulated the concept of the nucleated cell as a structural unit in plants [1]. Today, the nucleus is recognized as the site of numerous essential functions in eukaryotes, including storage and organization of the genetic material, DNA synthesis, DNA transcription, transcriptional regulation, and RNA processing. In cancer biology, much of the research has traditionally been focused on this "DNA-centric view," starting with the identification of oncogenes and tumor-suppressor genes to the establishment of the multiple "hits" (i.e., mutations) concept now commonly accepted as a requirement for cancer initiation and progression [2]. Recently, however, it has become apparent that in addition to these genetic components, it is necessary to take the physical, i.e., biomechanical, factors of tumor cells and their microenvironment into consideration. Research conducted within the last 10 years has revealed that cancer cells have reduced stiffness [3–7], generate increased contractile forces [8], and are strongly influenced by their biomechanical environment [9, 10]. Furthermore, not only can cancer cells be mechanically distinguished from non-tumorigenic cells, but physical measurements also allow telling apart highly invasive cells from less invasive cells, for example, by their increased cell deformability [4] and increased traction forces [8], yielding the promise of future

diagnostic and prognostic applications. Here, we focus on a particular aspect of cellular mechanics that has traditionally received less attention in cancer cell biology: the role of nuclear structure and mechanics in cancer progression.

Despite many advances in understanding the biology of cancer and its associated molecular changes, the most common and reliable diagnosis of cancer cells in tissue biopsies by pathologists still relies on the presence of morphological changes in nuclear structure, i.e., increased size, irregular shape and organization [11]. Nonetheless, the functional consequences of these characteristic changes have yet to be determined; thus, it remains unclear whether the observed morphological changes merely correlate with other, more difficult to observe cellular defects, or whether they can directly contribute to the disease progression.

In recent years, a growing number of studies have reported altered nuclear envelope composition in various cancers [12, 13]. The structure and composition of the nucleus, particularly the nuclear envelope, play an important role in cellular mechanics and function, ranging from determining nuclear deformability and fragility [14–17] to participating in mechanotransduction signaling, i.e., the sensing of biomechanical factors and the corresponding signaling response [15, 18]. One potential mechanism by which changes in nuclear envelope composition could contribute to cancer progression is that softer and more lobulated nuclei facilitate cancer cell invasion through dense tissues, where cells often have to pass through constrictions smaller than the nuclear diameter [19, 20]. Furthermore, the physical coupling between the nucleus and the cytoskeleton is critical for cytoskeletal organization and cell polarization [21–24], which could further affect cancer cell migration. In the following sections, we provide a brief review of normal nuclear structure and mechanics, highlight changes that occur during oncogenic transformation, and discuss recent findings suggesting an important role of nuclear mechanics and nucleocytoskeletal coupling in cancer progression.

Normal Nuclear Compartmentalization and Structure

The nucleus is a highly compartmentalized organelle that can be roughly subdivided into the nuclear envelope and the nuclear interior (Fig. 1), the latter representing most of the chromatin in diverse states of organization [25], the nucleolus, and diverse smaller subnuclear structures such as Cajal bodies and nuclear speckles [26–28]. In addition, the nuclear interior contains a still incompletely defined structural network (i.e., the nucleoskeleton or nuclear matrix), which may provide additional mechanical support and also act as scaffold for transcriptional complexes and other nuclear processes. The nuclear envelope forms the physical barrier between the nucleus and the cytoplasm. It consists of two phospholipid bilayers, the inner and the outer membranes, and the underlying nuclear lamina, a dense protein meshwork mostly comprising lamins. The inner and outer nuclear membranes are connected at the sites of nuclear pore complexes (NPCs) and encapsulate the perinuclear space or lumen.

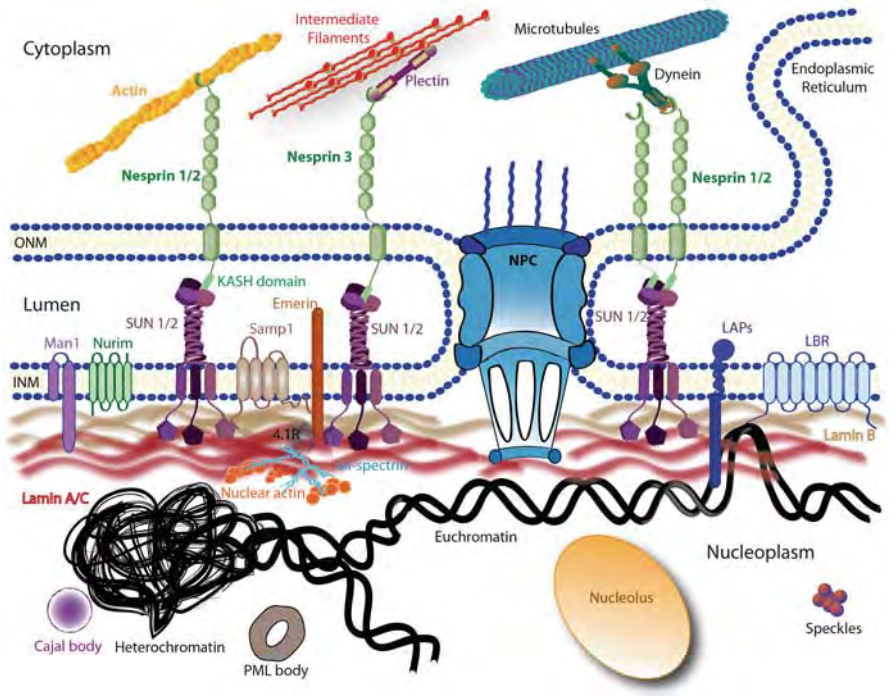

Fig. 1 Schematic overview of the nuclear structure and the LINC complex. The nuclear envelope is composed of the inner nuclear membrane (INM) and the outer nuclear membrane (ONM) punctuated by nuclear pore complexes (NPC). The ONM is continuous with the endoplasmic reticulum (ER). Several structures of the nuclear interior are depicted here, including the nucleolus, Cajal bodies, promyelocytic leukemia bodies (PML), and speckles. Chromatin is shown in its two states, very condensed (heterochromatin) and loosely organized (euchromatin). Only a subset of nuclear membrane proteins are portrayed in this picture: lamin B receptor (LBR), emerin, MAN1, and nurim. The schematic also illustrates some of the interactions between these proteins with the lamina meshwork (lamins B and A/C). The LINC complex is represented by nesprins, Sad1p/UNC-84 (SUN) proteins and Samp1. On the outer membrane, nesprin-1 and -2 can directly bind to actin filaments or indirectly interact with microtubules through motors proteins (dyneins or kinesin). Nesprin-3 is shown interacting with intermediate filaments via plectin

The Outer Nuclear Membrane

The outer nuclear membrane is continuous with the endoplasmic reticulum (ER); like the ER, its surface is scattered with ribosomes. The outer nuclear membrane exhibits a high degree of similarity to the ER membrane in terms of protein, enzyme, and lipid composition [29]. Nonetheless, recent studies have suggested that the outer nuclear membrane displays a certain degree of specialization [30] and participates in protein synthesis and processing [31]. The specialized protein composition of the outer nuclear membrane likely results from retention of specific proteins by

direct interaction with inner nuclear membrane proteins across the lumen, thereby enriching them compared to the ER fraction [32, 33]. In mammals, one particularly important family of outer nuclear membrane proteins is the nesprins [34], which play a central role in connecting the nucleus to the cytoskeleton [35–39].

The Nuclear Lumen and Nuclear Pore Complexes

The nuclear lumen, also commonly termed the perinuclear space, is a 30–50 nm wide aqueous space separating the inner from the outer nuclear membrane that is continuous with the ER lumen [40]. It accommodates the luminal domains of integral nuclear membrane proteins [41]. The inner and outer nuclear membranes come together at sites of NPC insertion [42]. NPCs act as the main gateway for molecules between the cytoplasm and the nuclear interior (and also proteins of the inner nuclear membrane). Small molecules can diffuse freely through the NPC, while the exchange of macromolecules larger than ~40 kDa is mediated by a tightly controlled import and export mechanism requiring nuclear import and export signals and interaction with specific transport molecules [43–45].

The Inner Nuclear Membrane

The inner nuclear membrane contains at least 70–100 unique membrane-associated and integral membrane proteins that are retained at the inner nuclear membrane through interaction with nucleoplasmic proteins (e.g., lamins) and chromatin [13]. Most of these proteins have only been identified in recent proteomic studies [46–50], and the function of several of the nuclear envelope transmembrane proteins remains unclear. Some well-characterized inner nuclear membrane proteins include lamin B receptor (LBR), lamina-associated polypeptides (LAPs) [30], emerin, MAN1, nurim, nesprins, and Sad1p/UNC-84 (SUN) proteins [13]. Mislocalization or loss of these proteins due to mutations in nuclear envelope proteins causes a spectrum of diseases collectively known as laminopathies that include certain types of muscular dystrophies (e.g., Emery–Dreifuss muscular dystrophy and limb-girdle muscular dystrophy), dilated cardiomyopathy, and the premature aging disease Hutchinson–Gilford progeria syndrome [51].

The Nuclear Lamina

The lamina corresponds to a dense meshwork of proteins mainly composed of lamins underlying the inner nuclear membrane [52]. Lamins are type V intermediate filaments [53, 54] and display the characteristic tripartite molecular organization of

all intermediate filaments, which consists of a central a-helical rod domain flanked by a short non-helical N-terminal "head" and a C-terminal "tail" domain that includes an Ig-like fold [55].

In vertebrates, lamins are classified into two major classes, A- and B-type lamins, depending on their sequence, expression pattern, and biochemical properties [56, 57]. A-type lamins, including lamins A, C, AΔ10, and C2, result from alternative splicing of the *LMNA* gene on chromosome 1. These proteins are expressed in a tissue-specific manner later in differentiation [58, 59], have neutral isoelectric points, and are dispersed upon phosphorylation of lamins during mitosis [60]. Lamin A and C can be distinguished by their unique C-terminal tail and processing: the C-terminus of prelamin A contains a CaaX motif, which is subject to a series of posttranslational modifications, including isoprenylation and proteolytic cleavage, to give rise to mature lamin A [61, 62]. In contrast, the shorter lamin C has a unique C-terminus that lacks the CaaX motif and does not require posttranslational processing. In addition to their localization at the nuclear lamina, A-type lamins are also present in the nuclear interior, where they form stable structures [63].

Unlike A-type lamins, B-type lamins are encoded by two separate genes: *LMNB1* for lamin B1 [64, 65] and *LMNB2* for lamin B2 and B3 [66, 67]. Only lamins B1 and B2 are found in somatic cells; expression of lamin B3 is restricted to germ cells. Unlike A-type lamins, at least one B-type lamin is expressed in all cells, including embryonic stem cells; B-type lamins are acidic and remain associated with membranes during mitosis [68]. The C-terminus of B-type lamins is also isoprenylated but, unlike prelamin A, does not undergo proteolytic cleavage. Consequently, B-type lamins remain permanently farnesylated, facilitating their attachment to the inner nuclear membrane.

The Nuclear Interior

In addition to DNA and histones, the nucleoplasm contains distinct structural and functional elements such as nucleoli [69], Cajal bodies [70], the Gemini of coiled bodies or gems [71], promyelocytic leukemia (PML) bodies [72], and splicing speckles [73]. The growing interest to decipher the detailed structure and composition of the nuclear interior has led to the recent discoveries that the nuclear interior contains actin [74, 75], myosin [76, 77], spectrin [78], and even titin [79]. It is now well established that actin oligomers or short polymers are present in the nucleus [80–82] and that all isoforms of actin contain nuclear export sequences [83], which may help prevent spontaneous assembly of actin filaments inside the nucleus. To date, many aspects of nuclear actin remain incompletely understood, including its precise structural organization [84]. Nonetheless, nuclear actin has been implicated in a number of functions highly relevant to tumorigenesis, including DNA organization, stabilization, and orientation during replication, determination of nuclear morphology, organization of gene regulatory complexes, and RNA synthesis [85]. The existence and function of the "nuclear matrix" or nucleoskeleton, typically defined as the insoluble

structure remaining after nuclease, detergent, and high salt treatment of isolated nuclei [86], remains a matter of lively debate, but given the plethora of structural proteins present in the nucleus and their often low diffusional mobility, it is likely that some (possibly local) structural frameworks exist in the nuclear interior.

Nuclear Mechanics and Mechanotransduction

In recent years, it has emerged that physical factors, such as the biomechanical properties of the microenvironment and the mechanical forces acting between cells and their environment, play an important role in cellular function [87]. With regard to cancer cells, modulation of cytoskeletal tension by Rho inhibition alone can be sufficient to phenotypically revert epithelial morphogenesis of malignant cells [10]. Rho proteins belong to the family of small signaling G-proteins (GTPases) that can act as "molecular switches" in regulating actin cytoskeleton dynamics, while also playing important roles in cell polarity, migration vesicle trafficking, mitosis, proliferation and apoptosis [88]. Furthermore, recent studies found that aggressive cancer cells can be distinguished from less invasive and non-tumorigenic cancer cells based on their cytoskeletal stiffness [3] and their contractile force generation [8]. What is now becoming apparent is that in addition to cytoskeletal stiffness and force generation, nuclear deformability, as well as the physical coupling between the nucleus and the cytoskeleton, play a critical role in cell motility in three-dimensional (3D) environments [19, 20]. In this section, we discuss the molecular players governing normal nuclear mechanics, i.e., nuclear deformability and nucleo-cytoskeletal coupling, as well as their potential contribution to cellular mechanosensing. Their involvement in cancer progression is then described in the subsequent section.

Nuclear Deformability and Stability

Over the years, a variety of experimental techniques have been developed to probe the mechanical properties of the nucleus, particularly its deformability under applied forces. These approaches include micropipette aspiration [89–93], atomic force microscopy [91, 94–96], cell stretching [14, 97–99], tracking of particles within the nucleoplasm [100], and, most recently, optical stretching [101] and measuring transit times through microfluidic constriction channels [102, 103]. These experiments have revealed that the nucleus exhibits both elastic (the nuclear lamina) and viscoelastic (the nuclear interior) behavior and is typically ~2–10 times stiffer than the surrounding cytoplasm [93, 99, 104, 105]. The precise measurements for the apparent Young's modulus, a measure of material elasticity, range from ~0.1 to 10 kPa, depending on the experimental conditions and technique. This broad range of stiffness measures likely reflects a large degree of cell-to-cell variability, as well as different domains and mechanical behavior probed by the diverse experimental

methods. For example, tracking of small particles within the nucleoplasm is sensitive to entanglement of the tracked particle within the nucleoskeleton/chromatin; in addition, the resulting measurements exclude contributions to nuclear stiffness from the nuclear envelope [90, 91]. In contrast, cell stretch experiments and other techniques that result in large nuclear deformations will yield "bulk" measurements that combine contributions from the nuclear interior and the nuclear envelope, but may also depend on the mechanical properties of the cytoskeleton and its connection to the nucleus [17].

Micropipette aspiration experiments [90–92] and computational modeling [105] indicate that the mechanical deformability of the nucleus is mainly governed by the nuclear lamina and the nuclear interior; the relative contribution of each component depends on diverse factors such as mechanical load (e.g., applied tension vs. compression), the specific cell type, differentiation state, and chromatin configuration. The contribution of the inner and outer nuclear membranes to the deformability of the nucleus is largely negligible [106], as lipid membranes exhibiting relatively low bending stiffness and a two-dimensional (2D) liquid-like behavior, i.e., they can flow in response to applied shear stress, with connections to a large membrane reservoir in the form of the ER [16, 106].

The importance of the nuclear lamina in providing structural support to the nucleus and controlling nuclear size is now well established [12, 17], with the nuclear lamina acting as a load-bearing, elastic shell surrounding a viscoelastic nuclear interior [90, 91, 107]. Experiments on cells from gene-modified mice lacking specific lamin isoforms [98] and *Xenopus* oocytes ectopically expressing human lamins [95] suggest that lamins A and C are the main contributors to nuclear stiffness, with loss of lamin A or C resulting in softer, more deformable nuclei, while increased expression of lamin A results in stiffer, less deformable nuclei. Given the structural similarities between A-type and B-type lamins, it may be somewhat surprising that these proteins have distinct roles in affecting nuclear deformability. However, recent findings suggest that A- and B-type lamins—and even lamins A and C—may form distinct but overlapping networks [108, 109], and that A-type lamins may form a thicker protein network at the nuclear envelope [110]; however, as imaging the nuclear lamina in intact somatic cells with sufficiently high resolution remains technically extremely challenging, the exact structure and organization of the lamina and the different lamin isoforms at the nuclear envelope remains unclear. Interaction of specific lamin isoforms with other nuclear (envelope) proteins may serve as additional explanation for the distinct roles of the diverse lamins in nuclear mechanics. For example, loss of the inner nuclear membrane protein emerin, which directly interacts with lamins A/C, results in more deformable nuclei, although to a lesser degree than functional loss of lamins A/C [92, 97]. In addition, functional loss of lamins due to mutations or (partial) deletion can also affects chromatin organization [111–114], which could affect nuclear deformability.

Further illustrating the importance of A-type lamins in nuclear mechanics, lamin A/C-deficient cells have more deformable nuclei that are more susceptible to rupture under mechanical stress [14, 115]. Of note, mutations in A-type lamins, as well as emerin, cause a spectrum of human diseases (laminopathies) that include

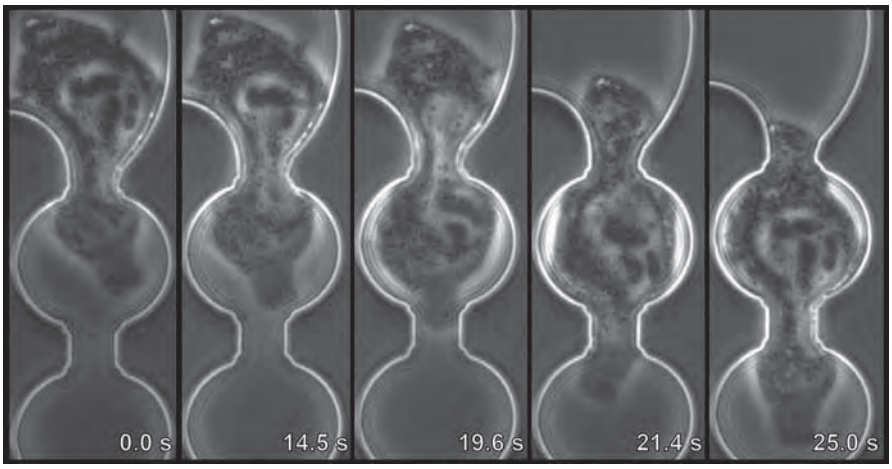

Fig. 2 Invasive cancer cell MDA-MB-231 squeezing into an 8 μm width constriction. Image sequences of a cancer cell being perfused through an 8 μm-wide constriction at a pressure difference (ΔP) of 10 psi. The viscoelastic deformation as the nucleus flows through the constriction is clearly visible

Emery–Dreifuss muscular dystrophy, limb-girdle muscular dystrophy, dilated cardiomyopathy, Dunnigan-type familial partial lipodystrophy, and Hutchinson–Gilford Progeria syndrome [51]. In many cases, cells from affected patients show characteristic features such as misshapen nuclei, increased nuclear fragility, and herniations [16]; furthermore, *LMNA* mutations resulting in disease affecting cardiac and skeletal muscle often cause defects in nuclear mechanics [116], providing a potential disease mechanism for the muscular laminopathies.

Importantly, lamins also interact with other inner nuclear membrane proteins (e.g., emerin, LAPs, and LBR), nuclear pore components, DNA, chromatin, and transcription factors (e.g., retinoblastoma protein [Rb], SREBPs, GCL, and MOK2), and structural proteins such as nuclear actin and titin [117]. These interactions could further modulate nuclear stiffness by forming nucleoskeletal structures or affecting chromatin organization and transcriptional regulation. For example, nuclear abnormalities have been observed in cells depleted of large repeat-domain proteins such as titin and αII-spectrin [118, 119]. On the other hand, the role of nuclear actin in providing structural support to the nucleus remains unclear [84]. Through their interaction with SUN proteins, nesprins, and Samp1, lamins also play an important role in connecting the nucleus to the surrounding cytoskeleton [120], as discussed in more detail below.

Besides the nuclear lamina, chromatin is an important contributor to nuclear stiffness. Unlike the mostly elastic nuclear lamina, chromatin exhibits more viscoelastic material behavior, i.e., it flows when subjected to forces (Fig. 2) and undergoes plastic deformations [106, 107]. Chromatin decondensation during initial lineage commitment of embryonic stem cells is associated with a significant softening of the nucleus [101]. Subsequently, the viscoelastic deformability of the cell nucleus in human embryonic stem cells changes during further cellular

differentiation [107], becoming 6 times stiffer and also less fluid-like during terminal differentiation. It remains unclear, however, to what extent this behavior is caused by changes in chromatin organization, e.g., switching from loose euchromatin to more compacted heterochromatin, or results from the increased expression of A-type lamins in differentiated cells.

Nucleo-cytoskeletal Coupling

Over the last 10 years, it has become well established that the nucleus is physically coupled to the surrounding cytoskeleton [120]. Many of the molecular components are highly preserved throughout evolution, being present in unicellular organisms such as yeast all the way to mice and humans [121]. Building on work in yeast and drosophila, several of the molecular details of nucleo-cytoskeletal coupling were first unraveled in *Caenorhabditis elegans*, where UNC84 and ANC-1, in conjunction with Ce-lamin, participate in the actin-dependent anchorage and positioning of the nucleus [32, 122–125]. Subsequent studies have confirmed that closely related proteins are also responsible for nucleo-cytoskeletal coupling in mammalian cells; this physical connection is now commonly referred to as the *Li*nker of *N*ucleoskeleton and *C*ytoskeleton (LINC) complex [126]. In the strictest definition, the LINC complex contains two essential parts: (1) a member of the trimeric inner nuclear membrane SUN- [127] domain protein family, which engages with nucleoplasmic proteins such as lamins [121, 128, 129]; (2), KASH- (Klarsicht, ANC-1, Syne Homology) domain containing nesprins located on the outer nuclear membrane that bind across the perinuclear space to the SUN domain of Sun1/Sun2 trimers [130]. The cytoplasmic ends of nesprins interact directly or indirectly with various components of the cytoskeleton, including actin, intermediate filaments (via plectin) [131], and microtubules (via microtubule-binding motors such as dynein and kinesin), thereby completing the physical connection across the nuclear envelope [121]. In many cases, lamins are considered an extended part of the LINC complex, as they bind to SUN proteins and inner membrane variants of nesprins and help tether these proteins to the nuclear interior [132]. Since the cytoskeleton also connects to focal adhesion and cell-cell junctions, cells contain a continuous mechanical network linking the nuclear interior and the extracellular matrix and neighboring cells, thereby allowing forces exerted from the cellular environment or the cytoskeleton to be transmitted directly to the nuclear interior [39, 120, 133, 134].

SUN Domain Proteins

The characteristic feature of SUN domain family proteins is a 115–175 amino acid domain that shares homology with the Sad1 protein from *Schizosaccharomyces pombe* [135] and the UNC84 protein from *C. elegans* [122]. Mammalian cells have five SUN domain proteins, with two of these proteins (SUN1 and SUN2) present on

the nuclear envelope in somatic cells (SUN3-5 are testis specific) [136]. SUN1 and SUN2 proteins consist of a helical N-terminal domain that can bind to lamins [137] and nuclear pore complex proteins [138, 139], a single pass transmembrane domain to anchor the protein in the inner nuclear membrane [140], a luminal helical domain required for trimerization of SUN proteins [130], and the C-terminal SUN domain, which interacts with the KASH domain of nesprins [126].

Nesprins and Other KASH Domain Proteins

Mammals have four nesprins (genes *SYNE 1–4*), with nesprins 1–3 having multiple isoforms resulting from alternative splicing, initiation, and termination [34, 120, 121]. Expression of various nesprin isoforms can be highly tissue-specific [34]. In skeletal muscle, levels of nesprin-1 (first described as Syne-1 for synaptic nuclear envelope protein-1) are highest in synaptic nuclei, suggesting that it might participate in the migration and anchoring of these specialized muscle nuclei [141]. Common to all nesprins is a central region containing multiple spectrin domains, whose number can greatly vary between isoforms [142]; all nesprins (but not all isoforms) contain a ~60 amino acid-long C-terminal KASH domain, consisting of a transmembrane domain and a short, highly conserved luminal domain, which is essential for anchoring nesprins to the nuclear envelop [59, 142]. The N-terminal domain of nesprins typically contains specific motifs to interact with different cytoskeletal proteins. For instance, the nesprin-1 and -2 "giant" isoforms (1,000 and 800 kDa in size, respectively) contain an actin-binding domain (ABD) composed of two calponin homology domains [35, 37, 143]; additionally, nesprins-1 and -2 can interact with the microtubule-associated motors dynein/dynactin and kinesin [120]. Nesprin-3 can connect to intermediate filaments via plectin [36]. Nesprin-4 binds the microtubule-associated motor kinesin, and ectopic expression of nesprin-4 induces dramatic changes in centrosome positioning in cells [144]. While localization of larger nesprin isoforms is restricted to the outer nuclear membrane, shorter isoforms can also be present at the inner nuclear membrane, where they can interact with lamins and emerin [38, 145–147]. Nesprin isoforms lacking the KASH domain may also be found in other cellular structures. In addition to nesprins 1–4, mammals express at least one additional KASH-domain protein, aptly named KASH5, which is found exclusively in spermatocytes and oocytes, where it plays a critical role in meiosis [148].

Other Molecules Involved in Nucleo-cytoskeletal Coupling

With the growing interest in understanding the mechanics of the nucleus and its connection to the cytoskeleton, several recent studies have focused on identifying additional molecular players involved in nucleo-cytoskeletal coupling. Based on experimental findings in emerin-deficient cells, one study has proposed that emerin binds to microtubules and that a subset of emerin located on the outer nuclear membrane is involved in coupling the centrosome to the nuclear envelope [149], but it

remains unclear whether the emerin-microtubule interaction is direct or mediated through other proteins such as nesprins.

A more recent candidate to be involved in nucleo-cytoskeletal coupling is the inner nuclear membrane protein Samp1 [150], which associates with lamin A/C, emerin, Sun1, and Sun2 [150–152]. During mitosis, Samp1 is associated with the mitotic spindle [150]; during interphase, however, Samp1 is an important component of transmembrane actin-associated nuclear (TAN) lines [152], which promote rearward nuclear movement in polarizing fibroblasts by connecting the nucleus to retrograde actin flow via nesprin-2giant and SUN2 [153]. The involvement of lamins A/C in nucleo-cytoskeletal coupling is further illustrated by the finding that lamin mutants associated with muscular dystrophies can disrupt this retrograde nuclear movement [132] and that lamin A/C is required for retaining Samp1 at the nuclear envelope [152]. Another potential mediator of nucleo-cytoskeletal coupling is the luminal protein torsinA, part of the AAA + ATPase superfamily. TorsinA interacts with the KASH domains of nesprins 1–3, and loss of torsinA results in mislocalization of nesprin-3 from the nuclear envelope and impaired cell polarization and migration [131]. Given the promiscuous interaction of SUN domain proteins and nesprins [154], it is likely that tissue-specific expression of their isoforms, as well as potential interaction with other nuclear envelope proteins such as Samp1, play an important role in the spatial and temporal control of nucleo-cytoskeletal coupling.

Nucleo-cytoskeletal Coupling Is Critical for Many Cell Functions

Studies investigating molecules involved in connecting chromatin and cytoskeletal structures have often focused on processes during mitosis and meiosis. For instance, analysis of chromosome condensation during yeast prophase has unraveled a direct interaction between Sad1 (a Sun homologue protein) and meiotic-specific bouquet (Bqt) proteins [155]. Sad1 has also been linked to Kms1 protein [156] and this interaction is known to couple telomeres to microtubules and cytoplasmic dynein [157, 158]. Similar results were obtained in *C. elegans*, where selective inactivation of Sun1 protein or Kdp-1 (KASH domain protein-1) protein delays cell cycle progression [159, 160]. In mammalian cells, lamins, SUN proteins, KASH5, and Samp1 have all been implicated in specific roles during mitosis and/or meiosis [148, 161], and loss of A-type lamins causes telomere shortening defects and overall genomic instability [162].

In recent years, research has increasingly focused on the role of LINC complex proteins in interphase cells and consequences of LINC complex disruption. In *C. elegans*, deletion of the nesprin and SUN1 orthologues ANC-1 and UNC-84 result in impaired nuclear positioning and anchoring in muscle cells [32, 122]. In mammalian cells, LINC complex disruption causes defects in nuclear positioning, cell polarization, and migration [133] by impairing force transmission between the nucleus and cytoskeleton [24, 153]. LINC complex proteins are particularly important during cell migration in 3D environments, for example, inside collagen matrices or tissues. In particular, lamins A/C, nesprin-2giant, and nesprin3 modulate

perinuclear actin organization and actin protrusions; consequently, deletion of lamins A/C or LINC complex disruption results in significantly impaired migration of cells in 3D collagen matrices [163]. The implications of impaired nucleo-cytoskeletal coupling in cancer progression are discussed in more detail below.

Nuclear Mechanics Stiffness and Nucleo-cytoskeletal Coupling in Mechanotransduction

As described above, the cytoskeleton physically connects the nucleus to the cellular microenvironment. Consequently, pulling on integrins on the surface of intact endothelial cells results not only in reorientation of cytoskeletal filaments, but also in distortion of the nucleus and spatial redistribution of subnuclear structures [134]. Similar results, including force-induced dissociation of nuclear protein complexes, have recently been obtained in HeLa cells subjected to forces applied via magnetic tweezers [164] and in human umbilical vein endothelial and osteosarcoma cells exposed to fluid shear stress [165]. It has long been speculated that such mechanically induced changes in nuclear structure and chromatin configuration could directly activate specific mechanosensitive genes, for example, by changing accessibility to transcription factors [18, 166]. This idea is further supported by studies that have found interactions between applied forces, Rho signaling, cell shape, and histone acetylation [167–169]. Nonetheless, direct evidence for such nuclear mechanosensing remains scarce, and the majority of data are rather correlative, making it difficult to discern whether mechanical forces acting on the nucleus are sufficient to directly induce changes in gene regulation, or whether the observed activation of mechanosensitive genes is the downstream result of signaling cascades originating in the cytoskeleton or the plasma membrane [15]. A recent study [24] addressing this question found that LINC complex disruption had no discernible effect on the mechanically induced expression of the mechanosensitive genes *Iex-1* and *Egr-1*, whose activation is impaired in lamin A/C-deficient cells [14, 170], even though LINC complex disruption resulted in substantially reduced nuclear deformation when the fibroblasts were subjected to substrate strain [24].

At the same time, changes in nuclear envelope composition undoubtedly affect cellular structure and function. For example, LINC complex disruption alters the mechanically induced proliferation of C2C12 myoblasts [171]; LINC complex depletion also causes impaired propagation of intracellular forces and disturbed organization of the perinuclear actin and intermediate filament networks, leading to defects in nuclear positioning and cell orientation [22, 24, 171]. In the case of impaired expression of mechanosensitive genes in lamin A/C- and emerin-deficient cells, it remains unclear whether this effect is due to direct mechanical defects or a consequence of altered interaction of lamins with specific transcriptional factors. An additional mechanism by which lamins and emerin can affect mechanotransduction signaling has recently been identified, revealing that the actin polymerization-promoting activity of emerin at the nuclear envelope can influence nuclear and

cytoskeletal actin dynamics, thereby modulating localization and activity of the mechanosensitive transcription factor MKL1 (also known as MRTF-A or MAL), whose localization is dependent on interaction with monomeric G-actin [172].

Relevance of Nuclear Mechanics and Mechanotransduction in Cancer Progression

With growing advances in the understanding of the physics of cell motility, the mechanical properties of cancer cells have become an increasing area of interest [3]. As the nucleus is typically the largest and stiffest organelle, often occupying a large fraction of the cell's volume, the properties of the nucleus can dominate the overall cellular mechanical response when cells are subjected to large deformations [17]. Several lines of evidence suggest that the ability of the nucleus to deform can impose a rate-limiting step in non-proteolytic cell migration in 3D environments, when cells attempt to squeeze through narrow constrictions imposed by extracellular matrix fibers and other cells (Fig. 3) [19, 20]. In this section, we summarize changes in nuclear structure and morphology observed in various cancers and describe the role of nuclear deformability in cell motility. In addition, we discuss the intricate feedback between the mechanics of the cellular microenvironment and intracellular organization and function.

Altered Nuclear Structure and Morphology in Cancer Cells

With few exceptions, the nuclei of normal cells have an ellipsoid shape with smooth outlines; in contrast, many cancer cells are easily identifiable by increased nuclear size, irregular nuclear contours, and disturbed chromatin distribution, making nuclear morphology one of the oldest and most commonly used cancer markers [11]. The irregular nuclear outline in cancer cells is mainly the result of grooving, convolutions and invaginations of the nuclear envelope [173]. While the characteristic changes in nuclear morphology in cancer cells are well documented, their cause and consequence remain unclear. Interestingly, the irregular nuclear morphology of cancer cells often bears striking resemblance to the abnormal nuclear shapes observed in cells lacking or expressing mutant nuclear envelope proteins such as lamins A/C, lamin B1/B2, or LBR [174, 175], suggesting a possible involvement of dysregulated nuclear envelope proteins [173, 176].

This idea is supported by a growing number of publications that report altered expression of lamins in a variety of human tumors, often associated with particularly malignant phenotypes (Table 1). Interestingly, while some cancers frequently show downregulation of lamin A/C [177–179], other cancers have upregulated levels of lamins A/C [177, 180, 181], and for some cancers, such as colon cancer, both increased [182] and decreased [183] levels of lamin A/C have been reported.

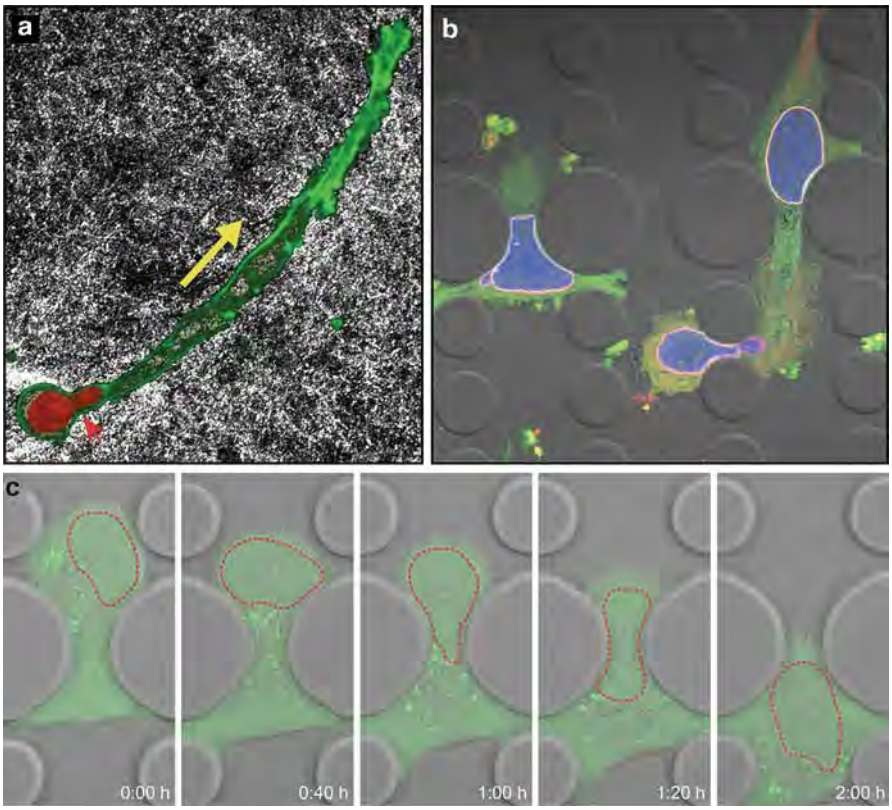

Fig. 3 Migration of cancer cell in a constrained environment. (**a**) Fibrosarcoma cell (HT1080 cell line) migrating through a dense collagen fiber matrix. The rat tail collagen matrix was imaged by reflection microscopy; the nucleus is visible in *red* (DAPI), F-actin in *green* (phalloidin). The cell body has already advanced in the direction of migration (*yellow arrow*), while the nucleus is still in the process of squeezing through constrictions in the collagen matrix (*red arrow head*). Image courtesy of Katarina Wolf, University of Nijmegen. (**b**) Fibrosarcoma cells (HT1080) migrating through 2 μm × 5 μm and 5 μm × 5 μm constrictions in a microfluidic channel. The cytoplasm is visible in *green*, the nucleus in *blue*, and the nuclear lamina (lamin B2) in *red*. (**c**) Time-lapse series of MDA-MB-231 breast cancer cell expressing a green fluorescent protein migrating through a 5 μm-wide constriction in a microfluidic channel. The nucleus is outlined in *red* (*dashed line*)

Furthermore, even within single tumors and individual cancer cell lines [184], highly heterogeneous expression levels of lamin A/C can be found [185]. Similarly, both high and low levels of lamins A/C have been considered poor prognostic markers for cancer patients, depending on the specific study and cancer subtype. For example, reduced lamin A/C expression is a sign of poor prognosis for patients with gastric carcinoma [186], and patients with stage II and III colon cancer have a significantly increased risk of cancer recurrence when their tumors are marked by loss of lamin A/C expression [183]. At the same time, another study found that patients with increased expression of lamins A/C in colorectal cancer tumors were almost

Table 1 Altered expression (and mutations) of nuclear envelope proteins in cancers

Protein	Cancer/tumor type	Reported change	Prognostic value	References
Emerin	Ovarian cancer	Loss of emerin		[222]
Lamins A/C	Lung cancer	Absence or very reduced expression in small cell lung carcinoma		[177]
	Colonic and gastric adenocarcinomas Other cancers: esophagus cancer, cervical and uterine cancer, breast cancer	Reduced levels and mislocalization (aberrant cytoplasmic immunolabelling)		[178]
	Basal cell skin carcinoma	Low levels or absence of lamin A	Increased proliferation	[179]
	Basal cell skin carcinoma	Low levels of lamin C	Low proliferation	[179]
	Skin cancer	High levels of lamin A and C in the basal cell layer of the epidermis overlying basal cell carcinomas, squamous cell carcinomas, and actinic keratosis (AK)	Proliferative capacity	[180]
	Leukemia and lymphomas	Loss of gene expression by epigenetic silencing in nodal diffuse large B-cell lymphomas and acute lymphoblastic leukemias.	Poor outcome/overall survival	[223]
	Colorectal cancer	Increased expression (mainly lamin A)	Promote tumor invasiveness Poor prognosis (risk indicator of tumor related mortality)	[187]
	Ovarian serous cancer	High levels in all stages of ovarian serous carcinomas; increased immunoreactivity in the higher stage of tumor	Correlates with advanced stage	[224]
	Primary gastric carcinoma	Low levels	Poor histological differentiation; poor prognosis	[186]
	Prostate cancer	Low expression in lower grade; increased levels in higher grade	Correlates with advanced stage	[225]
	Colon cancer	Low expression in stage II and III patients	Correlates with increased relapse	[183]
	Ovarian cancer	Heterogeneous lamin A/C protein expression pattern or absence of lamin A/C and aneuploidy		[185]
	Breast cancer	Mutated		[190]

Lamins A/C	Breast cancer	Loss of lamins A/C	Higher lamin A/C expression was associated with better clinical outcomes and with better overall and disease-free survival	[243, 244]
Lamin B	Colon cancer	Reduced expression		[178]
	Colorectal carcinoma	Increased levels		[226]
	Ovarian cancer	Increased levels of lamin B1 and B2 in malignant cell compared to benign		[227]
	Hepatocellular carcinoma	Increased levels of Lamin B1 in cirrhotic tissue		[228]
	Liver cancer	Increased levels of lamin B1 in every stage (cirrhosis, early stage, late stage); presence of soluble lamin B1 in the circulation	Potential biomarker Correlate with the tumor development	[229]
	Prostate cancer	Increased levels of lamin B	Correlate with the tumor development	[230]
	Pancreatic cancer	Increased levels of lamin B1	Correlate with decreased levels of tumor differentiation, high metastatic potential and, poor overall survival	[231]
Lamin B1	Breast cancer	Reduced mRNA levels of lamin B1	Expression of LMNB1 declined with worsening clinical outcome	[244]
LAP2	Malignant lymphocytes	Increased levels	LAP2β correlates with highly proliferative malignant cells	[232]
Nesprins	Ovarian cancer	Nesprin 1 polymorphism Downregulation of a transcript (shorter isoform)	Associated with invasive ovarian cancer risk	[191]
	Colorectal cancer	Nesprin 1 is a candidate cancer gene (mutated in cancer)		[189]
	Breast cancer	Nesprin 1 (mutations)		[190]
	Breast cancer	Nesprin 2 (mutations)		[189, 190]

(continued)

Table 1 (continued)

Protein	Cancer/tumor type	Reported change	Prognostic value	References
NUP 88	Ovarian cancer	Increased levels		[233]
	Different type of cancers: sarcomas, lymphomas, mesotheliomas, and breast cancer	Increased levels	Correlates with high-grade malignancies	[234–237]
	Colorectal cancer and hepatocellular carcinoma	Increased levels	Correlates with poor differentiation	[238, 239]
NUP 98	Leukemia	Increased levels; may act as a component of a chromosomal translocation		[240]
NUP 214	Uterine, stomach and rectal tumors, leukemias, breast cancer	Increased levels; may act as a multifunctional oncogene and as a component of a chromosomal translocation		[189, 240–242]

twice as likely to die of the disease than patients with tumors negative for lamin A/C [187], possibly by lamin A/C promoting cell motility [188]. These apparently inconsistent findings point at the multiple roles lamin can play in cancer progression, which will be discussed in more detail below.

In addition to lamins, other nuclear (envelope) proteins have recently been implicated in a variety of cancers. A genome-wide scan in several patients with either breast, colorectal or ovarian cancer revealed genetic alterations in nesprin-1 [189], and another genome-wide study identified mutations in nesprin-1, -2 and lamin A/C in a panel of 100 breast cancer patients [190]. Furthermore, downregulation and mutations in nesprin have been associated with an increased risk of invasive ovarian cancer [191]. Lastly, several "nuclear matrix" or nucleoskeletal-associated proteins such as NuMA or nucleoporin proteins (NUP 88, NUP 98) have been correlated with aggressive tumor phenotypes [192] and used as prognostic markers of disease [193].

Implications of Altered Nuclear Envelope Composition in Cancer

What is the impact of altered nuclear envelope composition on nuclear mechanics? As lamin expression and chromatin organization determine nuclear deformability, it is expected that changes in nuclear architecture will alter the rigidity of the nucleus. In cancer, increased nuclear deformability may benefit metastatic cells that need to pass through narrow interstitial spaces or small capillaries, while defects in nucleocytoskeletal coupling may impair migration in 3D tissues [20]. In addition to these mechanical functions, the nuclear envelope and nuclear interior play important roles in the processing of genetic information [194–196]. Thus, changes in nuclear organization could have consequences on gene expression or DNA stability with important implications in cancer progression.

Nuclear Deformability and Cell Motility

The abnormal nuclear shapes observed in cancer cells and their resemblance to lamin-deficient or mutant cells, combined with the increasing reports of altered expression of nuclear envelope proteins in various cancers (Table 1), suggests that cancer cells may have altered nuclear mechanics. While direct measurements of nuclear deformability in cancer cells have not yet been reported, studies that measure whole-cell deformability consistently find that cancer cells, particularly highly invasive ones, have increased cellular deformability [3, 4, 7]. Why should (nuclear) deformability matter in cancer progression? During the metastatic process, cancer cells must undergo modifications and large elastic deformations to invade the tissue surrounding the primary tumor, intravasate blood vessels, survive the physical stresses during circulation in the blood stream, extravasate at new sites in the body, and eventually proliferate in a nutrient-deprived microenvironment [197].

Particularly during invasion and intravasation and extravasation, cells penetrate through interstitial spaces and openings ranging in size from 2 to 30 μm [198, 199]. Cytoskeletal shape is highly adaptive, owing to the rapid cytoskeletal remodeling and plasma membrane flexibility; consequently, cytoskeletal protrusions can invade spaces of less than 1 μm^2 in cross section [200, 201]. In contrast, the ability of the nucleus to pass through narrow constrictions is more limited due to its size and stiffness. Transient nuclear deformations, resulting in hourglass- and cigar-shaped nuclei, as well as nuclear protrusions indicative of attempts to pass through narrow constrictions, can be observed (at least transiently) during cancer cell migration in vivo [20]. Importantly, a recent report by Friedl, Wolf, and colleagues [19] found that deformation of the nucleus poses a rate-limiting step during proteolysis-independent cell migration. They found that in the absence of proteolysis, e.g., during matrix metalloprotease (MMP) inhibition or knockdown, migration of cancer cells through 3D collagen matrices and polycarbonate filters is limited by the available pore size: cell migration speed and migration efficiency gradually drops with decreasing cross-sectional areas of the constrictions until cell body movement is completely stalled [19]. A similar size-dependent effect was observed by Tong and colleagues [202] when studying cell migration in microchannels with varying width. Indeed, decreasing channel width below 20 μm (at a fixed channel height of 10 μm) resulted in increasing reduction in migration speed. At the extreme, cells in 3 μm-wide channels had a 70 % reduction in migration speed compared to 50 and 20 μm-wide channels. Interestingly, the minimum size requirement for (non-proteolytic) migration through 3D environments was found to be independent of the shape of the constriction and only depends on the available cross-sectional area [19].

While these studies illustrate the importance of nuclear deformability in cell migration in confined environments, the role of the nuclear lamina and nuclear stiffness in this process remains to be explored [20]. At least in neutrophil-like cells, which normally have extremely low levels of lamins A/C and which can migrate through constrictions only a few micrometers in diameter, overexpression of lamin A results in less deformable nuclei that have reduced efficiency at crossing narrow constrictions and that take significantly longer to transit narrow microfluidic channels mimicking capillaries [103]. Similarly, fibroblasts expressing a mutant form of lamin A (progerin) that is responsible for Hutchinson–Gilford progeria syndrome have difficulties migrating through an array of microfabricated pillars spaced 6 μm apart [203], likely due to the increased nuclear stiffness caused by progerin [204, 205], as migration on non-constricted surfaces was comparable to cells from healthy controls [203]. Although these findings suggest an important role of lamins A/C in moderating the ability of cells to pass through narrow constrictions, Wolf and colleagues [19] found that the maximal deformation the nucleus could achieve during passage through narrow constrictions, indicated as the ratio of the nuclear cross section in the constriction to the undeformed nuclear cross section, was consistently around 1:10, regardless of the cell type studied. These findings suggest that the size limit for nuclear passage through small constriction may be governed by the maximal compressibility of the nucleus. The theoretically maximal compression depends on the solid fraction of the nucleus, as the chromatin (and other nucleoplasmic

proteins) can be no further compressed once all void spaces have been eliminated. This idea is consistent with the observed reduction in nuclear volume by up to 60 % during migration of skin fibroblasts through microfabricated constrictions [203] and with micropipette aspiration experiments that revealed that the nuclear volume can be compacted to about 20–40 % of its original size before reaching a state that resists further compression [92, 106].

But what about cancers in which increased, rather than decreased, levels of lamin A/C have been reported, which is expected to result in reduced nuclear deformability [98]? Cancer cells are highly plastic and heterogeneous in their gene expression, so it is likely that different subpopulations of cells with distinct roles in cancer progression exist. Increased lamin levels could help protect cells from mechanical stress caused by the high hydrostatic pressure inside solid tumors. At the same time, lamins are also involved in multiple signaling pathways [51, 117], which could modulate functions relevant to cancer progression. For example, increased levels of lamin A/C in prostate cancer cause changes in the PI3K/AKT/PTEN pathway [206], and upregulation of lamin A/C in colorectal cancer induces changes in cytoskeletal organization that promote cell motility [188]. As such, it is likely that different cells and tumors have found different approaches to find the best compromise between increasing nuclear deformability and activation of signaling pathways to increase cell motility and invasiveness.

Nuclear Rupture of Cancer Cells

As described earlier, the nuclear envelope forms a well-defined compartment that acts as a protective shield for the genetic material. In normal cells, nuclear envelope breakdown and reassembly is limited to mitosis and precisely regulated [207]. Recently, Vargas et al. [208] have reported that in many cancer cells, the nuclear envelope transiently ruptures and then reseals during interphase, resulting in temporary exchange between the nucleus and cytoplasm and the occasional entrapment of cytoplasmic organelles inside the nucleus. Nuclear envelope rupture was associated with the formation of micronuclei, portions of chromatin exiting the nuclear interior, and mislocalization of nucleoplasmic/cytoplasmic proteins. Importantly, the frequency of nuclear rupture events was increased in cells with small defects in the nuclear lamina [208]. These results are consistent with previous reports of increased nuclear fragility in lamin A/C-deficient mouse embryonic fibroblasts [14] and spontaneous (transient) nuclear rupture in these cells [209]. In our laboratory, we have frequently observed that cancer cells undergo transient nuclear rupture while migrating through narrow (~2 μm × 5 μm) microfluidic constrictions, with lamin-deficient cells displaying significantly increased rates of nuclear rupture (unpublished observations). Breakdown of the nuclear compartment during repetitive nuclear rupture could potentially result in increased genomic instability and chromatin rearrangements, which could further contribute to cancer progression, but this idea has not yet been experimentally tested.

Changes in Chromatin Organization in Cancer Cells

Epigenetic changes in chromatin configuration can directly impact nuclear stiffness. Therefore, the chromatin modifications frequently observed in cancer cells, including disturbed heterochromatin organization [11], could be associated with altered nuclear deformability and thereby affect 3D cell migration, in addition to their role in transcriptional activity. Importantly, there is a strong interplay between nuclear envelope proteins and chromatin organization. Lamin A regulates dynamics of heterochromatin proteins in early embryonic stem cells [25]; lamins A/C-deficiency and mutations in the *LMNA* gene result in loss of heterochromatin [111, 210]. Furthermore, lamins and lamin B receptor (LBR) play an important role in tethering specific chromatin regions to the nuclear periphery [211, 212], which typically serves as a transcriptionally repressive environment [195]. LBR also interacts with heterochromatin protein 1 [213] and histones H3/H4 [213]. Lamin-associated polypeptide-2β (LAP2β) can modulate gene expression by regulating higher order chromatin structure or binding the transcriptional repressors germ cell less (GCL) [214] and histone deacetylase 3 [215], resulting in deacetylation of histone H4 [215]. Emerin can directly associate with chromatin modifiers and transcriptional repressors such as the death promoting factor Btf [216], the splicing associated factor YT521-B [217], and the transcriptional repressor GCL [218]. Given these findings, it is tempting to speculate that the altered expression of nuclear envelope proteins found in various cancers (Table 1) can directly affect chromatin organization and gene expression. Of course, the observed changes in expression of nuclear envelope proteins could also be the consequence, rather than the cause of altered chromatin organization. In this case, the changes in nuclear envelope composition could still result in further modifications of nuclear structure and organization while also directly altering nuclear mechanics.

Conclusion and Future Perspectives

The field of cancer cell biology has dramatically changed since 1943, when George Papanicolaou published his book *Diagnosis of Uterine Cancer by the Vaginal Smear*, which laid the basis for the now abundant "pap smear" to detect early signs of cervical cancer. Since then, researchers and clinicians have learned not only to identify and assess cancer cells based on characteristic morphological changes, but also to peek inside the inner life of cancer cells, including their genetic changes, biochemical composition, and metabolic state. In recent years, these approaches have been complemented by a new research direction, focused on the biophysical changes in cancer cells and their microenvironment. This research has already led to striking discoveries, including the role of the extracellular matrix stiffness, composition and topology in cancer progression [219] and the characteristic difference in cell deformability of cancer cells, which may lead

to new diagnostic and prognostic applications [3]. Motivated by research in other diseases (laminopathies), it is now emerging that the mechanical properties of the cell nucleus, particularly its deformability and connection to the cytoskeleton, may play a similarly important role in cancer metastasis. The idea that deformation of the large and stiff nucleus presents a rate-limiting factor during the passage of metastatic cancer cells through tight interstitial spaces or narrow capillaries has recently found increasing experimental support [19, 103, 165]. Given the increasing reports of altered expression and mutations in nuclear envelope proteins responsible for determining nuclear stiffness, it is intriguing to speculate that (a subset of) cancer cells may have acquired specific adaptations in their nuclear structure and mechanics to promote metastatic spreading. Nonetheless, experimental verification of this idea is still lacking. Additional experiments, using sophisticated combinations of live cell imaging and measurements of subcellular mechanics, including primary tumor (and metastatic) cells from cancer patients and complemented by in vivo studies in mouse models, will be required to firmly establish this hypothesis. These experiments will also have to address why some cancers frequently have increased lamin levels while others have decreased or unchanged levels, and whether such changes in nuclear envelope composition can serve as reliable prognostic markers. Given the diverse functions of lamins, it is likely that (varying) combinations of altered cellular mechanics, cell signaling, and stem cell differentiation contribute to the increasingly emerging role of lamins in cancer progression. Done correctly, such experiments have the potential to not only address these key questions but to also produce novel insights into the dynamic nature of cancer cells, which may switch between different morphological and mechanical modes depending on their current role in cancer progression. Novel technology developments to probe single cell mechanics at substantial higher throughput than traditional methods [5, 102, 220, 221] will enable detection of rare cell subpopulations, which could play a crucial role in cancer progression. Identifying key (mechanical) parameters that govern cancer cell metastasis may reveal novel therapeutic targets for pharmacological inhibition.

These clinical translation-driven experiments should be complemented by research to address some of the more fundamental questions in cancer cell biology, including the molecular mechanisms by which cells manage to squeeze the nucleus through constrictions only one tenth the diameter of the nucleus in size, and whether induced nuclear deformations can directly contribute to cellular mechanosensing. We are only at the beginning of a long road ahead, the destination a complete understanding of the physics of cancer progression und the underlying biology, but it will be exciting to see what is awaiting us around the next corner.

Acknowledgements We apologize to all authors whose work could not be cited due to space constraints. This work was supported by National Institutes of Health awards [R01 NS059348 and R01 HL082792], a National Science Foundation CAREER award to J. L. [CBET-1254846], the Department of Defense Breast Cancer Idea Award [BC102152], and an award from the Progeria Research Foundation [PRF2011-0035].

References

1. Fawcett DW (1966) An Atlas of fine structure. The cell, 2nd edn. W. B. Saunders Company, PA
2. Hanahan D, Weinberg RA (2011) Hallmarks of cancer: the next generation. Cell 144(5): 646–674. doi:10.1016/j.cell.2011.02.013
3. Suresh S (2007) Biomechanics and biophysics of cancer cells. Acta Biomater 3(4):413–438. doi:10.1016/j.actbio.2007.04.002
4. Guck J, Schinkinger S, Lincoln B, Wottawah F, Ebert S, Romeyke M, Lenz D, Erickson HM, Ananthakrishnan R, Mitchell D, Käs J, Ulvick S, Bilby C (2005) Optical deformability as an inherent cell marker for testing malignant transformation and metastatic competence. Biophys J 88(5):3689–3698. doi:10.1529/biophysj.104.045476
5. Remmerbach TW, Wottawah F, Dietrich J, Lincoln B, Wittekind C, Guck J (2009) Oral cancer diagnosis by mechanical phenotyping. Cancer Res 69(5):1728–1732. doi:10.1158/0008-5472.can-08-4073
6. Byun S, Son S, Amodei D, Cermak N, Shaw J, Kang JH, Hecht VC, Winslow MM, Jacks T, Mallick P, Manalis SR (2013) Characterizing deformability and surface friction of cancer cells. Proc Natl Acad Sci U S A 110(19):7580–7585. doi:10.1073/pnas.1218806110
7. Cross SE, Jin YS, Rao J, Gimzewski JK (2007) Nanomechanical analysis of cells from cancer patients. Nat Nanotechnol 2(12):780–783. doi:10.1038/nnano.2007.388
8. Kraning-Rush CM, Califano JP, Reinhart-King CA (2012) Cellular traction stresses increase with increasing metastatic potential. PLoS One 7(2):e32572. doi:10.1371/journal.pone.0032572
9. Baker EL, Lu J, Yu D, Bonnecaze RT, Zaman MH (2010) Cancer cell stiffness: integrated roles of three-dimensional matrix stiffness and transforming potential. Biophys J 99(7): 2048–2057. doi:10.1016/j.bpj.2010.07.051
10. Paszek MJ, Zahir N, Johnson KR, Lakins JN, Rozenberg GI, Gefen A, Reinhart-King CA, Margulies SS, Dembo M, Boettiger D, Hammer DA, Weaver VM (2005) Tensional homeostasis and the malignant phenotype. Cancer Cell 8(3):241–254. doi:10.1016/j.ccr.2005.08.010
11. Zink D, Fischer AH, Nickerson JA (2004) Nuclear structure in cancer cells. Nat Rev Cancer 4(9):677–687. doi:10.1038/nrc1430
12. Ho CY, Lammerding J (2012) Lamins at a glance. J Cell Sci 125(Pt 9):2087–2093. doi:10.1242/jcs.087288
13. de Las Heras JI, Batrakou DG, Schirmer EC (2013) Cancer biology and the nuclear envelope: a convoluted relationship. Semin Cancer Biol 23(2):125–137. doi:10.1016/j.semcancer.2012.01.008
14. Lammerding J, Schulze PC, Takahashi T, Kozlov S, Sullivan T, Kamm RD, Stewart CL, Lee RT (2004) Lamin A/C deficiency causes defective nuclear mechanics and mechanotransduction. J Clin Invest 113(3):370–378. doi:10.1172/jci19670
15. Dahl KN, Ribeiro AJ, Lammerding J (2008) Nuclear shape, mechanics, and mechanotransduction. Circ Res 102(11):1307–1318. doi:10.1161/circresaha.108.173989
16. Zwerger M, Ho CY, Lammerding J (2011) Nuclear mechanics in disease. Annu Rev Biomed Eng 13:397–428. doi:10.1146/annurev-bioeng-071910-124736
17. Lammerding J (2011) Mechanics of the nucleus. Compr Physiol 1(2):783–807. doi:10.1002/cphy.c100038
18. Wang N, Tytell JD, Ingber DE (2009) Mechanotransduction at a distance: mechanically coupling the extracellular matrix with the nucleus. Nat Rev Mol Cell Biol 10(1):75–82. doi:10.1038/nrm2594
19. Wolf K, Te Lindert M, Krause M, Alexander S, Te Riet J, Willis AL, Hoffman RM, Figdor CG, Weiss SJ, Friedl P (2013) Physical limits of cell migration: control by ECM space and nuclear deformation and tuning by proteolysis and traction force. J Cell Biol 201(7): 1069–1084. doi:10.1083/jcb.201210152
20. Friedl P, Wolf K, Lammerding J (2011) Nuclear mechanics during cell migration. Curr Opin Cell Biol 23(1):55–64. doi:10.1016/j.ceb.2010.10.015

21. Hale CM, Shrestha AL, Khatau SB, Stewart-Hutchinson PJ, Hernandez L, Stewart CL, Hodzic D, Wirtz D (2008) Dysfunctional connections between the nucleus and the actin and microtubule networks in laminopathic models. Biophys J 95(11):5462–5475. doi:10.1529/biophysj.108.139428
22. Chancellor TJ, Lee J, Thodeti CK, Lele T (2010) Actomyosin tension exerted on the nucleus through nesprin-1 connections influences endothelial cell adhesion, migration, and cyclic strain-induced reorientation. Biophys J 99(1):115–123. doi:10.1016/j.bpj.2010.04.011
23. Schneider M, Lu W, Neumann S, Brachner A, Gotzmann J, Noegel AA, Karakesisoglou I (2011) Molecular mechanisms of centrosome and cytoskeleton anchorage at the nuclear envelope. Cell Mol Life Sci 68(9):1593–1610. doi:10.1007/s00018-010-0535-z
24. Lombardi ML, Jaalouk DE, Shanahan CM, Burke B, Roux KJ, Lammerding J (2011) The interaction between nesprins and sun proteins at the nuclear envelope is critical for force transmission between the nucleus and cytoskeleton. J Biol Chem 286(30):26743–26753. doi:10.1074/jbc.M111.233700
25. Melcer S, Hezroni H, Rand E, Nissim-Rafinia M, Skoultchi A, Stewart CL, Bustin M, Meshorer E (2012) Histone modifications and lamin A regulate chromatin protein dynamics in early embryonic stem cell differentiation. Nat Commun 3:910. doi:10.1038/ncomms1915
26. Handwerger KE, Gall JG (2006) Subnuclear organelles: new insights into form and function. Trends Cell Biol 16(1):19–26. doi:10.1016/j.tcb.2005.11.005
27. Zhao R, Bodnar MS, Spector DL (2009) Nuclear neighborhoods and gene expression. Curr Opin Genet Dev 19(2):172–179. doi:10.1016/j.gde.2009.02.007
28. Dundr M, Misteli T (2010) Biogenesis of nuclear bodies. Cold Spring Harb Perspect Biol 2(12):a000711. doi:10.1101/cshperspect.a000711
29. Franke WW, Scheer U, Krohne G, Jarasch ED (1981) The nuclear envelope and the architecture of the nuclear periphery. J Cell Biol 91(3 Pt 2):39s–50s
30. Schirmer EC, Foisner R (2007) Proteins that associate with lamins: many faces, many functions. Exp Cell Res 313(10):2167–2179. doi:10.1016/j.yexcr.2007.03.012
31. Puddington L, Lively MO, Lyles DS (1985) Role of the nuclear envelope in synthesis, processing, and transport of membrane glycoproteins. J Biol Chem 260(9):5641–5647
32. Starr DA, Han M (2002) Role of ANC-1 in tethering nuclei to the actin cytoskeleton. Science 298(5592):406–409. doi:10.1126/science.1075119
33. Fridkin A, Mills E, Margalit A, Neufeld E, Lee KK, Feinstein N, Cohen M, Wilson KL, Gruenbaum Y (2004) Matefin, a Caenorhabditis elegans germ line-specific SUN-domain nuclear membrane protein, is essential for early embryonic and germ cell development. Proc Natl Acad Sci U S A 101(18):6987–6992. doi:10.1073/pnas.0307880101
34. Rajgor D, Mellad JA, Autore F, Zhang Q, Shanahan CM (2012) Multiple novel nesprin-1 and nesprin-2 variants act as versatile tissue-specific intracellular scaffolds. PLoS One 7(7):e40098. doi:10.1371/journal.pone.0040098
35. Padmakumar VC, Abraham S, Braune S, Noegel AA, Tunggal B, Karakesisoglou I, Korenbaum E (2004) Enaptin, a giant actin-binding protein, is an element of the nuclear membrane and the actin cytoskeleton. Exp Cell Res 295(2):330–339. doi:10.1016/j.yexcr.2004.01.014
36. Wilhelmsen K, Litjens SH, Kuikman I, Tshimbalanga N, Janssen H, van den Bout I, Raymond K, Sonnenberg A (2005) Nesprin-3, a novel outer nuclear membrane protein, associates with the cytoskeletal linker protein plectin. J Cell Biol 171(5):799–810. doi:10.1083/jcb.200506083
37. Zhang Q, Skepper JN, Yang F, Davies JD, Hegyi L, Roberts RG, Weissberg PL, Ellis JA, Shanahan CM (2001) Nesprins: a novel family of spectrin-repeat-containing proteins that localize to the nuclear membrane in multiple tissues. J Cell Sci 114(Pt 24):4485–4498
38. Zhang Q, Ragnauth CD, Skepper JN, Worth NF, Warren DT, Roberts RG, Weissberg PL, Ellis JA, Shanahan CM (2005) Nesprin-2 is a multi-isomeric protein that binds lamin and emerin at the nuclear envelope and forms a subcellular network in skeletal muscle. J Cell Sci 118(Pt 4):673–687. doi:10.1242/jcs.01642
39. Chen D, Zhao M, Mundy G (2004) Bone morphogenetic proteins. Growth Factors 22(4): 233–241, doi:HHV6108EX6P056CA [pii]10.1080/08977190412331279890

40. Wischnitzer S (1958) An electron microscope study of the nuclear envelope of amphibian oocytes. J Ultrastruct Res 1(3):201–222
41. Gerace L, Foisner R (1994) Integral membrane proteins and dynamic organization of the nuclear envelope. Trends Cell Biol 4(4):127–131
42. Grossman E, Medalia O, Zwerger M (2012) Functional architecture of the nuclear pore complex. Annu Rev Biophys 41:557–584. doi:10.1146/annurev-biophys-050511-102328
43. Nakielny S, Dreyfuss G (1999) Transport of proteins and RNAs in and out of the nucleus. Cell 99(7):677–690
44. D'Angelo MA, Anderson DJ, Richard E, Hetzer MW (2006) Nuclear pores form de novo from both sides of the nuclear envelope. Science 312(5772):440–443. doi:10.1126/science.1124196
45. D'Angelo MA, Hetzer MW (2008) Structure, dynamics and function of nuclear pore complexes. Trends Cell Biol 18(10):456–466. doi:10.1016/j.tcb.2008.07.009
46. Dreger M, Bengtsson L, Schöneberg T, Otto H, Hucho F (2001) Nuclear envelope proteomics: novel integral membrane proteins of the inner nuclear membrane. Proc Natl Acad Sci U S A 98(21):11943–11948. doi:10.1073/pnas.211201898
47. Korfali N, Wilkie GS, Swanson SK, Srsen V, Batrakou DG, Fairley EA, Malik P, Zuleger N, Goncharevich A, de Las HJ, Kelly DA, Kerr AR, Florens L, Schirmer EC (2010) The leukocyte nuclear envelope proteome varies with cell activation and contains novel transmembrane proteins that affect genome architecture. Mol Cell Proteomics 9(12):2571–2585. doi:10.1074/mcp.M110.002915
48. Schirmer EC, Florens L, Guan T, Yates JR, Gerace L (2003) Nuclear membrane proteins with potential disease links found by subtractive proteomics. Science 301(5638):1380–1382. doi:10.1126/science.1088176
49. Wilkie GS, Korfali N, Swanson SK, Malik P, Srsen V, Batrakou DG, de las Heras J, Zuleger N, Kerr AR, Florens L, Schirmer EC (2011) Several novel nuclear envelope transmembrane proteins identified in skeletal muscle have cytoskeletal associations. Mol Cell Proteomics 10(1):M110.003129. doi:10.1074/mcp.M110.003129
50. Korfali N, Wilkie GS, Swanson SK, Srsen V, de Las HJ, Batrakou DG, Malik P, Zuleger N, Kerr AR, Florens L, Schirmer EC (2012) The nuclear envelope proteome differs notably between tissues. Nucleus 3(6):552–564. doi:10.4161/nucl.22257
51. Schreiber KH, Kennedy BK (2013) When lamins go bad: nuclear structure and disease. Cell 152(6):1365–1375. doi:10.1016/j.cell.2013.02.015
52. Paddy MR, Belmont AS, Saumweber H, Agard DA, Sedat JW (1990) Interphase nuclear envelope lamins form a discontinuous network that interacts with only a fraction of the chromatin in the nuclear periphery. Cell 62(1):89–106
53. Strelkov S, Herrmann H, Aebi U (2003) Molecular architecture of intermediate filaments. Bioessays 25(3):243–251. doi:10.1002/bies.10246
54. Aebi U, Cohn J, Buhle L, Gerace L (1986) The nuclear lamina is a meshwork of intermediate-type filaments. Nature 323(6088):560–564. doi:10.1038/323560a0
55. Herrmann H, Aebi U (2004) Intermediate filaments: molecular structure, assembly mechanism, and integration into functionally distinct intracellular Scaffolds. Annu Rev Biochem 73:749–789. doi:10.1146/annurev.biochem.73.011303.073823
56. Peter A, Reimer S (2012) Evolution of the lamin protein family: what introns can tell. Nucleus 3(1):44–59
57. Batsios P, Peter T, Baumann O, Stick R, Meyer I, Gräf R (2012) A lamin in lower eukaryotes? Nucleus 3(3):237–243. doi:10.4161/nucl.20149
58. Stuurman N, Heins S, Aebi U (1998) Nuclear lamins: their structure, assembly, and interactions. J Struct Biol 122(1–2):42–66. doi:10.1006/jsbi.1998.3987
59. Gruenbaum Y, Margalit A, Goldman RD, Shumaker DK, Wilson KL (2005) The nuclear lamina comes of age. Nat Rev Mol Cell Biol 6(1):21–31. doi:10.1038/nrm1550
60. Goldman RD, Gruenbaum Y, Moir RD, Shumaker DK, Spann TP (2002) Nuclear lamins: building blocks of nuclear architecture. Genes Dev 16(5):533–547. doi:10.1101/gad.960502

61. Kitten GT, Nigg EA (1991) The CaaX motif is required for isoprenylation, carboxyl methylation, and nuclear membrane association of lamin B2. J Cell Biol 113(1):13–23
62. Zastrow MS, Vlcek S, Wilson KL (2004) Proteins that bind A-type lamins: integrating isolated clues. J Cell Sci 117(Pt 7):979–987. doi:10.1242/jcs.01102
63. Dechat T, Gesson K, Foisner R (2010) Lamina-independent lamins in the nuclear interior serve important functions. Cold Spring Harb Symp Quant Biol 75:533–543. doi:10.1101/sqb.2010.75.018
64. Höger TH, Krohne G, Franke WW (1988) Amino acid sequence and molecular characterization of murine lamin B as deduced from cDNA clones. Eur J Cell Biol 47(2):283–290
65. Höger TH, Zatloukal K, Waizenegger I, Krohne G (1990) Characterization of a second highly conserved B-type lamin present in cells previously thought to contain only a single B-type lamin. Chromosoma 99(6):379–390
66. Lin F, Worman HJ (1993) Structural organization of the human gene encoding nuclear lamin A and nuclear lamin C. J Biol Chem 268(22):16321–16326
67. Lin F, Worman HJ (1995) Structural organization of the human gene (LMNB1) encoding nuclear lamin B1. Genomics 27(2):230–236. doi:10.1006/geno.1995.1036
68. Moir RD, Spann TP, Lopez-Soler RI, Yoon M, Goldman AE, Khuon S, Goldman RD (2000) Review: the dynamics of the nuclear lamins during the cell cycle—relationship between structure and function. J Struct Biol 129(2–3):324–334. doi:10.1006/jsbi.2000.4251
69. Raska I, Koberna K, Malínský J, Fidlerová H, Masata M (2004) The nucleolus and transcription of ribosomal genes. Biol Cell 96(8):579–594. doi:10.1016/j.biolcel.2004.04.015
70. Matera AG (2003) Cajal bodies. Curr Biol 13(13):R503
71. Matera AG, Frey MR (1998) Coiled bodies and gems: Janus or gemini? Am J Hum Genet 63(2):317–321. doi:10.1086/301992
72. Dellaire G, Bazett-Jones DP (2004) PML nuclear bodies: dynamic sensors of DNA damage and cellular stress. Bioessays 26(9):963–977. doi:10.1002/bies.20089
73. Nyman U, Hallman H, Hadlaczky G, Pettersson I, Sharp G, Ringertz NR (1986) Intranuclear localization of snRNP antigens. J Cell Biol 102(1):137–144
74. Pederson T, Aebi U (2002) Actin in the nucleus: what form and what for? J Struct Biol 140(1–3):3–9
75. Hofmann WA (2009) Cell and molecular biology of nuclear actin. Int Rev Cell Mol Biol 273:219–263. doi:10.1016/s1937-6448(08)01806-6
76. Nowak G, Pestic-Dragovich L, Hozák P, Philimonenko A, Simerly C, Schatten G, de Lanerolle P (1997) Evidence for the presence of myosin I in the nucleus. J Biol Chem 272(27):17176–17181
77. de Lanerolle P, Serebryannyy L (2011) Nuclear actin and myosins: life without filaments. Nat Cell Biol 13(11):1282–1288. doi:10.1038/ncb2364
78. Young KG, Kothary R (2005) Spectrin repeat proteins in the nucleus. Bioessays 27(2):144–152. doi:10.1002/bies.20177
79. Zastrow MS, Flaherty DB, Benian GM, Wilson KL (2006) Nuclear titin interacts with A- and B-type lamins in vitro and in vivo. J Cell Sci 119(Pt 2):239–249. doi:10.1242/jcs.02728
80. Rando OJ, Zhao K, Crabtree GR (2000) Searching for a function for nuclear actin. Trends Cell Biol 10(3):92–97
81. McDonald D, Carrero G, Andrin C, de Vries G, Hendzel MJ (2006) Nucleoplasmic beta-actin exists in a dynamic equilibrium between low-mobility polymeric species and rapidly diffusing populations. J Cell Biol 172(4):541–552. doi:10.1083/jcb.200507101
82. Gieni RS, Hendzel MJ (2009) Actin dynamics and functions in the interphase nucleus: moving toward an understanding of nuclear polymeric actin. Biochem Cell Biol 87(1):283–306. doi:10.1139/o08-133
83. Wada A, Fukuda M, Mishima M, Nishida E (1998) Nuclear export of actin: a novel mechanism regulating the subcellular localization of a major cytoskeletal protein. EMBO J 17(6):1635–1641. doi:10.1093/emboj/17.6.1635
84. Belin BJ, Cimini BA, Blackburn EH, Mullins RD (2013) Visualization of actin filaments and monomers in somatic cell nuclei. Mol Biol Cell 24(7):982–994. doi:10.1091/mbc.E12-09-0685

85. Visa N, Percipalle P (2010) Nuclear functions of actin. Cold Spring Harb Perspect Biol 2(4):a000620. doi:10.1101/cshperspect.a000620
86. Berezney R, Coffey DS (1977) Nuclear matrix. Isolation and characterization of a framework structure from rat liver nuclei. J Cell Biol 73(3):616–637
87. Jaalouk DE, Lammerding J (2009) Mechanotransduction gone awry. Nat Rev Mol Cell Biol 10(1):63–73. doi:10.1038/nrm2597
88. Heasman SJ, Ridley AJ (2008) Mammalian Rho GTPases: new insights into their functions from in vivo studies. Nat Rev Mol Cell Biol 9(9):690–701. doi:10.1038/nrm2476
89. Discher DE, Boal DH, Boey SK (1998) Simulations of the erythrocyte cytoskeleton at large deformation. II. Micropipette aspiration. Biophys J 75(3):1584–1597. doi:10.1016/s0006-3495(98)74076-7
90. Dahl KN, Kahn SM, Wilson KL, Discher DE (2004) The nuclear envelope lamina network has elasticity and a compressibility limit suggestive of a molecular shock absorber. J Cell Sci 117(Pt 20):4779–4786. doi:10.1242/jcs.01357
91. Dahl KN, Engler AJ, Pajerowski JD, Discher DE (2005) Power-law rheology of isolated nuclei with deformation mapping of nuclear substructures. Biophys J 89(4):2855–2864. doi:10.1529/biophysj.105.062554
92. Rowat AC, Lammerding J, Ipsen JH (2006) Mechanical properties of the cell nucleus and the effect of emerin deficiency. Biophys J 91(12):4649–4664. doi:10.1529/biophysj.106.086454
93. Guilak F, Tedrow JR, Burgkart R (2000) Viscoelastic properties of the cell nucleus. Biochem Biophys Res Commun 269(3):781–786. doi:10.1006/bbrc.2000.2360
94. Jiménez-García LF, Fragoso-Soriano R (2000) Atomic force microscopy of the cell nucleus. J Struct Biol 129(2–3):218–222. doi:10.1006/jsbi.2000.4233
95. Schäpe J, Prausse S, Radmacher M, Stick R (2009) Influence of lamin A on the mechanical properties of amphibian oocyte nuclei measured by atomic force microscopy. Biophys J 96(10):4319–4325. doi:10.1016/j.bpj.2009.02.048
96. Kaufmann A, Heinemann F, Radmacher M, Stick R (2011) Amphibian oocyte nuclei expressing lamin A with the progeria mutation E145K exhibit an increased elastic modulus. Nucleus 2(4):310–319. doi:10.4161/nucl.2.4.16119
97. Lammerding J, Hsiao J, Schulze PC, Kozlov S, Stewart CL, Lee RT (2005) Abnormal nuclear shape and impaired mechanotransduction in emerin-deficient cells. J Cell Biol 170(5):781–791. doi:10.1083/jcb.200502148
98. Lammerding J, Fong LG, Ji JY, Reue K, Stewart CL, Young SG, Lee RT (2006) Lamins A and C but not lamin B1 regulate nuclear mechanics. J Biol Chem 281(35):25768–25780. doi:10.1074/jbc.M513511200
99. Caille N, Thoumine O, Tardy Y, Meister JJ (2002) Contribution of the nucleus to the mechanical properties of endothelial cells. J Biomech 35(2):177–187
100. Tseng Y, Lee JS, Kole TP, Jiang I, Wirtz D (2004) Micro-organization and visco-elasticity of the interphase nucleus revealed by particle nanotracking. J Cell Sci 117(Pt 10):2159–2167. doi:10.1242/jcs.01073
101. Chalut KJ, Höpfler M, Lautenschläger F, Boyde L, Chan CJ, Ekpenyong A, Martinez-Arias A, Guck J (2012) Chromatin decondensation and nuclear softening accompany Nanog down-regulation in embryonic stem cells. Biophys J 103(10):2060–2070. doi:10.1016/j.bpj.2012.10.015
102. Isermann P, Davidson PM, Sliz JD, Lammerding J (2012) Assays to measure nuclear mechanics in interphase cells. Curr Protoc Cell Biol Chapter 22:Unit22.16. doi:10.1002/0471143030.cb2216s56
103. Rowat AC, Jaalouk DE, Zwerger M, Ung WL, Eydelnant IA, Olins DE, Olins AL, Herrmann H, Weitz DA, Lammerding J (2013) Nuclear envelope composition determines the ability of neutrophil-type cells to passage through micron-scale constrictions. J Biol Chem 288(12):8610–8618. doi:10.1074/jbc.M112.441535
104. Kha HN, Chen BK, Clark GM, Jones R (2004) Stiffness properties for Nucleus standard straight and contour electrode arrays. Med Eng Phys 26(8):677–685. doi:10.1016/j.medengphy.2004.05.001

105. Vaziri A, Mofrad MR (2007) Mechanics and deformation of the nucleus in micropipette aspiration experiment. J Biomech 40(9):2053–2062. doi:10.1016/j.jbiomech.2006.09.023
106. Rowat AC, Lammerding J, Herrmann H, Aebi U (2008) Towards an integrated understanding of the structure and mechanics of the cell nucleus. Bioessays 30(3):226–236. doi:10.1002/bies.20720
107. Pajerowski JD, Dahl KN, Zhong FL, Sammak PJ, Discher DE (2007) Physical plasticity of the nucleus in stem cell differentiation. Proc Natl Acad Sci U S A 104(40):15619–15624. doi:10.1073/pnas.0702576104
108. Shimi T, Pfleghaar K, Kojima S, Pack CG, Solovei I, Goldman AE, Adam SA, Shumaker DK, Kinjo M, Cremer T, Goldman RD (2008) The A- and B-type nuclear lamin networks: microdomains involved in chromatin organization and transcription. Genes Dev 22(24):3409–3421. doi:10.1101/gad.1735208
109. Kolb T, Maass K, Hergt M, Aebi U, Herrmann H (2011) Lamin A and lamin C form homodimers and coexist in higher complex forms both in the nucleoplasmic fraction and in the lamina of cultured human cells. Nucleus 2(5):425–433. doi:10.4161/nucl.2.5.17765
110. Goldberg MW, Huttenlauch I, Hutchison CJ, Stick R (2008) Filaments made from A- and B-type lamins differ in structure and organization. J Cell Sci 121(Pt 2):215–225. doi:10.1242/jcs.022020
111. Sullivan T, Escalante-Alcalde D, Bhatt H, Anver M, Bhat N, Nagashima K, Stewart CL, Burke B (1999) Loss of A-type lamin expression compromises nuclear envelope integrity leading to muscular dystrophy. J Cell Biol 147(5):913–920
112. Puckelwartz MJ, Depreux FF, McNally EM (2011) Gene expression, chromosome position and lamin A/C mutations. Nucleus 2(3):162–167. doi:10.1083/jcb.201101046, 10.4161/nucl.2.3.16003
113. Mewborn SK, Puckelwartz MJ, Abuisneineh F, Fahrenbach JP, Zhang Y, MacLeod H, Dellefave L, Pytel P, Selig S, Labno CM, Reddy K, Singh H, McNally E (2010) Altered chromosomal positioning, compaction, and gene expression with a lamin A/C gene mutation. PLoS One 5(12):e14342. doi:10.1371/journal.pone.0014342
114. Bridger JM, Foeger N, Kill IR, Herrmann H (2007) The nuclear lamina. Both a structural framework and a platform for genome organization. FEBS J 274(6):1354–1361
115. Broers JL, Ramaekers FC (2004) Dynamics of nuclear lamina assembly and disassembly. Symp Soc Exp Biol 56:177–192
116. Zwerger M, Jaalouk DE, Lombardi ML, Isermann P, Mauermann M, Dialynas G, Herrmann H, Wallrath LL, Lammerding J (2013) Myopathic lamin mutations impair nuclear stability in cells and tissue and disrupt nucleo-cytoskeletal coupling. Hum Mol Genet 22(12):2335–2349. doi:10.1093/hmg/ddt079
117. Simon DN, Wilson KL (2013) Partners and post-translational modifications of nuclear lamins. Chromosoma 122(1–2):13–31. doi:10.1007/s00412-013-0399-8
118. Zhong Z, Wilson KL, Dahl KN (2010) Beyond lamins other structural components of the nucleoskeleton. Methods Cell Biol 98:97–119. doi:10.1016/s0091-679x(10)98005-9
119. Dahl KN, Kalinowski A (2011) Nucleoskeleton mechanics at a glance. J Cell Sci 124(Pt 5):675–678. doi:10.1242/jcs.069096
120. Gundersen GG, Worman HJ (2013) Nuclear positioning. Cell 152(6):1376–1389. doi:10.1016/j.cell.2013.02.031
121. Rothballer A, Kutay U (2013) The diverse functional LINCs of the nuclear envelope to the cytoskeleton and chromatin. Chromosoma. doi:10.1007/s00412-013-0417-x
122. Malone CJ, Fixsen WD, Horvitz HR, Han M (1999) UNC-84 localizes to the nuclear envelope and is required for nuclear migration and anchoring during C. elegans development. Development 126(14):3171–3181
123. Lee KK, Starr D, Cohen M, Liu J, Han M, Wilson KL, Gruenbaum Y (2002) Lamin-dependent localization of UNC-84, a protein required for nuclear migration in Caenorhabditis elegans. Mol Biol Cell 13(3):892–901. doi:10.1091/mbc.01-06-0294
124. Malone CJ, Misner L, Le Bot N, Tsai MC, Campbell JM, Ahringer J, White JG (2003) The C. elegans hook protein, ZYG-12, mediates the essential attachment between the centrosome and nucleus. Cell 115(7):825–836

125. Starr DA, Han M (2003) ANChors away: an actin based mechanism of nuclear positioning. J Cell Sci 116(Pt 2):211–216
126. Crisp M, Liu Q, Roux K, Rattner JB, Shanahan C, Burke B, Stahl PD, Hodzic D (2006) Coupling of the nucleus and cytoplasm: role of the LINC complex. J Cell Biol 172(1):41–53. doi:10.1083/jcb.200509124
127. Starr DA, Fridolfsson HN (2010) Interactions between nuclei and the cytoskeleton are mediated by SUN-KASH nuclear-envelope bridges. Annu Rev Cell Dev Biol 26:421–444. doi:10.1146/annurev-cellbio-100109-104037
128. Wagner N, Krohne G (2007) LEM-Domain proteins: new insights into lamin-interacting proteins. Int Rev Cytol 261:1–46. doi:10.1016/s0074-7696(07)61001-8
129. Méjat A, Misteli T (2010) LINC complexes in health and disease. Nucleus 1(1):40–52. doi:10.4161/nucl.1.1.10530
130. Sosa BA, Rothballer A, Kutay U, Schwartz TU (2012) LINC complexes form by binding of three KASH peptides to domain interfaces of trimeric SUN proteins. Cell 149(5):1035–1047. doi:10.1016/j.cell.2012.03.046
131. Nery FC, Zeng J, Niland BP, Hewett J, Farley J, Irimia D, Li Y, Wiche G, Sonnenberg A, Breakefield XO (2008) TorsinA binds the KASH domain of nesprins and participates in linkage between nuclear envelope and cytoskeleton. J Cell Sci 121(Pt 20):3476–3486. doi:10.1242/jcs.029454
132. Folker ES, Ostlund C, Luxton GW, Worman HJ, Gundersen GG (2011) Lamin A variants that cause striated muscle disease are defective in anchoring transmembrane actin-associated nuclear lines for nuclear movement. Proc Natl Acad Sci U S A 108(1):131–136. doi:10.1073/pnas.1000824108
133. Lombardi ML, Lammerding J (2011) Keeping the LINC: the importance of nucleocytoskeletal coupling in intracellular force transmission and cellular function. Biochem Soc Trans 39(6):1729–1734. doi:10.1042/bst20110686
134. Maniotis AJ, Chen CS, Ingber DE (1997) Demonstration of mechanical connections between integrins, cytoskeletal filaments, and nucleoplasm that stabilize nuclear structure. Proc Natl Acad Sci U S A 94(3):849–854
135. Hagan I, Yanagida M (1995) The product of the spindle formation gene sad1+ associates with the fission yeast spindle pole body and is essential for viability. J Cell Biol 129(4):1033–1047
136. Sosa BA, Kutay U, Schwartz TU (2013) Structural insights into LINC complexes. Curr Opin Struct Biol 23(2):285–291. doi:10.1016/j.sbi.2013.03.005
137. Haque F, Lloyd DJ, Smallwood DT, Dent CL, Shanahan CM, Fry AM, Trembath RC, Shackleton S (2006) SUN1 interacts with nuclear lamin A and cytoplasmic nesprins to provide a physical connection between the nuclear lamina and the cytoskeleton. Mol Cell Biol 26(10):3738–3751. doi:10.1128/mcb.26.10.3738-3751.2006
138. Liu Q, Pante N, Misteli T, Elsagga M, Crisp M, Hodzic D, Burke B, Roux KJ (2007) Functional association of Sun1 with nuclear pore complexes. J Cell Biol 178(5):785–798. doi:10.1083/jcb.200704108
139. Lussi YC, Hügi I, Laurell E, Kutay U, Fahrenkrog B (2011) The nucleoporin Nup88 is interacting with nuclear lamin A. Mol Biol Cell 22(7):1080–1090. doi:10.1091/mbc.E10-05-0463
140. Razafsky D, Hodzic D (2009) Bringing KASH under the SUN: the many faces of nucleocytoskeletal connections. J Cell Biol 186(4):461–472. doi:10.1083/jcb.200906068
141. Apel ED, Lewis RM, Grady RM, Sanes JR (2000) Syne-1, a dystrophin- and Klarsicht-related protein associated with synaptic nuclei at the neuromuscular junction. J Biol Chem 275(41):31986–31995. doi:10.1074/jbc.M004775200
142. Mellad JA, Warren DT, Shanahan CM (2011) Nesprins LINC the nucleus and cytoskeleton. Curr Opin Cell Biol 23(1):47–54. doi:10.1016/j.ceb.2010.11.006
143. Zhen YY, Libotte T, Munck M, Noegel AA, Korenbaum E (2002) NUANCE, a giant protein connecting the nucleus and actin cytoskeleton. J Cell Sci 115(Pt 15):3207–3222
144. Roux KJ, Crisp ML, Liu Q, Kim D, Kozlov S, Stewart CL, Burke B (2009) Nesprin 4 is an outer nuclear membrane protein that can induce kinesin-mediated cell polarization. Proc Natl Acad Sci U S A 106(7):2194–2199. doi:10.1073/pnas.0808602106

145. Libotte T, Zaim H, Abraham S, Padmakumar VC, Schneider M, Lu W, Munck M, Hutchison C, Wehnert M, Fahrenkrog B, Sauder U, Aebi U, Noegel AA, Karakesisoglou I (2005) Lamin A/C-dependent localization of Nesprin-2, a giant scaffolder at the nuclear envelope. Mol Biol Cell 16(7):3411–3424. doi:10.1091/mbc.E04-11-1009
146. Mislow JM, Kim MS, Davis DB, McNally EM (2002) Myne-1, a spectrin repeat transmembrane protein of the myocyte inner nuclear membrane, interacts with lamin A/C. J Cell Sci 115(Pt 1):61–70
147. Mislow JM, Holaska JM, Kim MS, Lee KK, Segura-Totten M, Wilson KL, McNally EM (2002) Nesprin-1alpha self-associates and binds directly to emerin and lamin A in vitro. FEBS Lett 525(1–3):135–140
148. Morimoto A, Shibuya H, Zhu X, Kim J, Ishiguro K, Han M, Watanabe Y (2012) A conserved KASH domain protein associates with telomeres, SUN1, and dynactin during mammalian meiosis. J Cell Biol 198(2):165–172. doi:10.1083/jcb.201204085
149. Salpingidou G, Smertenko A, Hausmanowa-Petrucewicz I, Hussey PJ, Hutchison CJ (2007) A novel role for the nuclear membrane protein emerin in association of the centrosome to the outer nuclear membrane. J Cell Biol 178(6):897–904. doi:10.1083/jcb.200702026
150. Buch C, Lindberg R, Figueroa R, Gudise S, Onischenko E, Hallberg E (2009) An integral protein of the inner nuclear membrane localizes to the mitotic spindle in mammalian cells. J Cell Sci 122(Pt 12):2100–2107. doi:10.1242/jcs.047373
151. Gudise S, Figueroa RA, Lindberg R, Larsson V, Hallberg E (2011) Samp1 is functionally associated with the LINC complex and A-type lamina networks. J Cell Sci 124(Pt 12):2077–2085. doi:10.1242/jcs.078923
152. Borrego-Pinto J, Jegou T, Osorio DS, Auradé F, Gorjánácz M, Koch B, Mattaj IW, Gomes ER (2012) Samp1 is a component of TAN lines and is required for nuclear movement. J Cell Sci 125(Pt 5):1099–1105. doi:10.1242/jcs.087049
153. Luxton GW, Gomes ER, Folker ES, Vintinner E, Gundersen GG (2010) Linear arrays of nuclear envelope proteins harness retrograde actin flow for nuclear movement. Science 329(5994):956–959. doi:10.1126/science.1189072
154. Stewart-Hutchinson PJ, Hale CM, Wirtz D, Hodzic D (2008) Structural requirements for the assembly of LINC complexes and their function in cellular mechanical stiffness. Exp Cell Res 314(8):1892–1905. doi:10.1016/j.yexcr.2008.02.022
155. Scherthan H (2001) A bouquet makes ends meet. Nat Rev Mol Cell Biol 2(8):621–627. doi:10.1038/35085086
156. Miki F, Kurabayashi A, Tange Y, Okazaki K, Shimanuki M, Niwa O (2004) Two-hybrid search for proteins that interact with Sad1 and Kms1, two membrane-bound components of the spindle pole body in fission yeast. Mol Genet Genomics 270(6):449–461. doi:10.1007/s00438-003-0938-8
157. Chikashige Y, Tsutsumi C, Yamane M, Okamasa K, Haraguchi T, Hiraoka Y (2006) Meiotic proteins bqt1 and bqt2 tether telomeres to form the bouquet arrangement of chromosomes. Cell 125(1):59–69. doi:10.1016/j.cell.2006.01.048
158. Shimanuki M, Miki F, Ding DQ, Chikashige Y, Hiraoka Y, Horio T, Niwa O (1997) A novel fission yeast gene, kms1+, is required for the formation of meiotic prophase-specific nuclear architecture. Mol Gen Genet 254(3):238–249
159. Penkner A, Tang L, Novatchkova M, Ladurner M, Fridkin A, Gruenbaum Y, Schweizer D, Loidl J, Jantsch V (2007) The nuclear envelope protein Matefin/SUN-1 is required for homologous pairing in C. elegans meiosis. Dev Cell 12(6):873–885. doi:10.1016/j.devcel.2007.05.004
160. McGee MD, Stagljar I, Starr DA (2009) KDP-1 is a nuclear envelope KASH protein required for cell-cycle progression. J Cell Sci 122(Pt 16):2895–2905. doi:10.1242/jcs.051607
161. Ottaviani A, Schluth-Bolard C, Rival-Gervier S, Boussouar A, Rondier D, Foerster AM, Morere J, Bauwens S, Gazzo S, Callet-Bauchu E, Gilson E, Magdinier F (2009) Identification of a perinuclear positioning element in human subtelomeres that requires A-type lamins and CTCF. EMBO J 28(16):2428–2436. doi:10.1038/emboj.2009.201
162. Gonzalez-Suarez I, Redwood AB, Gonzalo S (2009) Loss of A-type lamins and genomic instability. Cell Cycle 8(23):3860–3865

163. Khatau SB, Bloom RJ, Bajpai S, Razafsky D, Zang S, Giri A, Wu PH, Marchand J, Celedon A, Hale CM, Sun SX, Hodzic D, Wirtz D (2012) The distinct roles of the nucleus and nucleus-cytoskeleton connections in three-dimensional cell migration. Sci Rep 2:488. doi:10.1038/srep00488
164. Poh YC, Shevtsov SP, Chowdhury F, Wu DC, Na S, Dundr M, Wang N (2012) Dynamic force-induced direct dissociation of protein complexes in a nuclear body in living cells. Nat Commun 3:866. doi:10.1038/ncomms1873
165. Booth-Gauthier EA, Alcoser TA, Yang G, Dahl KN (2012) Force-induced changes in subnuclear movement and rheology. Biophys J 103(12):2423–2431. doi:10.1016/j.bpj.2012.10.039
166. Maniotis AJ, Bojanowski K, Ingber DE (1997) Mechanical continuity and reversible chromosome disassembly within intact genomes removed from living cells. J Cell Biochem 65(1):114–130
167. Ingber DE (2003) Mechanobiology and diseases of mechanotransduction. Ann Med 35(8):564–577
168. Ingber DE (2006) Cellular mechanotransduction: putting all the pieces together again. FASEB J 20(7):811–827. doi:10.1096/fj.05-5424rev
169. Moore KA, Polte T, Huang S, Shi B, Alsberg E, Sunday ME, Ingber DE (2005) Control of basement membrane remodeling and epithelial branching morphogenesis in embryonic lung by Rho and cytoskeletal tension. Dev Dyn 232(2):268–281. doi:10.1002/dvdy.20237
170. Lammerding J, Lee RT (2005) The nuclear membrane and mechanotransduction: impaired nuclear mechanics and mechanotransduction in lamin A/C deficient cells. Novartis Found Symp 264:264–273, discussion 273–268
171. Brosig M, Ferralli J, Gelman L, Chiquet M, Chiquet-Ehrismann R (2010) Interfering with the connection between the nucleus and the cytoskeleton affects nuclear rotation, mechanotransduction and myogenesis. Int J Biochem Cell Biol 42(10):1717–1728. doi:10.1016/j.biocel.2010.07.001
172. Ho CY, Jaalouk DE, Vartiainen MK, Lammerding J (2013) Lamin A/C and emerin regulate MKL1-SRF activity by modulating actin dynamics. Nature 497(7450):507–511. doi:10.1038/nature12105
173. Dey P (2009) Nuclear margin irregularity and cancer: a review. Anal Quant Cytol Histol 31(5):345–352
174. Vigouroux C, Auclair M, Dubosclard E, Pouchelet M, Capeau J, Courvalin JC, Buendia B (2001) Nuclear envelope disorganization in fibroblasts from lipodystrophic patients with heterozygous R482Q/W mutations in the lamin A/C gene. J Cell Sci 114(Pt 24):4459–4468
175. Muchir A, Medioni J, Laluc M, Massart C, Arimura T, van der Kooi AJ, Desguerre I, Mayer M, Ferrer X, Briault S, Hirano M, Worman HJ, Mallet A, Wehnert M, Schwartz K, Bonne G (2004) Nuclear envelope alterations in fibroblasts from patients with muscular dystrophy, cardiomyopathy, and partial lipodystrophy carrying lamin A/C gene mutations. Muscle Nerve 30(4):444–450. doi:10.1002/mus.20122
176. Friedl P, Alexander S (2011) Cancer invasion and the microenvironment: plasticity and reciprocity. Cell 147(5):992–1009. doi:10.1016/j.cell.2011.11.016
177. Broers JL, Raymond Y, Rot MK, Kuijpers H, Wagenaar SS, Ramaekers FC (1993) Nuclear A-type lamins are differentially expressed in human lung cancer subtypes. Am J Pathol 143(1):211–220
178. Moss SF, Krivosheyev V, de Souza A, Chin K, Gaetz HP, Chaudhary N, Worman HJ, Holt PR (1999) Decreased and aberrant nuclear lamin expression in gastrointestinal tract neoplasms. Gut 45(5):723–729
179. Venables RS, McLean S, Luny D, Moteleb E, Morley S, Quinlan RA, Lane EB, Hutchison CJ (2001) Expression of individual lamins in basal cell carcinomas of the skin. Br J Cancer 84(4):512–519. doi:10.1054/bjoc.2000.1632
180. Tilli CM, Ramaekers FC, Broers JL, Hutchison CJ, Neumann HA (2003) Lamin expression in normal human skin, actinic keratosis, squamous cell carcinoma and basal cell carcinoma. Br J Dermatol 148(1):102–109
181. Hudson ME, Pozdnyakova I, Haines K, Mor G, Snyder M (2007) Identification of differentially expressed proteins in ovarian cancer using high-density protein microarrays. Proc Natl Acad Sci U S A 104(44):17494–17499. doi:10.1073/pnas.0708572104

182. Willis ND, Wilson RG, Hutchison CJ (2008) Lamin A: a putative colonic epithelial stem cell biomarker which identifies colorectal tumours with a more aggressive phenotype. Biochem Soc Trans 36(Pt 6):1350–1353. doi:10.1042/bst0361350
183. Belt EJ, Fijneman RJ, van den Berg EG, Bril H, Delis-van Diemen PM, Tijssen M, van Essen HF, de Lange-de Klerk ES, Beliën JA, Stockmann HB, Meijer S, Meijer GA (2011) Loss of lamin A/C expression in stage II and III colon cancer is associated with disease recurrence. Eur J Cancer 47(12):1837–1845. doi:10.1016/j.ejca.2011.04.025
184. Wolf K, Wu YI, Liu Y, Geiger J, Tam E, Overall C, Stack MS, Friedl P (2007) Multi-step pericellular proteolysis controls the transition from individual to collective cancer cell invasion. Nat Cell Biol 9(8):893–904. doi:10.1038/ncb1616
185. Capo-chichi CD, Cai KQ, Simpkins F, Ganjei-Azar P, Godwin AK, Xu XX (2011) Nuclear envelope structural defects cause chromosomal numerical instability and aneuploidy in ovarian cancer. BMC Med 9:28. doi:10.1186/1741-7015-9-28
186. Wu Z, Wu L, Weng D, Xu D, Geng J, Zhao F (2009) Reduced expression of lamin A/C correlates with poor histological differentiation and prognosis in primary gastric carcinoma. J Exp Clin Cancer Res 28:8. doi:10.1186/1756-9966-28-8
187. Willis ND, Cox TR, Rahman-Casañs SF, Smits K, Przyborski SA, van den Brandt P, van Engeland M, Weijenberg M, Wilson RG, de Bruïne A, Hutchison CJ (2008) Lamin A/C is a risk biomarker in colorectal cancer. PLoS One 3(8):e2988. doi:10.1371/journal.pone.0002988
188. Foster CR, Robson JL, Simon WJ, Twigg J, Cruikshank D, Wilson RG, Hutchison CJ (2011) The role of Lamin A in cytoskeleton organization in colorectal cancer cells: a proteomic investigation. Nucleus 2(5):434–443. doi:10.4161/nucl.2.5.17775
189. Sjöblom T, Jones S, Wood LD, Parsons DW, Lin J, Barber TD, Mandelker D, Leary RJ, Ptak J, Silliman N, Szabo S, Buckhaults P, Farrell C, Meeh P, Markowitz SD, Willis J, Dawson D, Willson JK, Gazdar AF, Hartigan J, Wu L, Liu C, Parmigiani G, Park BH, Bachman KE, Papadopoulos N, Vogelstein B, Kinzler KW, Velculescu VE (2006) The consensus coding sequences of human breast and colorectal cancers. Science 314(5797):268–274. doi:10.1126/science.1133427
190. Stephens PJ, Tarpey PS, Davies H, Van Loo P, Greenman C, Wedge DC, Nik-Zainal S, Martin S, Varela I, Bignell GR, Yates LR, Papaemmanuil E, Beare D, Butler A, Cheverton A, Gamble J, Hinton J, Jia M, Jayakumar A, Jones D, Latimer C, Lau KW, McLaren S, McBride DJ, Menzies A, Mudie L, Raine K, Rad R, Chapman MS, Teague J, Easton D, Langerød A, Lee MT, Shen CY, Tee BT, Huimin BW, Broeks A, Vargas AC, Turashvili G, Martens J, Fatima A, Miron P, Chin SF, Thomas G, Boyault S, Mariani O, Lakhani SR, van de Vijver M, van't Veer L, Foekens J, Desmedt C, Sotiriou C, Tutt A, Caldas C, Reis-Filho JS, Aparicio SA, Salomon AV, Børresen-Dale AL, Richardson AL, Campbell PJ, Futreal PA, Stratton MR, OBCC (2012) The landscape of cancer genes and mutational processes in breast cancer. Nature 486(7403):400–404. doi:10.1038/nature11017
191. Doherty JA, Rossing MA, Cushing-Haugen KL, Chen C, Van Den Berg DJ, Wu AH, Pike MC, Ness RB, Moysich K, Chenevix-Trench G, Beesley J, Webb PM, Chang-Claude J, Wang-Gohrke S, Goodman MT, Lurie G, Thompson PJ, Carney ME, Hogdall E, Kjaer SK, Hogdall C, Goode EL, Cunningham JM, Fridley BL, Vierkant RA, Berchuck A, Moorman PG, Schildkraut JM, Palmieri RT, Cramer DW, Terry KL, Yang HP, Garcia-Closas M, Chanock S, Lissowska J, Song H, Pharoah PD, Shah M, Perkins B, McGuire V, Whittemore AS, Di Cioccio RA, Gentry-Maharaj A, Menon U, Gayther SA, Ramus SJ, Ziogas A, Brewster W, Anton-Culver H, Pearce C, Group AOCSM, Cancer ACS, OCAC (2010) ESR1/SYNE1 polymorphism and invasive epithelial ovarian cancer risk: an Ovarian Cancer Association Consortium study. Cancer Epidemiol Biomarkers Prev 19(1):245–250. doi:10.1158/1055-9965.epi-09-0729
192. Barboro P, Repaci E, D'Arrigo C, Balbi C (2012) The role of nuclear matrix proteins binding to matrix attachment regions (Mars) in prostate cancer cell differentiation. PLoS One 7(7):e40617. doi:10.1371/journal.pone.0040617
193. Malonia SK, Sinha S, Lakshminarasimhan P, Singh K, Jalota-Badhwar A, Rampalli S, Kaul-Ghanekar R, Chattopadhyay S (2011) Gene regulation by SMAR1: role in cellular homeostasis and cancer. Biochim Biophys Acta 1815(1):1–12. doi:10.1016/j.bbcan.2010.08.003

194. Stein GS, Lian JB, van Wijnen AJ, Stein JL, Javed A, Montecino M, Zaidi SK, Young D, Choi JY, Gutierrez S, Pockwinse S (2004) Nuclear microenvironments support assembly and organization of the transcriptional regulatory machinery for cell proliferation and differentiation. J Cell Biochem 91(2):287–302. doi:10.1002/jcb.10777
195. Bickmore WA, van Steensel B (2013) Genome architecture: domain organization of interphase chromosomes. Cell 152(6):1270–1284. doi:10.1016/j.cell.2013.02.001
196. Burke B, Stewart CL (2013) The nuclear lamins: flexibility in function. Nat Rev Mol Cell Biol 14(1):13–24. doi:10.1038/nrm3488
197. Valastyan S, Weinberg RA (2011) Tumor metastasis: molecular insights and evolving paradigms. Cell 147(2):275–292. doi:10.1016/j.cell.2011.09.024
198. Stoitzner P, Pfaller K, Stössel H, Romani N (2002) A close-up view of migrating Langerhans cells in the skin. J Invest Dermatol 118(1):117–125. doi:10.1046/j.0022-202x.2001.01631.x
199. Weigelin B, Bakker G-J, Friedl P (2012) Intravital third harmonic generation microscopy of collective melanoma cell invasion. Principles of interface guidance and microvesicle dynamics. IntraVital 1(1):32–43
200. Shankar J, Messenberg A, Chan J, Underhill TM, Foster LJ, Nabi IR (2010) Pseudopodial actin dynamics control epithelial-mesenchymal transition in metastatic cancer cells. Cancer Res 70(9):3780–3790. doi:10.1158/0008-5472.can-09-4439
201. Schoumacher M, Goldman RD, Louvard D, Vignjevic DM (2010) Actin, microtubules, and vimentin intermediate filaments cooperate for elongation of invadopodia. J Cell Biol 189(3):541–556. doi:10.1083/jcb.200909113
202. Tong Z, Balzer EM, Dallas MR, Hung WC, Stebe KJ, Konstantopoulos K (2012) Chemotaxis of cell populations through confined spaces at single-cell resolution. PLoS One 7(1):e29211. doi:10.1371/journal.pone.0029211
203. Booth-Gauthier EA, Du V, Ghibaudo M, Rape AD, Dahl KN, Ladoux B (2013) Hutchinson-Gilford progeria syndrome alters nuclear shape and reduces cell motility in three dimensional model substrates. Integr Biol (Camb) 5(3):569–577. doi:10.1039/c3ib20231c
204. Verstraeten VL, Ji JY, Cummings KS, Lee RT, Lammerding J (2008) Increased mechanosensitivity and nuclear stiffness in Hutchinson-Gilford progeria cells: effects of farnesyltransferase inhibitors. Aging Cell 7(3):383–393. doi:10.1111/j.1474-9726.2008.00382.x
205. Dahl KN, Scaffidi P, Islam MF, Yodh AG, Wilson KL, Misteli T (2006) Distinct structural and mechanical properties of the nuclear lamina in Hutchinson-Gilford progeria syndrome. Proc Natl Acad Sci U S A 103(27):10271–10276. doi:10.1073/pnas.0601058103
206. Kong L, Schäfer G, Bu H, Zhang Y, Klocker H (2012) Lamin A/C protein is overexpressed in tissue-invading prostate cancer and promotes prostate cancer cell growth, migration and invasion through the PI3K/AKT/PTEN pathway. Carcinogenesis 33(4):751–759. doi:10.1093/carcin/bgs022
207. Wandke C, Kutay U (2013) Enclosing chromatin: reassembly of the nucleus after open mitosis. Cell 152(6):1222–1225. doi:10.1016/j.cell.2013.02.046
208. Vargas JD, Hatch EM, Anderson DJ, Hetzer MW (2012) Transient nuclear envelope rupturing during interphase in human cancer cells. Nucleus 3(1):88–100. doi:10.4161/nucl.18954
209. De Vos WH, Houben F, Kamps M, Malhas A, Verheyen F, Cox J, Manders EM, Verstraeten VL, van Steensel MA, Marcelis CL, van den Wijngaard A, Vaux DJ, Ramaekers FC, Broers JL (2011) Repetitive disruptions of the nuclear envelope invoke temporary loss of cellular compartmentalization in laminopathies. Hum Mol Genet 20(21):4175–4186. doi:10.1093/hmg/ddr344
210. McCord RP, Nazario-Toole A, Zhang H, Chines PS, Zhan Y, Erdos MR, Collins FS, Dekker J, Cao K (2013) Correlated alterations in genome organization, histone methylation, and DNA-lamin A/C interactions in Hutchinson-Gilford progeria syndrome. Genome Res 23(2):260–269. doi:10.1101/gr.138032.112
211. Solovei I, Wang AS, Thanisch K, Schmidt CS, Krebs S, Zwerger M, Cohen TV, Devys D, Foisner R, Peichl L, Herrmann H, Blum H, Engelkamp D, Stewart CL, Leonhardt H, Joffe B (2013) LBR and lamin A/C sequentially tether peripheral heterochromatin and inversely regulate differentiation. Cell 152(3):584–598. doi:10.1016/j.cell.2013.01.009

212. Timp W, Feinberg AP (2013) Cancer as a dysregulated epigenome allowing cellular growth advantage at the expense of the host. Nat Rev Cancer 13(7):497–510. doi:10.1038/nrc3486
213. Polioudaki H, Kourmouli N, Drosou V, Bakou A, Theodoropoulos PA, Singh PB, Giannakouros T, Georgatos SD (2001) Histones H3/H4 form a tight complex with the inner nuclear membrane protein LBR and heterochromatin protein 1. EMBO Rep 2(10):920–925. doi:10.1093/embo-reports/kve199
214. Nili E, Cojocaru GS, Kalma Y, Ginsberg D, Copeland NG, Gilbert DJ, Jenkins NA, Berger R, Shaklai S, Amariglio N, Brok-Simoni F, Simon AJ, Rechavi G (2001) Nuclear membrane protein LAP2beta mediates transcriptional repression alone and together with its binding partner GCL (germ-cell-less). J Cell Sci 114(Pt 18):3297–3307
215. Somech R, Shaklai S, Geller O, Amariglio N, Simon AJ, Rechavi G, Gal-Yam EN (2005) The nuclear-envelope protein and transcriptional repressor LAP2beta interacts with HDAC3 at the nuclear periphery, and induces histone H4 deacetylation. J Cell Sci 118(Pt 17):4017–4025. doi:10.1242/jcs.02521
216. Haraguchi T, Holaska JM, Yamane M, Koujin T, Hashiguchi N, Mori C, Wilson KL, Hiraoka Y (2004) Emerin binding to Btf, a death-promoting transcriptional repressor, is disrupted by a missense mutation that causes Emery-Dreifuss muscular dystrophy. Eur J Biochem 271(5):1035–1045
217. Wilkinson FL, Holaska JM, Zhang Z, Sharma A, Manilal S, Holt I, Stamm S, Wilson KL, Morris GE (2003) Emerin interacts in vitro with the splicing-associated factor, YT521-B. Eur J Biochem 270(11):2459–2466
218. Holaska JM, Lee KK, Kowalski AK, Wilson KL (2003) Transcriptional repressor germ cell-less (GCL) and barrier to autointegration factor (BAF) compete for binding to emerin in vitro. J Biol Chem 278(9):6969–6975. doi:10.1074/jbc.M208811200
219. Lu P, Takai K, Weaver VM, Werb Z (2011) Extracellular matrix degradation and remodeling in development and disease. Cold Spring Harb Perspect Biol 3(12). doi:10.1101/cshperspect.a005058
220. Di Carlo D, Tse HT, Gossett DR (2012) Introduction: why analyze single cells? Methods Mol Biol 853:1–10. doi:10.1007/978-1-61779-567-1_1
221. Zhang W, Kai K, Choi DS, Iwamoto T, Nguyen YH, Wong H, Landis MD, Ueno NT, Chang J, Qin L (2012) Microfluidics separation reveals the stem-cell-like deformability of tumor-initiating cells. Proc Natl Acad Sci U S A 109(46):18707–18712. doi:10.1073/pnas.1209893109
222. Capo-chichi CD, Cai KQ, Testa JR, Godwin AK, Xu XX (2009) Loss of GATA6 leads to nuclear deformation and aneuploidy in ovarian cancer. Mol Cell Biol 29(17):4766–4777. doi:10.1128/mcb.00087-09
223. Agrelo R, Setien F, Espada J, Artiga MJ, Rodriguez M, Pérez-Rosado A, Sanchez-Aguilera A, Fraga MF, Piris MA, Esteller M (2005) Inactivation of the lamin A/C gene by CpG island promoter hypermethylation in hematologic malignancies, and its association with poor survival in nodal diffuse large B-cell lymphoma. J Clin Oncol 23(17):3940–3947. doi:10.1200/jco.2005.11.650
224. Wang Y, Wu R, Cho KR, Thomas DG, Gossner G, Liu JR, Giordano TJ, Shedden KA, Misek DE, Lubman DM (2009) Differential protein mapping of ovarian serous adenocarcinomas: identification of potential markers for distinct tumor stage. J Proteome Res 8(3):1452–1463. doi:10.1021/pr800820z
225. Skvortsov S, Schäfer G, Stasyk T, Fuchsberger C, Bonn GK, Bartsch G, Klocker H, Huber LA (2011) Proteomics profiling of microdissected low- and high-grade prostate tumors identifies Lamin A as a discriminatory biomarker. J Proteome Res 10(1):259–268. doi:10.1021/pr100921j
226. Alfonso P, Cañamero M, Fernández-Carbonié F, Núñez A, Casal JI (2008) Proteome analysis of membrane fractions in colorectal carcinomas by using 2D-DIGE saturation labeling. J Proteome Res 7(10):4247–4255. doi:10.1021/pr800152u
227. Bengtsson S, Krogh M, Szigyarto CA, Uhlen M, Schedvins K, Silfverswärd C, Linder S, Auer G, Alaiya A, James P (2007) Large-scale proteomics analysis of human ovarian cancer for biomarkers. J Proteome Res 6(4):1440–1450. doi:10.1021/pr060593y

228. Lim SO, Park SJ, Kim W, Park SG, Kim HJ, Kim YI, Sohn TS, Noh JH, Jung G (2002) Proteome analysis of hepatocellular carcinoma. Biochem Biophys Res Commun 291(4):1031–1037. doi:10.1006/bbrc.2002.6547
229. Sun S, Xu MZ, Poon RT, Day PJ, Luk JM (2010) Circulating Lamin B1 (LMNB1) biomarker detects early stages of liver cancer in patients. J Proteome Res 9(1):70–78. doi:10.1021/pr9002118
230. Coradeghini R, Barboro P, Rubagotti A, Boccardo F, Parodi S, Carmignani G, D'Arrigo C, Patrone E, Balbi C (2006) Differential expression of nuclear lamins in normal and cancerous prostate tissues. Oncol Rep 15(3):609–613
231. Li L, Du Y, Kong X, Li Z, Jia Z, Cui J, Gao J, Wang L, Xie K (2013) Lamin B1 is a novel therapeutic target of betulinic acid in pancreatic cancer. Clin Cancer Res. doi:10.1158/1078-0432.ccr-12-3630
232. Somech R, Gal-Yam EN, Shaklai S, Geller O, Amariglio N, Rechavi G, Simon AJ (2007) Enhanced expression of the nuclear envelope LAP2 transcriptional repressors in normal and malignant activated lymphocytes. Ann Hematol 86(6):393–401. doi:10.1007/s00277-007-0275-9
233. Martínez N, Alonso A, Moragues MD, Pontón J, Schneider J (1999) The nuclear pore complex protein Nup88 is overexpressed in tumor cells. Cancer Res 59(21):5408–5411
234. Agudo D, Gómez-Esquer F, Martínez-Arribas F, Núñez-Villar MJ, Pollán M, Schneider J (2004) Nup88 mRNA overexpression is associated with high aggressiveness of breast cancer. Int J Cancer 109(5):717–720. doi:10.1002/ijc.20034
235. Brustmann H, Hager M (2009) Nucleoporin 88 expression in normal and neoplastic squamous epithelia of the uterine cervix. Ann Diagn Pathol 13(5):303–307. doi:10.1016/j.anndiagpath.2009.05.005
236. Emterling A, Skoglund J, Arbman G, Schneider J, Evertsson S, Carstensen J, Zhang H, Sun XF (2003) Clinicopathological significance of Nup88 expression in patients with colorectal cancer. Oncology 64(4):361–369, doi:70294
237. Gould VE, Orucevic A, Zentgraf H, Gattuso P, Martinez N, Alonso A (2002) Nup88 (karyoporin) in human malignant neoplasms and dysplasias: correlations of immunostaining of tissue sections, cytologic smears, and immunoblot analysis. Hum Pathol 33(5):536–544
238. Knoess M, Kurz AK, Goreva O, Bektas N, Breuhahn K, Odenthal M, Schirmacher P, Dienes HP, Bock CT, Zentgraf H, zur Hausen A (2006) Nucleoporin 88 expression in hepatitis B and C virus-related liver diseases. World J Gastroenterol 12(36):5870–5874
239. Zhang ZY, Zhao ZR, Jiang L, Li JC, Gao YM, Cui DS, Wang CJ, Schneider J, Wang MW, Sun XF (2007) Nup88 expression in normal mucosa, adenoma, primary adenocarcinoma and lymph node metastasis in the colorectum. Tumour Biol 28(2):93–99. doi:10.1159/000099154
240. Xu S, Powers MA (2009) Nuclear pore proteins and cancer. Semin Cell Dev Biol 20(5):620–630. doi:10.1016/j.semcdb.2009.03.003
241. Cervoni N, Detich N, Seo SB, Chakravarti D, Szyf M (2002) The oncoprotein Set/TAF-1beta, an inhibitor of histone acetyltransferase, inhibits active demethylation of DNA, integrating DNA methylation and transcriptional silencing. J Biol Chem 277(28):25026–25031. doi:10.1074/jbc.M202256200
242. Hernández P, Solé X, Valls J, Moreno V, Capellá G, Urruticoechea A, Pujana MA (2007) Integrative analysis of a cancer somatic mutome. Mol Cancer 6:13. doi:10.1186/1476-4598-6-13
243. Capo-chichi CD, Cai KQ, Smedberg J, Ganjei-Azar P, Godwin AK, Xu XX. Loss of A-type lamin expression compromises nuclear envelope integrity in breast cancer. Chin J Cancer. 2011 Jun;30(6):415–425. http://www.ncbi.nlm.nih.gov/pubmed/21627864
244. Wazir U, Ahmed MH, Bridger JM, Harvey A, Jiang WG, Sharma AK, Mokbel K. The clinicopathological significance of lamin A/C, lamin B1 and lamin B receptor mRNA expression in human breast cancer. Cell Mol Biol Lett. 2013 Dec;18(4):595-611. doi: 10.2478/s11658-013-0109-9. Epub 2013 Nov 30. http://www.ncbi.nlm.nih.gov/pubmed/24293108

Author's personal copy

Review

CellPress

Broken nuclei – lamins, nuclear mechanics, and disease

Patricia M. Davidson[1] and Jan Lammerding[2]

[1] Weill Institute for Cell and Molecular Biology, Cornell University, 526 Campus Road, Ithaca, NY 14853, USA
[2] Department of Biomedical Engineering/Weill Institute for Cell and Molecular Biology, Cornell University, 526 Campus Road, Ithaca, NY 14853, USA

Mutations in lamins, which are ubiquitous nuclear intermediate filaments, lead to a variety of disorders including muscular dystrophy and dilated cardiomyopathy. Lamins provide nuclear stability, help connect the nucleus to the cytoskeleton, and can modulate chromatin organization and gene expression. Nonetheless, the diverse functions of lamins remain incompletely understood. We focus here on the role of lamins on nuclear mechanics and their involvement in human diseases. Recent findings suggest that lamin mutations can decrease nuclear stability, increase nuclear fragility, and disturb mechanotransduction signaling, possibly explaining the muscle-specific defects in many laminopathies. At the same time, altered lamin expression has been reported in many cancers, where the resulting increased nuclear deformability could enhance the ability of cells to transit tight interstitial spaces, thereby promoting metastasis.

Lamins and disease

Since the discovery in 1999 that mutations in the nuclear envelope proteins lamin A/C cause Emery–Dreifuss muscular dystrophy (EDMD) [1] lamins and lamin-associated proteins have garnered increasing interest in the scientific and medical community, resulting in the discovery of over 450 disease-associated lamin mutations to date (see http://www.umd.be/LMNA/). These 'laminopathies' include EDMD, dilated cardiomyopathy (DCM), Dunnigan-type familial partial lipodystrophy (FPLD), and Hutchinson–Gilford progeria syndrome (HGPS), a premature aging disorder [2]. Given that lamins A/C are expressed in nearly all cells and tissues, the high degree of tissue-specificity and the broad range of diseases caused by different mutations in the same gene are perplexing. Despite extensive research efforts, the molecular mechanisms underlying laminopathies remain to be fully explained.

In addition to providing structural support to the nucleus, lamins also contribute to nucleo-cytoskeletal coupling, chromatin organization, epigenetic modifications, DNA replication, transcriptional regulation and repair, and responses to oxidative stress [2]. In this review we focus on the mechanical aspects of lamin functions, including governing nuclear deformability and fragility, physically connecting the nucleus and the cytoskeleton, and contributing to mechanotransduction signaling – in other words, the ability of the cells to respond to mechanical stimuli. These functions could be particularly relevant to muscular dystrophies and cardiomyopathies caused by mutations in lamins A/C. At the same time, striking new reports suggest that nuclear deformability, which is modulated by the expression of specific lamin isoforms, can constitute a rate-limiting factor in the ability of cells to pass through micrometer-sized constrictions in 3D environments [3,4], and this has important implications for cancer progression, immune cell function, and development.

Lamins – primary components of the nuclear lamina

The lamina is a dense protein meshwork underlying the inner nuclear membrane that is composed of lamins and lamina-associated proteins. In somatic cells the predominant lamins are lamins A and C (referred to as A-type lamins), resulting from alternative splicing of the *LMNA* gene, and the B-type lamins, lamin B1 and B2. Although most differentiated cells express at least one A-type lamin, embryonic stem cells, the lower layer of epidermis [5], and the central nervous system [6] produce little to no lamin A. These latter findings may explain why the central nervous system is typically spared in diseases arising from *LMNA* mutations. By contrast, striated muscles and many mesenchymal cells have particularly high levels of A-type lamins, and this may contribute to their prominent involvement in many laminopathies.

Unlike A-type lamins, B-type lamins are expressed by all cells throughout development. B-type lamins were previously considered to be essential for cell viability, based on knockdown studies in human cells [7] and *Caenorhabditis elegans* [8], but recent studies indicate that, at least in mice, B-type lamins are dispensable in many cell types, including embryonic stem cells [9,10] and skin cells [11]. Nonetheless, lamins B1 and B2 are necessary for organogenesis [9], and mice lacking lamins B1 and/or B2 die shortly after birth with severe defects in neuronal development and migration [12]. These contrasting findings may reflect changes in experimental conditions (acute knockdown in the human and *C. elegans* cells versus

Corresponding author: Lammerding, J. (jan.lammerding@cornell.edu).
Keywords: protein assembly/structure; cell mechanics; gene regulation; cytoskeleton; laminopathy.

0962-8924/$ – see front matter
© 2013 Elsevier Ltd. All rights reserved. http://dx.doi.org/10.1016/j.tcb.2013.11.004

Author's personal copy

selection of stable lamin B-deficient embryonic stem cells) or they may result from cell- or species-specific differences. Regardless, the findings consistently point to an important role of B-type lamins in organ development, particularly the brain, and should stimulate further research into the function of lamins during tissue development. A growing number of reports further suggest an involvement of lamin B1 in regulating cellular senescence [13]. B-type lamins have recently been linked to two diseases, adult-onset leukodystrophy, caused by a duplication of the *LMNB1* gene [14], and acquired partial lipodystrophy (Barraquer–Simons syndrome) arising from mutations in the *LMNB2* gene [15]. Nonetheless, the number of identified disease-causing mutations remains far fewer than for lamins A/C, suggesting that many lamin B mutations may result in embryonic lethality in humans.

Structural organization of nuclear lamins

Lamins, which are type V intermediate filaments, assemble into a dense network in the nuclear lamina (Figure 1). Lamins A and C, however, are also present in the nuclear interior [16]. Owing to the difficulty of imaging the chromatin- and nuclear membrane-associated lamina at high resolution *in situ*, and the challenge of accurately reconstituting the nuclear envelope environment *in vitro*, the ultrastructural organization of the nuclear lamina in mammalian cells remains incompletely understood. Advances in cryo-electron tomography may eventually enable more

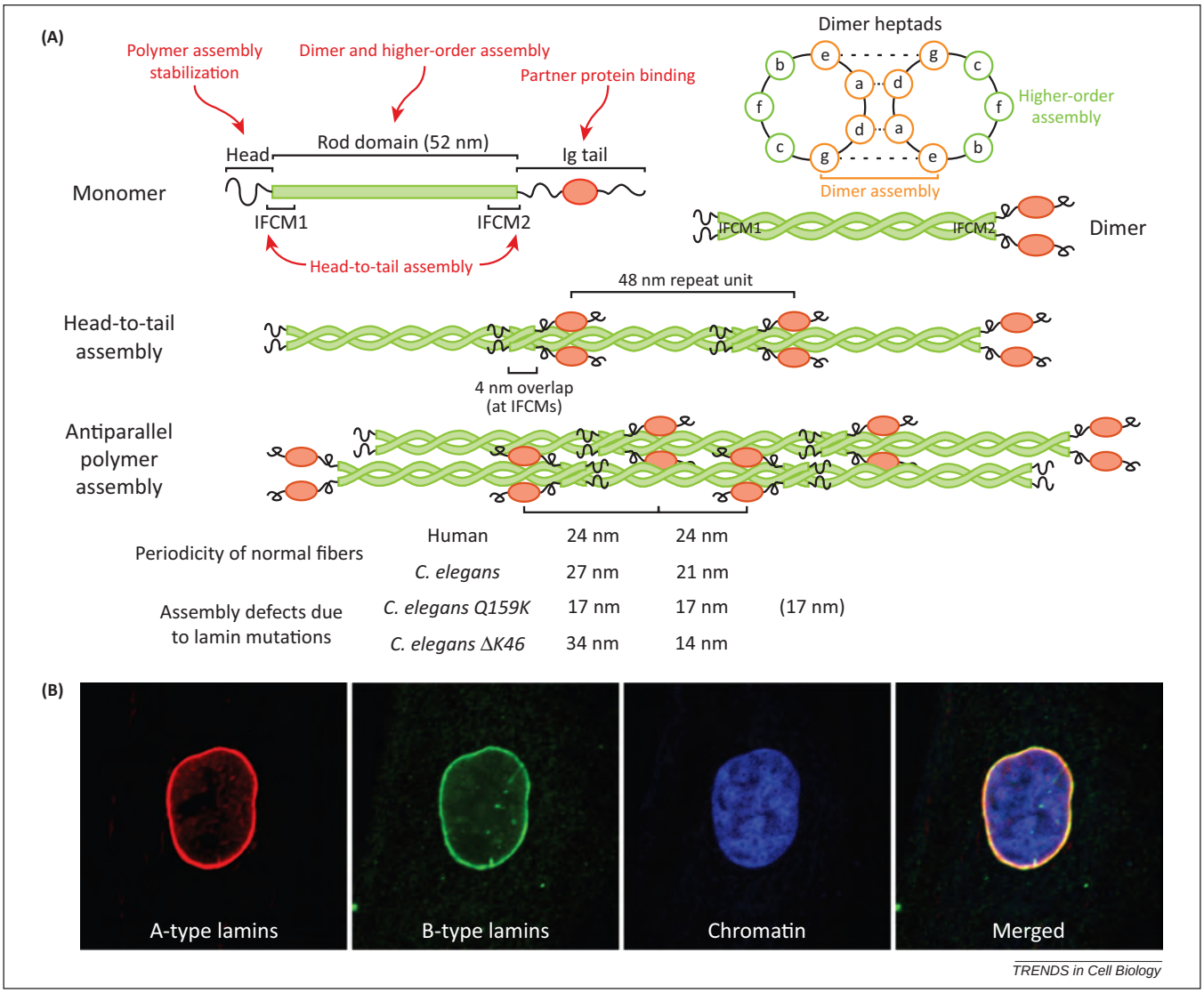

Figure 1. Lamin assembly and defects caused by lamin mutations. **(A)** Experiments with mutated and truncated lamins suggest that different parts of the lamin proteins play distinct roles in lamin assembly (red text). Two parallel lamin monomers (top left) form dimers (top right) through coiled-coil interaction of the heptad repeats in their central rod domains. These dimers assemble head-to-tail by overlapping their rod domains at the two intermediate filament (IF) consensus motifs (IFCM). The head-to-tail assemblies form non-polar protofilaments composed of two antiparallel polymers which then laterally assemble to form mature filaments (and paracrystals) with specific repeat units that are visible by electron microscopy and have been identified as the site of the globular immunoglobulin (Ig)-fold motif. Defects in lamin assembly can be identified *in vitro* by changes in the spacing of the repeat unit, as demonstrated for two mutants in *Caenorhabditis elegans* (bottom) or by failure to form lamin filaments or paracrystals. Note that, in the case of the Q159K mutation, it is likely that the spacing is 17/17/17, approximately corresponding to the 48 nm repeat unit, indicating a combination of three overlapping polymers instead of two. Inset, top right: a cross-sectional view of the heptad repeats of the coiled coil illustrates how the inner amino acids play a role in dimer assembly, whereas amino acids that point outwards can affect higher-order assembly. **(B)** Immunofluorescence images of human skin fibroblasts stained for lamins A/C (red), B-type lamins (green), and DNA (blue).

Author's personal copy

accurate visualization of the nuclear lamina in somatic cells [17]. Ectopic expression of human lamins in *Xenopus* oocytes indicates that A-type lamins form a thick (up to 100 nm) network and that B-type lamins form a thin fibrous meshwork closely associated with the inner nuclear membrane, likely due to their farnesyl lipid anchor [18,19] (see Box 1 for a comparison of the common animal models used to study lamins). Although A-type and B-type lamins can form mixed polymers during *in vitro* assembly [20], immunofluorescence and photobleaching studies suggest that A- and B-type lamins form separate but overlapping networks in somatic cells [21]. Even lamins A and C segregate and assemble as homodimers *in vivo*, despite their ability to form heterodimers *in vitro* [22]. Whether the diverse lamin networks are interpenetrating or simply adjacent remains to be determined, as well as to what extent specific lamins can compensate for one another. Mice that express only prelamin A, only lamin C, or only mature lamin A lack obvious disease phenotypes [23,24], and in *Drosophila* ectopic expression of an A-type lamin can compensate for loss of B-type lamins in cyst stem cells [25], indicating that lamins may have (partially) redundant or overlapping roles. However, unlike lamin A, ectopic expression of lamin C only partially rescues the native stiffness of lamin A/C-deficient cells [26], suggesting a more important role for lamin A in nuclear stability.

Box 1. Common animal models for the study of lamins

***Xenopus* oocytes.** In the large amphibian oocytes, which express only a B-type lamin (lamin LIII), the lamina lacks the tight association with chromatin seen in somatic cells, allowing easy access to the nuclear lamina and isolation for structural observation by electron microscopy. Its native lamina is organized into orthogonal filaments 10.5 nm wide and spaced 52 nm apart [107]. Lamins from other species ectopically expressed in amphibian oocytes assemble into a nuclear lamina, thereby enabling ultrastructural analysis. *Xenopus* oocytes currently provide the only model in which the *in vivo* lamina structure can be studied.

***Caenorhabditis elegans*.** These worms express a single lamin, Ce-lamin, that is functionally similar to both A- and B-type lamins [108]. Ce-lamin can be assembled into 10 nm filaments *in vitro*, resembling the organization of the *Xenopus* lamina, although it has been suggested that the 10 nm filaments obtained *in vitro* may represent a transitory phase that remains stable only under specific conditions [108]. The effects of specific lamin mutations in various tissues and their functional consequences can be assessed *in vivo* [58].

***Drosophila*.** Flies express two lamin proteins, A-type lamin C and B-type lamin Dm0 [109]. Human lamins expressed in *Drosophila* localize correctly, and many protein interactions are conserved. Many human laminopathies can be modeled by introducing corresponding mutations into *Drosophila* lamin C. Effects on nuclear structure and organization, as well as functional consequences such as locomotion and lethality, can be assessed in larval and adult animals [109].

***Mus musculus*.** Mice provide important mammalian models to study laminopathies, including *Lmna* mutations causing DCM (N195K, H222P), EDMD (M371K), HGPS (G608G, L530P), and Charcot–Marie–Tooth disease (R298C), as well as various models lacking specific lamin isoforms. The frequently used lamin A/C-null model ($Lmna^{-/-}$), which develops skeletal and cardiac defects, was recently found to express a short (54 kDa) fragment of A-type lamin by skipping exons 8–11 [110]. In a newer *Lmna*-null mouse model [111], homozygous mice develop more severe phenotypes whereas heterozygotes remain healthy, implying residual function and mild toxicity of the LmnaΔ8–11 fragment. However, ectopic expression of wild type lamin A in the original $Lmna^{+/-}$ cells completely rescues nuclear stiffness in these cells [43], indicating that the LmnaΔ8–11 fragment has no dominant-negative effect on nuclear mechanics. Although mouse models enable the study of the effect of human lamin mutations in mammals, many models require homozygous expression of the mutant lamin, unlike the often heterozygous expression in human laminopathy patients.

Lamin binding partners

For A-type lamins at least 54 binding-partners have been identified to date; for the less-studied lamins B1 and B2 a combined 25 partners have been reported, some of which are also common to A-type lamins [27]. As a note of caution, some of the reported interactions may be indirect or might not occur under physiological conditions, and expression of many binding partners is likely cell type-specific [27,28]. Many nuclear envelope proteins and potential lamin-binding partners are still incompletely characterized, and new partners continue to be discovered. Recent examples include Samp1 [29], MLIP [30], and SLAP75 [31]. Broadly speaking, lamin binding partners can be categorized into structural proteins (such as actin, nesprin, SUN proteins, and titin) and signaling molecules and transcription factors (e.g., pRb, ERK1/2, c-Fos, and SREBP), although several proteins may possess both structural and regulatory functions. Importantly, interaction between lamins and lamin-binding partners can take place at the nuclear envelope and/or the nuclear interior, and this may provide an additional mechanism to regulate interactions. For a comprehensive overview of lamin binding partners and their diverse functions see a recent review [27].

Broken nuclei lead to broken hearts (and muscle) – the effect of lamin mutations

It remains unclear how mutations in lamins, which are nearly ubiquitously expressed, can lead to often highly tissue-specific disorders [2]. The 'structural hypothesis' suggests that lamin mutations increase nuclear fragility, resulting in cell death and progressive failure in tissues such as muscle that are exposed to repetitive mechanical stress. The 'gene regulation hypothesis' proposes that lamin mutations interfere with tissue-specific genes: lamin mutations may inhibit binding to tissue-specific factors [27] or lead to abnormal gene activation/silencing during differentiation [32]. A third hypothesis proposes that lamin mutations impair stem cell function: mutations may cause abnormal differentiation or depletion of the stem cell niche through defects in proliferation, survival, or differentiation efficiency [25]. These hypotheses are not mutually exclusive, and it is likely that laminopathies arise from a combination of defects in lamin function [2]. For example, abnormal differentiation could be related to dysregulated signaling pathways and disturbed chromatin organization, but also to mechanical defects such as impaired nucleocytoskeletal coupling [33]. Recent results provide support for each of these hypotheses, as detailed below.

Lamin mutations can reduce nuclear stability

Nuclear deformability is largely determined by nuclear lamina composition [34–36] and chromatin organization [37,38], which are sensitive to changes in lamin expression [39]. Consequently, expression levels of lamins A (and C) can help to predict nuclear deformability, with increasing

Author's personal copy

Table 1. Consequences of lamin mutations for nuclear structure and mechanics

Evidence of altered nuclear stability	Experimental system	Refs
Nuclear rupture	*In vitro*: in patient fibroblasts carrying mutations that lead to HGPS, FPLD, RD, and HCM *In vivo*: in the heart tissue of human and mouse carrying DCM mutations	[41,48,49]
Stiffer nuclei	*In vitro*: in HGPS patient cells and in *Xenopus* oocytes overexpressing lamin A with a mutation that causes HGPS	[19,50]
Softer nuclei	*In vitro*: in fibroblasts carrying mutations that lead to DCM and EDMD *In situ*: in *Drosophila* larval muscle expressing dominant-negative lamin mutations	[43]
Elongated nuclei *in vivo*	In the heart tissue of human, mice, and flies carrying DCM mutations	[43–47]
Defects in lamin assembly	*In vitro* assembly of lamin filaments and paracrystals from recombinant lamin	[43,56–59]

levels corresponding to stiffer and more viscous nuclei [26,40]. Lamin A/C-deficient nuclei are not only more deformable but are also more fragile: lamin A/C-deficient cells show spontaneous transient nuclear rupture [41] and are more susceptible to nuclear breakage and cell death when exposed to mechanical stress [36]. B-type lamins undoubtedly play an important role in nuclear structure and contribute to nuclear shape and stability, particularly in cells lacking A-type lamins. However, in cells expressing both types of lamins, levels of A-type lamins correlate more strongly with nuclear stiffness than B-type lamins [26,40], suggesting that lamins A and C play a more dominant role in determining nuclear stiffness. This functional difference may be due to different structural properties of the diverse lamin networks because experiments ectopically expressing human lamins in *Xenopus* oocytes found that A-type lamins assembled into substantially thicker networks than B-type lamins [42]. In addition to lamin content, several other factors may influence nuclear deformability by affecting the organization of the lamin network, including the phosphorylation status of lamins and the structural contribution of lamin-binding proteins.

Although earlier studies were directed at cells lacking specific lamins, techniques to assess nuclear mechanics and fragility (e.g., micropipette aspiration, microindentation, and substrate strain application) are now finding widespread application to investigate the effects of specific disease-causing lamin mutations. A recent study of a broad panel of lamin A mutants expressed in lamin A/C-deficient cells found that, whereas reintroduction of wild type lamin A completely restored nuclear stiffness to levels of wild type cells, many mutations linked to EDMD and DCM failed to restore nuclear stiffness; by contrast, FPLD mutations were functionally indistinguishable from wild type lamin A [43]. *In vivo*, muscle tissue from EDMD patients [44], and from mouse [45,46] and *Drosophila* models of EDMD and DCM [43,47], contain severely elongated nuclei, indicative of reduced nuclear stiffness. Importantly, lamin mutations responsible for striated muscle disease also increase nuclear envelope fragility. Cultured laminopathy patient fibroblasts have higher rates of nuclear rupture *in vitro* [41], and skeletal muscle and cardiac tissue of mice and of human patients carrying EDMD and DCM mutations, respectively, show anecdotal evidence of nuclear rupture *in vivo*, including mitochondria inside the nucleus [48] and discontinuities in the nuclear envelope visible by electron microscopy [49]. Taken together, these results point to a disease mechanism by which lamin mutations cause muscle-specific disease by compromising nuclear envelope stability and integrity (Table 1), resulting in nuclear rupture and consequently cell death in tissues subjected to mechanical stress.

In contrast to the effects of EDMD- and DCM-causing mutations, lamin A mutations responsible for HGPS cause increased stiffness in HGPS patient cells [50,51] and when expressed in *Xenopus* oocytes [19]. Interestingly, fibroblasts from HGPS patients nonetheless have an increased susceptibility to mechanically induced cell death [50]. Increased sensitivity to mechanical stress is particularly relevant to vascular smooth muscle cells in HGPS because patients and mouse models exhibit progressive loss of vascular smooth-muscle cells in large arteries, which are subjected to repetitive vessel strains.

Lamin mutations cause defects in lamin assembly

The mechanical defects described above are likely caused by aberrations in nuclear lamina assembly. Similarly to other intermediate filament (IF) family members, lamins are composed of a mostly α-helical central rod domain flanked by a short N-terminal head and a long tail domain, which contains a globular immunoglobulin (Ig)-fold [52]. In contrast to cytoplasmic IFs, many questions remain regarding the higher-order assembly of nuclear lamins. Most *in vitro* studies have focused on lamins from *C. elegans* (Ce-lamin) which form filaments with a diameter of ~10 nm *in vitro*, resembling those observed in the lamina of *Xenopus* oocytes (Box 1). Mammalian lamins can be induced to assemble into various structures *in vitro*, ranging from short head-to-tail polymers and filaments to paracrystals, depending on the experimental conditions [43,52]. The physiological relevance of these varying lamin forms remains unclear.

Owing to the challenge of crystallizing filamentous proteins, crystallographic analysis has been restricted to smaller lamin fragments, including the coil 2B of lamin A/C [53] and lamin B1 [54], as well as the lamin A/C globular tail [55]. Combined with *in vitro* assembly experiments using lamin mutations and partial deletions, these studies indicate that the supramolecular assembly of lamins largely depends on interactions within the lamin rod domains and the N-terminal head domain [52]. These studies have recently been expanded to investigate the effect of specific mutations on lamin assembly. Mutations causing DCM, EDMD, or HGPS in the first IF consensus motif and in coil 2 of human [43] and *C. elegans* lamin [56–59] disturb lamin assembly, leading to shortened and irregular filament and paracrystal assembly *in vitro* and increased mobility and solubility of mutant lamins *in vivo* (Figure 1). The EDMD

Author's personal copy

and DCM-causing mutations in the lamin rod domain impair head-to-tail polymer assembly or lateral filament association rather than lamin dimerization [43], although some mutations could also disturb dimer formation [60,61]. Supporting the notion that EDMD and DCM mutations primarily affect higher-order assembly of lamins A/C, the crystal structure of coil2B was recently solved for two DCM mutations, and neither mutation altered the secondary structure of the wild type protein [62]. Intriguingly, studies with a fragment of the lamin A/C coil 2B domain, comprising a small portion of the tail (residues 328–398), suggest that, in addition to the typical left-handed heptad, lamins can form right-handed quindecad coiled-coils [63] such that during head-to-tail polymer formation the IF consensus motifs may 'unzip' from the heptad and latch onto the adjacent lamin dimer. Head-to-tail polymer assembly might therefore require that the IF consensus motifs can be easily disassembled, and mutations that increase heptad stability may impede higher-order assembly [60].

Although the rod and head domains are essential for lamin assembly, other regions are also important for proper protein function. The lamin A/C tail domain, including the globular Ig-fold, harbors most of the interaction sites for lamin-binding partners [27]. Specific mutations can affect the Ig-fold structure in distinct ways. Mutations causing striated muscle disease are typically located in the interior of the Ig-fold β-sandwich, which can destabilize the Ig-fold [55]. By contrast, mutations responsible for FPLD are clustered in a small region on the surface of the Ig-fold. The FPLD mutations, as shown for the R482W mutant, do not affect the crystal structure of the Ig-fold [64] but may instead impair interaction with specific binding partners such as SREBP1 [55]. Lastly, the HGPS mutation that results in a 50 amino acid deletion in the lamin A tail leads to stronger intramolecular binding, impeding molecular interactions that would require accessibility of the Ig-fold [65].

Lamin mutations can disrupt nucleo-cytoskeletal coupling

Although many lamin mutations that cause DCM and EDMD impair nuclear stability, other mutations have little or no effect on nuclear stiffness [43], suggesting that alternative mechanisms must contribute to the disease. One potential mechanism that has gained increasing prominence is the role of lamins in nucleo-cytoskeletal coupling through interactions with LINC (linker of nucleoskeleton to cytoskeleton complex) components. The LINC complex is composed of SUN protein trimers at the inner nuclear membrane that connect across the luminal space to nesprins proteins on the outer nuclear membrane, and these in turn can interact with various cytoskeletal components [66,67]. Intact LINC complex function was recently identified to be crucial for a multitude of cellular functions, including force transmission between the nucleus and the cytoskeleton [68], nuclear positioning in secretory epithelial cells [69], retrograde nuclear movement in migrating fibroblasts via transmembrane actin-associated nuclear (TAN) lines [70], positioning of synaptic nuclei in muscle fibers [71] and the retina [72], and cytoskeletal organization [36]. Many molecular details underlying LINC complex function, including its dynamic regulation, remain incompletely understood, and recent studies have implicated additional nuclear envelope proteins in nucleo-cytoskeletal coupling, including Samp1 [29,73] and emerin [74]. Lamins A/C can bind to SUN1 [75], SUN2 [76], Samp1 [73], emerin, and various nesprin isoforms [77], highlighting their importance in nucleo-cytoskeletal coupling, presumably by anchoring LINC complex components to the nuclear lamina and interior.

Loss of lamins A/C and mutations associated with striated muscle disease can interfere with coupling to SUN proteins [77,78], emerin [59,77], Klaroid (a *Drosophila* nesprin analog) [79], Nesprin-1 [78], Nesprin-2 [80], nuclear pore components [79], and DNA [81]. Conversely, other mutations increase binding to SUN [77] and emerin [82]. Consequently, loss of lamins A/C and lamin mutations responsible for EDMD and DCM can disrupt nucleo-cytoskeletal coupling and related functions. Cells carrying EDMD and DCM mutations have defective intracellular force transmission between the cytoskeleton and nucleus [43], and expression of EDMD and DCM mutations, but not of the FPLD mutation, prevents retrograde nuclear movement because TAN lines fail to anchor to the nucleus [83]. Lamins also contribute to proper cytoskeletal organization and lamin A/C-deficient cells have reduced cytoskeletal stiffness and disturbed cytoskeletal networks [36], similar to the defects observed in cells after LINC complex disruption. Evidence of impaired nucleo-cytoskeletal coupling can also be found in tissues from EDMD and DCM patients, and from mouse and *Drosophila* models, which display discontinuous neuromuscular junctions, reduced numbers of synaptic nuclei, abnormal clustering of nuclei, and sarcomere disorganization around the nucleus [44,78,84]. These aberrations could provide further explanation for the muscle-specific phenotype of particular laminopathies.

The role of B-type lamins in nucleo-cytoskeletal coupling is slowly emerging. Lamin B1-deficient cells have spontaneously rotating nuclei, indicating loss of nuclear anchoring, and lamin B1 and B2 are essential for neuronal migration during brain development, a process that involves nuclear movement along microtubules [15,85]. However, the underlying molecular defects remain unclear.

Lamins, mechanotransduction, and gene regulation

The cell nucleus has long been proposed to act as a cellular mechanosensor [86]. Thus, altered nucleo-cytoskeletal coupling and nuclear deformability resulting from lamin mutations may also affect the ability of cells to translate mechanical stimuli into biochemical signals, as evidenced by impaired activation of mechanosensitive genes in lamin A/C- and emerin-deficient cells *in vitro* [36,87] and *in vivo* [88]. However, it remains unclear whether the diminished mechanotransduction signaling results from impaired nuclear mechanosensing or from altered downstream signaling. On the one hand, disruption of nucleo-cytoskeletal coupling with dominant-negative nesprin and SUN protein constructs, which abolish nuclear deformation when cells are subjected to mechanical strain, has no effect on the mechanical activation of the genes impaired in lamin A/C-deficient cells [68], arguing against a role of the nucleus as

Author's personal copy

a mechanosensor. On the other hand, externally applied forces can alter intranuclear protein mobility [89,90], and depletion of lamins A/C prevents force-induced dissociation of protein complexes inside Cajal bodies [89]. A recent report further found that exposing isolated nuclei to shear stress causes partial unfolding of the lamin A/C Ig-fold, exposing a buried cysteine, and this could trigger further signaling events [40]. Furthermore, the ratio of A-type lamins to B-type lamins in cells and tissues strongly correlates with the overall stiffness of the surrounding tissue, with most of the effect being attributed to higher levels of A-type lamins in response to increased tissue stiffness [40]; *in vitro*, increasing substrate stiffness results in higher levels of lamins A/C and suppresses their phosphorylation [40], and this could further increase nuclear stiffness. These findings support the notion that applied forces can directly induce structural changes and signaling inside the nucleus, with the nucleus and the nuclear lamina in particular playing a central role in cellular mechanosensing and adaptation of cells to their mechanical environment. Interestingly, loss of lamin A/C or mutations leading to emerin mislocalization result in impaired intracellular localization of the mechanosensitive transcriptional cofactor myocardin-related transcription factor A (MRTF-A) which plays important roles in cardiac development and function [91]. This effect was caused by dysregulation of the actin-polymerizing function of emerin at the nuclear envelope, affecting nuclear (and cytoskeletal) actin dynamics that are crucial in regulating MRTF-A intracellular localization, and impairing activation of MRTF-A/SRF downstream genes [91].

Lamins may also modulate gene expression independently of mechanical stimulation because lamins A/C associate with several transcriptional regulators, including c-Fos, ERK1/2, SREBP1, and pRb [27]. Mutations and (functional) loss of lamins can affect intranuclear localization and stability of these transcription factors as well as the affinity of lamins for specific binding partners. In addition, lamins can modulate gene expression by controlling gene positioning through lamina-associated domains (LADs), which may control the silencing and activation of tissue-specific genes [92]. A detailed discussion of the various gene-regulatory roles of lamins can be found elsewhere [2,27].

Given these facts, it is not surprising that lamin mutations can disturb numerous important signaling pathways: striated muscle disease mutations result in abnormal activation of mitogen-activated protein kinases (MAPK) ERK [45], JNK [93], and p38α [94], as well as target of rapamycin (mTOR) [95,96]; HGPS mutations cause abnormalities in the Wnt pathway [97] and SIRT1 activity [98]. The identification of abnormal signaling pathways provides attractive targets for the development of therapies for laminopathies: treatments with MAPK inhibitors [45,93,94] or rapamycin [95,96] have already been shown to improve phenotypes in EDMD and DCM mouse models. For patients with HGPS, clinical trials with farnesyltransferase inhibitors (FTIs), statins, and bisphosphonates, aimed at modulating the abnormal processing of mutant lamin A, are currently underway [99]. An initial study with farnesyltransferase inhibitors resulted in modestly improved cardiovascular symptoms but did not rescue the stunted growth of the patients [100]. Although the various therapeutic approaches may not always address the root cause of the disease, they nonetheless present powerful means to alleviate many of the most pressing symptoms, immediately benefiting laminopathy patients.

Lamins, cell migration, and cancer

An increasing number of reports have recently implicated lamins in human cancers because cancers of the ovary, colon, gut, blood, prostate, lung, and breast often have altered expression of lamins (reviewed in [101]). In the case of colorectal cancer, both increased [102] and decreased levels of lamin A/C [103] have been shown to correlate with increased aggressiveness, and decreased levels are associated with tumor recurrence in advanced stage patients [103]. Given the diverse functions of lamins, changes in lamin expression may affect cancer progression through a variety of mechanisms, including altered proliferation, signaling, and migration [101,104]. One possible model to explain how low levels of lamins A/C can contribute to cancer progression is based on the emerging importance of nuclear deformability during cell motility in 3D environments. It is now becoming clear that nuclear deformability can constitute a rate-limiting factor in the passage of cells through narrow constrictions, as convincingly demonstrated for cancer cells and immune cells migrating through dense collagen matrices [3], breast cancer cells migrating through microfabricated channels [105], and neutrophils passing through microfluidic constrictions [4]. In the latter case, cells with decreased levels of lamin A were able to pass more easily through constrictions smaller than the size of the nucleus [4]. Conversely, expression of an HGPS lamin variant, progerin, which stiffens the nucleus, impairs cell migration through confining 3D environments [106], further supporting the idea that nuclear deformability is an important factor in 3D migration. These findings suggest that downregulation of A-type lamins, whether during physiological processes such as granulopoiesis or in a subpopulation of cancer cells, results in increased nuclear deformability – and can thereby facilitate transit of cells through narrow constrictions, for example, in the interstitial space or during intra- and extravasation and passage through narrow capillaries. However, given that lamin levels are not uniformly altered across different cancer types, and lamin expression even varies within individual tumors, it remains unclear whether lamins primarily modulate cancer metastasis by changing the mechanical properties of cells or through effects of lamins on cell proliferation, signaling, and differentiation.

Concluding remarks

Inside the body, cells are continuously exposed to physical forces and the mechanical constraints of their microenvironment. It is now emerging that lamins play a crucial role in the ability of cells to adapt to their mechanical environment by providing structural support to the nucleus and modulating mechanotransduction signaling. However, it remains unclear to what extent lamins and other nuclear proteins act as direct nuclear mechanosensors or whether

Author's personal copy

they primarily serve as signaling and structural hubs at the nuclear/cytoskeletal interface. Similarly, the role of lamins in stem cell function and differentiation – for example, by responding to mechanical cues or tethering genes to transcriptionally repressive locations – remains to be addressed in more detail because embryonic stem cells lacking all lamins still undergo normal differentiation *in vitro* and *in vivo*. In addition, more work will be necessary to address the specific effects of lamin mutations associated with different diseases. Patient-derived induced pluripotent stem cells (iPSCs) that can be differentiated into various cell types provide an important tool to study tissue-specific defects of lamin mutations and are finding increasing use in investigating laminopathies. Understanding

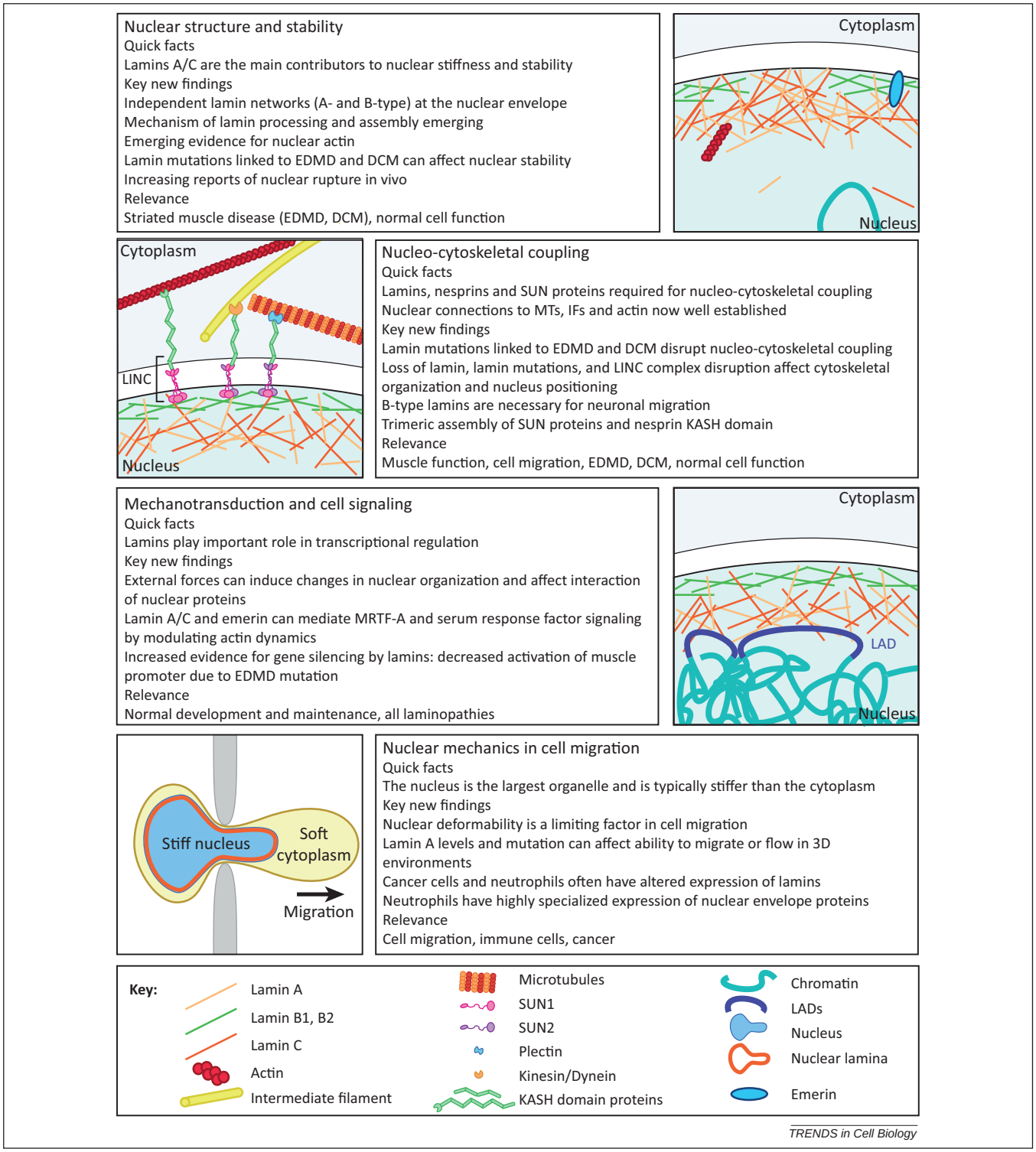

Figure 2. Overview of the diverse functions of lamins in nuclear and cellular mechanics and mechanotransduction. Abbreviations: EDMD, Emery–Dreifuss muscular dystrophy; DCM, dilated cardiomyopathy; IF, intermediate filament LAD, lamina-associated domain; LINC, linker of nucleoskeleton to cytoskeleton complex; MRTF-A, myocardin-related transcription factor A.

Author's personal copy

whether muscle-specific laminopathies primarily result from structural defects or from disturbed signaling is particularly relevant to the development of therapeutic approaches; correcting altered signaling is currently more amenable to treatment with small molecules than are structural defects, which may require gene therapy or silencing of the mutant gene(s). Although much of our current understanding of the diverse functions of lamins has come from studying the effects of disease-causing lamin mutations, it is now becoming apparent that lamins may also play an important role in cancer progression, whether by providing physical limits to the ability of the nucleus deform through microscopic constrictions in interstitial spaces or by modulating cytoskeletal dynamics and other cell functions.

Lamins provide an ideal research avenue to study the interplay between (nuclear) structure and cellular function, given their central role in modulating nuclear and cytoskeletal structure, gene expression, and a plethora of other cellular functions (Figure 2). Enormous progress has been made in recent years in the understanding of lamins, with insights gained from these studies providing hope and promise to the many patients affected by devastating laminopathies.

Acknowledgments

We apologize to all authors whose work could not be cited due to space constraints. This work was supported by National Institutes of Health awards (R01 NS059348 and R01 HL082792), a National Science Foundation CAREER award (CBET-1254846), a Department of Defense Breast Cancer Idea Award (BC102152), an award from the Progeria Research Foundation (PRF2011-0035), and a Pilot Project Award by the Cornell Center on the Microenvironment and Metastasis through Award Number U54CA143876 from the National Cancer Institute. The content is solely the responsibility of the authors and does not necessarily represent the official views of the National Cancer Institute or the National Institutes of Health.

References

1 Bonne, G. *et al.* (1999) Mutations in the gene encoding lamin A/C cause autosomal dominant Emery–Dreifuss muscular dystrophy. *Nat. Genet.* 21, 285–288
2 Schreiber, K. and Kennedy, B. (2013) When lamins go bad: nuclear structure and disease. *Cell* 152, 1365–1375
3 Wolf, K. *et al.* (2013) Physical limits of cell migration: control by ECM space and nuclear deformation and tuning by proteolysis and traction force. *J. Cell Biol.* 201, 1069–1084
4 Rowat, A.C. *et al.* (2013) Nuclear envelope composition determines the ability of neutrophil-type cells to passage through micron-scale constrictions. *J. Biol. Chem.* 288, 8610–8618
5 Hanif, M. *et al.* (2009) Differential expression of A-type and B-type lamins during hair cycling. *PLoS ONE* 4, e4114
6 Jung, H-J. *et al.* (2012) Regulation of prelamin A but not lamin C by miR-9, a brain-specific microRNA. *Proc. Natl. Acad. Sci. U.S.A.* 109, E423–E431
7 Harborth, J. *et al.* (2001) Identification of essential genes in cultured mammalian cells using small interfering RNAs. *J. Cell Sci.* 114, 4557–4565
8 Liu, J. *et al.* (2000) Essential roles for *Caenorhabditis elegans* lamin gene in nuclear organization, cell cycle progression, and spatial organization of nuclear pore complexes. *Mol. Biol. Cell* 11, 3937–3947
9 Kim, Y. *et al.* (2011) Mouse B-type lamins are required for proper organogenesis but not by embryonic stem cells. *Science* 334, 1706–1710
10 Kim, Y. *et al.* (2013) Proliferation and differentiation of mouse embryonic stem cells lacking all lamins. *Cell Res.* http://dx.doi.org/10.1038/cr.2013.118
11 Yang, S.H. *et al.* (2011) An absence of both lamin B1 and lamin B2 in keratinocytes has no effect on cell proliferation or the development of skin and hair. *Hum. Mol. Genet.* 20, 3537–3544
12 Coffinier, C. *et al.* (2011) Deficiencies in lamin B1 and lamin B2 cause neurodevelopmental defects and distinct nuclear shape abnormalities in neurons. *Mol. Biol. Cell* 22, 4683–4693
13 Dreesen, O. *et al.* (2013) Lamin B1 fluctuations have differential effects on cellular proliferation and senescence. *J. Cell Biol.* 200, 605–617
14 Dittmer, T.A. and Misteli, T. (2011) The lamin protein family. *Genome Biol.* 12, 222
15 Coffinier, C. *et al.* (2010) LINCing lamin B2 to neuronal migration: growing evidence for cell-specific roles of B-type lamins. *Nucleus* 1, 407–411
16 Adam, S. and Goldman, R. (2012) Insights into the differences between the A-and B-type nuclear lamins. *Adv. Biol. Regul.* 52, 108–113
17 Fridman, K. *et al.* (2012) Advances in tomography: probing the molecular architecture of cells. *Nat. Rev. Mol. Cell Biol.* 13, 736–742
18 Jung, H-J. *et al.* (2013) Farnesylation of lamin B1 is important for retention of nuclear chromatin during neuronal migration. *Proc. Natl. Acad. Sci. U.S.A.* 110, E1923–E1932
19 Kaufmann, A. *et al.* (2011) Amphibian oocyte nuclei expressing lamin A with the progeria mutation E145K exhibit an increased elastic modulus. *Nucleus* 2, 310–319
20 Kapinos, L.E. *et al.* (2010) Characterization of the head-to-tail overlap complexes formed by human lamin A, B1 and B2 'half-minilamin' dimers. *J. Mol. Biol.* 396, 719–731
21 Shimi, T. *et al.* (2008) The A- and B-type nuclear lamin networks: microdomains involved in chromatin organization and transcription. *Genes Dev.* 22, 3409–3421
22 Kolb, T. *et al.* (2011) Lamin A and lamin C form homodimers and coexist in higher complex forms both in the nucleoplasmic fraction and in the lamina of cultured human cells. *Nucleus* 2, 425–433
23 Davies, B.S. *et al.* (2011) Investigating the purpose of prelamin A processing. *Nucleus* 2, 4–9
24 Fong, L. and Ng, J. (2006) Prelamin A and lamin A appear to be dispensable in the nuclear lamina. *J. Clin. Invest.* 116, 743–752
25 Chen, H. *et al.* (2013) The nuclear lamina regulates germline stem cell niche organization via modulation of EGFR signaling. *Cell Stem Cell* 13, 73–86
26 Lammerding, J. *et al.* (2006) Lamins A and C but not lamin B1 regulate nuclear mechanics. *J. Biol. Chem.* 281, 25768–25780
27 Simon, D.N. and Wilson, K.L. (2013) Partners and post-translational modifications of nuclear lamins. *Chromosoma* 122, 13–31
28 Korfali, N. *et al.* (2012) The nuclear envelope proteome differs notably between tissues. *Nucleus* 3, 552–564
29 Gudise, S. *et al.* (2011) Samp1 is functionally associated with the LINC complex and A-type lamina networks. *J. Cell Sci.* 124, 2077–2085
30 Ahmady, E. *et al.* (2011) Identification of a novel muscle A-type lamin-interacting protein (MLIP). *J. Biol. Chem.* 286, 19702–19713
31 Roux, K.J. *et al.* (2012) A promiscuous biotin ligase fusion protein identifies proximal and interacting proteins in mammalian cells. *J. Cell Biol.* 196, 801–810
32 Peric-Hupkes, D. *et al.* (2010) Molecular maps of the reorganization of genome–nuclear lamina interactions during differentiation. *Mol. Cell* 38, 603–613
33 Lombardi, M.L. and Lammerding, J. (2011) Keeping the LINC: the importance of nucleocytoskeletal coupling in intracellular force transmission and cellular function. *Biochem. Soc. Trans.* 39, 1729–1734
34 Dahl, K.N. *et al.* (2004) The nuclear envelope lamina network has elasticity and a compressibility limit suggestive of a molecular shock absorber. *J. Cell Sci.* 117, 4779–4786
35 Broers, J.L.V. *et al.* (2004) Decreased mechanical stiffness in LMNA$^{-/-}$ cells is caused by defective nucleo-cytoskeletal integrity: implications for the development of laminopathies. *Hum. Mol. Genet.* 13, 2567–2580
36 Lammerding, J. *et al.* (2004) Lamin A/C deficiency causes defective nuclear mechanics and mechanotransduction. *J. Clin. Invest.* 113, 370–378

Author's personal copy

37 Pajerowski, J.D. *et al.* (2007) Physical plasticity of the nucleus in stem cell differentiation. *Proc. Natl. Acad. Sci. U.S.A.* 104, 15619–15624
38 Rowat, A.C. *et al.* (2008) Towards an integrated understanding of the structure and mechanics of the cell nucleus. *Bioessays* 30, 226–236
39 Sullivan, T. *et al.* (1999) Loss of A-type lamin expression compromises nuclear envelope integrity leading to muscular dystrophy. *J. Cell Biol.* 147, 913–920
40 Swift, J. *et al.* (2013) Nuclear lamin-A scales with tissue stiffness and enhances matrix-directed differentiation. *Science* 341, 1240104
41 De Vos, W.H. *et al.* (2011) Repetitive disruptions of the nuclear envelope invoke temporary loss of cellular compartmentalization in laminopathies. *Hum. Mol. Genet.* 20, 4175–4186
42 Schäpe, J. *et al.* (2009) Influence of lamin A on the mechanical properties of amphibian oocyte nuclei measured by atomic force microscopy. *Biophys. J.* 96, 4319–4325
43 Zwerger, M. *et al.* (2013) Myopathic lamin mutations impair nuclear stability in cells and tissue and disrupt nucleo-cytoskeletal coupling. *Hum. Mol. Genet.* 22, 2335–2349
44 Roncarati, R. *et al.* (2013) Doubly heterozygous LMNA and TTN mutations revealed by exome sequencing in a severe form of dilated cardiomyopathy. *Eur. J. Hum. Genet.* 21, 1105–1111
45 Muchir, A. *et al.* (2009) Inhibition of extracellular signal-regulated kinase signaling to prevent cardiomyopathy caused by mutation in the gene encoding A-type lamins. *Hum. Mol. Genet.* 18, 241–247
46 Mounkes, L.C. *et al.* (2005) Expression of an LMNA-N195K variant of A-type lamins results in cardiac conduction defects and death in mice. *Hum. Mol. Genet.* 14, 2167–2180
47 Dialynas, G. *et al.* (2010) The role of *Drosophila* Lamin C in muscle function and gene expression. *Development* 137, 3067–3077
48 Gupta, P. *et al.* (2010) Genetic and ultrastructural studies in dilated cardiomyopathy patients: a large deletion in the lamin A/C gene is associated with cardiomyocyte nuclear envelope disruption. *Basic Res. Cardiol.* 105, 365–377
49 Cattin, M-E. *et al.* (2013) Heterozygous LmnadelK32 mice develop dilated cardiomyopathy through a combined pathomechanism of haploinsufficiency and peptide toxicity. *Hum. Mol. Genet.* 22, 3152–3164
50 Verstraeten, V.L.R.M. *et al.* (2008) Increased mechanosensitivity and nuclear stiffness in Hutchinson–Gilford progeria cells: effects of farnesyltransferase inhibitors. *Aging Cell* 7, 383–393
51 Dahl, K.N. *et al.* (2006) Distinct structural and mechanical properties of the nuclear lamina in Hutchinson–Gilford progeria syndrome. *Proc. Natl. Acad. Sci. U.S.A.* 103, 10271–10276
52 Herrmann, H. *et al.* (2009) Intermediate filaments: primary determinants of cell architecture and plasticity. *J. Clin. Invest.* 119, 1772–1783
53 Strelkov, S.V. *et al.* (2004) Crystal structure of the human lamin A coil 2B dimer: implications for the head-to-tail association of nuclear lamins. *J. Mol. Biol.* 343, 1067–1080
54 Ruan, J. *et al.* (2012) Crystal structures of the coil 2B fragment and the globular tail domain of human lamin B1. *FEBS Lett.* 586, 314–318
55 Dhe-Paganon, S. *et al.* (2002) Structure of the globular tail of nuclear lamin. *J. Biol. Chem.* 277, 17381–17384
56 Wiesel, N. *et al.* (2008) Laminopathic mutations interfere with the assembly, localization, and dynamics of nuclear lamins. *Proc. Natl. Acad. Sci. U.S.A.* 105, 180–185
57 Ben-Harush, K. *et al.* (2009) The supramolecular organization of the *C. elegans* nuclear lamin filament. *J. Mol. Biol.* 386, 1392–1402
58 Bank, E.M. *et al.* (2012) Structural and physiological phenotypes of disease-linked lamin mutations in *C. elegans*. *J. Struct. Biol.* 177, 106–112
59 Bank, E.M. *et al.* (2011) A laminopathic mutation disrupting lamin filament assembly causes disease-like phenotypes in *Caenorhabditis elegans*. *Mol. Biol. Cell* 22, 2716–2728
60 Gangemi, F. and Degano, M. (2013) Disease-associated mutations in the coil 2B domain of human lamin A/C affect structural properties that mediate dimerization and intermediate filament formation. *J. Struct. Biol.* 181, 17–28
61 Bhattacharjee, P. *et al.* (2013) Structural alterations of lamin a protein in dilated cardiomyopathy. *Biochemistry* 52, 4229–4241
62 Bollati, M. *et al.* (2012) Structures of the lamin A/C R335W and E347K mutants: implications for dilated cardiolaminopathies. *Biochem. Biophys. Res. Commun.* 418, 217–221
63 Kapinos, L.E. *et al.* (2011) Simultaneous formation of right- and left-handed anti-parallel coiled-coil interfaces by a coil2 fragment of human lamin A. *J. Mol. Biol.* 408, 135–146
64 Magracheva, E. *et al.* (2009) Structure of the lamin A/C R482W mutant responsible for dominant familial partial lipodystrophy (FPLD). *Acta Crystallogr. Sect. F: Struct. Biol. Cryst. Commun.* 65, 665–670
65 Qin, Z. *et al.* (2011) Structure and stability of the lamin A tail domain and HGPS mutant. *J. Struct. Biol.* 175, 425–433
66 Sosa, B.A. *et al.* (2012) LINC complexes form by binding of three KASH peptides to domain interfaces of trimeric SUN proteins. *Cell* 149, 1035–1047
67 Gundersen, G.G. and Worman, H.J. (2013) Nuclear positioning. *Cell* 152, 1376–1389
68 Lombardi, M.L. *et al.* (2011) The interaction between nesprins and sun proteins at the nuclear envelope is critical for force transmission between the nucleus and cytoskeleton. *J. Biol. Chem.* 286, 1–20
69 Roux, K.J. *et al.* (2009) Nesprin 4 is an outer nuclear membrane protein that can induce kinesin-mediated cell polarization. *Proc. Natl. Acad. Sci. U.S.A.* 106, 2194–2199
70 Luxton, G.W.G. *et al.* (2010) Linear arrays of nuclear envelope proteins harness retrograde actin flow for nuclear movement. *Science* 329, 956–959
71 Lei, K. *et al.* (2009) SUN1 and SUN2 play critical but partially redundant roles in anchoring nuclei in skeletal muscle cells in mice. *Proc. Natl. Acad. Sci. U.S.A.* 106, 10207–10212
72 Yu, J. *et al.* (2011) KASH protein Syne-2/Nesprin-2 and SUN proteins SUN1/2 mediate nuclear migration during mammalian retinal development. *Hum. Mol. Genet.* 20, 1061–1073
73 Borrego-Pinto, J. *et al.* (2012) Samp1 is a component of TAN lines and is required for nuclear movement. *J. Cell Sci.* 125, 1099–1105
74 Salpingidou, G. *et al.* (2007) A novel role for the nuclear membrane protein emerin in association of the centrosome to the outer nuclear membrane. *J. Cell Biol.* 178, 897–904
75 Ostlund, C. *et al.* (2009) Dynamics and molecular interactions of linker of nucleoskeleton and cytoskeleton (LINC) complex proteins. *J. Cell Sci.* 122, 4099–4108
76 Liang, Y. *et al.* (2011) Subcellular localization of SUN2 is regulated by Lamin A and Rab5. *PLoS ONE* 6, e20507
77 Haque, F. *et al.* (2010) Mammalian SUN protein interaction networks at the inner nuclear membrane and their role in laminopathy disease processes. *J. Biol. Chem.* 285, 3487–3498
78 Méjat, A. *et al.* (2009) Lamin A/C-mediated neuromuscular junction defects in Emery–Dreifuss muscular dystrophy. *J. Cell Biol.* 184, 31–44
79 Dialynas, G. *et al.* (2012) LMNA variants cause cytoplasmic distribution of nuclear pore proteins in *Drosophila* and human muscle. *Hum. Mol. Genet.* 21, 1544–1556
80 Yang, L. *et al.* (2013) Mutations in LMNA modulate the lamin A–nesprin-2 interaction and cause LINC complex alterations. *PLoS ONE* 8, e71850
81 Bruston, F. *et al.* (2010) Loss of a DNA binding site within the tail of prelamin A contributes to altered heterochromatin anchorage by progerin. *FEBS Lett.* 584, 2999–3004
82 Rajendran, V. *et al.* (2012) In silico investigation of molecular mechanism of laminopathy caused by a point mutation (R482W) in lamin A/C protein. *Amino Acids* 43, 603–615
83 Folker, E.S. *et al.* (2011) Lamin A variants that cause striated muscle disease are defective in anchoring transmembrane actin-associated nuclear lines for nuclear movement. *Proc. Natl. Acad. Sci. U.S.A.* 108, 131–136
84 Park, Y-E. *et al.* (2009) Nuclear changes in skeletal muscle extend to satellite cells in autosomal dominant Emery–Dreifuss muscular dystrophy/limb-girdle muscular dystrophy 1B. *Neuromuscul. Disord.* 19, 29–36
85 Ji, J.Y. *et al.* (2007) Cell nuclei spin in the absence of lamin B1. *J. Biol. Chem.* 282, 20015–20026
86 Wang, N. *et al.* (2009) Mechanotransduction at a distance: mechanically coupling the extracellular matrix with the nucleus. *Nat. Rev. Mol. Cell Biol.* 10, 75–82
87 Lammerding, J. *et al.* (2005) Abnormal nuclear shape and impaired mechanotransduction in emerin-deficient cells. *J. Cell Biol.* 170, 781–791

Author's personal copy

88 Cupesi, M. *et al.* (2010) Attenuated hypertrophic response to pressure overload in a lamin A/C haploinsufficiency mouse. *J. Mol. Cell. Cardiol.* 48, 1290–1297
89 Poh, Y-C. *et al.* (2012) Dynamic force-induced direct dissociation of protein complexes in a nuclear body in living cells. *Nat. Commun.* 3, 866
90 Booth-Gauthier, E.A. *et al.* (2012) Force-induced changes in subnuclear movement and rheology. *Biophys. J.* 103, 2423–2431
91 Ho, C.Y. *et al.* (2013) Lamin A/C and emerin regulate MKL1-SRF activity by modulating actin dynamics. *Nature* 497, 507–511
92 Guelen, L. *et al.* (2008) Domain organization of human chromosomes revealed by mapping of nuclear lamina interactions. *Nature* 453, 948–951
93 Muchir, A. (2012) MEK1/2 Inhibitors to treat dilated cardiomyopathy caused by LMNA mutations. In *Advances in Protein Kinases* (Da Silva Xavier, G., ed.), Intech Chapter 4
94 Muchir, A. *et al.* (2012) Abnormal p38α mitogen-activated protein kinase signaling in dilated cardiomyopathy caused by lamin A/C gene mutation. *Hum. Mol. Genet.* 21, 4325–4333
95 Ramos, F.J. *et al.* (2012) Rapamycin reverses elevated mTORC1 signaling in lamin A/C-deficient mice, rescues cardiac and skeletal muscle function, and extends survival. *Sci. Transl. Med.* 4, 144ra103
96 Choi, J.C. *et al.* (2012) Temsirolimus activates autophagy and ameliorates cardiomyopathy caused by lamin A/C gene mutation. *Sci. Transl. Med.* 4, 144ra102
97 Meshorer, E. and Gruenbaum, Y. (2008) Gone with the Wnt/Notch: stem cells in laminopathies, progeria, and aging. *J. Cell Biol.* 181, 9–13
98 Liu, B. *et al.* (2012) Resveratrol rescues SIRT1-dependent adult stem cell decline and alleviates progeroid features in laminopathy-based progeria. *Cell Metab.* 16, 738–750
99 Young, S.G. *et al.* (2013) Targeting protein prenylation in progeria. *Sci. Transl. Med.* 5, 171ps3
100 Gordon, L. and Kleinman, M. (2012) Clinical trial of a farnesyltransferase inhibitor in children with Hutchinson–Gilford progeria syndrome. *Proc. Natl. Acad. Sci. U.S.A.* 109, 1–6
101 De Las Heras, J.I. *et al.* (2012) Cancer biology and the nuclear envelope: a convoluted relationship. *Semin. Cancer Biol.* 23, 125–137
102 Willis, N.D. *et al.* (2008) Lamin A/C is a risk biomarker in colorectal cancer. *PLoS ONE* 3, e2988
103 Belt, E.J.T. *et al.* (2011) Loss of lamin A/C expression in stage II and III colon cancer is associated with disease recurrence. *Eur. J. Cancer* 47, 1837–1845
104 Kong, L. *et al.* (2012) Lamin A/C protein is overexpressed in tissue-invading prostate cancer and promotes prostate cancer cell growth, migration and invasion through the PI3K/AKT/PTEN pathway. *Carcinogenesis* 33, 751–759
105 Fu, Y. *et al.* (2012) Nuclear deformation during breast cancer cell transmigration. *Lab Chip* 12, 3774–3778
106 Booth-Gauthier, E.A. *et al.* (2013) Hutchinson–Gilford progeria syndrome alters nuclear shape and reduces cell motility in three dimensional model substrates. *Integr. Biol. (Camb.)* 5, 569–577
107 Aebi, U. *et al.* (1986) The nuclear lamina is a meshwork of intermediate-type filaments. *Nature* 323, 560–564
108 Bank, E.M. and Gruenbaum, Y. (2011) *Caenorhabditis elegans* as a model system for studying the nuclear lamina and laminopathic diseases. *Nucleus* 2, 350–357
109 Schulze, S.R. *et al.* (2009) A comparative study of *Drosophila* and human A-type lamins. *PLoS ONE* 4, e7564
110 Jahn, D. *et al.* (2012) A truncated lamin A in the Lmna$^{-/-}$ mouse line: implications for the understanding of laminopathies. *Nucleus* 3, 463–474
111 Kubben, N. *et al.* (2011) Post-natal myogenic and adipogenic developmental: defects and metabolic impairment upon loss of A-type lamins. *Nucleus* 2, 195–207

LETTER

doi:10.1038/nature12105

Lamin A/C and emerin regulate MKL1–SRF activity by modulating actin dynamics

Chin Yee Ho[1,2], Diana E. Jaalouk[2]†, Maria K. Vartiainen[3] & Jan Lammerding[1,2]

Laminopathies, caused by mutations in the *LMNA* gene encoding the nuclear envelope proteins lamins A and C, represent a diverse group of diseases that include Emery–Dreifuss muscular dystrophy (EDMD), dilated cardiomyopathy (DCM), limb-girdle muscular dystrophy, and Hutchison–Gilford progeria syndrome[1]. Most *LMNA* mutations affect skeletal and cardiac muscle by mechanisms that remain incompletely understood. Loss of structural function and altered interaction of mutant lamins with (tissue-specific) transcription factors have been proposed to explain the tissue-specific phenotypes[1]. Here we report in mice that lamin-A/C-deficient (*Lmna*$^{-/-}$) and *Lmna*$^{N195K/N195K}$ mutant cells have impaired nuclear translocation and downstream signalling of the mechanosensitive transcription factor megakaryoblastic leukaemia 1 (MKL1), a myocardin family member that is pivotal in cardiac development and function[2]. Altered nucleo-cytoplasmic shuttling of MKL1 was caused by altered actin dynamics in *Lmna*$^{-/-}$ and *Lmna*$^{N195K/N195K}$ mutant cells. Ectopic expression of the nuclear envelope protein emerin, which is mislocalized in *Lmna* mutant cells and also linked to EDMD and DCM, restored MKL1 nuclear translocation and rescued actin dynamics in mutant cells. These findings present a novel mechanism that could provide insight into the disease aetiology for the cardiac phenotype in many laminopathies, whereby lamin A/C and emerin regulate gene expression through modulation of nuclear and cytoskeletal actin polymerization.

MKL1 (also known as MAL or MRTF-A) is a mechanosensitive transcription factor with important roles in the cardiovascular system[2,3]. Intracellular localization of MKL1 is regulated via changes in actin polymerization[4,5]. Normally, MKL1 is localized in the cytoplasm by binding to cytoplasmic G actin and constitutive nuclear export. Mitogenic or mechanical stimulation triggers RhoA-mediated actin polymerization, liberating MKL1 from G actin and exposing a nuclear localization sequence (NLS) within the actin-binding domain of MKL1 (refs 6, 7). Increased nuclear import, coupled with decreased export, causes accumulation of MKL1 in the nucleus, where it co-activates serum response factor (SRF) to turn on genes regulating cellular motility and contractility, including vinculin, actin and SRF itself[8]. Because cells from lamin-A/C-deficient mice have impaired activation of mechanosensitive genes *in vitro*[9] and *in vivo*[10], we investigated whether loss of lamin A/C could affect MKL1–SRF signalling. Nuclear translocation of endogenous MKL1 in response to serum stimulation was severely abrogated in *Lmna*$^{-/-}$ mouse embryonic fibroblasts (MEFs) compared to wild-type controls (Fig. 1a, c and Supplementary Fig. 1a). We confirmed these findings by time-lapse microscopy of cells expressing MKL1–green fluorescent protein (GFP) (Figs 1b and 2a) and in lamin-A/C-downregulated HeLa cells (Supplementary Fig. 2a, b), indicating that impaired MKL1 translocation is a general effect of loss of lamin A/C. To test whether similar defects could also result from lamin mutations associated with DCM, we investigated cells from the *Lmna*$^{N195K/N195K}$ mouse model (subsequently referred to as *Lmna* N195K cells), which develops severe DCM but lacks skeletal muscle involvement[11]. *Lmna* N195K MEFs

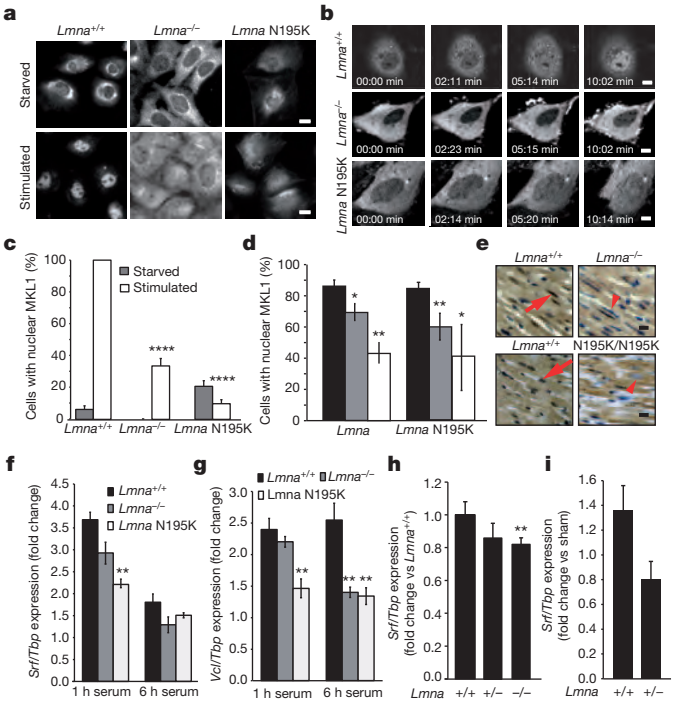

Figure 1 | Impaired nuclear translocation of MKL1 in lamin-A/C-deficient and *Lmna* N195K mutant cells. **a**, *Lmna*$^{-/-}$ and *Lmna* N195K MEFs had a lower fraction of nuclear MKL1 after serum stimulation than *Lmna*$^{+/+}$ cells, on the basis of MKL1 immunofluorescence. Scale bars, 10 μm. **b**, Time-lapse sequences of cells expressing MKL1–GFP stimulated with serum (see Supplementary Videos 1–3). Scale bars, 10 μm. **c**, Quantitative analysis of MEFs with positive nuclear MKL1 staining in response to serum stimulation ($n \approx 50$ per cell line). **d**, Quantitative analysis of myocytes with nuclear MKL1 in cardiac sections from *Lmna*$^{-/-}$ and *Lmna*$^{N195K/N195K}$ mice as well as littermate controls ($n = 3$ for each). **e**, Representative histological cardiac tissue sections from *Lmna*$^{-/-}$ and *Lmna*$^{N195K/N195K}$ mice and age-matched wild-type littermates stained for MKL1 (brown). Red arrows denote example of MKL1-positive nucleus; arrowhead denotes an MKL1-negative nucleus. Scale bars, 20 μm. **f**, **g**, Gene expression of serum response factor (*Srf*) and vinculin (*Vcl*) in *Lmna*$^{+/+}$, *Lmna*$^{-/-}$ and *Lmna* N195K MEFs after 1 h and 6 h of serum stimulation. Values were based on three independent experiments and were normalized to TATA binding protein (*Tbp*). **h**, Gene expression of *Srf* in *Lmna*$^{+/+}$ ($n = 9$), *Lmna*$^{+/-}$ ($n = 11$) and *Lmna*$^{-/-}$ ($n = 10$) cardiac tissue. Values were normalized to *Tbp*. **i**, Gene expression of *Srf* in *Lmna*$^{+/+}$ ($n = 5$) and *Lmna*$^{+/-}$ ($n = 7$) cardiac tissue collected 1 week after transverse aortic constriction (TAC) surgery. Values were normalized to *Tbp* and compared to those from sham mice. Statistical significance determined by Student's *t*-test, compared to *Lmna*$^{+/+}$ MEFs; $*P \leq 0.05$; $**P \leq 0.01$; $****P \leq 0.0001$. Error bars indicate s.e.m.

[1]Cornell University, Weill Institute for Cell and Molecular Biology/Department of Biomedical Engineering, Ithaca, New York 14853, USA. [2]Brigham and Women's Hospital/Harvard Medical School, Department of Medicine, Boston 02115, Massachusetts, USA. [3]Institute of Biotechnology, University of Helsinki, 00014 Helsinki, Finland. †Present address: American University of Beirut, Department of Biology, Beirut 1107 2020, Lebanon.

©2013 Macmillan Publishers Limited. All rights reserved

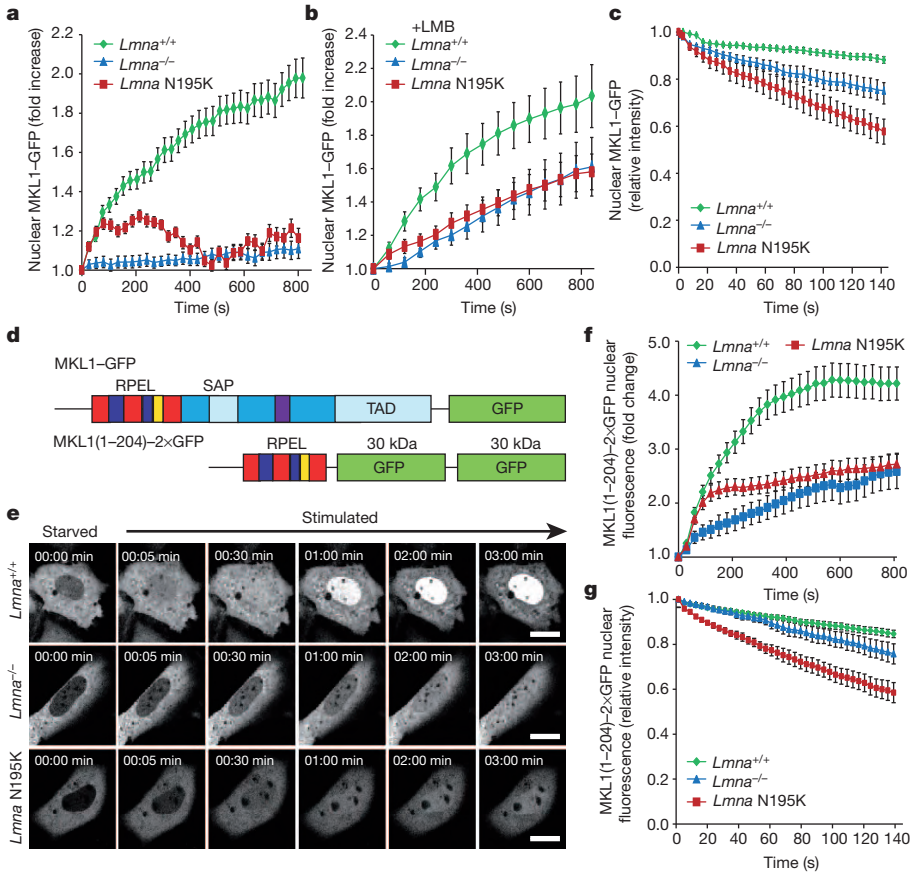

Figure 2 | Changes in nuclear import and export are specific to MKL1 and are caused by altered actin dynamics in *Lmna*$^{-/-}$ and *Lmna* N195K cells. **a**, **b**, Change in nuclear fluorescence intensity over time upon serum stimulation in *Lmna*$^{+/+}$, *Lmna*$^{-/-}$ and *Lmna* N195K MEFs expressing MKL1–GFP in the absence (**a**) or presence (**b**) of leptomycin B. Values were normalized to the initial nuclear fluorescence intensity before serum addition. $n = 20$ for each cell line. **c**, Fluorescence loss in photobleaching (FLIP) experiments of MKL1–GFP to measure nuclear export. Increased loss of nuclear fluorescence indicates a higher rate of nuclear export of MKL1–GFP in lamin mutant cells. $n = 10$ for each cell line. **d**, Schematic representation (not drawn to scale) of full-length MKL1–GFP (top) and MKL1(1–204)–2×GFP (bottom), consisting of the N-terminal actin-binding domain of MKL1 fused to two GFP moieties. RPEL motifs are depicted in blue and red; NLS in yellow; DNA-binding domain (SAP) and transcriptional activation domain (TAD) in light blue; coiled-coil domain in purple; other parts of the C terminus in dark blue. **e**, Representative frames from time-lapse series of *Lmna*$^{+/+}$, *Lmna*$^{-/-}$ and *Lmna* N195K MEFs expressing MKL1(1–204)–2×GFP after serum stimulation (see Supplementary Videos 4–6). Scale bars, 10 μm. **f**, *Lmna*$^{+/+}$ MEFs showed rapid accumulation of MKL1(1–204)–2×GFP in the nucleus upon serum stimulation, whereas nuclear accumulation was slower in *Lmna*$^{-/-}$ and *Lmna* N195K cells. Nuclear fluorescence intensity was normalized to the initial nuclear fluorescence before serum stimulation. $n = 60$ for each cell line. **g**, FLIP experiments in cells expressing MKL1(1–204)–2×GFP. Fluorescence intensity values were normalized to the initial nuclear fluorescence intensity before bleaching of a cytoplasmic region. $n = 10$ for each cell line. Error bars indicate s.e.m.

(Fig. 1a–c and Supplementary Fig. 1a) and bone-marrow-derived mesenchymal stem cells (Supplementary Fig. 1b) had impaired nuclear translocation of MKL1. Notably, cardiac sections from *Lmna*$^{-/-}$ and *Lmna*$^{N195K/N195K}$ mice had significantly reduced fractions of cardiomyocytes with nuclear MKL1 (Fig. 1d, e), confirming MKL1 translocation defects *in vivo* and implicating altered MKL1 signalling in the development of cardiomyopathies in these animals.

To characterize the consequences of altered MKL1 translocation, we assessed expression of select MKL1–SRF target genes. *Lmna*$^{-/-}$ and *Lmna* N195K MEFs had impaired serum-induced expression of *Srf* and vinculin (Fig. 1f, g) and had fewer focal adhesions than wild-type controls (Supplementary Fig. 3c, d); expression of an SRF-dependent luciferase reporter was also significantly reduced (Supplementary Fig. 3e). Cardiac tissues from *Lmna*$^{-/-}$ mice had lower *Srf* and actin transcript levels than those from wild-type littermates, and activation of *Srf* expression in response to left ventricular pressure overload was impaired in *Lmna*$^{+/-}$ mice (Fig. 1h, i and Supplementary Fig. 3a, b), demonstrating altered MKL1–SRF mechanosignalling *in vivo*.

Experiments with an NLS–GFP–NES reporter construct consisting of GFP fused to an NLS and a nuclear export sequence (NES) revealed that general nuclear import and export were preserved in *Lmna*$^{-/-}$ and *Lmna* N195K cells (Supplementary Fig. 4), as were levels and localization of the nuclear transport factor Ran and its regulator, RCC1 (Supplementary Fig. 2c–f). We then devised experiments to assess independently nuclear import and export of MKL1. Nuclear import was measured by monitoring nuclear accumulation of MKL1–GFP while blocking nuclear export with leptomycin B[8]. *Lmna*$^{-/-}$ and *Lmna* N195K mutant cells had significantly reduced nuclear import of MKL1 in response to serum stimulation than wild-type controls (Fig. 2b), which we confirmed with photoactivatable MKL1–PAGFP (Supplementary Fig. 5; see also Supplementary Videos 7–9). Fluorescence loss in photobleaching (FLIP) experiments revealed that lamin mutant MEFs had a significantly faster decrease in nuclear MKL1–GFP (Fig. 2c) than wild-type cells, indicating increased nuclear export of MKL1 in *Lmna*$^{-/-}$ and mutant MEFs.

Nuclear import and export of MKL1 are regulated by actin polymerization[8], requiring interaction between MKL1 and G actin via three amino-terminal RPEL motifs[12]. We expressed a truncated MKL1 construct, MKL1(1–204)–2×GFP, which contains the RPEL motifs but lacks the transcriptional domains (Fig. 2d) and recapitulates the actin-binding characteristics and serum-inducible translocation of full-length MKL1 (ref. 12). Nuclear accumulation of MKL1(1–204)–2×GFP was substantially

©2013 Macmillan Publishers Limited. All rights reserved

lower in *Lmna*$^{-/-}$ and *Lmna* N195K cells than in wild-type cells (Fig. 2e, f), indicating that impaired nuclear translocation of MKL1 was caused by altered actin dynamics in the lamin mutant cells. As seen with full-length MKL1–GFP, FLIP studies showed that nuclear export of MKL1(1–204)–2×GFP was significantly increased in the mutant cells (Fig. 2g). In contrast, abrogation of G-actin binding by mutating all three RPEL motifs (MKL1(1–204)XXX–2×GFP) or disrupting the interaction between G actin and MKL1 with cytochalasin D resulted in nuclear accumulation of MKL1(1–204)XXX–2×GFP (Supplementary Fig. 6a) and endogenous MKL1 (Supplementary Fig. 6b), respectively, in all cell types, indicating that MKL1 can enter the nucleus of *Lmna*$^{-/-}$ and *Lmna* N195K cells when decoupled from actin dynamics.

We subsequently compared actin organization between mutant and wild-type cells. Fluorescence recovery after photobleaching (FRAP) revealed that nuclear actin, which modulates nuclear export of MKL1 (ref. 8), was more mobile in *Lmna*$^{-/-}$ cells than in wild-type controls (Supplementary Fig. 7). *Lmna*$^{-/-}$ and *Lmna* N195K MEFs also had a larger fraction of highly mobile cytoplasmic actin (Fig. 3a). Furthermore, *Lmna*$^{-/-}$ and *Lmna* N195K cells were slower to reassemble stress fibres after disruption of actin filaments with cytochalasin D (Fig. 3b, c). In addition, whereas wild-type cells increased their ratio of F actin to G actin upon serum stimulation, *Lmna*$^{-/-}$ and *Lmna* N195K MEFs had a consistently weaker response (Fig. 3d). These findings indicate that actin polymerization is altered in *Lmna*$^{-/-}$ and *Lmna* N195K cells and that altered actin organization may be responsible for the impaired nuclear translocation of MKL1.

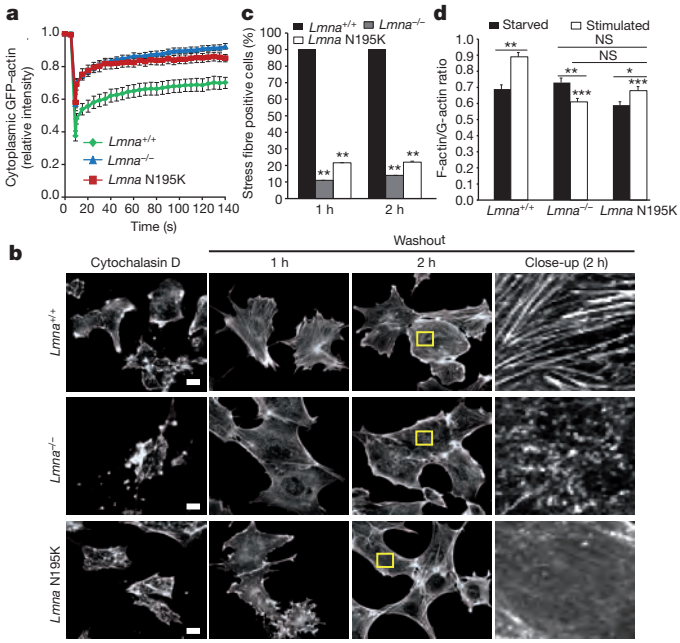

Figure 3 | *Lmna*$^{-/-}$ and *Lmna* N195K cells have altered actin dynamics and polymerization kinetics. **a**, Fluorescence recovery after photobleaching (FRAP) studies with GFP–actin revealed increased cytoplasmic actin mobility in *Lmna*$^{-/-}$ and *Lmna* N195K cells relative to *Lmna*$^{+/+}$ controls. $n = 20$ for each cell line. **b**, Representative images of *Lmna*$^{+/+}$, *Lmna*$^{-/-}$ and *Lmna* N195K MEFs stained for actin stress fibres with phalloidin after cytochalasin D washout. The right column contains close-up images of the regions marked by the yellow rectangle. Scale bars, 10 μm. **c**, *Lmna*$^{+/+}$ MEFs had a larger fraction of cells containing stress fibres at 1 h and 2 h after cytochalasin D washout than *Lmna*$^{-/-}$ and *Lmna* N195K cells. $n = 50$ for each cell line. **d**, Comparison of F-actin/G-actin ratio in starved and serum-stimulated *Lmna*$^{+/+}$, *Lmna*$^{-/-}$ and *Lmna* N195K MEFs based on phalloidin (F actin) and DNase 1 (G actin) staining. Difference in the F-actin/G-actin ratio in serum-starved cells was not statistically significant (NS); $n = 35$ for each cell line. $^{*}P \leq 0.05$; $^{**}P \leq 0.01$; $^{***}P \leq 0.001$; all comparisons relative to corresponding *Lmna*$^{+/+}$ cells unless indicated otherwise by horizontal bars. Error bars indicate s.e.m.

What causes disturbed actin organization in lamin mutant cells? Because lamins contribute to nucleo-cytoskeletal coupling and impaired nucleo-cytoskeletal coupling can disturb perinuclear actin organization, we tested whether disrupting nucleo-cytoskeletal coupling with dominant-negative nesprin mutants (consisting of the KASH domain of nesprin) could reproduce defects in MKL1 translocation. However, expression of dominant-negative KASH had no effect on MKL1 localization (Supplementary Fig. 8). Emerin, an inner nuclear membrane protein associated with X-linked EDMD[13], is an actin pointed-end capping protein that promotes actin polymerization *in vitro*[14] and requires lamin A/C for proper localization. In *Lmna*$^{-/-}$ and *Lmna* N195K MEFs, emerin was more mobile and mislocalized from the nuclear envelope compared with wild-type cells (Fig. 4a and Supplementary Fig. 9a). Hemizygous emerin-null male mice (*Emd*$^{-/Y}$) MEFs displayed the same impaired nuclear translocation of MKL1 as lamin mutant cells, which could be rescued by re-introduction of exogenous emerin (Fig. 4b–d). FRAP studies in *Emd*$^{-/Y}$ MEFs demonstrated that exogenous emerin completely restored actin mobility to levels of wild-type cells (Fig. 4e, f). Ectopic expression of emerin also markedly improved nuclear translocation of MKL1 in *Lmna*$^{-/-}$ and *Lmna* N195K cells (Fig. 4d and Supplementary Fig. 9b) by increasing the amount of emerin available at the nuclear envelope. In contrast, expression of emerin mutants unable to bind actin and to promote actin polymerization[14] failed to restore nuclear translocation of MKL1 and caused dominant-negative defects in wild-type cells (Fig. 4d). These data indicate that emerin is a crucial modulator of actin polymerization and that loss of emerin from the nuclear envelope causes disturbed actin dynamics and impaired MKL1 signalling.

Taken together, our data suggest a novel mechanism for nuclear envelope proteins to regulate MKL1–SRF signalling by modulating actin polymerization. We propose that emerin primarily affects nuclear actin polymerization, which controls nuclear export and transcriptional activity of MKL1 (refs 2, 8). Altered MKL1–SRF signalling could then further affect cytoskeletal actin, as MKL1 and SRF are master regulators for numerous cytoskeletal proteins, including actin and actin-binding proteins, consistent with the reduced cytoskeletal stiffness reported in *Lmna*$^{-/-}$ MEFs[9,15,16]. Given the low levels of emerin at the outer nuclear membrane[17] and the fact that the fraction of emerin at the endoplasmic reticulum increases in *Lmna*$^{-/-}$ and *Lmna* N195K cells (Supplementary Fig. 10), it is likely that emerin has only a limited direct effect on cytoplasmic actin polymerization. Nonetheless, we cannot exclude the possibility that emerin (and lamins) may have additional effects on MKL1. For example, direct interaction of lamin A/C with nuclear G actin[18] could further contribute to the altered actin dynamics in *Lmna*$^{-/-}$ and *Lmna* N195K cells, as lamins, together with emerin and spectrin IIa, may form a nuclear cortical actin network[14]. Furthermore, emerin can inhibit or reduce the nuclear accumulation of other transcription factors, including β-catenin, Lmo7 and phospho-ERK1/2 (ref. 19).

Lmna$^{-/-}$ and *Lmna*$^{N195K/N195K}$ mice develop DCM and have defects in cytoskeletal organization and focal adhesions[9,20,21], consistent with impaired MKL1–SRF signalling[22]. Underscoring the crucial role of MKL1–SRF in cardiac function, cardiac-specific deletion of SRF in adult mice results in DCM[23]. Considering the marked similarity of the cardiac phenotype observed in these mice with those in EDMD and DCM patients, we propose that impaired MKL1–SRF signalling and the resulting alterations in cytoskeletal organization may have a pivotal role in the development of cardiac defects and muscle phenotypes in various laminopathies. Surprisingly, although *Emd*$^{-/Y}$ cells have obvious defects in nuclear stability and mechanotransduction signalling[24,25], emerin-deficient mice—unlike human patients with emerin mutations—lack an overt muscular phenotype[26], indicating additional layers of complexity, species-specific differences, and possible compensation in the *Emd*$^{-/Y}$ mice. Nonetheless, *Emd*$^{-/Y}$ animals show delays in muscle repair[26], consistent with a role of MKL1 in satellite cells and skeletal muscle regeneration[27] and providing additional support for the involvement of impaired MKL1 signalling in nuclear envelopathies.

©2013 Macmillan Publishers Limited. All rights reserved

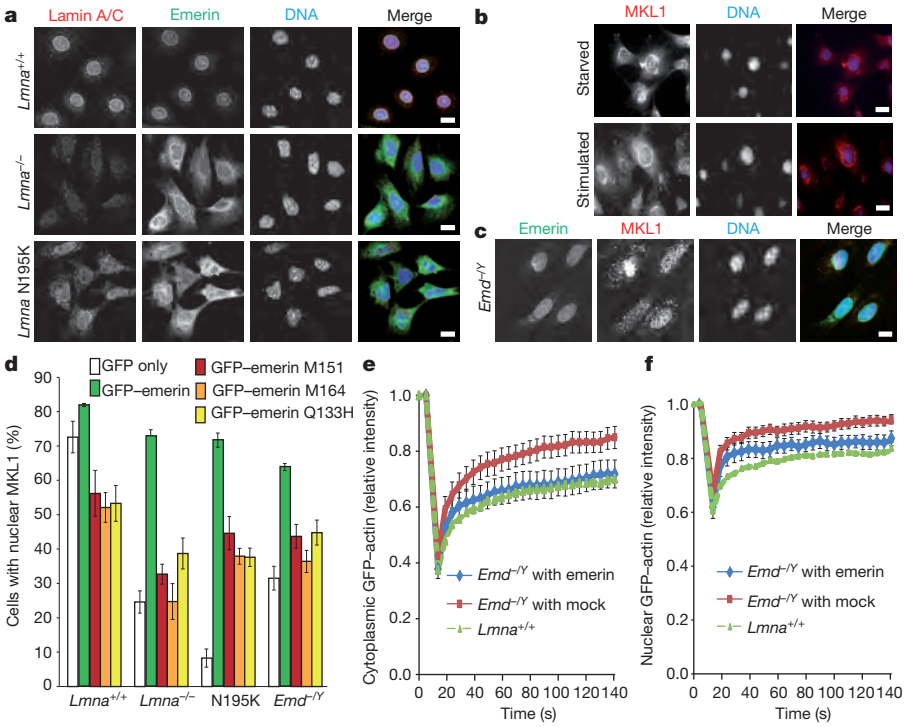

Figure 4 | Emerin expression rescues actin dynamics and restores MKL1 nuclear translocation in *Lmna*$^{-/-}$ and *Lmna* N195K cells. **a**, Representative immunofluorescence images showing mislocalization of emerin from the nuclear envelope in *Lmna*$^{-/-}$ and *Lmna* N195K MEFs. Scale bar, 10 μm. **b**, *Emd*$^{-/Y}$ MEFs had the same defects in MKL1 translocation as lamin mutant cells (compare with Fig. 1a). Scale bar, 10 μm. **c**, Stable expression of HA–emerin in *Emd*$^{-/Y}$ MEFs restored normal nuclear MKL1 localization (71.1 ± 6.02%) in response to serum stimulation. Scale bar, 10 μm. **d**, Quantification of nuclear MKL1 localization upon serum stimulation in *Lmna*$^{+/+}$, *Lmna*$^{-/-}$, *Lmna* N195K and *Emd*$^{-/Y}$ MEFs transiently expressing GFP–emerin, emerin mutants that do not bind to actin (GFP–M151, GFP–M164, GFP–Q133H), or GFP vector alone. Cells were categorized as either having 'nuclear' or 'diffuse/cytoplasmic' localization of MKL1. Expression of GFP–emerin restored serum-induced nuclear localization of MKL1 in *Lmna*$^{-/-}$, *Lmna* N195K and *Emd*$^{-/Y}$ cells. $n = 50$ for each cell line. Statistical significance determined by one-way analysis of variance (ANOVA) ($P \leq 0.001$) with Dunnett multiple comparison post test. Each group was compared to *Lmna*$^{+/+}$ expressing GFP–emerin. **e**, **f**, FRAP analysis of GFP–actin mobility in the cytoplasm (**e**) and in the nucleus (**f**) of *Emd*$^{-/Y}$ MEFs stably expressing either HA–emerin or a mock control. $n = 10$ for each cell line. *Lmna*$^{+/+}$ data reproduced from Fig. 3a for comparison. Error bars indicate s.e.m.

Our findings further illustrate the wide-ranging impacts of mutations in nuclear envelope proteins. Treatment of lamin and emerin mutant mice with MAPK inhibitors can reduce cardiac and skeletal phenotypes[28], which may be attributed at least in part to the effect on MKL1 signalling, as inhibiting ERK1/2 activity is expected to increase nuclear localization of MKL1 by reducing its nuclear export[20]. These findings encourage further approaches to correct impaired MKL1–SRF signalling to ameliorate the devastating cardiac disease associated with many laminopathies.

METHODS SUMMARY

Details for standard cell biology techniques (western blotting, immunofluorescence labelling, time-lapse microscopy and photobleaching experiments) can be found in the Methods. Mouse models have been described previously[11,26,29]. All animal work was conducted in accordance with relevant guidelines and regulations.

Full Methods and any associated references are available in the online version of the paper.

Received 24 July 2012; accepted 20 March 2013.
Published online 5 May 2013.

1. Ho, C. Y. & Lammerding, J. Lamins at a glance. *J. Cell Sci.* **125,** 2087–2093 (2012).
2. Olson, E. N. & Nordheim, A. Linking actin dynamics and gene transcription to drive cellular motile functions. *Nature Rev. Mol. Cell Biol.* **11,** 353–365 (2010).
3. Parmacek, M. S. Myocardin-related transcription factors: critical coactivators regulating cardiovascular development and adaptation. *Circ. Res.* **100,** 633–644 (2007).
4. Miralles, F., Posern, G., Zaromytidou, A. I. & Treisman, R. Actin dynamics control SRF activity by regulation of its coactivator MAL. *Cell* **113,** 329–342 (2003).
5. Mouilleron, S., Guettler, S., Langer, C. A., Treisman, R. & McDonald, N. Q. Molecular basis for G-actin binding to RPEL motifs from the serum response factor coactivator MAL. *EMBO J.* **27,** 3198–3208 (2008).
6. Hirano, H. & Matsuura, Y. Sensing actin dynamics: structural basis for G-actin-sensitive nuclear import of MAL. *Biochem. Biophys. Res. Commun.* **414,** 373–378 (2011).
7. Pawłowski, R., Rajakyla, E. K., Vartiainen, M. K. & Treisman, R. An actin-regulated importin α/β-dependent extended bipartite NLS directs nuclear import of MRTF-A. *EMBO J.* **29,** 3448–3458 (2010).
8. Vartiainen, M. K., Guettler, S., Larijani, B. & Treisman, R. Nuclear actin regulates dynamic subcellular localization and activity of the SRF cofactor MAL. *Science* **316,** 1749–1752 (2007).
9. Lammerding, J. *et al.* Lamin A/C deficiency causes defective nuclear mechanics and mechanotransduction. *J. Clin. Invest.* **113,** 370–378 10.1172/JCI19670 (2004).
10. Cupesi, M. *et al.* Attenuated hypertrophic response to pressure overload in a lamin A/C haploinsufficiency mouse. *J. Mol. Cell. Cardiol.* **48,** 1290–1297 (2010).
11. Mounkes, L. C., Kozlov, S. V., Rottman, J. N. & Stewart, C. L. Expression of an LMNA-N195K variant of A-type lamins results in cardiac conduction defects and death in mice. *Hum. Mol. Genet.* **14,** 2167–2180 (2005).
12. Guettler, S., Vartiainen, M. K., Miralles, F., Larijani, B. & Treisman, R. RPEL motifs link the serum response factor cofactor MAL but not myocardin to Rho signaling via actin binding. *Mol. Cell. Biol.* **28,** 732–742 (2008).
13. Fairley, E. A., Kendrick-Jones, J. & Ellis, J. A. The Emery-Dreifuss muscular dystrophy phenotype arises from aberrant targeting and binding of emerin at the inner nuclear membrane. *J. Cell Sci.* **112,** 2571–2582 (1999).
14. Holaska, J. M., Kowalski, A. K. & Wilson, K. L. Emerin caps the pointed end of actin filaments: evidence for an actin cortical network at the nuclear inner membrane. *PLoS Biol.* **2,** e231 (2004).
15. Nikolova-Krstevski, V. *et al.* Nesprin-1 and actin contribute to nuclear and cytoskeletal defects in lamin A/C-deficient cardiomyopathy. *J. Mol. Cell. Cardiol.* **50,** 479–486 (2011).
16. Hale, C. M. *et al.* Dysfunctional connections between the nucleus and the actin and microtubule networks in laminopathic models. *Biophys. J.* **95,** 5462–5475 (2008).
17. Salpingidou, G., Smertenko, A., Hausmanowa-Petrucewicz, I., Hussey, P. J. & Hutchison, C. J. A novel role for the nuclear membrane protein emerin in association of the centrosome to the outer nuclear membrane. *J. Cell Biol.* **178,** 897–904 (2007).
18. Simon, D. N., Zastrow, M. S. & Wilson, K. L. Direct actin binding to A- and B-type lamin tails and actin filament bundling by the lamin A tail. *Nucleus* **1,** 264–272 (2010).

©2013 Macmillan Publishers Limited. All rights reserved

19. Wilson, K. L. & Berk, J. M. The nuclear envelope at a glance. *J. Cell Sci.* **123,** 1973–1978 (2010).
20. Muehlich, S. *et al.* Serum-induced phosphorylation of the serum response factor coactivator MKL1 by the extracellular signal-regulated kinase 1/2 pathway inhibits its nuclear localization. *Mol. Cell. Biol.* **28,** 6302–6313 (2008).
21. Nikolova, V. *et al.* Defects in nuclear structure and function promote dilated cardiomyopathy in lamin A/C-deficient mice. *J. Clin. Invest.* **113,** 357–369 (2004).
22. Morita, T., Mayanagi, T. & Sobue, K. Reorganization of the actin cytoskeleton via transcriptional regulation of cytoskeletal/focal adhesion genes by myocardin-related transcription factors (MRTFs/MAL/MKLs). *Exp. Cell Res.* **313,** 3432–3445 (2007).
23. Parlakian, A. *et al.* Temporally controlled onset of dilated cardiomyopathy through disruption of the SRF gene in adult heart. *Circulation* **112,** 2930–2939 (2005).
24. Lammerding, J. *et al.* Abnormal nuclear shape and impaired mechanotransduction in emerin-deficient cells. *J. Cell Biol.* **170,** 781–791 (2005).
25. Rowat, A. C., Lammerding, J. & Ipsen, J. H. Mechanical properties of the cell nucleus and the effect of emerin deficiency. *Biophys. J.* **91,** 4649–4664 (2006).
26. Melcon, G. *et al.* Loss of emerin at the nuclear envelope disrupts the Rb1/E2F and MyoD pathways during muscle regeneration. *Hum. Mol. Genet.* **15,** 637–651 (2006).
27. Mokalled, M. H., Johnson, A. N., Creemers, E. E. & Olson, E. N. MASTR directs MyoD-dependent satellite cell differentiation during skeletal muscle regeneration. *Genes Dev.* **26,** 190–202 (2012).
28. Muchir, A., Shan, J., Bonne, G., Lehnart, S. E. & Worman, H. J. Inhibition of extracellular signal-regulated kinase signaling to prevent cardiomyopathy caused by mutation in the gene encoding A-type lamins. *Hum. Mol. Genet.* **18,** 241–247 (2009).
29. Sullivan, T. *et al.* Loss of A-type lamin expression compromises nuclear envelope integrity leading to muscular dystrophy. *J. Cell Biol.* **147,** 913–920 (1999).

Supplementary Information is available in the online version of the paper.

Acknowledgements We thank C. Stewart for the mouse models and cell lines. We thank J. Gannon for TAC surgeries and M. Cupesi for collecting the cardiac samples from the pressure-overload model. This work was supported by National Institutes of Health awards (R01 NS059348 and R01 HL082792); the Department of Defense Breast Cancer Idea Award (BC102152); an award from the Progeria Research Foundation (PRF 2011-035); and a postdoctoral fellowship from the American Heart Association to D.E.J. (AHA award 09POST2320042). The work in the laboratory of M.K.V. is funded by the Academy of Finland and the Sigrid Juselius Foundation.

Author Contributions C.Y.H., D.E.J. and J.L. conceived and designed the overall project, with valuable help from M.K.V. C.Y.H. and D.E.J. performed the experiments. C.Y.H., D.E.J. and J.L. analysed data. C.Y.H. and J.L. wrote the paper.

Author Information Reprints and permissions information is available at www.nature.com/reprints. The authors declare no competing financial interests. Readers are welcome to comment on the online version of the paper. Correspondence and requests for materials should be addressed to J.L. (jan.lammerding@cornell.edu).

©2013 Macmillan Publishers Limited. All rights reserved

METHODS

Plasmids. MKL1–GFP was a gift from A. Kapus; MKL1(1–204)–2×GFP, MKL1 (1–204)XXX–2×GFP, NLS–GFP–NES and MKL1–PAGFP were obtained from M. Vartiainen. The NLS–GFP–NES reporter construct consists of GFP fused to an NLS and an importin α/β-dependent NES, using the same import/export mechanism as MKL1 (ref. 30). The MKL1(1–204)XXX–2×GFP construct contains alanine substitutions in all three of the MKL1 RPEL motifs, which abrogates binding to G actin and leads to constitutively nuclear localization independent of actin polymerization[12]. GFP–RCC1 was obtained from B. Paschal. GFP–actin was from F. Gertler and emerin–GFP was obtained from H. Worman.

Lamin and emerin mouse models. *Lmna*$^{-/-}$ mice along with heterozygous (*Lmna*$^{+/-}$) and wild-type (*Lmna*$^{+/+}$) littermates were obtained from crossing *Lmna*$^{+/-}$ mice. Similarly, *Lmna*$^{N195K/N195K}$ and heterozygous (*Lmna*$^{N195K/+}$) and wild-type (*Lmna*$^{+/+}$) littermates resulted from breeding *Lmna*$^{N195K/+}$ animals. *Lmna*$^{-/-}$ mice develop severe muscular dystrophy and cardiomyopathy and die at 4–8 weeks of age[29]. *Lmna*$^{N195K/N195K}$ mice develop severe dilated cardiomyopathy and die prematurely around 12–16 weeks of age[11]. Genotype was determined by polymerase chain reaction of genomic tail DNA, as described previously[29]. The mouse colonies were derived from breeders provided by C. Stewart[11,26,29]. All mice were maintained in the animal facility at Cornell University following protocols approved by the Cornell University Institutional Animal Care and Use Committee (IACUC).

Cell lines, transfection and drug treatment. Immortalized MEFs from *Lmna*$^{+/+}$, *Lmna*$^{-/-}$, *Lmna*$^{N195K/N195K}$ and *Emd*$^{-/Y}$ mice were a gift from C. Stewart. Cells were maintained in Dulbecco's Eagle's Modified Media (DMEM) with GlutaMax (Gibco, Invitrogen) containing 10% fetal bovine serum (FBS) (PAA), and 1% penicillin/streptomycin at 37 °C in a humidified atmosphere with 5% carbon dioxide. Serum starvation was done by withdrawing serum and incubating the cells in 0.3% FBS for 24 h. Starved cells were stimulated with DMEM with 15% FBS. Transient transfection was carried out using Lipofectamine Reagent (Invitrogen) according to manufacturer's protocol. 1 μg of plasmid DNA was used per transfection reaction. For cytochalasin D (Sigma Aldrich) treatment, a stock of 1 mM was prepared by reconstituting the drug in DMSO and a working concentration of 1 μM was used for all experiments. For leptomycin B (Sigma Aldrich) treatment, a working concentration of 5 nM was used for all experiments.

Antibodies and immunofluorescence staining. Goat anti-MKL1 (C-19 and H-180), goat anti-actin (C-11) conjugated with horseradish peroxidase (HRP) and goat anti-lamin A/C (N-18) antibodies were purchased from Santa Cruz Biotechnology. Mouse anti-Ran antibody (610341) was purchased from BD Biosciences. Mouse anti-emerin antibody (NCL-emerin) was a product from Novocastra. Mouse anti-paxillin (05-417) was purchased from Millipore. Rabbit anti-tubulin (ab6046) was purchased from Abcam. Secondary antibodies conjugated to Alexa-488 or Alexa-568 fluorophores were purchased from Molecular Probes (Invitrogen). For immunofluorescence staining, cells grown at subconfluency were collected and fixed with 4% paraformaldehyde/phosphate-buffered saline (PBS) and permeabilized with 0.2% Triton X-100 in PBS for 10 min at room temperature. Cells were grown at similar subconfluency for all cell lines tested. Primary antibodies in 4% bovine serum albumin in Tris-buffered saline (TBS) with 0.05% Tween 20 were incubated for 1 h at room temperature or overnight at 4 °C. Cells were washed three times and incubated with appropriate secondary antibodies for 1 h at room temperature. Slides were mounted in Prolong Gold Anti-Fade medium with 4′,6-diamidino-2-phenylindole (DAPI) (Molecular Probes, Invitrogen). Images were collected and analysed on a Zeiss LSM 700 confocal microscope (Carl Zeiss). Images were captured using identical exposure times for each cell line.

Immunohistochemistry. Hearts from 4-week-old *Lmna*$^{-/-}$ mice and 8-week-old *Lmna*$^{N195K/N195K}$ mice along with wild-type and heterozygous littermate controls were collected and fixed in 4% paraformaldehyde in PBS before processing for paraffin embedding and cutting. The sections were deparaffinized with xylene and rehydrated. Antigen retrieval was performed by incubation with sodium citrate buffer (10 mM sodium citrate, 0.05% Tween 20, pH 6.0) (Invitrogen Inc.) at 95 °C for 20 min. The sections were then incubated with 3% hydrogen peroxide (H_2O_2) for 20 min to quench endogenous peroxidase activity. Blocking of nonspecific sites was done by incubating the slices with 10% horse serum in PBS for 20 min. Anti-MKL1 antibody (Santa Cruz Biotechnologies) was used at 1:50 dilution at 4 °C for 12–16 h to detect endogenous MKL1. A biotinylated anti-goat IgG secondary antibody (Vector Laboratories Inc.) was used at 1:400 dilution at room temperature for 1 h. The biotinylated secondary antibody was then detected using the VECTASTAIN ABC system (Vector Laboratories Inc.) which uses a preformed macromolecular complex between avidin and biotinylated horseradish peroxidase. A working solution of 3,3′-diaminobenzidine (DAB) was used as a substrate for the peroxidase. The sections were then counterstained with haematoxylin before air-drying and mounting. Images were acquired using a Zeiss Aviovert 200 inverted microscope (Carl Zeiss) equipped with a ×20 objective with an AxioCam ICc1. The number of cells positive for nuclear MKL1 was counted manually on at least five random microscopic fields per section and normalized to the total number of cardiac myocytes.

Western blotting. Cells were lysed using radioimmunoprecipitation assay (RIPA) buffer with freshly added protease inhibitor cocktail. The cells were scraped off using a cell scraper and incubated on ice for 30 min. The lysate was then cleared by centrifuging at 13,200 r.p.m. at 4 °C. Protein concentration was estimated by Bradford assay. Thirty micrograms of protein re-suspended in Laemmli sample buffer was loaded per sample. Cytoplasmic and nuclear fractions were prepared using the Pierce NE-PER Nuclear and Cytoplasmic Extraction kit according to manufacturer's instructions. Denatured proteins were resolved on 4–15% Nu-PAGE bis-tris polyacrylamide gels and blotted to a polyvinylidene fluoride (PVDF) membrane. Blocking was done with incubation in 10% non-fat dry milk in TBS with 0.1% Tween-20. The membrane was then probed with primary antibodies in 5% milk in TBST at 4 °C overnight and sequentially detected with horseradish peroxidase conjugated secondary antibodies. The signal was revealed by autoradiography using enhanced chemiluminescence (ECL) (Pierce, Thermo Fisher Scientific Inc.).

F- and G-actin assays. For the cytochalasin D washout experiment, MEFs were treated with 1 μM cytochalasin D (Sigma Aldrich) for 30 min; subsequent drug washout was performed by rinsing the cells with three changes of medium. Cells were fixed with 4% paraformaldehyde/PBS at 1 h or 2 h after washout and then permeabilized with 0.2% Triton X-100 in PBS. Stress fibres were visualized using Phalloidin-Alexa 568. For fluorescence labelling of F and G actin, starved and stimulated *Lmna*$^{+/+}$, *Lmna*$^{-/-}$ and *Lmna* N195K MEFs were fixed and permeabilized as described above. Cells were then stained with Phalloidin-Alexa 568 to label F actin and DNase 1-Alexa 488 (Invitrogen) to label G actin[31]. Slides were mounted in Prolong Gold Anti-Fade medium with DAPI (Invitrogen). Images were collected and analysed on a Zeiss LSM 700 confocal microscope (Carl Zeiss). Images were captured using identical exposure times for each cell line.

Real-time PCR. Total RNA from cell lines was extracted using the Qiagen RNeasy kit (Qiagen) according to manufacturer's instructions. Total RNA from cryopreserved tissues was extracted using TRIzol Reagent (Life Technologies, Invitrogen Inc.) according to manufacturer's instructions. RNA was reverse-transcribed to cDNA using the High-Capacity cDNA Reverse Transcription kit (Applied Biosystems). Real-time PCR was carried out using SYBR-Green technology (Applied Biosystems) in a total volume of 25 μl. Gene expression for *Srf* and *Vcl* was quantified. Values were normalized to an endogenous control, TATA binding protein (*Tbp*), and compared to unstimulated samples with the $\Delta\Delta C_t$ method. Data are based on results from three independent experiments.

SRE-luciferase assay. SRF forms a complex over the SRE/CArG element upon receiving upstream signals from the MAPK pathway and/or the RhoA pathway. SRE activity was measured using the Dual-Glo SRE-Luciferase Assay (Promega) according to manufacturer's instructions. Briefly, *Lmna*$^{+/+}$, *Lmna*$^{-/-}$ and *Lmna* N195K MEFs were transfected with either the SRE reporter construct or positive and negative controls. Dual-luciferase data from starved and serum-stimulated transfected cells were then collected on a luminometer. The fold change of SRE activity for each cell line was determined by comparing normalized luciferase activities of the reporter in stimulated versus starved samples.

Time-lapse microscopy and photobleaching experiments. For live cell imaging, a Zeiss LSM 700 confocal microscope (Carl Zeiss) equipped with a ×63 oil immersion objective (Carl Zeiss) was used. Cells were maintained at 37 °C in HEPES-buffered DMEM for the duration of the time-lapse acquisition. Images were recorded at 30 s or 1 min intervals and analysed using the Zen software (Carl Zeiss). For photobleaching experiments, cells were plated on a coverslip and mounted onto a glass slide with a depression containing culture media. Fluorescence loss in photobleaching (FLIP) experiments were performed on a Zeiss LSM 700 confocal microscope (Carl Zeiss) using the 488 nm laser line. Cells had been serum-stimulated for 30 min before the experiments. Relative loss in nuclear fluorescence during continuous photobleaching of cytoplasmic MKL1–GFP was computed by normalizing nuclear fluorescence intensity to pre-bleach values ($t = 0$). Increased loss of nuclear fluorescence indicates a higher rate of nuclear export of MKL1–GFP. For FLIP experiments, two single scans were acquired, followed by repeated photobleaching using a single bleach pulse at intervals of 1 s for 200 iterations in defined regions of approximately 30 μm^2 in the cytoplasm. Single section images were then collected at 1 s intervals. For imaging, the laser power was attenuated to 2% of the bleach intensity. The relative fluorescence intensity in a region of interest was determined by normalizing fluorescence intensity in the region to the total fluorescence in the same region during prebleach. This method provides a means of quantifying nuclear export as the cytoplasmic pool of fluorescent protein is rapidly bleached and subsequent loss of fluorescence signal from the nucleus reflects nuclear export. For FRAP experiments, the cells were scanned

©2013 Macmillan Publishers Limited. All rights reserved

two times before photobleaching by scanning the region of interest 80 times at 100% laser intensity of a 488-nm laser line. Single section images were then collected at 5-s intervals with laser power attenuated to 2% of the bleach intensity. The fluorescence intensity at the region of interest at each time point was normalized to the change in total fluorescence due to bleaching and imaging, as described previously[32]. For actin FRAP experiments, cells were photobleached in defined ~2 μm diameter nuclear and cytoplasmic regions with 2 μm thickness[33]. Values were normalized to the whole-cell fluorescence or nuclear fluorescence at each time point, for cytoplasmic and nuclear actin FRAP, respectively. For photoactivation experiments, cells expressing MKL1–PAGFP were plated on glass-bottom dishes and starved for 24 h before stimulation with 15% FBS in phenol-red free DMEM for 30 min. Imaging was performed at 37 °C using an LSM 700 confocal microscope (Carl Zeiss). Photoactivation of cytoplasmic MKL1–PAGFP was carried out using the 405-nm laser at 50% laser power for 30 iterations. Sequential imaging after photoactivation was performed using a ×63 oil immersion objective using excitation from a 488-nm laser line with 2% laser intensity. The increase of fluorescence was normalized to the initial fluorescence of the cytoplasmic activation area.

Statistical analysis. Statistical analysis was performed using GraphPad Prism (GraphPad Software Inc.). Data are presented as mean ± s.e.m. unless stated otherwise. Two-tailed unpaired *t*-test and one-way ANOVA were used as detailed in respective figure legends. Statistical significance was defined as $P < 0.05$. All results are derived from three independent experiments.

30. Kudo, N. *et al.* Leptomycin B inhibition of signal-mediated nuclear export by direct binding to CRM1. *Exp. Cell Res.* **242,** 540–547 (1998).
31. Knowles, G. C. & McCulloch, C. A. Simultaneous localization and quantification of relative G and F actin content: optimization of fluorescence labeling methods. *J. Histochem. Cytochem.* **40,** 1605–1612 (1992).
32. Phair, R. D. & Misteli, T. High mobility of proteins in the mammalian cell nucleus. *Nature* **404,** 604–609 (2000).
33. McDonald, D., Carrero, G., Andrin, C., de Vries, G. & Hendzel, M. J. Nucleoplasmic beta-actin exists in a dynamic equilibrium between low-mobility polymeric species and rapidly diffusing populations. *J. Cell Biol.* **172,** 541–552 (2006).

©2013 **Macmillan Publishers Limited. All rights reserved**

Current Biology 23, R1113–R1121, December 16, 2013 ©2013 Elsevier Ltd All rights reserved http://dx.doi.org/10.1016/j.cub.2013.11.009

Nuclear Mechanics and Mechanotransduction in Health and Disease

Review

Philipp Isermann[1] and Jan Lammerding[1,*]

The nucleus is the defining feature of eukaryotic cells and often represents the largest organelle. Over the past decade, it has become apparent that the nucleus is tightly integrated into the structural network of the cell through so-called LINC (linker of the nucleoskeleton and cytoskeleton) complexes, which enable transmission of forces between the nucleus and cytoskeleton. This physical connection between the nucleus and the cytoskeleton is essential for a broad range of cellular functions, including intracellular nuclear movement and positioning, cytoskeletal organization, cell polarization, and cell migration. Recent reports further indicate that forces transmitted from the extracellular matrix to the nucleus via the cytoskeleton may also directly contribute to the cell's ability to probe its mechanical environment by triggering force-induced changes in nuclear structures. In addition, it is now emerging that the physical properties of the nucleus play a crucial role during cell migration in three-dimensional (3D) environments, where cells often have to transit through narrow constrictions that are smaller than the nuclear diameter, e.g., during development, wound healing, or cancer metastasis. In this review, we provide a brief overview of how LINC complex proteins and lamins facilitate nucleo-cytoskeletal coupling, highlight recent findings regarding the role of the nucleus in cellular mechanotransduction and cell motility in 3D environments, and discuss how mutations and/or changes in the expression of these nuclear envelope proteins can result in a broad range of human diseases, including muscular dystrophy, dilated cardiomyopathy, and premature aging.

Introduction

Mechanotransduction defines the process by which cells 'translate' mechanical stimuli into biochemical signals, enabling cells to sense their physical environment and adjust their structure and function accordingly. While mechanotransduction was first studied in specialized sensory cells, such as the inner hair cells involved in hearing, we now know that virtually all cells respond to mechanical stimulation. A growing body of work over the past two decades has led to the suggestion that, rather than relying on a single central 'mechanosensor', cells utilize a variety of mechanosensitive elements to sense applied forces and substrate stiffness, ranging from stretch-activated ion channels in the plasma membrane, conformational changes in proteins at focal adhesions and inside the cytoskeleton, to force-induced unfolding of extracellular matrix proteins, [1–3]. Recent findings have further fueled the speculation that the nucleus itself may act as a cellular mechanosensor, bypassing diffusion-based mechano-signaling through the cytoplasm to directly modulate expression of mechanosensitive genes [3].

Department of Biomedical Engineering & Weill Institute for Cell and Molecular Biology, Cornell University, Ithaca, NY 14853, USA.
[1]These authors contributed equally to this work.
*E-mail: jan.lammerding@cornell.edu

A central role in this mechanosensory process has been attributed to lamins, which are type V nuclear intermediate filaments that constitute the major components of the nuclear lamina — a dense protein network underlying the inner nuclear membrane — and that also form stable structures within the nucleoplasm [4]. Lamins can be separated into A-type and B-type lamins, with lamins A and C as the major A-type isoforms, and lamins B1 and B2 being the major B-type isoforms in somatic cells [4]. Lamins interact with a variety of nuclear envelope proteins, including emerin, lamin B receptor, and the nesprin and SUN protein families [5], as well as with numerous transcriptional regulators [4,5]. Lamins can also directly interact with chromatin [6] and help tether specific chromatin regions known as lamina-associated domains (LADs) to the nuclear periphery [7]; loss of lamins results in changes in chromatin organization, including the loss of peripheral heterochromatin [8]. Lamins, in particular lamins A and C, provide structural support to the nucleus [9,10] and play an important role in physically connecting the nucleus to the cytoskeleton, thereby enabling forces to be transmitted from the cytoskeleton and extracellular matrix to the nuclear interior [11–14].

Lamins are an extended part of the LINC (linker of nucleoskeleton and cytoskeleton) complex [15], which enables force transmission across the nuclear envelope. The LINC complex itself is composed of two protein families — SUN domain proteins at the inner nuclear membrane and KASH domain proteins at the outer nuclear membrane — that engage across the luminal space via their conserved SUN and KASH domains (Figure 1). SUN domain proteins interact with the nuclear lamina, nuclear pore proteins, and other nuclear proteins at the nuclear interior; in the cytoplasm, KASH domain proteins can bind to all major cytoskeletal filament networks, including actin filaments (through the actin-binding domain of the giant isoforms of nesprin-1 and -2), intermediate filaments (via interaction of nesprin-3 with the cytoskeletal linker plectin), and microtubules (via kinesin and dynein motor proteins binding to nesprin-1, -2, -4 and KASH5) [16]. We refer the reader to excellent recent reviews regarding the detailed molecular organization of the LINC complex [16], its evolutionary history [17], and the diverse role of lamins and other nuclear envelope proteins in other cellular functions [18].

The importance of nuclear mechanics and nucleo-cytoskeletal coupling in cellular function has become strikingly evident over the past decade by the identification of a growing number of diseases resulting from mutations in lamins and LINC complex components. In particular, mutations in the *LMNA* gene, encoding the nuclear envelope proteins lamin A and C, cause a variety of human diseases (laminopathies) that include Emery-Dreifuss muscular dystrophy, dilated cardiomyopathy, limb-girdle muscular dystrophy, and Hutchinson-Gilford progeria syndrome [18]. For many of these diseases, the molecular disease mechanism remains incompletely understood, but recent reports demonstrate that mutations in lamins A and C can disrupt LINC complex function and cause defects in skeletal and cardiac muscle [16,19,20]. In addition to its role in muscle, proper nucleo-cytoskeletal coupling is also essential in cell migration, for example, during wound healing, inflammation, cancer metastasis, and development [13,16,21].

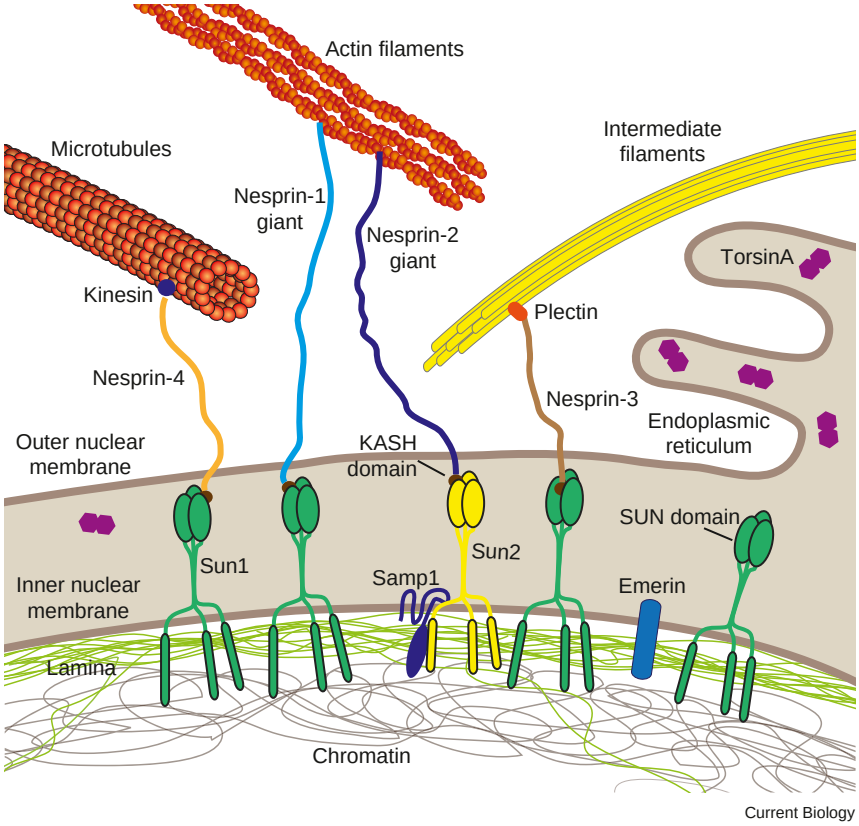

Figure 1. Schematic overview of LINC complex proteins and their connections to the cytoskeleton and nuclear interior.

SUN proteins at the inner nuclear membrane bind to the nuclear lamina and other nucleoplasmic proteins while interacting with KASH domain proteins at the outer nuclear membrane. KASH domain proteins directly or indirectly interact with cytoskeletal filaments, thereby forming a physical connection between the nuclear interior and cytoskeleton. Please note that SUN and KASH domain proteins can exist in multiple isoforms encoded by several genes. In human somatic cells, the most predominant KASH domain proteins are nesprin-1, -2, and -3 and their various isoforms, and Sun1 and Sun2 are the predominant SUN proteins [16]. Illustrated are only the largest isoforms for nesprin-1–4; cells express many additional shorter nesprin isoforms, including some lacking the KASH domain. Smaller nesprin isoforms may also be located on the inner nuclear membrane. Note that nesprin-1, -2, -4 and KASH5 can also interact with kinesin and/or dynein. Samp1 and torsinA are involved in the regulation of the LINC complex. Not depicted are KASH5 and the SUN protein isoforms Sun3–5, as their expression is restricted to germ cells. The nuclear lamina comprises A-type and B-type lamins. Note that torsinA can be localized in the endoplasmic reticulum and the perinuclear space, with the distribution varying depending on expression levels.

Cytoskeletal forces are required to dynamically position the nucleus during migration on 2D substrates [21]. In 3D environments, the cell and nucleus face additional challenges, as the dense fibrous extracellular matrix network and tight interstitial spaces often create constrictions smaller than the size of the nucleus, so that the deformation of the typically large and relatively stiff nucleus can become a rate-limiting step [22].

In this Review, we provide an overview of the current understanding of the role of the nucleus and the nuclear envelope in cellular mechanosensing and mechanotransduction signaling and discuss how changes in nuclear structure and disturbed nucleo-cytoskeletal coupling can contribute to human disease. We conclude with a brief outlook on new directions in this exciting research field and discuss how improved insights into nucleo-cytoskeletal coupling and nuclear mechanosensing may eventually point to novel therapeutic approaches for the various nuclear envelopathies.

The Role of the Nucleus in Mechanotransduction

In its literal definition, mechanotransduction refers only to the immediate cellular processes in which mechanical stimuli are transduced into biochemical signals; however, the term mechanotransduction is often applied more broadly to describe the overall cellular response to changes in its mechanical environment, for example, activation of specific genes or changes in cellular structure and organization. In the following, we use the term ‘mechanosensing’ to describe the initiating mechanotransduction events, while denoting the downstream signaling and changes in gene expression as ‘mechanotransduction signaling’.

Given the central role of the nucleus in transcriptional regulation, it has long been speculated that the nucleus could act as a cellular mechanosensor that can directly modulate gene expression in response to mechanical disturbances. It is well established that external forces applied to a cell are transmitted from the plasma membrane via the cytoskeleton to the nucleus, resulting in (intra-)nuclear deformations [23–25]. These deformations could alter chromatin structure or induce conformational changes in nuclear proteins, such as the release of transcriptional regulators or translocation of chromatin segments away from transcriptionally repressive regions, thereby activating (or repressing) mechanosensitive genes (Figure 2). Support for this idea comes from three recent studies. Dahl and colleagues [26] found that fluid shear stress and compressive stress application increase intranuclear movement of fluorescent fusion proteins binding to ribosomal DNA and RNA in a number of cell lines, indicating that externally applied forces can indeed alter chromatin organization and accessibility. Going a step further, Wang and co-workers [27] reported that application of approximately nanonewton forces to the surface of HeLa cells via magnetic microspheres results in rapid (less than 1 s) dissociation of two major structural Cajal body proteins, coilin and SMN, and that disruption of the actin cytoskeleton or depletion of lamins A and C abolishes this response. Most recently, Discher and colleagues [28] revealed an additional mechanism by which force-induced nuclear deformation could initiate biochemical responses, focusing on the role of nuclear lamins. Application of fluid shear stress to isolated nuclei caused the immunoglobulin (Ig) domain of lamin A to unfold, exposing a previously buried cysteine residue [28]. While these findings indicate that the nuclear lamina could

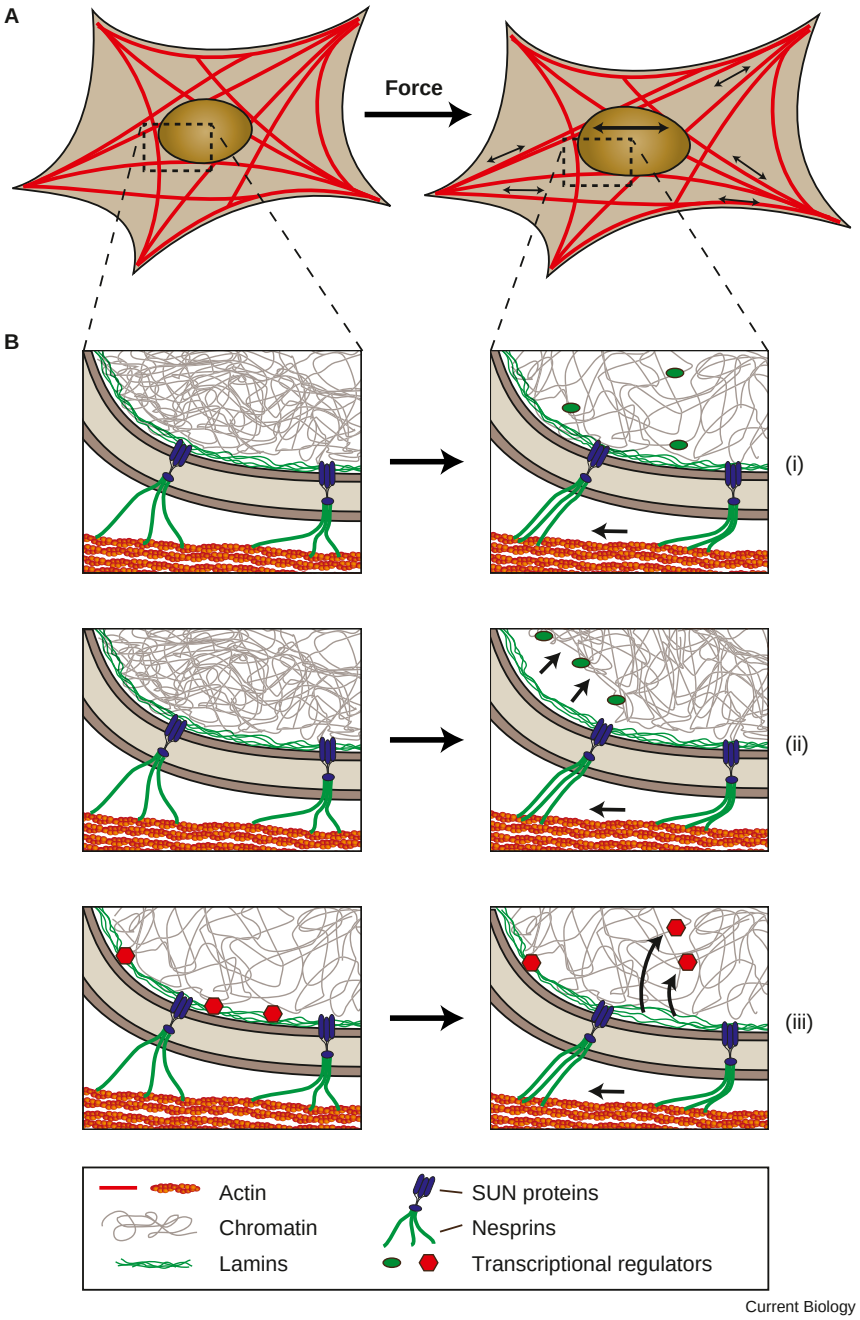

Figure 2. Potential mechanisms of nuclear mechanosensing.

Schematic illustration of how force-induced nuclear deformation could modulate expression of mechano-responsive genes. (A) A cell exposed to a uniaxial stretch, resulting in nuclear deformation by forces transmitted from focal adhesions through the (actin) cytoskeleton to the nucleus. (B) Potential molecular mechanisms for nuclear mechanosensing. (i) Opening of chromatin structures under force, enabling access of transcriptional regulators to the chromatin. (ii) Chromatin detachment from the lamina, freeing genes from the often transcriptionally repressive nuclear periphery; this process could also result in further changes in chromatin structure, promoting access to transcriptional regulators. (iii) Stretching the lamina could result in conformational changes or partial unfolding of lamins, altering their interaction with transcriptional regulators. Shown here is the release of transcription factors, which can then interact with their target genes. Phosphorylation and other post-translational modifications of nuclear envelope proteins could further contribute to nuclear mechanosensing.

function as a nuclear force sensor, in their current study, Discher and colleagues [28] did not observe any exposed cysteines in intact cells, which may suggest that forces acting on the nucleus under physiological conditions are insufficient to cause (partial) protein unfolding. Furthermore, it remains to be seen whether any partial unfolding of lamins could alter the interaction with their diverse binding partners to initiate further changes in transcriptional regulation.

Interestingly, the same study by Discher and colleagues [28] also investigated the expression levels and phosphorylation state of lamins in response to changes in the cellular mechanical environment, revealing that the expression of lamins A and C (relative to B-type lamins) scales with the substrate stiffness *in vitro* and *in vivo*. In addition, softer substrates, which correspond to reduced cytoskeletal tension, were associated with higher levels of lamin A/C phosphorylation [28], indicative of a more soluble and mechanically weaker lamin network. As lamins A and C are the main contributors to nuclear stiffness and stability, it is easily conceivable that cells adapt the expression and organization of lamins to their mechanical environment, for example, resulting in high levels of lamins A and C in mechanically stressed tissues, such as skeletal and cardiac muscle, and low levels of lamins A and C in brain or adipose tissue, thereby normalizing the mechanical stress acting on the lamin network. However, at the current time, it remains to be seen whether this intriguing correlation is caused by a direct role of lamins in mechanosensing and a corresponding feedback loop to control lamin levels, or whether transcriptional regulation of lamins in response to substrate stiffness is downstream of other mechanotransduction signaling pathways.

Arguing, at least in part, against the idea that induced nuclear deformations are essential for cellular mechanosensing and mechanotransduction signaling is a recent study that found that disruption of LINC complex proteins by dominant-negative nesprin and SUN constructs almost completely abolishes nuclear deformation when cells are subjected to substrate strain, yet the mechanoresponsive genes tested by the authors were activated normally [24]. While these experiments do not exclude the possibility that some mechanosensitive genes exist that directly respond to nuclear deformation, they lead to the suggestion that mechanosensors in the plasma membrane and/or the

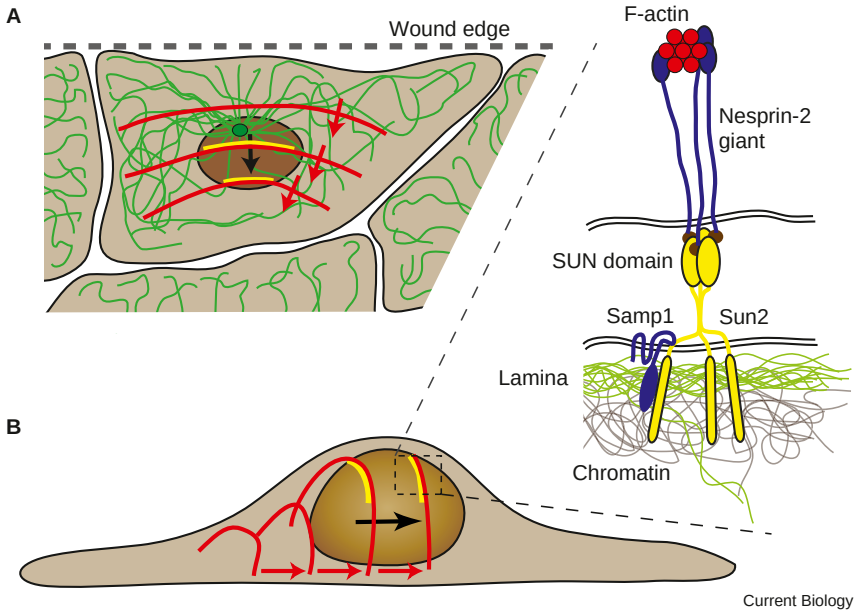

Figure 3. Nuclear positioning during cell polarization via TAN lines.

Schematic depiction of retrograde nuclear movement during early polarization in a scratch wound assay. (A) The nucleus moves to the rear end of the cell, resulting in the centrosome (green, with microtubule network) to become located towards the leading edge (i.e., the wound edge) of the cell. Nuclear translocation is mediated by rearward moving dorsal actin cables (red), which form stable connections to complexes of nesprin-2, Sun2 and Samp1 (yellow), referred to as TAN lines. (B) Schematic side view of the process by which rearward moving actin cables move the nucleus towards the rear of the cell. The inset shows a close-up of the molecular structure of the TAN lines: F-actin cables interact with the actin-binding domain of nesprin-2 molecules, which bind to Sun2 homotrimers across the perinuclear space. Sun2 also interacts with Samp1 and the underlying nuclear lamina and chromatin.

cytoskeleton may be sufficient to initiate mechanotransduction pathways that are then transmitted via biochemical signals to the nucleus.

On the other hand, nuclear envelope proteins undoubtedly play an important role in cellular mechanotransduction signaling. LINC complex disruption impairs intracellular force transmission from the cytoskeleton to the nucleus and, at least in C2C12 myoblasts, LINC complex disruption can interfere with stretch-induced proliferation [29]. In endothelial cells, nesprins play an important role in the response to fluid shear stress, with depletion of nesprin-3 causing altered cell morphology and impaired cell polarization and migration in the direction of the fluid flow [30]. Even more dramatic changes are observed in cells lacking lamins A and C or emerin, which have impaired activation of mechanoresponsive genes *in vitro* and *in vivo* [10,31–33]. The molecular details underlying impaired activation of the mechanosensitive transcription factor myocardin-related transcription factor-A (MRTF-A, also known as MKL1 or MAL) were recently elucidated [32]. MRTF-A, which plays a critical role in cardiac development and function, is normally sequestered in the cytoplasm by interaction with monomeric actin; stimulation by mechanical stress or serum induces the assembly of actin filaments, resulting in the release of MRTF-A and its translocation to the nucleus, where it serves as co-activator for the transcription factor serum response factor (SRF) to initiate expression of genes with a serum response element (SRE) that include vinculin, actin, and SRF itself [34]. Nuclear activity and export of MRTF-A are further modulated by polymerization of nuclear actin [34,35]. Since emerin, which can directly bind actin and promote its polymerization [36], requires lamin A/C for its localization to the inner nuclear membrane, functional loss of lamin A/C or emerin reduces nuclear and cytoskeletal actin dynamics and results in impaired translocation and activation of MRTF-A [32], demonstrating how structural changes mediated by lamin A/C and emerin can affect gene regulation.

Importantly, lamins and other proteins involved in nucleo-cytoskeletal coupling also directly interact with chromatin and numerous transcriptional regulators, including: retinoblastoma protein (pRb), c-Fos, and ERK1/2 for lamins A/C; α-catenin and ERK1/2 for nesprin-2; and β-catenin, barrier-to-autointegration factor (BAF), germ cell-less (GCL) and the splicing-associated factor YT521-B for emerin [4,5,37]. Consequently, defects in mechanotransduction signaling in lamin A/C- or emerin-deficient cells may also be attributed to the loss of the interaction of lamins or emerin with these transcriptional modulators, rather than the loss of their role in nucleo-cytoskeletal coupling and nuclear stability, although more experimental evidence is needed to distinguish between these (non-mutually exclusive) hypotheses.

As these findings demonstrate, nuclear structure and deformability, as well as force transmission between the cytoskeleton and nucleus, play crucial roles in activating or modulating cellular mechanotransduction signaling. At the same time, nuclear mechanics and nucleo-cytoskeletal coupling can also directly affect other cellular functions that require the physical movement and positioning/anchoring of the nucleus within the cell. Examples include the rearward nuclear position in (most) migrating cells, the peripheral nuclear placement in striated muscle cells, or the basal nuclear position in stem cells asymmetrically dividing in their niche [16].

Nuclear Positioning in 2D Cell Migration

Many cells cultured on flat substrates show a characteristic cellular reorientation (polarization) before initiating migration [38]. Scratch wound assays reveal that, during the polarization process, the nucleus moves rearwards, away from the wound edge, resulting in the centrally located centrosome to be positioned ahead of the nucleus, towards the wound edge (Figure 3). This process requires intact nucleo-cytoskeletal coupling because LINC complex disruption or depletion of lamins prevents rearward nuclear movement [12,21,24].

A seminal study by Luxton and colleagues [21] uncovered that the nuclear repositioning during cell polarization is mediated by coupling the nucleus to dorsal actin cables

that — driven by Cdc42 and actin–myosin II interactions — originate near the leading edge of the cell and move rearward, thereby dragging the nucleus backwards (Figure 3) [21]. These so-called TAN (transmembrane actin-associated nuclear) lines are composed of actin filaments, nesprin-2 giant at the outer nuclear membrane, and Sun2 at the inner nuclear membrane [21], and, as recently discovered, the inner nuclear membrane protein Samp1 [39]. The mobility of nesprins that are part of the TAN lines is significantly lower than in other parts of the nucleus, indicating that they are part of a stable complex [21]. This complex formation may be mediated by Samp1, as depletion of Samp1 results in failure to reposition the nucleus [39]. Similarly, when the LINC complex is disrupted by RNAi-mediated depletion of lamin A or Sun2, the TAN lines drift across the nuclear envelope without becoming sufficiently anchored, resulting in lack of nuclear movement and defects in cell polarization and migration [21]. In single-cell migration assays, LINC complex disruption causes reduced migration speed and decreased directional persistence [24], further demonstrating the importance of intact nucleo-cytoskeletal coupling. We refer the reader to a recent review [16] for a more detailed discussion of nucleo-cytoskeletal coupling in 2D cell migration.

Cell Migration in 3D Environments

Most *in vitro* migration assays are conducted on 2D surfaces; in contrast, cell motility *in vivo* — for example, cell migration during early development, infiltration of immune cells into sites of infection, or invasion of cancer cells into adjacent tissues — typically takes place in 3D environments. An emerging field of research suggests that cell migration in 3D environments differs substantially from 2D migration (discussed in [40]).

Nuclear Deformability as a Rate-Limiting Step in 3D Cell Migration

While much of the research in cell migration — both in 2D and 3D environments — has been focused on processes at the leading edge, particularly the dynamics of the actin cytoskeleton, it is now becoming evident that the mechanical properties of the cell nucleus and its connection to the cytoskeleton play an essential role in 3D migration [22,41]. When cells encounter constrictions in the interstitial space that are smaller than their nuclear diameter, cells can either proteolytically degrade the constricting extracellular matrix or attempt to squeeze through the narrow opening, requiring substantial cellular deformation. During non-proteolytic migration, the highly adaptable and dynamic cytoskeleton and plasma membrane can penetrate spaces less than 1 μm in diameter [22], but the large and stiff nucleus is much more resistant to large deformations and imposes a rate-limiting step during migration through narrow constrictions [22,42]. Recent studies of cells migrating through 3D collagen matrices, polycarbonate filters, or microfabricated channels with well-defined pore sizes demonstrate that decreasing pore sizes beyond 20 μm gradually reduces migration speed [22,43]. Movement of the cell body and nucleus stalls completely when encountering constrictions smaller than ~10% of the initial nuclear diameter [22], suggesting a finite limit of the compressibility of the nucleus [22,44].

Given the prominent role of nuclear envelope proteins, particularly lamins A and C, in determining nuclear deformability, it is intriguing to speculate to what extent nuclear envelope composition can affect cell migration in 3D environments. Cells expressing a lamin A mutation that increases nuclear stiffness [45,46] have difficulties navigating through 6 μm wide constrictions, even though they have similar migration speeds in unconfined spaces as control cells [47]. Conversely, neutrophils have evolved highly lobulated nuclei almost completely lacking lamins A and C, making them well suited to pass through narrow capillaries and narrow constrictions during extravasation and interstitial migration [48]. Ectopic expression of lamin A in HL-60-derived neutrophil-like cells induces rounder nuclei and an impaired ability to pass through narrow constrictions during perfusion and migration [42], further illustrating the importance of nuclear deformability in 3D cell motility.

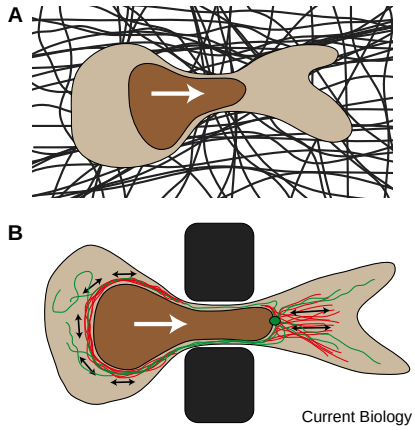

Figure 4. Nuclear deformation during cell migration through tight constrictions.

(A) Schematic depiction of a cross-section of a cell migrating through a constriction in the dense extracellular matrix (dark fibers) that is smaller than the nuclear diameter. The white arrow denotes the direction of cell migration. The nucleus is depicted in brown. (B) Side view of a cell migrating through a polycarbonate filter or microfabricated device used to study nuclear deformation during cell migration through precisely defined pores. Illustrated in red are actin–myosin networks, applying contractile forces (black arrows) to the nucleus, either posterior to the nucleus, resulting in a pushing force, or anterior, pulling on the nucleus. Molecular motors on the microtubule network (green, with centrosome) may apply additional forces to the nucleus, particularly during neuronal migration. White arrow indicates the direction of migration.

Does the Cytoskeleton Pull or Push the Nucleus during 3D Migration?

The nuclear deformation during cell passage through narrow constrictions requires substantial cytoskeletal forces acting on the nucleus. One can imagine several non-mutual exclusive possibilities explaining how forces could be applied to the nucleus to move it through tight constrictions. The cytoskeleton could exert forces from the cell front, pulling on the nucleus, or it could apply contractile forces from the rear, pushing and squeezing the nucleus through the constriction (Figure 4). Pulling forces could result from molecular motors such as dynein attached to the nuclear surface via LINC complex proteins, moving the nucleus along the microtubule network towards the centrosome on the other side of the constriction. Actin–myosin interactions could exert contractile forces between forward-based focal adhesions and the anterior edge of the nucleus. The contribution of pulling forces is supported by the finding that integrin- and actomyosin-dependent force generation is

Table 1. List of proteins/genes involved in nucleo-cytoskeletal coupling and the diseases associated with specific mutations.

Protein (Gene)	Diseases [Reference]
Lamin A/C (*LMNA*)	Emery-Dreifuss muscular dystrophy [78]
	Limb-girdle muscular dystrophy [79]
	Dilated cardiomyopathy [80]
	Congenital muscular dystrophy (dropped head) [81]
	Heart-hand syndrome [82]
	Dunnigan-type familial partial lipodystrophy [83]
	Generalized lipoatrophy [84]
	Mandibuloacral dysplasia [85]
	Charcot-Marie-Tooth syndrome [86]
	Atypical Werner syndrome [87]
	Hutchinson-Gilford progeria syndrome [86,88]
	Restrictive dermopathy [89]
Lamin B1 (*LMNB1*)	Adult onset leukodystrophy (caused by duplication) [66]
Lamin B2 (*LMNB2*)	Partial lipodystrophy [67,68]
Emerin (*STA*/*EMD*)	Emery-Dreifuss muscular dystrophy [90]
Nesprin-1 (*SYNE1*)	Emery-Dreifuss muscular dystrophy [91]
	Dilated cardiomyopathy [92]
	Cerebellar ataxia [61]
	Arthrogryposis [62]
Nesprin-2 (*SYNE2*)	Emery-Dreifuss muscular dystrophy [91]
	Dilated cardiomyopathy [91]
Nesprin-3 (*SYNE3*)	None reported to date
Nesprin-4 (*NESP4*)	Hearing loss [64]
SUN1 (*SUN1*)	None reported to date
SUN2 (*SUN2*)	Emery-Dreifuss muscular dystrophy (patient also carried other mutations) [65]
TorsinA (*TOR1A*)	Early-onset generalized torsion dystonia [93]

Not included here are mutations in cytoskeletal and motor proteins that can result in muscular dystrophies, cardiomyopathies, and lissencephaly due to impaired neuronal migration [16].

required for non-proteolytic cell migration through dense collagen matrices [22] and observations of herniations of the nuclear membrane at the anterior edge of the nucleus along with detachment of the chromatin from the nuclear envelope in lamin B1-mutant neurons during migration [49].

At the same time, actomyosin-generated contraction can also serve as the pushing force for the nucleus, as seen in the interkinetic nuclear migration of neurons in the retina of zebrafish [50]. Unlike in mammalian cells, where interkinetic nuclear movement is mainly driven by microtubule-associated motors [51], zebrafish neurons rely on myosin II activity at the rear of the nucleus to push the nucleus forward [50], possibly reflecting species- or cell-shape-dependent differences [51]. While non-muscle myosin-IIa is located near the leading edge of cells [52–54], non-muscle myosin-IIb is present in the actin network surrounding the nucleus [55]. The idea of a contractile network consisting of F-actin and myosin-II at the side and rear of the cell responsible for pushing the nucleus through the constriction is consistent with data observed by Wolf *et al.* [22], who found that inhibition of myosin light chain activity reduced cell migration in dense collagen matrices, and further supported by the finding that in breast cancer cells invading Matrigel scaffolds, actomyosin-based cytoskeletal contraction is limited to the rear of the cells, and inhibition of actomyosin-based contraction abolishes invasion [56].

As squeezing the fluid-filled nucleus from the rear may produce similar nuclear protrusions into the constriction as expected in a pulling model (Figure 4B), it is challenging to distinguish between the two major modes — i.e., pulling or pushing the nucleus through the constriction — by observation of nuclear deformations alone. Further research is necessary to elucidate the molecular details involved in overcoming the nuclear resistance during cell migration in 3D environments. Importantly, it remains to be seen to what extent these processes require nucleo-cytoskeletal coupling through the LINC complex. While at least one study reported that LINC complex disruption impairs cell migration in 3D environments [57], a contractile actomyosin network at the rear of the nucleus may not necessarily require LINC complex function to transmit forces to the nucleus. Furthermore, a nuclear positioning mechanism independent of the LINC complex has been observed during the migration of nuclei in *Drosophila* oocytes, where polymerizing microtubules at the rear of the nucleus propel the nucleus forward [58].

In light of the emerging importance of nuclear mechanics during cell migration in 3D environments, it is intriguing to speculate whether cells are capable of dynamically adjusting the mechanical properties of the nucleus. An example of long-term adjustment can be seen during granulopoiesis, when cells downregulate expression of lamins while increasing expression of the lamin B receptor, resulting in highly lobulated and deformable nuclei in granulocytes that promote passage through tight spaces [42,59]. Given the recent report of changes in lamin expression and phosphorylation in response to substrate stiffness [28], it is not too far-fetched to envision that cells may dynamically reduce or partially depolymerize the nuclear lamin network to transiently increase nuclear deformability, similar to the process of nuclear envelope breakdown during mitosis. Alternatively, cells could enhance migration through narrow constrictions by increasing the cytoskeletal tension, thereby exerting more forces on the nucleus. This could be particularly relevant in the spreading of cancer cells, as cells with increased metastatic potential were recently shown to generate higher cytoskeletal forces [60].

LINC Complex-Associated Proteins and Human Diseases

Given the range of cellular functions that require intact nucleo-cytoskeletal coupling, it comes as no surprise that mutations in LINC complex-associated proteins can result in a large number of human diseases (Table 1). The majority of diseases are caused by mutations in the *LMNA* gene, encoding lamins A and C. These laminopathies range from highly tissue-specific diseases affecting striated muscle, adipose tissue, or peripheral nerves to systemic disorders and include Emery-Dreifuss muscular dystrophy, limb-girdle muscular dystrophy, dilated cardiomyopathy, familial partial lipodystrophy, Charcot-Marie-Tooth and the accelerated aging disorder Hutchinson-Gilford progeria syndrome (reviewed in [18]).

Interestingly, diseases affecting striated muscle, i.e., Emery-Dreifuss muscular dystrophy and dilated cardiomyopathy, can also be caused by mutations in emerin (*STA* or *EMD* gene), nesprin-1 (*SYNE1*), and nesprin-2 (*SYNE2*), suggesting a LINC complex-associated disease mechanism [16]. In addition to these muscular phenotypes, nesprin-1 mutations are also responsible for autosomal recessive cerebellar ataxia [61] and arthrogryposis [62], which is characterized by congenital joint contractures resulting from reduced fetal movements. Mutations in nesprin-4, for which expression is limited to secretory epithelial cells and hair cells of the inner ear [63], result in progressive

high-frequency hearing loss, a phenotype that can be recapitulated in mice lacking either nesprin-4 or Sun1 [64]. In contrast, no disease-causing mutations have been reported for either of the SUN proteins, although a novel mutation in Sun2 was recently described in a patient with Emery-Dreifuss muscular dystrophy who was also carrying a mutation in nesprin-1α1, which by itself is considered non-pathogenic [65]. Interestingly, the same study also identified a patient with Duchenne muscular dystrophy caused by a mutation in the dystrophin gene (*DMD*) also carrying a nesprin-1α2 mutation, suggesting that mutations in LINC complex proteins can act as modifier genes in other muscular dystrophies. Mutations and gene duplications have also been described for B-type lamins [18]. Duplication of *LMNB1* results in adult onset leukodystrophy [66], characterized by demyelination in the central nervous system. Mutations in *LMNB2* cause acquired partial lipodystrophy, which involves a progressive loss of subcutaneous fat tissue [67,68].

The disease etiology for the broad spectrum of nuclear envelopathies remains incompletely understood. Patient cells are often characterized by abnormal nuclear morphology and altered distribution of nuclear envelope proteins, including mislocalization of lamins, nesprins, and SUN proteins [16], and lamin mutations linked to striated muscle diseases result in impaired nucleo-cytoskeletal force transmission and reduced nuclear stability [11,20]. These findings suggest that, at least for the diseases affecting cardiac and skeletal muscle, which are exposed to particularly high levels of mechanical stress, defects in nucleo-cytoskeletal coupling and nuclear mechanics could directly contribute to the disease phenotype. Nonetheless, it is likely that additional mechanisms, such as impaired mechanotransduction signaling, disturbed transcriptional regulation, or impaired stem cell function, further contribute to the disease development and are responsible for the broad spectrum of human diseases [18].

One interesting and unexpected disease mechanism emerged from the recent crossing of lamin A/C-deficient and Sun1-deficient mouse models. Mice that lack lamins A and C develop severe muscular dystrophy and dilated cardiomyopathy and die at 4–8 weeks of age [69]. Surprisingly, when crossed with Sun1-deficient mice, which lack an overt phenotype, the resulting double deletion of lamin A/C and Sun1 expands the lifetime of the animals, possibly by preventing toxic accumulation of Sun1 in the Golgi apparatus [70]. Similarly increased survival was observed in mice lacking exon 9 of the *Lmna* gene, which causes a progeria-like phenotype when crossed with Sun1-deficient mice [70]. These findings suggest that, in addition to disrupting their normal role in nucleo-cytoskeletal coupling, displacement of nuclear envelope proteins may cause further cellular defects by inducing Golgi stress and compromising Golgi functionality.

Recently, altered expression of nuclear envelope proteins, particularly lamins, has been reported in a number of cancers. For example, lamins A/C are downregulated in breast cancer, leukemias, lymphomas, colon cancer, and gastric carcinoma, whereas expression of A-type lamins is upregulated in prostate, skin and ovarian cancers [4,71,72]. Furthermore, a recent genome-wide analysis of 100 cancer patients identified mutations in lamins A/C, nesprin-1, and nesprin-2, which, albeit unlikely to be driver mutations, could represent modulators of cancer progression [73]. In cancer cells, altered lamin function could directly affect the nuclear deformability required for interstitial migration or act through diverse signaling pathways that promote cell motility [72,74]. These changes in nuclear envelope composition, which may provide an explanation for the often severe abnormal nuclear shape in cancer cells, could directly contribute to the disease progression, either by altering the mechanical properties of the cell nucleus [41] or by modulating signaling pathways and cytoskeletal organization associated with changes in lamin expression [75].

Outlook

Over the past decade, numerous novel nuclear envelope proteins involved in nucleo-cytoskeletal coupling and force transmission to the nucleus have been identified, including nesprins and SUN proteins, the core components of the LINC complex. Nonetheless, many questions remain unanswered. What is the role of nuclear envelope proteins in cellular mechanotransduction? Can these proteins act as nuclear mechanosensors, or do they primarily serve as processing hubs in the cellular mechanotransduction signaling network? In the context of intracellular force transmission, given the broad distribution of nesprins and SUN proteins along the nuclear surface, how is the interaction of LINC complex proteins regulated to promote (dynamic) anchoring to specific cytoskeletal structures while avoiding 'locking up' the nucleus by unwanted interaction with other cytoskeletal elements? Which proteins are involved in this regulation? Where does the regulation take place — at the cytoplasm, the nucleoplasm, or the luminal interaction between the SUN and KASH domains? Are there other, yet-to-be characterized proteins involved in linking the nucleus to the cytoskeleton independent of LINC complex proteins?

Answering these questions will not only advance our understanding of normal cellular processes but also aid in the development of therapeutic approaches, targeting the many diseases resulting from mutations in LINC-complex-associated proteins. As of now, it remains unclear to what extent direct mechanical defects such as impaired nuclear anchoring as opposed to impaired transcriptional regulation or stem cell dysfunction contribute to the disease mechanisms, and whether these defects are interrelated [11,18]. Treating impaired signaling provides a more rapidly attainable goal and has already produced some promise in cardiac laminopathies [76], but may be insufficient to overcome structural defects.

Twenty years from now, we will probably look back with a smile at the limitations of our current knowledge of nucleo-cytoskeletal coupling and nuclear mechanotransduction. The concept of transmembrane connections between the actin cytoskeleton and the extracellular matrix, leading to the discovery of integrins, is almost 40 years old [77]. That work has evolved into a tremendously successful research field spanning cell migration, stem cell differentiation and anti-cancer therapies. Is nucleo-cytoskeletal coupling headed the same way? We will not find out for a while, but it is certainly an exciting ride, wherever it may lead us.

Acknowledgements

We apologize to all authors whose work could not be cited due to space constraints. This work was supported by National Institutes of Health awards (R01 NS059348, R01 HL082792), a National Science Foundation CAREER award (CBET-1254846), the Department of Defense Breast Cancer Idea Award (BC102152), an award from the Progeria Research Foundation (PRF2011-0035), and a Pilot Project

Award by the Cornell Center on the Microenvironment & Metastasis through Award Number U54CA143876 from the National Cancer Institute. The content is solely the responsibility of the authors and does not necessarily represent the official views of the National Cancer Institute or the National Institutes of Health.

References

1. Jaalouk, D.E., and Lammerding, J. (2009). Mechanotransduction gone awry. Nat. Rev. Mol. Cell Biol. *10*, 63–73.
2. Eyckmans, J., Boudou, T., Yu, X., and Chen, C.S. (2011). A hitchhiker's guide to mechanobiology. Dev. Cell *21*, 35–47.
3. Wang, N., Tytell, J.D., and Ingber, D.E. (2009). Mechanotransduction at a distance: mechanically coupling the extracellular matrix with the nucleus. Nat. Rev. Mol. Cell Biol. *10*, 75–82.
4. Ho, C.Y., and Lammerding, J. (2012). Lamins at a glance. J. Cell Sci. *125*, 2087–2093.
5. Wilson, K.L., and Berk, J.M. (2010). The nuclear envelope at a glance. J. Cell Sci. *123*, 1973–1978.
6. Dechat, T., Pfleghaar, K., Sengupta, K., Shimi, T., Shumaker, D.K., Solimando, L., and Goldman, R.D. (2008). Nuclear lamins: major factors in the structural organization and function of the nucleus and chromatin. Genes Dev. *22*, 832–853.
7. Bickmore, W.A., and van Steensel, B. (2013). Genome architecture: domain organization of interphase chromosomes. Cell *152*, 1270–1284.
8. Solovei, I., Wang, A.S., Thanisch, K., Schmidt, C.S., Krebs, S., Zwerger, M., Cohen, T.V., Devys, D., Foisner, R., Peichl, L., *et al*. (2013). LBR and lamin A/C sequentially tether peripheral heterochromatin and inversely regulate differentiation. Cell *152*, 584–598.
9. Lammerding, J., Fong, L.G., Ji, J.Y., Reue, K., Stewart, C.L., Young, S.G., and Lee, R.T. (2006). Lamins A and C but not lamin B1 regulate nuclear mechanics. J. Biol. Chem. *281*, 25768–25780.
10. Lammerding, J., Schulze, P.C., Takahashi, T., Kozlov, S., Sullivan, T., Kamm, R.D., Stewart, C.L., and Lee, R.T. (2004). Lamin A/C deficiency causes defective nuclear mechanics and mechanotransduction. J. Clin. Invest. *113*, 370–378.
11. Zwerger, M., Jaalouk, D.E., Lombardi, M.L., Isermann, P., Mauermann, M., Dialynas, G., Herrmann, H., Wallrath, L.L., and Lammerding, J. (2013). Myopathic lamin mutations impair nuclear stability in cells and tissue and disrupt nucleo-cytoskeletal coupling. Hum. Mol. Genet. *22*, 2335–2349.
12. Folker, E.S., Ostlund, C., Luxton, G.W., Worman, H.J., and Gundersen, G.G. (2011). Lamin A variants that cause striated muscle disease are defective in anchoring transmembrane actin-associated nuclear lines for nuclear movement. Proc. Natl. Acad. Sci. USA *108*, 131–136.
13. Luxton, G.G., Gomes, E.R., Folker, E.S., Worman, H.J., and Gundersen, G.G. (2011). TAN lines: a novel nuclear envelope structure involved in nuclear positioning. Nucleus *2*, 173–181.
14. Ostlund, C., Folker, E.S., Choi, J.C., Gomes, E.R., Gundersen, G.G., and Worman, H.J. (2009). Dynamics and molecular interactions of linker of nucleoskeleton and cytoskeleton (LINC) complex proteins. J. Cell Sci. *122*, 4099–4108.
15. Crisp, M., Liu, Q., Roux, K., Rattner, J.B., Shanahan, C., Burke, B., Stahl, P.D., and Hodzic, D. (2006). Coupling of the nucleus and cytoplasm: role of the LINC complex. J. Cell Biol. *172*, 41–53.
16. Gundersen, G.G., and Worman, H.J. (2013). Nuclear positioning. Cell *152*, 1376–1389.
17. Rothballer, A., and Kutay, U. (2013). The diverse functional LINCs of the nuclear envelope to the cytoskeleton and chromatin. Chromosoma *122*, 415–429.
18. Schreiber, K.H., and Kennedy, B.K. (2013). When lamins go bad: nuclear structure and disease. Cell *152*, 1365–1375.
19. Mejat, A., and Misteli, T. (2010). LINC complexes in health and disease. Nucleus *1*, 40–52.
20. Folker, E.S., Ostlund, C., Luxton, G.W., Worman, H.J., and Gundersen, G.G. (2010). Lamin A variants that cause striated muscle disease are defective in anchoring transmembrane actin-associated nuclear lines for nuclear movement. Proc. Natl. Acad. Sci. USA *108*, 131–136.
21. Luxton, G.W., Gomes, E.R., Folker, E.S., Vintinner, E., and Gundersen, G.G. (2010). Linear arrays of nuclear envelope proteins harness retrograde actin flow for nuclear movement. Science *329*, 956–959.
22. Wolf, K., Te Lindert, M., Krause, M., Alexander, S., Te Riet, J., Willis, A.L., Hoffman, R.M., Figdor, C.G., Weiss, S.J., and Friedl, P. (2013). Physical limits of cell migration: Control by ECM space and nuclear deformation and tuning by proteolysis and traction force. J. Cell Biol. *201*, 1069–1084.
23. Morimoto, A., Shibuya, H., Zhu, X., Kim, J., Ishiguro, K., Han, M., and Watanabe, Y. (2012). A conserved KASH domain protein associates with telomeres, SUN1, and dynactin during mammalian meiosis. J. Cell Biol. *198*, 165–172.
24. Lombardi, M.L., Jaalouk, D.E., Shanahan, C.M., Burke, B., Roux, K.J., and Lammerding, J. (2011). The interaction between nesprins and sun proteins at the nuclear envelope is critical for force transmission between the nucleus and cytoskeleton. J. Biol. Chem. *286*, 26743–26753.
25. Caille, N., Tardy, Y., and Meister, J.J. (1998). Assessment of strain field in endothelial cells subjected to uniaxial deformation of their substrate. Ann. Biomed. Eng. *26*, 409–416.
26. Booth-Gauthier, E.A., Alcoser, T.A., Yang, G., and Dahl, K.N. (2012). Force-induced changes in subnuclear movement and rheology. Biophys. J. *103*, 2423–2431.
27. Poh, Y.C., Shevtsov, S.P., Chowdhury, F., Wu, D.C., Na, S., Dundr, M., and Wang, N. (2012). Dynamic force-induced direct dissociation of protein complexes in a nuclear body in living cells. Nat. Commun. *3*, 866.
28. Swift, J., Ivanovska, I.L., Buxboim, A., Harada, T., Dingal, P.C., Pinter, J., Pajerowski, J.D., Spinler, K.R., Shin, J.W., Tewari, M., *et al*. (2013). Nuclear lamin-A scales with tissue stiffness and enhances matrix-directed differentiation. Science *341*, 1240104.
29. Brosig, M., Ferralli, J., Gelman, L., Chiquet, M., and Chiquet-Ehrismann, R. (2010). Interfering with the connection between the nucleus and the cytoskeleton affects nuclear rotation, mechanotransduction and myogenesis. Int. J. Biochem. Cell Biol. *42*, 1717–1728.
30. Morgan, J.T., Pfeiffer, E.R., Thirkill, T.L., Kumar, P., Peng, G., Fridolfsson, H.N., Douglas, G.C., Starr, D.A., and Barakat, A.I. (2011). Nesprin-3 regulates endothelial cell morphology, perinuclear cytoskeletal architecture, and flow-induced polarization. Mol. Biol. Cell *22*, 4324–4334.
31. Cupesi, M., Yoshioka, J., Gannon, J., Kudinova, A., Stewart, C.L., and Lammerding, J. (2010). Attenuated hypertrophic response to pressure overload in a lamin A/C haploinsufficiency mouse. J. Mol. Cell. Cardiol. *48*, 1290–1297.
32. Ho, C.Y., Jaalouk, D.E., Vartiainen, M.K., and Lammerding, J. (2013). Lamin A/C and emerin regulate MKL1-SRF activity by modulating actin dynamics. Nature *497*, 507–511.
33. Lammerding, J., Hsiao, J., Schulze, P.C., Kozlov, S., Stewart, C.L., and Lee, R.T. (2005). Abnormal nuclear shape and impaired mechanotransduction in emerin-deficient cells. J. Cell Biol. *170*, 781–791.
34. Olson, E.N., and Nordheim, A. (2010). Linking actin dynamics and gene transcription to drive cellular motile functions. Nat. Rev. Mol. Cell Biol. *11*, 353–365.
35. Baarlink, C., Wang, H., and Grosse, R. (2013). Nuclear actin network assembly by formins regulates the SRF coactivator MAL. Science *340*, 864–867.
36. Holaska, J.M., Kowalski, A.K., and Wilson, K.L. (2004). Emerin caps the pointed end of actin filaments: evidence for an actin cortical network at the nuclear inner membrane. PLoS Biol. *2*, E231.
37. Neumann, S., Schneider, M., Daugherty, R.L., Gottardi, C.J., Eming, S.A., Beijer, A., Noegel, A.A., and Karakesisoglou, I. (2010). Nesprin-2 interacts with {alpha}-catenin and regulates Wnt signaling at the nuclear envelope. J. Biol. Chem. *285*, 34932–34938.
38. Gomes, E.R., Jani, S., and Gundersen, G.G. (2005). Nuclear movement regulated by Cdc42, MRCK, myosin, and actin flow establishes MTOC polarization in migrating cells. Cell *121*, 451–463.
39. Borrego-Pinto, J., Jegou, T., Osorio, D.S., Aurade, F., Gorjanacz, M., Koch, B., Mattaj, I.W., and Gomes, E.R. (2012). Samp1 is a component of TAN lines and is required for nuclear movement. J. Cell Sci. *125*, 1099–1105.
40. Friedl, P., Sahai, E., Weiss, S., and Yamada, K.M. (2012). New dimensions in cell migration. Nat. Rev. Mol. Cell Biol. *13*, 743–747.
41. Friedl, P., Wolf, K., and Lammerding, J. (2011). Nuclear mechanics during cell migration. Curr. Opin. Cell Biol. *23*, 55–64.
42. Rowat, A.C., Jaalouk, D.E., Zwerger, M., Ung, W.L., Eydelnant, I.A., Olins, D.E., Olins, A.L., Herrmann, H., Weitz, D.A., and Lammerding, J. (2013). Nuclear envelope composition determines the ability of neutrophil-type cells to passage through micron-scale constrictions. J. Biol. Chem. *288*, 8610–8618.
43. Tong, Z., Balzer, E.M., Dallas, M.R., Hung, W.C., Stebe, K.J., and Konstantopoulos, K. (2012). Chemotaxis of cell populations through confined spaces at single-cell resolution. PLoS One *7*, e29211.
44. Rowat, A.C., Lammerding, J., Herrmann, H., and Aebi, U. (2008). Towards an integrated understanding of the structure and mechanics of the cell nucleus. BioEssays *30*, 226–236.
45. Dahl, K.N., Scaffidi, P., Islam, M.F., Yodh, A.G., Wilson, K.L., and Misteli, T. (2006). Distinct structural and mechanical properties of the nuclear lamina in Hutchinson-Gilford progeria syndrome. Proc. Natl. Acad. Sci. USA *103*, 10271–10276.
46. Verstraeten, V.L., Ji, J.Y., Cummings, K.S., Lee, R.T., and Lammerding, J. (2008). Increased mechanosensitivity and nuclear stiffness in Hutchinson-Gilford progeria cells: effects of farnesyltransferase inhibitors. Aging Cell *7*, 383–393.
47. Booth-Gauthier, E.A., Du, V., Ghibaudo, M., Rape, A.D., Dahl, K.N., and Ladoux, B. (2013). Hutchinson-Gilford progeria syndrome alters nuclear shape and reduces cell motility in three dimensional model substrates. Integr. Biol. *5*, 569–577.
48. Olins, A.L., Hoang, T.V., Zwerger, M., Herrmann, H., Zentgraf, H., Noegel, A.A., Karakesisoglou, I., Hodzic, D., and Olins, D.E. (2009). The LINC-less granulocyte nucleus. Eur. J. Cell Biol. *88*, 203–214.
49. Jung, H.J., Nobumori, C., Goulbourne, C.N., Tu, Y., Lee, J.M., Tatar, A., Wu, D., Yoshinaga, Y., de Jong, P.J., Coffinier, C., *et al*. (2013). Farnesylation of lamin B1 is important for retention of nuclear chromatin during neuronal migration. Proc. Natl. Acad Sci. USA *110*, E1923–1932.

50. Norden, C., Young, S., Link, B.A., and Harris, W.A. (2009). Actomyosin is the main driver of interkinetic nuclear migration in the retina. Cell *138*, 1195–1208.

51. Cooper, J.A. (2013). Cell biology in neuroscience: mechanisms of cell migration in the nervous system. J. Cell Biol. *202*, 725–734.

52. Vicente-Manzanares, M., Zareno, J., Whitmore, L., Choi, C.K., and Horwitz, A.F. (2007). Regulation of protrusion, adhesion dynamics, and polarity by myosins IIA and IIB in migrating cells. J. Cell Biol. *176*, 573–580.

53. Cai, Y., Biais, N., Giannone, G., Tanase, M., Jiang, G., Hofman, J.M., Wiggins, C.H., Silberzan, P., Buguin, A., Ladoux, B., *et al*. (2006). Nonmuscle myosin IIA-dependent force inhibits cell spreading and drives F-actin flow. Biophys. J. *91*, 3907–3920.

54. Vicente-Manzanares, M., Koach, M.A., Whitmore, L., Lamers, M.L., and Horwitz, A.F. (2008). Segregation and activation of myosin IIB creates a rear in migrating cells. J. Cell Biol. *183*, 543–554.

55. Lo, C.M., Buxton, D.B., Chua, G.C., Dembo, M., Adelstein, R.S., and Wang, Y.L. (2004). Nonmuscle myosin IIb is involved in the guidance of fibroblast migration. Mol. Biol. Cell *15*, 982–989.

56. Poincloux, R., Collin, O., Lizarraga, F., Romao, M., Debray, M., Piel, M., and Chavrier, P. (2011). Contractility of the cell rear drives invasion of breast tumor cells in 3D Matrigel. Proc. Natl. Acad. Sci. USA *108*, 1943–1948.

57. Khatau, S.B., Bloom, R.J., Bajpai, S., Razafsky, D., Zang, S., Giri, A., Wu, P.H., Marchand, J., Celedon, A., Hale, C.M., *et al*. (2012). The distinct roles of the nucleus and nucleus-cytoskeleton connections in three-dimensional cell migration. Sci. Rep. *2*, 488.

58. Zhao, T., Graham, O.S., Raposo, A., and St Johnston, D. (2012). Growing microtubules push the oocyte nucleus to polarize the Drosophila dorsal-ventral axis. Science *336*, 999–1003.

59. Olins, A.L., Zwerger, M., Herrmann, H., Zentgraf, H., Simon, A.J., Monestier, M., and Olins, D.E. (2008). The human granulocyte nucleus: Unusual nuclear envelope and heterochromatin composition. Eur. J. Cell Biol. *87*, 279–290.

60. Kraning-Rush, C.M., Califano, J.P., and Reinhart-King, C.A. (2012). Cellular traction stresses increase with increasing metastatic potential. PLoS One *7*, e32572.

61. Gros-Louis, F., Dupre, N., Dion, P., Fox, M.A., Laurent, S., Verreault, S., Sanes, J.R., Bouchard, J.P., and Rouleau, G.A. (2007). Mutations in SYNE1 lead to a newly discovered form of autosomal recessive cerebellar ataxia. Nat. Genet. *39*, 80–85.

62. Attali, R., Warwar, N., Israel, A., Gurt, I., McNally, E., Puckelwartz, M., Glick, B., Nevo, Y., Ben-Neriah, Z., and Melki, J. (2009). Mutation of SYNE-1, encoding an essential component of the nuclear lamina, is responsible for autosomal recessive arthrogryposis. Hum. Mol. Genet. *18*, 3462–3469.

63. Roux, K.J., Crisp, M.L., Liu, Q., Kim, D., Kozlov, S., Stewart, C.L., and Burke, B. (2009). Nesprin 4 is an outer nuclear membrane protein that can induce kinesin-mediated cell polarization. Proc. Natl. Acad. Sci. USA *106*, 2194–2199.

64. Horn, H.F., Brownstein, Z., Lenz, D.R., Shivatzki, S., Dror, A.A., Dagan-Rosenfeld, O., Friedman, L.M., Roux, K.J., Kozlov, S., Jeang, K.T., *et al*. (2013). The LINC complex is essential for hearing. J. Clin. Invest. *123*, 740–750.

65. Taranum, S., Vaylann, E., Meinke, P., Abraham, S., Yang, L., Neumann, S., Karakesisoglou, I., Wehnert, M., and Noegel, A.A. (2012). LINC complex alterations in DMD and EDMD/CMT fibroblasts. Eur. J. Cell Biol. *91*, 614–628.

66. Padiath, Q.S., Saigoh, K., Schiffmann, R., Asahara, H., Yamada, T., Koeppen, A., Hogan, K., Ptacek, L.J., and Fu, Y.H. (2006). Lamin B1 duplications cause autosomal dominant leukodystrophy. Nat. Genet. *38*, 1114–1123.

67. Hegele, R.A., Cao, H., Liu, D.M., Costain, G.A., Charlton-Menys, V., Rodger, N.W., and Durrington, P.N. (2006). Sequencing of the reannotated LMNB2 gene reveals novel mutations in patients with acquired partial lipodystrophy. Am J. Hum. Genet. *79*, 383–389.

68. Gao, J., Li, Y., Fu, X., and Luo, X. (2012). A Chinese patient with acquired partial lipodystrophy caused by a novel mutation with LMNB2 gene. J. Ped. Endocrin. Metab *25*, 375–377.

69. Sullivan, T., Escalante-Alcalde, D., Bhatt, H., Anver, M., Bhat, N., Nagashima, K., Stewart, C.L., and Burke, B. (1999). Loss of A-type lamin expression compromises nuclear envelope integrity leading to muscular dystrophy. J. Cell Biol. *147*, 913–920.

70. Chen, C.Y., Chi, Y.H., Mutalif, R.A., Starost, M.F., Myers, T.G., Anderson, S.A., Stewart, C.L., and Jeang, K.T. (2012). Accumulation of the inner nuclear envelope protein Sun1 is pathogenic in progeric and dystrophic laminopathies. Cell *149*, 565–577.

71. Foster, C.R., Przyborski, S.A., Wilson, R.G., and Hutchison, C.J. (2010). Lamins as cancer biomarkers. Biochem. Soc. Trans. *38*, 297–300.

72. de Las Heras, J.I., Batrakou, D.G., and Schirmer, E.C. (2013). Cancer biology and the nuclear envelope: a convoluted relationship. Semin. Cancer Biol. *23*, 125–137.

73. Stephens, P.J., Tarpey, P.S., Davies, H., Van Loo, P., Greenman, C., Wedge, D.C., Nik-Zainal, S., Martin, S., Varela, I., Bignell, G.R., *et al*. (2012). The landscape of cancer genes and mutational processes in breast cancer. Nature *486*, 400–404.

74. Kong, L., Schafer, G., Bu, H., Zhang, Y., Zhang, Y., and Klocker, H. (2012). Lamin A/C protein is overexpressed in tissue-invading prostate cancer and promotes prostate cancer cell growth, migration and invasion through the PI3K/AKT/PTEN pathway. Carcinogenesis *33*, 751–759.

75. Foster, C.R., Robson, J.L., Simon, W.J., Twigg, J., Cruikshank, D., Wilson, R.G., and Hutchison, C.J. (2011). The role of Lamin A in cytoskeleton organization in colorectal cancer cells: a proteomic investigation. Nucleus *2*, 434–443.

76. Cattin, M.E., Muchir, A., and Bonne, G. (2013). 'State-of-the-heart' of cardiac laminopathies. Curr. Opin. Cardiol. *28*, 297–304.

77. Hynes, R.O. (2004). The emergence of integrins: a personal and historical perspective. Matrix Biol. *23*, 333–340.

78. Bonne, G., Di Barletta, M.R., Varnous, S., Becane, H.M., Hammouda, E.H., Merlini, L., Muntoni, F., Greenberg, C.R., Gary, F., Urtizberea, J.A., *et al*. (1999). Mutations in the gene encoding lamin A/C cause autosomal dominant Emery-Dreifuss muscular dystrophy. Nat. Genet. *21*, 285–288.

79. Muchir, A., Bonne, G., van der Kooi, A.J., van Meegen, M., Baas, F., Bolhuis, P.A., de Visser, M., and Schwartz, K. (2000). Identification of mutations in the gene encoding lamins A/C in autosomal dominant limb girdle muscular dystrophy with atrioventricular conduction disturbances (LGMD1B). Hum. Mol. Genet. *9*, 1453–1459.

80. Fatkin, D., MacRae, C., Sasaki, T., Wolff, M.R., Porcu, M., Frenneaux, M., Atherton, J., Vidaillet, H.J., Jr., Spudich, S., De Girolami, U., *et al*. (1999). Missense mutations in the rod domain of the lamin A/C gene as causes of dilated cardiomyopathy and conduction-system disease. New Engl. J. Med. *341*, 1715–1724.

81. Quijano-Roy, S., Mbieleu, B., Bonnemann, C.G., Jeannet, P.Y., Colomer, J., Clarke, N.F., Cuisset, J.M., Roper, H., De Meirleir, L., D'Amico, A., *et al*. (2008). De novo LMNA mutations cause a new form of congenital muscular dystrophy. Ann. Neurol. *64*, 177–186.

82. Renou, L., Stora, S., Yaou, R.B., Volk, M., Sinkovec, M., Demay, L., Richard, P., Peterlin, B., and Bonne, G. (2008). Heart-hand syndrome of Slovenian type: a new kind of laminopathy. J. Med. Genet. *45*, 666–671.

83. Shackleton, S., Lloyd, D.J., Jackson, S.N., Evans, R., Niermeijer, M.F., Singh, B.M., Schmidt, H., Brabant, G., Kumar, S., Durrington, P.N., *et al*. (2000). LMNA, encoding lamin A/C, is mutated in partial lipodystrophy. Nat. Genet. *24*, 153–156.

84. Caux, F., Dubosclard, E., Lascols, O., Buendia, B., Chazouilleres, O., Cohen, A., Courvalin, J.C., Laroche, L., Capeau, J., Vigouroux, C., *et al*. (2003). A new clinical condition linked to a novel mutation in lamins A and C with generalized lipoatrophy, insulin-resistant diabetes, disseminated leukomelanodermic papules, liver steatosis, and cardiomyopathy. J. Clin. Endocrinol. Metab *88*, 1006–1013.

85. Novelli, G., and D'Apice, M.R. (2003). The strange case of the "lumper" lamin A/C gene and human premature ageing. Trends Mol. Med. *9*, 370–375.

86. De Sandre-Giovannoli, A., Chaouch, M., Kozlov, S., Vallat, J.M., Tazir, M., Kassouri, N., Szepetowski, P., Hammadouche, T., Vandenberghe, A., Stewart, C.L., *et al*. (2002). Homozygous defects in LMNA, encoding lamin A/C nuclear-envelope proteins, cause autosomal recessive axonal neuropathy in human (Charcot-Marie-Tooth disorder type 2) and mouse. Am J. Hum. Genet. *70*, 726–736.

87. Chen, L., Lee, L., Kudlow, B.A., Dos Santos, H.G., Sletvold, O., Shafeghati, Y., Botha, E.G., Garg, A., Hanson, N.B., Martin, G.M., *et al*. (2003). LMNA mutations in atypical Werner's syndrome. Lancet *362*, 440–445.

88. Eriksson, M., Brown, W.T., Gordon, L.B., Glynn, M.W., Singer, J., Scott, L., Erdos, M.R., Robbins, C.M., Moses, T.Y., Berglund, P., *et al*. (2003). Recurrent de novo point mutations in lamin A cause Hutchinson-Gilford progeria syndrome. Nature *423*, 293–298.

89. Navarro, C.L., De Sandre-Giovannoli, A., Bernard, R., Boccaccio, I., Boyer, A., Genevieve, D., Hadj-Rabia, S., Gaudy-Marqueste, C., Smitt, H.S., Vabres, P., *et al*. (2004). Lamin A and ZMPSTE24 (FACE-1) defects cause nuclear disorganization and identify restrictive dermopathy as a lethal neonatal laminopathy. Hum. Mol. Genet. *13*, 2493–2503.

90. Bione, S., Maestrini, E., Rivella, S., Mancini, M., Regis, S., Romeo, G., and Toniolo, D. (1994). Identification of a novel X-linked gene responsible for Emery-Dreifuss muscular dystrophy. Nat. Genet. *8*, 323–327.

91. Zhang, Q., Bethmann, C., Worth, N.F., Davies, J.D., Wasner, C., Feuer, A., Ragnauth, C.D., Yi, Q., Mellad, J.A., Warren, D.T., *et al*. (2007). Nesprin-1 and -2 are involved in the pathogenesis of Emery-Dreifuss muscular dystrophy and are critical for nuclear envelope integrity. Hum. Mol. Genet. *16*, 2816–2833.

92. Puckelwartz, M.J., Kessler, E.J., Kim, G., Dewitt, M.M., Zhang, Y., Earley, J.U., Depreux, F.F., Holaska, J., Mewborn, S.K., Pytel, P., *et al*. (2010). Nesprin-1 mutations in human and murine cardiomyopathy. J. Mol. Cell. Cardiol *48*, 600–608.

93. Breakefield, X.O., Blood, A.J., Li, Y., Hallett, M., Hanson, P.I., and Standaert, D.G. (2008). The pathophysiological basis of dystonias. Nat. Rev. Neurosci. *9*, 222–234.

THE JOURNAL OF BIOLOGICAL CHEMISTRY VOL. 288, NO. 12, pp. 8610–8618, March 22, 2013
© 2013 by The American Society for Biochemistry and Molecular Biology, Inc. Published in the U.S.A.

Nuclear Envelope Composition Determines the Ability of Neutrophil-type Cells to Passage through Micron-scale Constrictions*[S]

Received for publication, December 1, 2012, and in revised form, January 15, 2013 Published, JBC Papers in Press, January 25, 2013, DOI 10.1074/jbc.M112.441535

Amy C. Rowat[‡§¶1], Diana E. Jaalouk[§2], Monika Zwerger[§3], W. Lloyd Ung[¶], Irwin A. Eydelnant[¶], Don E. Olins[‖], Ada L. Olins[‖], Harald Herrmann[**], David A. Weitz[¶], and Jan Lammerding[§‡‡]

From the [‡]Department of Integrative Biology and Physiology, UCLA, Los Angeles, California 90095, the [§]Department of Medicine, Brigham and Women's Hospital, Harvard Medical School, Cambridge, Massachusetts 02139, the [¶]Department of Physics and School of Engineering and Applied Sciences, Harvard University, Cambridge, Massachusetts 02138, the [‖]Department of Pharmaceutical Sciences, College of Pharmacy, University of New England, Portland, Maine 04103, the [**]Division of Molecular Genetics, German Cancer Research Center, D-69120 Heidelberg, Germany, and the [‡‡]Weill Institute for Cell and Molecular Biology, Department of Biomedical Engineering, Cornell University, Ithaca, New York 14853

Background: The unusual nuclear shape of neutrophils has been speculated to facilitate their passage through confined spaces.
Results: Levels of nuclear protein lamin A modulate cell passage through micron-scale pores.
Conclusion: The unique protein composition of neutrophil nuclei facilitates their deformation; lobulated nuclear shape is not essential.
Significance: Altered nuclear envelope composition, as reported in cancer cells, could impact cell passage through physiological gaps.

Neutrophils are characterized by their distinct nuclear shape, which is thought to facilitate the transit of these cells through pore spaces less than one-fifth of their diameter. We used human promyelocytic leukemia (HL-60) cells as a model system to investigate the effect of nuclear shape in whole cell deformability. We probed neutrophil-differentiated HL-60 cells lacking expression of lamin B receptor, which fail to develop lobulated nuclei during granulopoiesis and present an *in vitro* model for Pelger-Huët anomaly; despite the circular morphology of their nuclei, the cells passed through micron-scale constrictions on similar timescales as scrambled controls. We then investigated the unique nuclear envelope composition of neutrophil-differentiated HL-60 cells, which may also impact their deformability; although lamin A is typically down-regulated during granulopoiesis, we genetically modified HL-60 cells to generate a subpopulation of cells with well defined levels of ectopic lamin A. The lamin A-overexpressing neutrophil-type cells showed similar functional characteristics as the mock controls, but they had an impaired ability to pass through micron-scale constrictions. Our results suggest that levels of lamin A have a marked effect on the ability of neutrophils to passage through micron-scale constrictions, whereas the unusual multilobed shape of the neutrophil nucleus is less essential.

The passage of cells through narrow spaces is critical in physiological and disease processes from immune response to metastasis. For example, neutrophils are required to rapidly traverse constrictions that are much smaller than their own diameter of 7–8 μm: during perfusion through capillaries with diameters as small as 2 μm or during migration through transendothelial and interstitial spaces ranging from 0.1 to 10 μm (1). The ability of neutrophils to transit through narrow constrictions is essential; increased cell stiffness results in retention of neutrophils in arteries and capillaries (2), as well as accumulation in postcapillary venules leading to inflammation in the vascular bed (3).

Although the mechanical properties of neutrophils can be regulated by cytoskeletal filaments such as actin (4–6) and microtubules (7), the hallmark multilobed nuclear morphology has long been thought to facilitate the deformation of neutrophils through narrow spaces (8, 9); a round-shaped nucleus could sterically hinder the deformation of a cell through a narrow pore, whereas the multilobed neutrophil nucleus could aid cell passage as individual lobes could be sequentially "threaded" through constrictions. Indeed, cells with lobulated nuclear shape show less retention in 8-μm porous membranes as compared with their progenitors with round nuclei (10). However, it remains unclear to what extent this hyperlobulated nuclear shape is required for neutrophils to deform through narrow gaps; tightly regulated modifications in nuclear envelope protein composition also occur during granulopoiesis. Specifically,

* This work was supported by a Cross-Disciplinary Fellowship of the International Human Frontiers Science Program (HFSP) (to A. C. R.) and National Institutes of Health Grants R01 NS059348 and R01 HL082792 and Department of Defense Breast Cancer Idea Award BC102152 (to J. L.). This work was also supported by the Natural Sciences and Engineering Research Council of Canada (NSERC) (to W. L. U. and I. A. E.), an American Heart Association fellowship (AHA Award 09POST2320042) (to D. E. J.), and HFSP Grant RGP0004/2005-C102, National Science Foundation (NSF) Contracts DMR-1006546 and DBI-649865, and Harvard Materials Research Science and Engineering Center (MRSEC) Contract DMR-0820484.
[S] This article contains supplemental Methods and Figs. S1–S5.
[1] To whom correspondence should be addressed: Dept. of Integrative Biology and Physiology, Terasaki Life Sciences Bldg. 1125, 610 Charles E. Young Dr. S., Los Angeles, CA 90095. Tel.: 310-825-4026; Fax: 310-206-9184; E-mail: rowat@ucla.edu.
[2] Present address: Dept. of Biology, American University of Beirut, Beirut 1107 2020, Lebanon.
[3] Present address: Dept. of Biochemistry, University of Zurich, 8057 Zurich, Switzerland.

Downloaded from http://www.jbc.org/ at Cornell University Library on December 14, 2013

during the process of granulopoiesis, as recapitulated *in vitro* using human promyelocytic leukemia (HL-60)[4] cells, major alterations occur in the expression levels of two key nuclear envelope proteins; the integral nuclear membrane protein, lamin B receptor (LBR), is strongly up-regulated, whereas there is a concurrent decrease in levels of lamin A, a key structural protein that forms a network underlying the inner nuclear membrane and imparts the nucleus with mechanical stability (11–13). Thus, although the unique shape of the neutrophil nucleus could facilitate the passage of these cells through narrow constrictions, we hypothesized that reduced levels of lamin A could enhance nuclear deformability and thereby facilitate the passage of cells through micron-scale constrictions.

To dissect the role of nuclear shape and nuclear envelope composition in the passage of cells through constrictions that mimic physiological gaps, we used all-*trans*-retinoic acid (ATRA)-stimulated HL-60 cells to recapitulate granulopoiesis; this *in vitro* system is widely used for structural and functional assays of white blood cells (14–16). We probed the ability of cells to transit through micron-scale constrictions and investigated the effects of both altered nuclear shape and altered lamin A expression levels. Our results show that levels of lamin A have a predominant effect on the ability of cells to passage through narrow constrictions, whereas the altered shape of the neutrophil nucleus is not essential for rapid passage through micron-scale pores.

EXPERIMENTAL PROCEDURES

Cell Culture—HL-60/S4 cells were maintained in RPMI 1640 medium with L-glutamine (Invitrogen), 10% fetal bovine serum (FBS), and 1% penicillin:streptomycin (Gemini Bio-Products, West Sacramento, CA). We generated scrambled control cells to compare with HL-60/S4 cells with stable shRNA-mediated knockdown of LBR (LBR KD cells) (17). To induce differentiation into neutrophil-type cells, we added ATRA at a final concentration of 5 μM to 1×10^5 cells/ml; ethanol was used as vehicle control. We probed nuclear shape and nuclear envelope composition at days 0, 3, and 5 after ATRA treatment; we performed functional assays of neutrophil-type cells at 4 days after ATRA treatment, when cells display characteristics of neutrophils (11, 18).

Microfluidic Deformation—Soft lithography was used to fabricate microfluidic channels in polydimethylsiloxane (Sylgard 184 silicone elastomer, Dow Corning) (19). Devices were bonded to #1.5-thickness coverglasses. We drove the flow of cells by applying 28 kilopascals (4 p.s.i.) of pressure to a tube of 2.5×10^6 cells/ml with 0.1% F127 (Pluoronic F-127, Invitrogen) to minimize surface adhesion (20). Images were acquired at 300 frames/s with a high speed camera (Miro ex4, Vision Research, Wayne, NJ) mounted on an inverted light microscope (Zeiss Observer) with 10×/0.25 Ph1 objective (A-Plan, Zeiss). The resulting image sequences were analyzed using a custom-written program (MATLAB) to extract the time for cell passage through the first constriction.

Retroviral Transduction—We generated the stably modified lamin A-overexpressing (LamA OE) cells from the parent HL-60/S4 cell line by retroviral transduction (21–23) with the bicistronic vector (pRetroX-IRES-ZsGreen1, Clontech) for lamin A and the fluorophore reporter *Zoanthus* green fluorescent protein (ZsGreen1) with the 5′ Moloney murine leukemia virus LTR as the promoter. Cloning of the wild-type prelamin A into the bicistronic retroviral vector was performed as follows: the insert was generated by cutting pSVK3-prelamin A (24) (kind gift from Howard J. Worman) with SmaI and SalI; this was ligated to the vector obtained from cutting pEGFP-C1 (Clontech) with Ecl136II and SalI resulting in a shuttle vector, which was subsequently digested with XmaI, blunted with Klenow, and then cut with BglII. The insert from the latter digestion was then ligated to the vector generated from cutting the pRetroX-IRES-ZsGreen1 with BamHI and blunted with Klenow followed by BglII digestion. Transfection of the resultant pRetro-prelamin A-IRES-ZsGreen 1 expression vector into the 293GPG retroviral packaging cell line (kind gift from Richard C. Mulligan) was performed using Lipofectamine Plus reagent (Invitrogen) based on the manufacturer's specifications and previous protocols with minor modifications (21–23). A ZsGreen1 retrovector without lamin A insert was used to generate the mock control cells. Viral supernatant was collected daily for 6 consecutive days, filtered through 0.45-μm pores, and stored at −20 °C. Later, the viral supernatants collected per batch were thawed and pooled, and viral titer was determined by viral infection of mouse embryo fibroblasts. Two rounds of viral transduction of HL-60/S4 cells were then performed using unconcentrated viral supernatant supplemented with 6–8 μg/ml Polybrene (Sigma-Aldrich) at a multiplicity of infection of 25–50. Gene transfer efficiency was assayed 5 days after retroviral infection by flow cytometry probing ZsGreen1 levels; because ZsGreen1 and lamin A are derived from the same bicistronic mRNA transcript, we sorted individual cells based on ZsGreen1 levels into a subpopulation of cells with well defined, elevated expression levels by fluorescence-activated cell sorting (Aria II, BD Biosciences or MoFlo, Beckman Coulter) into calcium-free PBS buffer. The resulting subpopulation does not derive from a single clone, but is rather generated by the highest expressing cells that may contain multiple insertions; the 5′ LTR promoter is relatively weak, and we observed an ~20–30-fold increase in lamin A levels in comparison with the mock controls.

Analysis of Protein Expression—Cell lysates were prepared from 5×10^6 cells using urea lysis buffer with final concentrations of 9 M urea, 10 mM Tris-HCl (pH 8), 10 μM EDTA, 500 μM phenylmethylsulfonyl fluoride, 20 μl of β-mercaptoethanol, and 1 μl/ml protease inhibitor mixture (Sigma). All steps were performed at 4 °C. Proteins were separated on a 4-12% Bis-Tris gel with 1× MOPS running buffer and then transferred onto activated transfer membranes, blocked, and labeled using horseradish peroxidase-conjugated antibodies (Bio-Rad). We used protein standard (Invitrogen SeeBlue Plus2) for size calibration and used β-tubulin as a loading control because its levels remain constant throughout differentiation (11). Primary antibodies used for probing are described in the supplemental Methods.

[4] The abbreviations used are: HL-60, human promyelocytic leukemia; LamA OE, lamin A-overexpressing; LBR, lamin B receptor; LBR KD, LBR knockdown; ATRA, all-*trans*-retinoic acid; Bis-Tris, 2-(bis(2-hydroxyethyl)amino)-2-(hydroxymethyl)propane-1,3-diol.

Downloaded from http://www.jbc.org/ at Cornell University Library on December 14, 2013

Expression levels were quantified by optical density analysis using ImageJ (National Institutes of Health).

Cell Surface Marker Analysis—To assay expression levels of CD11b, we used Fc receptor polyclonal human IgG (Sigma) as a blocking agent and labeled 10^6 cells with Alexa Fluor 700 mouse anti-human-CD11b (BD Pharmingen). We analyzed fluorescence levels by flow cytometry (LSR II, BD Biosciences).

Respiratory Burst Assay—We determined superoxide radical production of day 4/ATRA-treated cells using luminol-enhanced chemiluminescence (Diogenes reagent, National Diagnostics, Atlanta, GA) following stimulation by phorbol 12-myristate 13-acetate (25, 26), as per the manufacturer's instructions. Cells were activated by the addition of phorbol 12-myristate 13-acetate (stock solution 1 mg/ml dimethyl sulfoxide (DMSO), Sigma) to a final concentration of 11 μM; we recorded luminescence values after 30 min using a plate reader (SpectraMax M5).

Nuclear Shape Analysis—We incubated cells with Hoechst 33342 (1 μg/ml, Invitrogen) for 30 min at 37 °C. We then placed the cells on a glass slide pretreated with poly-L-lysine (0.01% w/v in water) by centrifuging a 20-μl drop of cell suspension at 1,000 rpm for 5 s. Images were acquired using a 20×/0.5 Ph2 objective (EC Plan Neofluar, Zeiss), DAPI filter set, and charge-coupled device camera (AxioCam MRm, Zeiss). Analysis of nuclear geometry was performed using ImageJ. Circularity for a nuclear cross-section is $4\pi A/P^2$, where A is the cross-sectional area and P is the perimeter.

Transwell Migration Assay—We used membranes with 3- and 8-μm pore sizes (Millipore) and FBS as chemoattractant (27, 28). Day 4/ATRA-treated cells were resuspended to 5×10^6 cells/ml in RPMI without FBS. We placed media with and without FBS in the bottom well and cells in the top well and then incubated the plate at 37 °C, 5% CO_2 for 2 h. We then removed the membrane insert, labeled cells in the bottom well with Hoechst, and imaged each well by microscopy using a 10×/0.25 Ph1 objective (A-Plan, Zeiss), charge-coupled device camera (AxioCam MRm, Zeiss), and DAPI filter set. We determined the number of cells per well using image analysis (ImageJ).

Two-dimensional Migration Assay—Glass-bottomed dishes (World Precision Instruments, Sarasota, FL) were coated with human fibronectin (10 μg/ml in Hanks' balanced salt solution without calcium and magnesium, Gemini Bio-products). Cells were seeded onto the dishes, and images were acquired at 1-min intervals over 3 h (5% CO_2, 37 °C) using a Zeiss microscope outfitted with an automated stage (Applied Scientific Instruments, Eugene, OR), 10×/0.3 Ph objective (EC-Plan Neofluar, Zeiss), and charge-coupled device camera (AxioCam MRm, Zeiss); x-y positions of cells were extracted from the resultant movies (ImageJ), and trajectory analysis was performed using MATLAB.

RESULTS

Lobulated Nuclear Shape Is Not Essential for Cell Transit—To probe the ability of neutrophil-type cells with round or lobulated nuclei to deform through narrow gaps, we designed a microfluidic device with precisely defined constrictions of 5-μm width (Fig. 1*A*); this width is less than the typical 7–10-μm diameter of HL-60 nuclei, such that nuclear deformation is required for a cell to passage through a pore (supplemental Fig. S1). We forced the neutrophil-type cells (day 4/ATRA-treated HL-60 cells) to transit through these micron-scale pores using pressure to drive a flow of cell suspension through the channels; we monitored the passage of cells as a function of time. When a cell arrives at a constriction, it is subjected to physical forces resulting from external stresses due to the pressure drop across the cell trapped in the constriction; these stresses cause the cell to deform and passage through the pore. Given the dimensions of a single pore, a pressure of 28 kilopascals corresponds to approximately micronewton-scale forces. The rate at which the cell deforms largely depends on the applied stress (driving pressure) as well as the global mechanical properties of the cell and nucleus (5, 29–32) As individual cells deformed through the 5-μm constrictions of the microfluidic device, we imaged their passage using a high speed camera (Fig. 1, *B* and *D*). By automated image analysis, we determined the time required for the cell to passage through the first 5-μm constriction, which we define as its passage time. Given these millisecond timescales of cell passage at a driving pressure of 28

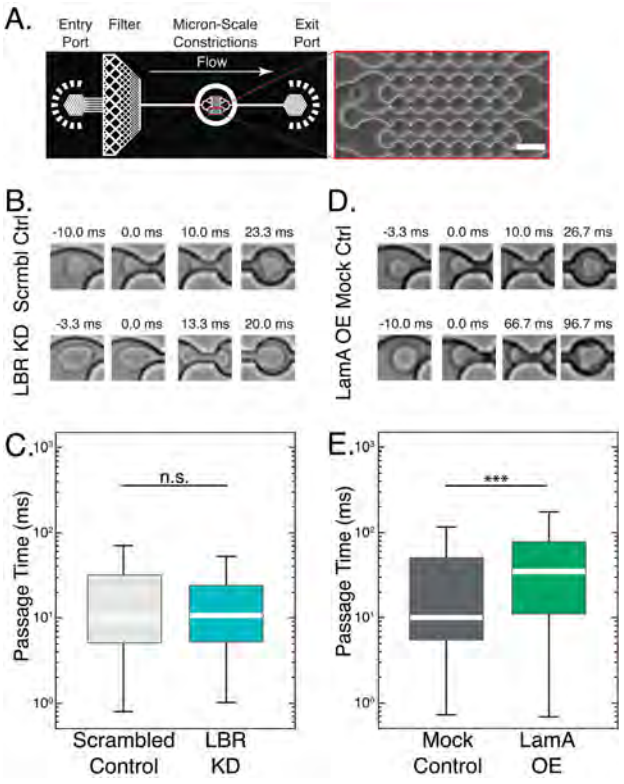

FIGURE 1. **Ectopic expression of lamin A increases passage time through microfluidic constriction channels.** *A*, schematic overview of the microfluidic device and close-up of the 5-μm constrictions. Pressurizing the reservoir drives the cell suspension through the inlet, and cells passage through the channels with 5-μm constrictions, as shown in the *inset*. *Scale bar*, 20 μm. *B*, time-sequence images of day 4/ATRA-treated cells passaging through 5-μm constrictions. *Scrmbl Ctrl*, scrambled control; *Mock Ctrl*, mock control. *C*, LBR KD cells have similar passage times as the scrambled controls despite the round shape of their nucleus, which has been speculated to sterically hinder the passage of cells through narrow pores. *D* and *E*, LamA OE cells take longer to passage the constrictions than mock control cells. In all box plots, the *white bar* denotes the population median, *boxes* are the 25th and 75th percentiles, and *lines* show the 10th and 90th percentiles. *n.s.*, $p > 0.05$ for LBR KD *versus* scrambled control; ***, $p < 0.001$ for LamA OE *versus* mock control. $n > 300$ cells for each cell type. *Error bars* represent S.E. over three independent experiments.

Downloaded from http://www.jbc.org/ at Cornell University Library on December 14, 2013

kilopascals, this microfluidic assay primarily probes the passive mechanical behavior of the cell, as actin remodeling and protein expression changes occur on timescales of several minutes and more (33). Although actin can contribute to the cortical stiffness of neutrophils (4–6), we confirmed that the actin makes little contribution to these measurements by treating a subset of neutrophil-type cells with cytochalasin D to disrupt actin polymerization; this treatment had no effect on passage times (data not shown), indicating that the deformability of the nucleus has a pivotal role in the passage of cells through micron-scale pores.

To assess the effect of hypolobulated or round-shaped nuclei on the passage of neutrophil-type cells through micron-scale constrictions, we used LBR KD cells as an *in vitro* system. In contrast to the control cells that exhibit strong up-regulation of LBR during differentiation and develop lobulated nuclei, LBR KD cells show only trace levels of LBR expression and maintain round nuclei (17). Nevertheless, despite their round nuclei, LBR KD cells exhibited similar passage times as compared with the scrambled control cells (Fig. 1*B*). These observations suggest that the multilobed shapes of nuclei in mature neutrophils provide no significant advantage in the time required for cells to deform through 5-μm constrictions.

Generating Neutrophil-type Cells with Increased Lamin A Expression—Because the above experiments indicate that lobulated nuclear shape is not essential for neutrophil-type cell passage through narrow constrictions, we hypothesized that the unique molecular composition of the nuclear envelope in neutrophils could determine the ability of cells to deform. One possible origin may be the low levels of the key structural protein of the nucleus, lamin A; this protein is normally down-regulated by over 90% in ATRA-stimulated HL-60 cells after 4–5 days of stimulation (Fig. 2*B*) (11, 14). Given the essential role of lamin A in nuclear mechanical stability (12, 13, 30), we postulated that preventing lamin A down-regulation could reduce nuclear deformability and impair cell passage through pores. Because the LBR KD neutrophil-type cells that have round nuclei have similar reduced lamin A expression levels as unmodified and mock-modified cells, this may also explain their unaltered passage times (17).

To test the effect of *increased* lamin A levels on cell passage through narrow constrictions, we generated a LamA OE HL-60 cell line by retroviral transduction. The resulting subpopulation of high expressing cells exhibits lamin A levels that are about 20–30-fold higher than the mock-modified cells (supplemental Fig. S2*A*). Although lamin A expression levels in the LamA OE cells are greater than those in unmodified HL-60 cells, they are comparable with physiological levels in other somatic cells such as mouse embryo fibroblast cells (supplemental Fig. S2*B*). To confirm that the ectopic lamin A is properly localized to the nuclear envelope, we conducted immunofluorescence and confocal imaging (supplemental Fig. S3).

Protein Composition of LamA OE Cells—To characterize how protein levels of the LamA OE cells change during granulopoiesis, we monitored expression levels of major structural proteins over the differentiation time course; we induced the HL-60 cells to differentiate into neutrophil-type cells by ATRA treatment, collected cell lysates at days 0, 3, and 5 following

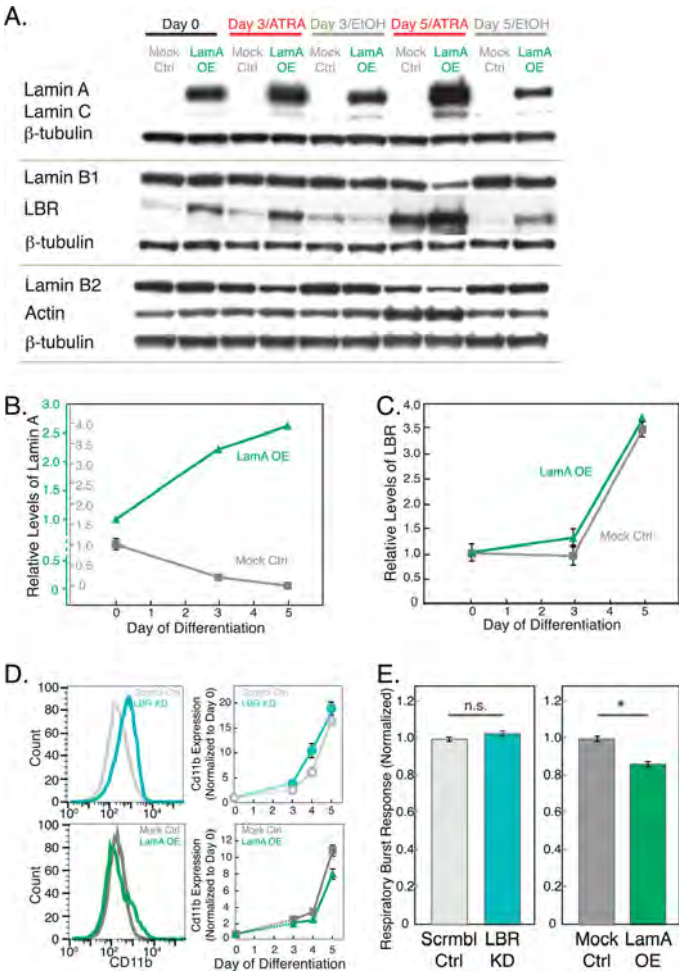

FIGURE 2. **Genetically modified HL-60 cells show typical characteristics of neutrophils after ATRA stimulation.** *A*, representative immunoblots for lamins A/C, B1, B2, and LBR with β-tubulin as loading control. Cell lysates are collected from LamA OE and mock control (*Mock Ctrl*) cells at days 0, 3, and 5 after ATRA stimulation. *B* and *C*, quantitative analysis of lamin A and LBR protein levels normalized first to β-tubulin and then to day 0 for each protein in each cell line. *Error bars* represent S.E. of 3–5 independent experiments; where not visible, they are smaller than the symbols. Based on immunoblot analysis, base-line levels of lamin A are estimated to be ~20–30× greater in the LamA OE cells as compared with the mock control cells (supplemental Fig. S2); for this reason, two separate axes are plotted for each cell line. *D*, expression levels of the cell surface antigen, CD11b, a hallmark of neutrophils, increase during differentiation for all cell lines. *Left*, representative histograms of data from a single flow cytometry experiment showing the distribution of CD11b expression levels at day 4 after ATRA stimulation. *Right*, graphs showing median values of CD11b after ATRA treatment with the values for each cell line normalized to day 0 for each independent experiment. *Error bars* represent S.E. over three independent experiments. *Scrmbl Ctrl*, scrambled control. *E*, respiratory burst assay that probes superoxide production using a luminescence assay 30 min after stimulation by phorbol myristate acetate, indicating that all cells show normal functional characteristics of neutrophils. Luminescence values are relative to the mock and scrambled control for the *left* and *right panels*, respectively. Data represent the average of three independent experiments; *error bars* represent the S.E. *n.s.*, $p > 0.05$ for LBR KD *versus* scrambled control; *, $p < 0.05$ for LamA OE *versus* mock control.

ATRA treatment, and performed immunoblotting (Fig. 2*A*). As expected, unmodified and mock-modified cells displayed a strong up-regulation of LBR during granulopoiesis with a concurrent decrease in lamin A levels (Fig. 2, *B* and *C*), confirming previous observations (11). In contrast, LamA OE cells have increased levels of lamin A that further increased during granulopoiesis (Fig. 2, *B* and *C*), possibly due to an ATRA-sensitive element in the ectopic promoter region. LamA OE cells showed

Downloaded from http://www.jbc.org/ at Cornell University Library on December 14, 2013

elevated basal levels of LBR as compared with the mock controls, with a similar ~4-fold increase in LBR levels during granulocytic differentiation. We also probed levels of other structural proteins that could contribute to cell deformability (4–6); during differentiation in both the mock-modified and LamA OE cells, actin levels showed minor variations, and other structural nuclear proteins, including lamin B1 and B2, showed a decrease in expression levels (Fig. 2) (34). Although we cannot exclude the possible contribution of lamin B1 and B2 down-regulation to altered cellular mechanical properties, we anticipate that the observed changes in lamin B1/B2 levels would have little effect on nuclear mechanical properties in comparison with the lamin A up-regulation; lamins A/C have a predominant role in nuclear shape stability and stiffness (12, 13, 30), whereas lamin B1 does not have any significant effect on nuclear mechanical stability (13).

Genetically Modified Cells Display Characteristics of Neutrophils—To test whether the genetically modified HL-60 cells still undergo normal granulopoiesis, we assayed essential functional, biochemical, and proteomic characteristics that define neutrophils. One metric to assess the differentiation of HL-60 cells into neutrophil-type cells is to measure cell density following ATRA stimulation; decreased proliferation rates are an indicator of successful differentiation as cells exit the cell cycle to commit to their differentiation into neutrophils (35). Both LBR KD and LamA OE cells showed a similar progressive decrease in proliferation rates over the days following ATRA treatment as compared with the scrambled and mock controls (supplemental Fig. S4). As a more direct assay of differentiation into neutrophil-type cells, we measured expression levels of the cell surface marker, CD11b, a subunit of a heterodimeric adhesion glycoprotein, which is widely used as a marker for neutrophils (36). After 4 days of ATRA treatment, CD11b levels were increased for all cell types as compared with the undifferentiated HL-60 cells and vehicle-treated controls (supplemental Fig. S5). These results confirmed that the HL-60 cells are differentiating into neutrophil-type cells. Importantly, we observed that all cell lines show significant increase in CD11b levels following ATRA stimulation, with levels varying slightly between cell lines (Fig. 2*D*); this demonstrates that the changes in nuclear envelope composition do not markedly affect differentiation efficiency.

Another hallmark of neutrophil cells is their respiratory burst response upon exposure to phagocytotic stimuli, such as yeast or bacteria. To probe this functional characteristic of the modified neutrophil-type cells, we stimulated cells with phorbol myristate acetate and measured subsequent superoxide production (Fig. 2*E*). LBR KD cells showed similar response as compared with the scrambled controls. LamA OE cells exhibited a small yet statistically significant 15% reduction in superoxide production as compared with the mock controls. Overall, these experiments suggest that the functional and biochemical characteristics of the genetically modified neutrophil-type cells are generally maintained despite their altered nuclear envelope composition.

Lamin A Expression Alters Nuclear Lobulations during Granulopoiesis—A key hallmark of granulopoiesis is the transition from round to multilobed nuclear shape, which is observed in

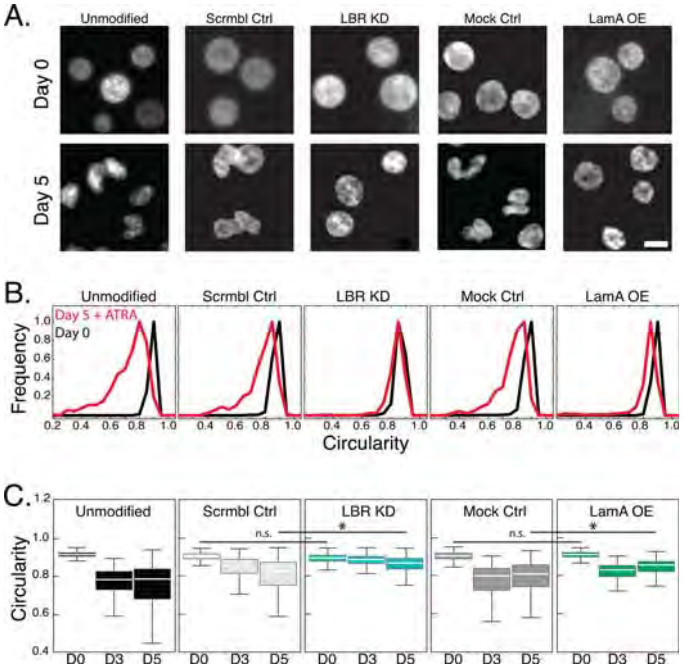

FIGURE 3. **Nuclear shape transition during granulopoiesis requires lamin A down-regulation and LBR up-regulation.** *A*, fluorescent images of Hoechst-stained nuclei acquired at day 0 and day 5 after ATRA treatment. All images were acquired at the same magnification. *Scale bar*, 5 μm. *B*, to quantitatively describe nuclear shape, the circularity of the nucleus is defined as $4\pi A/P^2$. Histograms show the distribution for each cell type at days 0 and 5 after ATRA treatment. *C*, box plots show the circularity of nuclei at days 0, 3, and 5 after ATRA treatment. The *white bar* denotes the population median, *boxes* are the 25th and 75th percentiles, and *lines* show the 10th and 90th percentiles. To evaluate statistical significance, we compared the medians of at least 3 independent experiments for each cell type. Day 0, unmodified to scrambled control. *n.s.*, $p > 0.05$; *, $p < 0.05$. Nuclei from over 300 individual cells were analyzed for each cell type.

HL-60 cells after 3–5 days following ATRA treatment (11, 18). To investigate the effect of altered nuclear envelope composition on this shape transition, we imaged Hoechst-stained nuclei by fluorescence microscopy over the differentiation time course. To quantify changes in nuclear shape, we analyzed the circularity of nuclei, defined as $4\pi A/P^2$, where A is the cross-sectional area and P is the perimeter of an individual nuclear cross-section. For a perfect circle, the circularity value equals one; lower values reflect deviations from a circular shape. In the undifferentiated state, all cell lines have nuclei with predominantly circular shape and similarly high circularity values, representative of round nuclei (Fig. 3, *A*–*C*).

After 3 days of ATRA treatment, the unmodified, mock, and scrambled control cells exhibited nuclei with large invaginations; circularity values correspondingly showed a lower median and greater variability, reflecting these irregular nuclear shapes. By contrast, LBR KD cells retained their round shape, as reflected by the higher circularity values, even after 5 days of ATRA treatment (Fig. 3*A*) (17). The nuclei of LamA OE cells showed some morphological changes but failed to develop the characteristic lobulations seen in the unmodified and mock control cells (Fig. 3*A*, supplemental Fig. S3); the lack of severe lobulation that is typical for normal neutrophil cells illustrates that down-regulation of lamin A expression during neutrophil differentiation could also be required for the lobulated nuclear shape of mature neutrophils.

Downloaded from http://www.jbc.org/ at Cornell University Library on December 14, 2013

Increased Lamin A Expression Delays Cell Passage through Pores—Lamin A is a crucial modulator of nuclear deformability (13, 30, 37). To probe the effects of increased lamin A levels on the ability of cells to deform through physiological gaps, we measured the passage time of LamA OE neutrophil-type cells and mock controls when forced through the 5-μm constrictions of our microfluidic device (Fig. 1, *A* and *D*). The LamA OE neutrophil-type cells exhibited a 3-fold increase in median passage time as compared with the mock controls (Fig. 1*E*); these results indicate that increased density of lamin protein at the nuclear envelope may impair the ability of LamA OE neutrophil-type cells to passage through the 5-μm constrictions. Taken together, our results show that lamin A levels have an important effect on the ability of cells to passage through 5-μm constrictions; physiological *down-regulation* of lamin A following ATRA-induced differentiation of HL-60 cells results in *faster passage* through the micron-scale constrictions, whereas ectopically *increased expression* of lamin A results in *slower passage* of LamA OE-neutrophils through the 5-μm constrictions.

Active Migration through Pores Is Impaired in LamA OE Cells—The results of our microfluidic experiments illustrate that altered expression of lamin A can substantially alter the passive deformability of cells. However, a critical function of neutrophils is their ability to *actively* migrate through narrow constrictions. To test migration efficiency, we used a transwell migration assay to probe the ability of cells to migrate through 3- and 8-μm pores; we monitored the number of cells that migrate through the pores after 2 h and determined the migration efficiency relative to the respective control cells. As seen in the passive deformation results obtained by microfluidic assays, the LBR KD cells exhibited similar migration efficiency as the scrambled control cells (Fig. 4, *A* and *B*), further substantiating that neutrophil-type cells with round nuclei can exhibit equivalent passage efficiency through micron-scale pores. By contrast, the LamA OE cells showed a marked reduction in migration through 3-μm pores (Fig. 4, *D* and *E*). The impaired migration was less severe in the experiments with 8-μm pores (Fig. 4, *D* and *E*); because deformation through 8-μm pores requires smaller deformations of nuclei, these results are consistent with our observations that nuclear deformation rate-limits the passage of cells through micron-scale constrictions.

To address the possibility that a general migration defect underlies the impaired transwell migration efficiency of the LamA OE cells, we performed two-dimensional migration assays; cells exhibited velocities from 2 to 5 μm/min, consistent with previous observations of neutrophil migration (38). The LBR KD cells showed a slightly increased velocity as compared with the scrambled control cells (Fig. 4*C*). Importantly, LamA OE cells exhibited similar migration velocities as the mock control cells (Fig. 4*F*), indicating that the observed differences in the transwell assay cannot be attributed to general defects in their migration. Taken together, our experiments indicate that the density of lamin A at the nuclear envelope is crucial in facilitating the passage of cells through micron-scale constrictions.

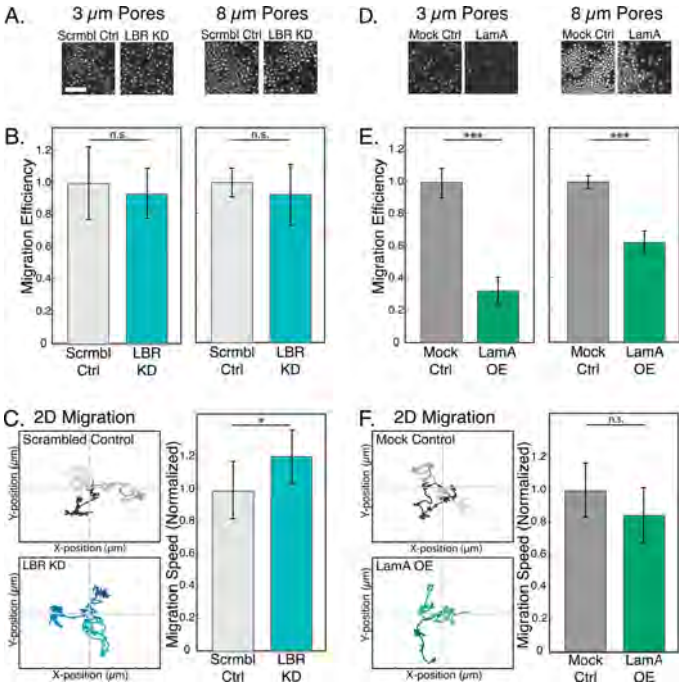

FIGURE 4. **Impaired migration of LamA OE cells through narrow constrictions.** To probe the active migration of cells through micron-scale pores, we use a Transwell migration assay. *A* and *D*, representative images from a single experiment showing Hoechst-stained nuclei of cells that have passed through 3- or 8-μm pores. *Scale bar*, 100 μm. *Ctrl*, control; *Scrmbl Ctrl*, scrambled control; *Mock Ctrl*, mock control. *B* and *E*, migration efficiency is defined as the number of cells that passaged through the porous membrane relative to the corresponding scrambled or mock control. *Bars* represent averages from at least three independent experiments; *error bars* represent S.E. ***, $p < 0.001$ for LamA OE *versus* mock control. *C* and *F*, two-dimensional migration experiments were performed by tracking the positions of individual cells at 1-min intervals over 3 h. Traces of three representative cells for each cell type show the total distance traveled and the directionality of movement over the three-hour time-lapse experiment. Axes are 150 μm with 50-μm increments. Migration speed over the entire trajectory is computed from the individual traces of over 50 cells for each cell type. Mean values for each LBR KD and LamA OE cells are normalized to their respective controls. *n.s.*, $p > 0.05$; *, $p < 0.05$; ***, $p < 0.001$. Absolute velocities of cells are: LBR KD, 4.4–5.1 μm/min; scrambled control, 3.5–4.2 μm/min; LamA OE, 2.2–4.7 μm/min; mock control, 2.8–4.8 μm/min.

DISCUSSION

It has long been speculated that the lobulated shape of the neutrophil nucleus is "a special adaptation for passing through vessel walls" (8). However, here we show that nuclear shape alone does not always determine the timescale for neutrophil deformation through micron-scale pores; neutrophil-type cells with round nuclei resulting from LBR knockdown (17) show unaltered passage efficiency through pores down to 3 μm, as probed using both passive deformation through 5-μm microfluidic constrictions, as well as active migration through 3- and 8-μm porous membranes.

These LBR KD cells also provide an *in vitro* model for Pelger-Huët anomaly; the nuclei from neutrophils of these individuals are round or bilobulated (36, 37) due to a complete or partial lack of functional LBR. The extent to which the altered nuclear shape of Pelger-Huët anomaly neutrophils affects their ability to passage through micron-scale constrictions has been inconclusive (26, 39–41). Some previous studies of these neutrophils discovered altered migration (26, 39, 40); however, these primary neutrophils also exhibited bilobular nuclei, and differ-

Downloaded from http://www.jbc.org/ at Cornell University Library on December 14, 2013

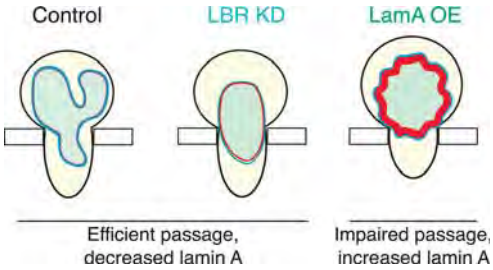

FIGURE 5. **Lamin A levels, rather than nuclear shape, are a primary determinant of the efficiency of cell passage through narrow constrictions.** A schematic illustration summarizing the effects of nuclear shape and lamin A expression levels on the ability of cells to deform through narrow constrictions is shown. The ratio of LamA to LBR expression levels is estimated from immunoblots. Undifferentiated (unmodified or mock-modified) HL-60 cells, as well as the LBR KD neutrophil-type cells, exhibit efficient passage, despite their round nuclear shape. By contrast, lamin A overexpression results in impaired passage, both through the constricted 5-μm channels of a microfluidic device, as well as the 3- and 8-μm pores of the transwell migration assay. Undifferentiated LamA OE cells with more circular nuclei and lower levels of LBR require even longer time to passage through narrow constrictions.

ences in migratory ability could result from other phenotypic differences. Here we used LBR KD cells as an *in vitro* system to specifically investigate the effect of the hypolobulated nucleus on cell passage through micron-scale constrictions. Despite the round shape of LBR KD nuclei, which could sterically hinder the passage of nuclei through constrictions, these cells exhibited similar passage efficiencies through micron-scale constrictions as compared with the scrambled control cells with multilobed nuclei (Fig. 1).

Although LBR KD neutrophil-type cells have an atypical round nuclear shape, they have similarly low levels of lamin A as the unmodified controls (17). Here, we show that lamin A expression levels, rather than the shape of the cell nucleus, can be a major determinant of the timescale of cell passage through micron-scale gaps (Fig. 5). By contrast, nonmechanical functions of these cells are not substantially affected by changes in nuclear envelope composition. Although other types of white blood cells with ovoid-shaped nuclei, such as macrophages, also undergo transendothelial migration, their deformations occur on a slower timescale as compared with neutrophils (31). Indeed, monocyte/macrophage-differentiated HL-60 cells also show increased levels of lamin A/C expression relative to neutrophil-type cells (34).

If irregular nuclear shape is not essential for the deformability of neutrophil cells, then why do their nuclei exhibit this distinct shape? One possibility is that the multilobed nucleus could simply result from the marked changes in nuclear envelope protein composition. Indeed, lamin A levels impact the mechanical stability of the nuclear envelope, whereas ectopic overexpression of LBR can increase nuclear membrane surface area (42, 43) (Fig. 5). Alternatively, the unusual multilobed nuclear shape may facilitate other neutrophil functions, such as phagocytosis, the formation of neutrophil extracellular traps, or migration through even smaller $<$1-μm constrictions of the endothelium, either between or through cells (44).

Here we have used HL-60 cells, which are a well established *in vitro* model system to study white blood cell lineages; for example, the resulting neutrophil-type cells show similar structural and functional characteristics as primary neutrophils (14–16). HL-60 cells also exhibit similar mechanical properties; recent measurements of cell compliance using an optical stretcher confirmed that *in vitro* differentiation of HL-60 cells into neutrophil-type cells recapitulates the 3–6-fold increase in cell deformability observed in primary neutrophils and their CD34+ precursor cells (31). A direct comparison of the absolute passage times through micron-sized constriction between primary neutrophils and HL-60-derived neutrophil-type cells is complicated by the fact that HL-60 cells are typically larger than primary neutrophils (~12-μm *versus* 7–8-μm median diameter, respectively) and exhibit substantially larger transit times through microfluidic constriction channels (29). Consequently, we have focused our study on HL-60 cells and vary protein levels within the same cell type; this has enabled us to clearly illustrate the importance of nuclear envelope composition, particularly the levels of lamins A/C, on the ability of cells to pass through narrow constrictions during perfusion and migration.

It is intriguing to speculate that changes in levels of lamin A expression may have implications for cellular deformability in a variety of physiological processes and diseases (45). For example, certain types of cancer cells have reduced levels of lamin A expression as compared with their nonmalignant progenitors (46, 47). Akin to neutrophils, large deformations of cancer cells and their nuclei are required during deformation through micron-scale constrictions (48) in extravasation and metastasis. Ultimately, a deeper knowledge of the molecular basis of cellular and nuclear deformability will provide unique insights into the mechanical aspects of cell biology and possibly new therapeutic approaches.

Acknowledgments—We acknowledge the Center for Nanoscale Systems, Harvard University, for access to the profilometer and Bino Varghese for advice on data analysis protocols. Cell sorting was performed by Brian Tilton, Bauer Center at Harvard University, and Jeff Calimlim in the UCLA Jonsson Comprehensive Cancer Center (JCCC) and Center for AIDS Research Flow Cytometry Core Facility. The UCLA JCCC and Center for AIDS Research Flow Cytometry Core Facility are supported by National Institutes of Health Awards CA-16042 and AI-28697 and by the JCCC, the UCLA AIDS Institute, the David Geffen School of Medicine at UCLA, and the UCLA Chancellor's Office.

REFERENCES

1. Doerschuk, C. M., Beyers, N., Coxson, H. O., Wiggs, B., and Hogg, J. C. (1993) Comparison of neutrophil and capillary diameters and their relation to neutrophil sequestration in the lung. *J. Appl. Physiol.* **74,** 3040–3045
2. Worthen, G. S., Schwab, B., 3rd, Elson, E. L., and Downey, G. P. (1989) Mechanics of stimulated neutrophils: cell stiffening induces retention in capillaries. *Science* **245,** 183–186
3. Downey, G. P., Worthen, G. S., Henson, P. M., and Hyde, D. M. (1993) Neutrophil sequestration and migration in localized pulmonary inflammation. Capillary localization and migration across the interalveolar septum. *Am. Rev. Respir. Dis.* **147,** 168–176
4. Tsai, M. A., Waugh, R. E., and Keng, P. C. (1998) Passive mechanical behavior of human neutrophils: effects of colchicine and paclitaxel. *Biophys. J.* **74,** 3282–3291
5. Tsai, M. A., Frank, R. S., and Waugh, R. E. (1994) Passive mechanical behavior of human neutrophils: effect of cytochalasin B. *Biophys. J.* **66,** 2166–2172

Downloaded from http://www.jbc.org/ at Cornell University Library on December 14, 2013

6. Ting-Beall, H. P., Lee, A. S., and Hochmuth, R. M. (1995) Effect of cytochalasin D on the mechanical properties and morphology of passive human neutrophils. *Ann. Biomed. Eng.* **23,** 666–671
7. Lautenschläger, F., Paschke, S., Schinkinger, S., Bruel, A., Beil, M., and Guck, J. (2009) The regulatory role of cell mechanics for migration of differentiating myeloid cells. *Proc. Natl. Acad. Sci. U.S.A.* **106,** 15696–15701
8. Hirsch, J. G. (1959) Immunity to infectious diseases: review of some concepts of Metchnikoff. *Bacteriol. Rev.* **23,** 48–60
9. Erzurum, S. C., Kus, M. L., Bohse, C., Elson, E. L., and Worthen, G. S. (1991) Mechanical properties of HL60 cells: role of stimulation and differentiation in retention in capillary-sized pores. *Am. J. Respir. Cell Mol. Biol.* **5,** 230–241
10. Downey, G. P., Doherty, D. E., Schwab, B., 3rd, Elson, E. L., Henson, P. M., and Worthen, G. S. (1990) Retention of leukocytes in capillaries: role of cell size and deformability. *J. Appl. Physiol.* **69,** 1767–1778
11. Olins, A. L., Herrmann, H., Lichter, P., and Olins, D. E. (2000) Retinoic acid differentiation of HL-60 cells promotes cytoskeletal polarization. *Exp. Cell Res.* **254,** 130–142
12. Lammerding, J., Schulze, P. C., Takahashi, T., Kozlov, S., Sullivan, T., Kamm, R. D., Stewart, C. L., and Lee, R. T. (2004) Lamin A/C deficiency causes defective nuclear mechanics and mechanotransduction. *J. Clin. Invest.* **113,** 370–378
13. Lammerding, J., Fong, L. G., Ji, J. Y., Reue, K., Stewart, C. L., Young, S. G., and Lee, R. T. (2006) Lamins A and C but not lamin B1 regulate nuclear mechanics. *J. Biol. Chem.* **281,** 25768–25780
14. Olins, A. L., Buendia, B., Herrmann, H., Lichter, P., and Olins, D. E. (1998) Retinoic acid induction of nuclear envelope-limited chromatin sheets in HL-60. *Exp. Cell Res.* **245,** 91–104
15. Collins, S. J. (1987) The HL-60 promyelocytic leukemia cell line: proliferation, differentiation, and cellular oncogene expression. *Blood* **70,** 1233–1244
16. Gallagher, R., Collins, S., Trujillo, J., McCredie, K., Ahearn, M., Tsai, S., Metzgar, R., Aulakh, G., Ting, R., Ruscetti, F., and Gallo, R. (1979) Characterization of the continuous, differentiating myeloid cell line (HL-60) from a patient with acute promyelocytic leukemia. *Blood* **54,** 713–733
17. Olins, A. L., Ernst, A., Zwerger, M., Herrmann, H., and Olins, D. E. (2010) An *in vitro* model for Pelger-Huët anomaly: stable knockdown of lamin B receptor in HL-60 cells. *Nucleus* **1,** 506–512
18. Meyer, P. A., and Kleinschnitz, C. (1990) Retinoic acid induced differentiation and commitment in HL-60 cells. *Environ. Health Perspect.* **88,** 179–182
19. Duffy, D. C., McDonald, J. C., Schueller, O. J. A., and Whitesides, G. M. (1998) Rapid prototyping of microfluidic systems in poly(dimethylsiloxane). *Anal. Chem.* **70,** 4974–4984
20. Gómez-Sjöberg, R., Leyrat, A. A., Pirone, D. M., Chen, C. S., and Quake, S. R. (2007) Versatile, fully automated, microfluidic cell culture system. *Anal Chem.* **79,** 8557–8563
21. Ory, D. S., Neugeboren, B. A., and Mulligan, R. C. (1996) A stable human-derived packaging cell line for production of high titer retrovirus/vesicular stomatitis virus G pseudotypes. *Proc. Natl. Acad. Sci. U.S.A.* **93,** 11400–11406
22. Jaalouk, D. E., Lejeune, L., Couture, C., and Galipeau, J. (2006) A self-inactivating retrovector incorporating the IL-2 promoter for activation-induced transgene expression in genetically engineered T-cells. *Virol. J.* **3,** 97
23. Spitzer, D., Wu, X., Ma, X., Xu, L., Ponder, K. P., and Atkinson, J. P. (2006) Cutting edge: treatment of complement regulatory protein deficiency by retroviral *in vivo* gene therapy. *J. Immunol.* **177,** 4953–4956
24. Boguslavsky, R. L., Stewart, C. L., and Worman, H. J. (2006) Nuclear lamin A inhibits adipocyte differentiation: implications for Dunnigan-type familial partial lipodystrophy. *Hum. Mol. Genet.* **15,** 653–663
25. Teufelhofer, O., Weiss, R. M., Parzefall, W., Schulte-Hermann, R., Micksche, M., Berger, W., and Elbling, L. (2003) Promyelocytic HL60 cells express NADPH oxidase and are excellent targets in a rapid spectrophotometric microplate assay for extracellular superoxide. *Toxicol. Sci.* **76,** 376–383
26. Gaines, P., Tien, C. W., Olins, A. L., Olins, D. E., Shultz, L. D., Carney, L., and Berliner, N. (2008) Mouse neutrophils lacking lamin B-receptor expression exhibit aberrant development and lack critical functional responses. *Exp. Hematol.* **36,** 965–976
27. Auguste, K. I., Jin, S., Uchida, K., Yan, D., Manley, G. T., Papadopoulos, M. C., and Verkman, A. S. (2007) Greatly impaired migration of implanted aquaporin-4-deficient astroglial cells in mouse brain toward a site of injury. *FASEB J.* **21,** 108–116
28. Muinonen-Martin, A. J., Veltman, D. M., Kalna, G., and Insall, R. H. (2010) An improved chamber for direct visualisation of chemotaxis. *PLoS One* **5,** e15309
29. Rosenbluth, M. J., Lam, W. A., and Fletcher, D. A. (2008) Analyzing cell mechanics in hematologic diseases with microfluidic biophysical flow cytometry. *Lab. Chip* **8,** 1062–1070
30. Pajerowski, J. D., Dahl, K. N., Zhong, F. L., Sammak, P. J., and Discher, D. E. (2007) Physical plasticity of the nucleus in stem cell differentiation. *Proc. Natl. Acad. Sci. U.S.A.* **104,** 15619–15624
31. Ekpenyong, A. E., Whyte, G., Chalut, K., Pagliara, S., Lautenschläger, F., Fiddler, C., Paschke, S., Keyser, U. F., Chilvers, E. R., and Guck, J. (2012) Viscoelastic properties of differentiating blood cells are fate- and function-dependent. *PLoS One* **7,** e45237
32. Bathe, M., Shirai, A., Doerschuk, C. M., and Kamm, R. D. (2002) Neutrophil transit times through pulmonary capillaries: the effects of capillary geometry and fMLP-stimulation. *Biophys. J.* **83,** 1917–1933
33. Cano, M. L., Lauffenburger, D. A., and Zigmond, S. H. (1991) Kinetic analysis of F-actin depolymerization in polymorphonuclear leukocyte lysates indicates that chemoattractant stimulation increases actin filament number without altering the filament length distribution. *J. Cell Biol.* **115,** 677–687
34. Olins, A. L., Herrmann, H., Lichter, P., Kratzmeier, M., Doenecke, D., and Olins, D. E. (2001) Nuclear envelope and chromatin compositional differences comparing undifferentiated and retinoic acid- and phorbol ester-treated HL-60 cells. *Exp. Cell Res.* **268,** 115–127
35. Fleck, R. A., Athwal, H., Bygraves, J. A., Hockley, D. J., Feavers, I. M., and Stacey, G. N. (2003) Optimization of nb-4 and hl-60 differentiation for use in opsonophagocytosis assays. *In Vitro Cell Dev. Biol. Anim.* **39,** 235–242
36. Gaines, P., and Berliner, N. (2005) Differentiation and characterization of myeloid cells. in *Current Protocols in Immunology*, Unit 22F 5, John Wiley & Sons, Inc., New York
37. Rowat, A. C., Lammerding, J., Herrmann, H., and Aebi, U. (2008) Towards an integrated understanding of the structure and mechanics of the cell nucleus. *BioEssays* **30,** 226–236
38. Gonzalez, A. L., El-Bjeirami, W., West, J. L., McIntire, L. V., and Smith, C. W. (2007) Transendothelial migration enhances integrin-dependent human neutrophil chemokinesis. *J. Leukocyte Biol.* **81,** 686–695
39. Park, B. H., Dolen, J., and Snyder, B. (1977) Defective chemotactic migration of polymorphonuclear leukocytes in Pelger-Huet anomaly. *Proc. Soc. Exp. Biol. Med.* **155,** 51–54
40. Repo, H., Vuopio, P., Leirisalo, M., Jansson, S. E., and Kosunen, T. U. (1979) Impaired neutrophil chemotaxis in Pelger-Huët anomaly. *Clin. Exp. Immunol.* **36,** 326–333
41. Matsumoto, T., Harada, Y., Yamaguchi, K., Matsuzaki, H., Sanada, I., Yoshimura, T., Honda, M., and Tanaka, R. (1984) Cytogenetic and functional studies of leukocytes with Pelger-Huët anomaly. *Acta Haematol.* **72,** 264–273
42. Ellenberg, J., Siggia, E. D., Moreira, J. E., Smith, C. L., Presley, J. F., Worman, H. J., and Lippincott-Schwartz, J. (1997) Nuclear membrane dynamics and reassembly in living cells: targeting of an inner nuclear membrane protein in interphase and mitosis. *J. Cell Biol.* **138,** 1193–1206
43. Ma, Y., Cai, S., Lv, Q., Jiang, Q., Zhang, Q., Sodmergen, Zhai, Z., and Zhang, C. (2007) Lamin B receptor plays a role in stimulating nuclear envelope production and targeting membrane vesicles to chromatin during nuclear envelope assembly through direct interaction with importin β. *J. Cell Sci.* **120,** 520–530
44. Feng, D., Nagy, J. A., Pyne, K., Dvorak, H. F., and Dvorak, A. M. (1998) Neutrophils emigrate from venules by a transendothelial cell pathway in response to FMLP. *J. Exp. Med.* **187,** 903–915

Downloaded from http://www.jbc.org/ at Cornell University Library on December 14, 2013

45. Campbell, M. S., Lovell, M. A., and Gorbsky, G. J. (1995) Stability of nuclear segments in human neutrophils and evidence against a role for microfilaments or microtubules in their genesis during differentiation of HL60 myelocytes. *J. Leukoc. Biol.* **58,** 659–666
46. de Las Heras, J. I., Batrakou, D. G., and Schirmer, E. C. (2012) Cancer biology and the nuclear envelope: A convoluted relationship. *Semin. Cancer Biol.*, in press
47. Zink, D., Fischer, A. H., and Nickerson, J. A. (2004) Nuclear structure in cancer cells. *Nat. Rev. Cancer* **4,** 677–687
48. Fu, Y., Chin, L. K., Bourouina, T., Liu, A. Q., and VanDongen, A. M. (2012) Nuclear deformation during breast cancer cell transmigration. *Lab. Chip* **12,** 3774–3778

Downloaded from http://www.jbc.org/ at Cornell University Library on December 14, 2013

Supplementary Information

SI METHODS

Cell culture. We ensure > 90% of the population of the LamA OE cells has increased lamin A expression by monitoring ZsGreen1 expression and resorting cells when necessary. To control for spontaneous differentiation that can arise due to increased cell density, we monitor cell density each day during the differentiation time-course of five days (Coulter Counter, Beckman Coulter) and dilute the culture to 1×10^5 cells/ml with 5 µM ATRA in RPMI media. ATRA is stored as 1 mM stock in ethanol (Sigma). Before conducting microfluidic assays, cells are prefiltered to remove large aggregates by passing the suspension through a cell strainer (35 µm mesh size, BD).

Antibodies. For immunblotting we use the following antibodies: goat anti-lamin A/C (N-18, sc6215) and anti-lamin B1 (M-20, sc6217; Santa Cruz Biotechnology, Inc., Santa Cruz, USA); mouse monoclonal anti-lamin B2 (65147C; PROGEN Biotechnik GmbH, Heidelberg, Germany); guinea pig serum against LBR, generated in the laboratory of Harald Herrmann[1,2]; rabbit anti-β-tubulin (6046-100; Abcam, Cambridge, USA); and rabbit anti-actin (A5060; Sigma). In between probings, membranes are stripped with 0.2 N NaOH for 60 min at room temperature.

Microfluidic device fabrication. In brief, the desired design is printed onto quartz with 3 µm features (California NanoSystems Institute, UCLA). SU8-2005 (Microchem, Newton, MA, USA) is spin-coated (G3P-12 Spincoater, Specialty Coating Systems, Indianapolis, IN) onto a cleaned silicon wafer to a final thickness of 5.6 µm following the protocol described by the manufacturer. Exposure to UV light (200 - 250 mJ, OAI, San Jose, CA, USA) crosslinks the exposed pattern, and the non-exposed photoresist is removed using propylene glycol monomethyl ether acetate (PGMEA). We confirm the channel height using a stylus profilometer (KLA Tencor, Milpitas, USA). PDMS with 10% (w/w) crosslinking agent is thoroughly degassed and then poured onto the SU8-mold. After baking overnight at 65°C, the structure is carefully peeled off the mold. Holes connecting to the channels are formed using biopsy punches (0.75 mm diameter, Harris Uni-Core, Ted Pella, Inc., Redding, CA, USA). The device is backlit to facilitate punching holes into the shallow channels [3], and is then rinsed with isopropanol and dried before oxygen plasma treatment (Femto, Diener Electronic, Reading, PA) and bonding to a glass coverslip of No. 1.5 thickness.

Microfluidic device operation. Cell suspension is placed in a flow cytometer tube (BD), and a custom-fabricated cap that maintains a pressure seal is placed on top, allowing us to pressurize the tube. The cap connects to both a source of compressed air (Air with 5% CO_2, Airgas), as well as tubing that extends into the cell suspension and connects to the microfluidic device (1/32" OD PEEK tubing, Vici Valco Instruments, Co. Inc. Houston, TX, USA). Maintaining a constant pressure drop across the device enables optimal measurement throughput and consistency.

Nuclear shape. Image analysis is performed on thresholded images that are corrected for background inhomogeneities.

Two-dimensional migration assay. After washing with buffer, 5×10^5 cells/ml in RPMI are placed on the dish, allowed to settle for 15 min at 37°C, and then washed with prewarmed RPMI media supplemented with 10 mM HEPES (Gemini BioProducts,

Calabasas, USA); heavy mineral oil (Sigma) is placed on top to prevent evaporation. Cells that divided or interacted with other cells are excluded from the analysis.

Statistical analysis. Paired samples t-tests were performed to evaluate the statistical significance of data sets over at least 3 independent experiments. Values of $P < 0.05$ was considered as statistically significant. To compare larger data sets of passage times and circularity values, we conducted non-parametric tests due to the observed non-Gaussian distributions of the data. All data are reported as mean ± standard error of the mean (s.e.m.) unless indicated otherwise.

REFERENCES

1. Dreger CK, Konig AR, Spring H, Lichter P, Herrmann H. Investigation of nuclear architecture with a domain-presenting expression system. J Struct Biol. 2002;140:100-115.
2. Zwerger M, Kolb T, Richter K, Karakesisoglou I, Herrmann H. Induction of a massive endoplasmic reticulum and perinuclear space expansion by expression of lamin B receptor mutants and the related sterol reductases TM7SF2 and DHCR7. Mol Biol Cell. 2010;21:354-368.
3. Rowat AC, Weitz DA. Chips & Tips: punch holes easily in a PDMS microfluidic device Lab-on-a-Chip. 2008.

SI FIGURES

SI Figure S1 – Deformation of nucleus is required for passage of cell through 5-micron constrictions. Image of LBR KD neutrophils with Hoechst 33342 labeled nuclei passaging through microfluidic constriction channels. The image is acquired with fluorescence and low levels of transmitted light to show the outline of the microfluidic channels. Scale, 20 μm.

SI Figure S2 – Western blots analyses for lamin A expression. A. Lamin A levels during granulopoiesis of HL60/S4 mock and LamA OE cells in response to ATRA treatment. In the mock controls, lamin A levels decrease during differentiation; in contrast, LamA OE cells express substantially higher levels of lamin A at baseline that further increase in response to ATRA treatment. The same blot as shown in Fig. 1A is shown here with a much shorter exposure time. **B.** Comparative analysis of lamin A levels across different cell types. HL60/S4 cells have naturally low lamin A expression levels, as revealed by Western blot analysis. LamA OE HL60/S4 cells show roughly ~20 to 30× higher lamin A levels compared to the non-modified HL60/S4 cells; these levels are comparable to physiological levels of lamin A in mouse embryo fibroblasts.

SI Figure S3 – Confocal microscopy reveals more details of nuclear morphology in lamA OE cells and mock controls after ATRA treatment. Cells are immunolabeled four days after ATRA treatment with antibodies against lamin A and LBR; DNA is stained by Hoechst 33342. Confocal images confirm that lamin A is correctly localized to the nuclear envelope in the lamA OE cells, and that lamA OE nuclei do not develop the typical lobulations of the mock control cells following ATRA stimulation; instead revealing invaginations of the nuclear envelope over 1 – 2 μm length scales. Both LamA OE and mock controls show distinct LBR staining at the nuclear periphery. Scale, 10 μm.

SI Figure S4 – Cell proliferation progressively decreases following ATRA treatment for all cell lines. Cell density decreases within 3 to 5 days following ATRA treatment. This behavior is characteristic of HL60/S4 cells following ATRA treatment, which drives them to exit the cell cycle and differentiate into neutrophil-type cells followed by apoptosis. The genetically modified LamA OE and LBR KD cells show similar behavior as the control cell lines.

SI Figure S5 – CD11b expression levels increase following ATRA treatment in all cell lines. Flow cytometry results of cells labeled with CD11b-Alexa Fluor 700 performed at day 0 on non-differentiated HL60 cells and their genetic variants, and at day 4 after ATRA stimulation for **(A)** non-modified HL60 cells; **(B)** mock control cells; **(C)** lamA OE cells; **(D)** scrambled control cells; and **(E)** LBR KD cells.

SI FIGURE S1.

SI FIGURE S2.

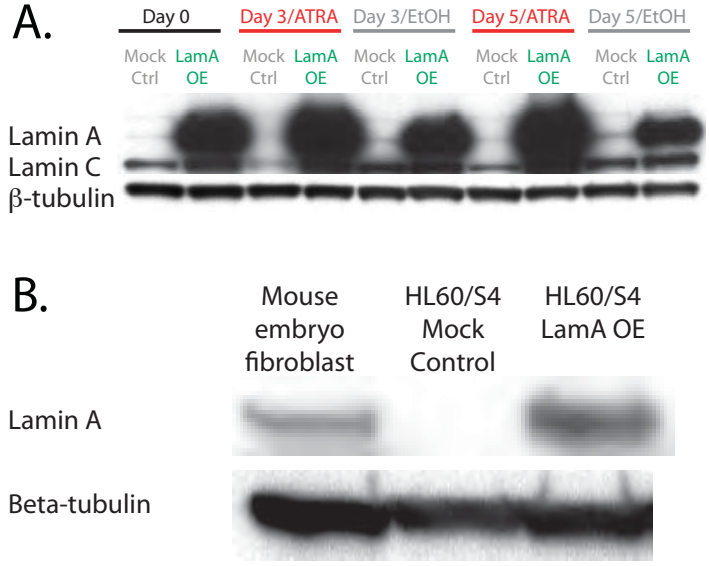
A.
Day 0
Day 3/ATRA
Day 3/EtOH
Day 5/ATRA
Day 5/EtOH
Mock Ctrl
LamA OE
Lamin A
Lamin C
β-tubulin
B.
Mouse embryo fibroblast
HL60/S4 Mock Control
HL60/S4 LamA OE
Lamin A
Beta-tubulin

SI FIGURE S3.

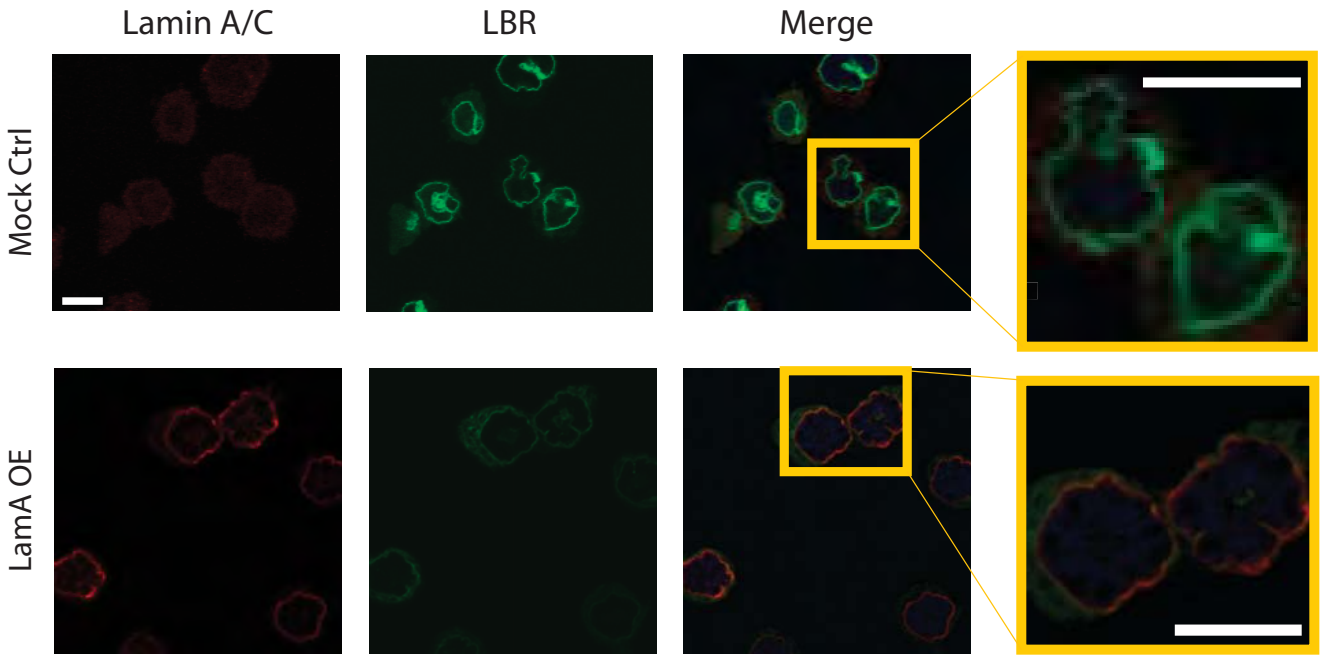

SI FIGURE S4.

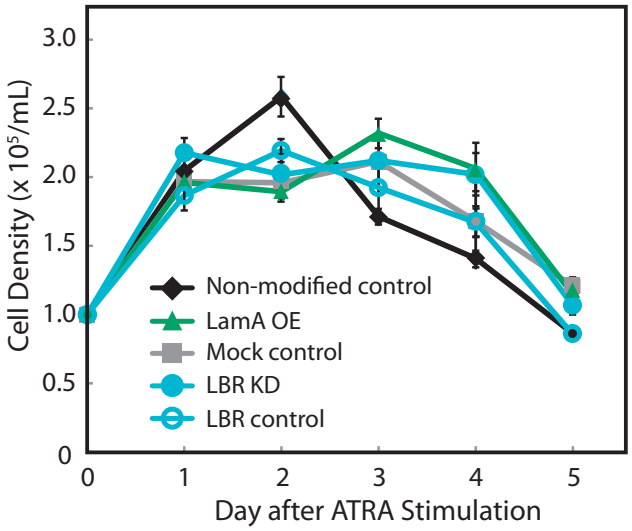
Cell Density (x 10⁵/mL)
3.0
2.5
2.0
1.5
1.0
0.5
0
0
1
2
3
4
5
Day after ATRA Stimulation
Non-modified control
LamA OE
Mock control
LBR KD
LBR control

SI FIGURE S5.

A. HL60

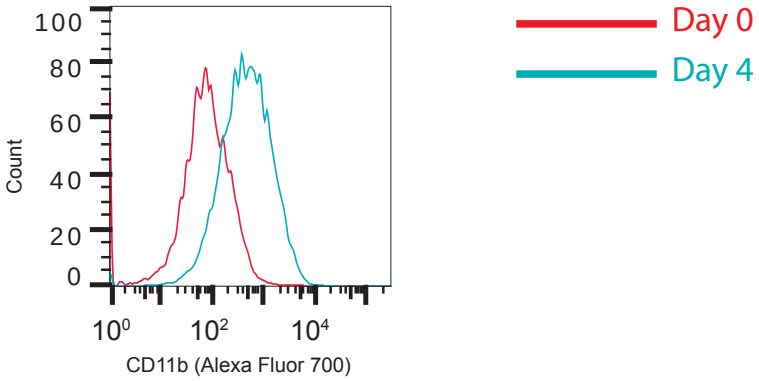

B. MOCK CTRL

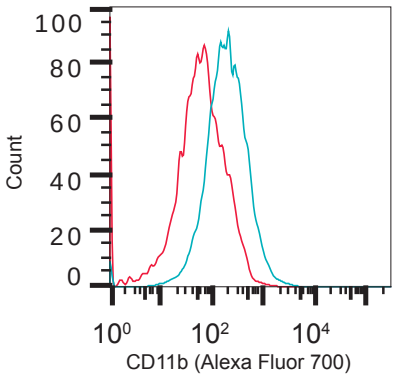

C. LAMA OE

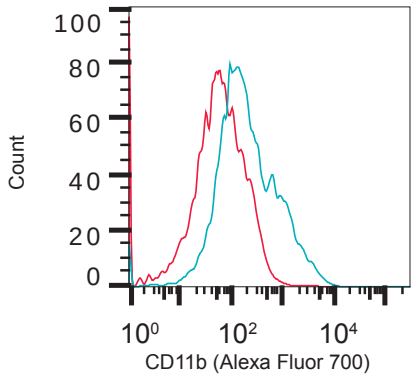

D. SCRAMBLED CTRL

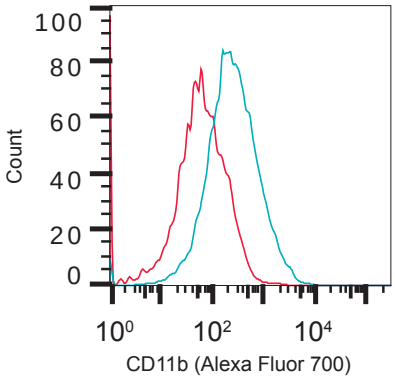

E. LBR KD

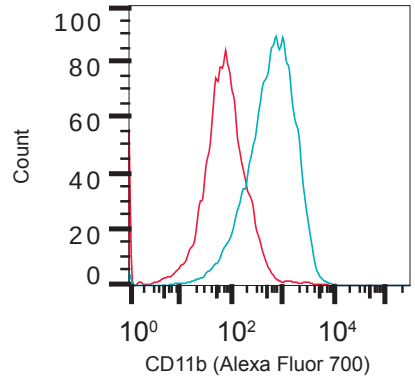

Human Molecular Genetics, 2013, Vol. 22, No. 12 **2335–2349**
doi:10.1093/hmg/ddt079
Advance Access published on February 19, 2013

Myopathic lamin mutations impair nuclear stability in cells and tissue and disrupt nucleo-cytoskeletal coupling

Monika Zwerger[1,3], Diana E. Jaalouk[1,4], Maria L. Lombardi[1], Philipp Isermann[1,2], Monika Mauermann[5], George Dialynas[6], Harald Herrmann[5], Lori L. Wallrath[6] and Jan Lammerding[1,2,*]

[1]Department of Medicine, Brigham and Women's Hospital/Harvard Medical School, Boston, MA 02115, USA, [2]Weill Institute for Cell and Molecular Biology and Department of Biomedical Engineering, Cornell University, Weill Hall, Ithaca, NY 14853, USA, [3]Department of Biochemistry, University of Zurich, 8057 Zurich, Switzerland, [4]Department of Biology, American University of Beirut, Beirut 1107 2020, Lebanon, [5]Functional Architecture of the Cell, German Cancer Research Center (DKFZ), 69120 Heidelberg, Germany and [6]Department of Biochemistry, University of Iowa, Iowa City, IA 52242, USA

Received December 15, 2012; Revised February 7, 2013; Accepted February 13, 2013

Lamins are intermediate filament proteins that assemble into a meshwork underneath the inner nuclear membrane, the nuclear lamina. Mutations in the *LMNA* gene, encoding lamins A and C, cause a variety of diseases collectively called laminopathies. The disease mechanism for these diverse conditions is not well understood. Since lamins A and C are fundamental determinants of nuclear structure and stability, we tested whether defects in nuclear mechanics could contribute to the disease development, especially in laminopathies affecting mechanically stressed tissue such as muscle. Using skin fibroblasts from laminopathy patients and lamin A/C-deficient mouse embryonic fibroblasts stably expressing a broad panel of laminopathic lamin A mutations, we found that several mutations associated with muscular dystrophy and dilated cardiomyopathy resulted in more deformable nuclei; in contrast, lamin mutants responsible for diseases without muscular phenotypes did not alter nuclear deformability. We confirmed our results in intact muscle tissue, demonstrating that nuclei of transgenic *Drosophila melanogaster* muscle expressing myopathic lamin mutations deformed more under applied strain than controls. *In vivo* and *in vitro* studies indicated that the loss of nuclear stiffness resulted from impaired assembly of mutant lamins into the nuclear lamina. Although only a subset of lamin mutations associated with muscular diseases caused increased nuclear deformability, almost all mutations tested had defects in force transmission between the nucleus and cytoskeleton. In conclusion, our results indicate that although defective nuclear stability may play a role in the development of muscle diseases, other factors, such as impaired nucleo-cytoskeletal coupling, likely contribute to the muscle phenotype.

INTRODUCTION

The mammalian nucleus is the largest organelle within the cell. It is separated from the cytoplasm by the nuclear envelope. The nuclear envelope consists of the outer nuclear membrane, which is continuous with the rough endoplasmic reticulum, the inner nuclear membrane and the nuclear lamina (1). The lamina is a proteinaceous network located underneath the inner nuclear membrane and is tightly connected to nuclear pore complexes and nuclear envelope transmembrane proteins. The lamina is primarily formed by two distinct types of proteins, referred to as A- and B-type

*To whom correspondence should be addressed at: Weill Hall, Room 235, Cornell University, Ithaca, NY 14853, USA. Tel: +1 607 2551700; Fax: +1 607 2555961; Email: jan.lammerding@cornell.edu

© *The Author 2013. Published by Oxford University Press. All rights reserved.*
For Permissions, please email: journals.permissions@oup.com

Downloaded from http://hmg.oxfordjournals.org/ at Cornell University Library on November 14, 2013

lamins (2). Lamins are type-V intermediate filaments (3,4), i.e. fibrous proteins with a characteristic tripartite structural organization: an extended, central α-helical 'rod' domain flanked by non-α-helical N- and C-terminal domains. Lamins form coiled-coil dimers through interactions of the central rod heptad sequence repeats and further assemble into higher order structures (5,6). In mammalian somatic cells, the most abundant isoforms are lamins A and C, which arise from a single gene, *LMNA*, by alternative splicing (7), and lamin B1 and B2, encoded by the genes *LMNB1* and *LMNB2*, respectively (8,9). Lamins A/C form interactions with a multitude of nuclear components and are involved in many major nuclear processes, including DNA replication and repair, chromatin organization, transcriptional regulation and stem-cell maintenance and differentiation (reviewed in 10). The recent discovery that mutations in the *LMNA* gene cause a large variety of human diseases, collectively termed laminopathies, resulted in a rapidly growing interest in the biological functions of lamins A and C. Laminopathies include the autosomal dominant form of Emery–Dreifuss muscular dystrophy (EDMD), limb–girdle muscular dystrophy, dilated cardiomyopathy (DCM), familial partial lipodystrophy (FPLD) and the segmental aging disease Hutchison–Gilford progeria syndrome (11–13). Despite much progress, it remains unclear how mutations in a single, nearly ubiquitously expressed gene can cause such a variety of disorders and why the majority of the more than 400 mutations identified to date primarily affect muscle tissue, whereas other laminopathies mostly lack muscular phenotypes (11,13). Intriguingly, lamin mutations resulting in the same disease are often scattered across the length of the gene, whereas in other cases, different mutations in the same amino acid can cause distinct disease phenotypes (13).

Different, non-mutually exclusive hypotheses have been proposed to explain the broad range of laminopathies: the 'structural hypothesis' postulates that mutated lamins assemble into a structurally impaired lamina and lead to more fragile nuclei that rupture and result in cell death, especially in mechanically stressed tissue such as muscle. A variation of the 'structural hypothesis' is that mutations in lamins do not affect nuclear stability directly, but rather affect lamin interactions with components of the linker of nucleoskeleton and cytoskeleton (LINC) complex (14), which provides a physical connection between the nuclear interior and the cytoskeleton (15,16). Decreased LINC complex formation might result in impaired nucleo-cytoskeletal coupling, and thereby cause disease. The 'gene expression hypothesis' proposes that mutations in lamins A/C can alter gene regulation, and that misregulated, tissue-specific signaling pathways give rise to the various disease phenotypes (17–20). Other hypotheses include altered stem-cell conservation and differentiation, which could result in impaired tissue maintenance and regeneration in laminopathies (21).

Previous studies have identified lamins A and C as fundamental determinants of nuclear mechanical properties and demonstrated that loss of lamin A/C causes weaker, more deformable nuclei (19,22,23). However, the effect of specific disease-causing lamin mutations on nuclear mechanics has never been systematically tested. Therefore, it remains unclear whether mutations responsible for muscular phenotypes have more severe effects on nuclear mechanics compared with mutations linked to other laminopathies. In this study, we systematically tested the effect of laminopathic mutations on various aspects of nuclear mechanics, including nuclear stiffness (i.e. the extent to which the nucleus resists deformation) and nuclear fragility, both aspects of the stability of a nucleus under mechanical stress, as well as nucleo-cytoskeletal coupling, which describes the ability to transmit intracellular forces between the cytoskeleton and nuclear interior. We evaluated nuclear stiffness in skin fibroblasts from patients with EDMD and FPLD, in a panel of $Lmna^{+/-}$ mouse embryonic fibroblasts (MEFs) genetically modified to stably express physiological levels of mutant or wild-type lamin A, and in intact *Drosophila melanogaster* larval body wall muscle tissue expressing various EDMD mutations. We complemented these studies with assays to evaluate the effect of specific mutations on lamin assembly *in vivo* and *in vitro* and on force transmission between the nucleus and cytoskeleton. Our results suggest that specific myopathic lamin A mutations interfere with normal lamin assembly and result in a loss of nuclear stability that likely contributes to muscle-specific phenotypes, but that also other factors, such as impaired nucleo-cytoskeletal coupling, play a role in the development of muscular laminopathies.

RESULTS

Fibroblasts from EDMD patients show increased nuclear deformability

Cells and biopsies from laminopathy patients and mouse models often display misshapen or ruptured nuclei (24–29), providing anecdotal support for the hypothesis that mutated lamins may alter the lamina structure in a way that renders nuclei more susceptible to mechanical stress (30,31). To test whether lamin A/C mutations linked to muscular diseases (e.g. EDMD, DCM) cause particularly strong defects in nuclear mechanics and thereby promote muscular phenotypes, we assessed the mechanical properties of nuclei in primary skin fibroblasts from EDMD patients and compared them with cells from FPLD patients and healthy controls. Nuclear stiffness of adherent cells was inferred from the induced nuclear deformations in response to substrate strain application (32). We found that nuclei of cells from two EDMD patients, carrying the *LMNA* mutations ΔK32 and E358K, respectively, deformed significantly more than those from passage-matched healthy controls (Fig. 1A), indicating increased nuclear deformability in the EDMD cells. In contrast, cells from two FPLD patients with the *LMNA* mutations R482Q and R482L, respectively, had normal nuclear stiffness. In addition, we observed that cells from EDMD patients became more frequently damaged during the strain application than cells from healthy controls, indicating increased sensitivity to mechanical stress (Supplementary Material, Fig. S1A and B). In particular, close to 12% of EDMD fibroblasts with the *LMNA* E358K mutation were damaged during strain application, whereas $<1\%$ of cells were damaged in the three control cell lines (Supplementary Material, Fig. S1C).

Downloaded from http://hmg.oxfordjournals.org/ at Cornell University Library on November 14, 2013

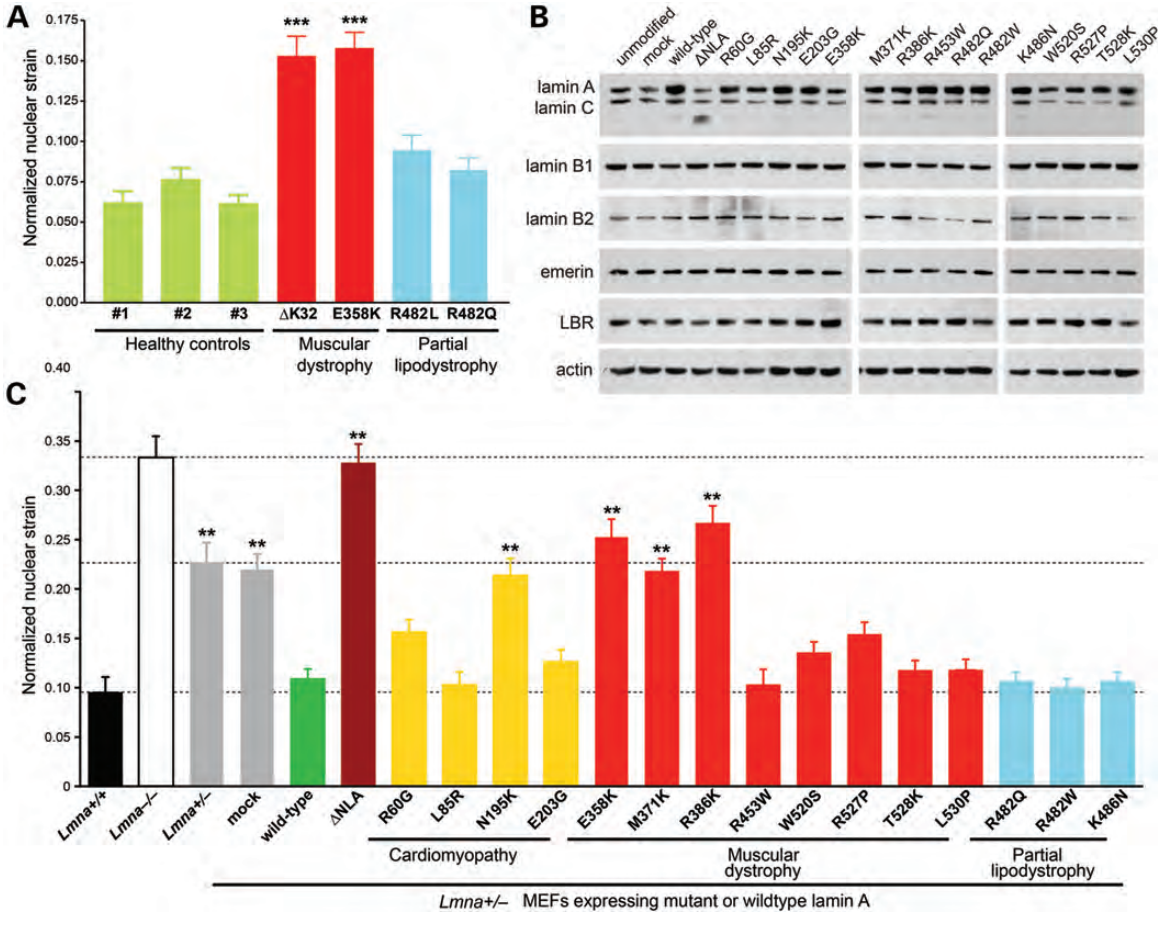

Figure 1. Myopathic mutations in LMNA have variable effects on nuclear stiffness. (**A**) Normalized nuclear strain measurements of skin fibroblasts from healthy controls (green) and human patients with *LMNA* mutations that cause EDMD (red) or FPLD (blue). Measurements were performed at passage numbers between P8 and P15. In our experiments, we observed no correlation between passage number and nuclear deformability. $^{***}P < 0.001$, versus healthy controls. (**B**) Expression levels of nuclear envelope proteins in $Lmna^{+/-}$ MEFs stably expressing the empty vector (mock), wild-type lamin A, head-truncated ΔNLA or disease-specific lamin A mutations. Actin was used as loading control. (**C**) Normalized nuclear strain measurements of unmodified $Lmna^{+/+}$, $Lmna^{-/-}$ and $Lmna^{+/-}$ fibroblasts, as well as of $Lmna^{+/-}$ fibroblasts expressing specific lamin A mutations, wild-type lamin A, head-truncated ΔNLA or the empty vector (mock). Expression of wild-type lamin A rescued nuclear stiffness to levels comparable with $Lmna^{+/+}$ cells; in contrast, ΔNLA resulted in stiffness comparable with $Lmna^{-/-}$ fibroblasts. $^{**}P < 0.01$ and $^{***}P < 0.001$, compared with $Lmna^{+/-}$ MEFs expressing wild-type lamin A.

Lamin mutations causing EDMD or DCM, but not FPLD, fail to restore nuclear stiffness

Since analysis of patient fibroblasts is limited by the heterogeneous genetic background and the limited availability of samples, we developed a comprehensive approach to test a wider panel of lamin A mutations associated with EDMD, DCM and FPLD in a genetically uniform background. We ectopically expressed mutant or wild-type lamin A in MEFs lacking a single *Lmna* allele ($Lmna^{+/-}$ MEFs), which express only ~50% of the normal levels of lamin A/C (33,34). The lamin mutations were introduced with a bicistronic retroviral construct consisting of non-tagged human lamin A and a ZsGreen fluorescent reporter. Since both proteins are translated from a single bicistronic mRNA transcript and expressed at similar levels, we were able to sort for cells with physiological levels of ectopically expressed lamin A by fluorescence-activated cell sorting for ZsGreen. The resulting model system closely resembles the situation in laminopathy patients, who typically carry autosomal dominant *LMNA* mutations and express approximately equal amounts of mutant and wild-type lamins. Furthermore, expressing the mutations in the $Lmna^{+/-}$ MEF background and comparing them with $Lmna^{+/+}$ and $Lmna^{-/-}$ MEFs enabled us to distinguish whether any observed effects of specific mutations were dominant-negative or caused by a loss-of-function of the mutant lamin A protein (i.e. haploinsufficiency). We tested a total of 15 mutations, representing EDMD (8 mutations), DCM (4 mutations) and FPLD (3 mutations) (summarized in Table 1). For comparison, we evaluated $Lmna^{+/-}$ MEFs stably expressing either the empty vector (mock control) or wild-type lamin A. As an additional control, we assessed the effect of a lamin A mutant lacking the N-terminal 33 amino acids (ΔNLA), which are critical for the assembly of higher order lamin structures. When expressed in mammalian cells, ΔNLA fails to assemble into the lamina and disrupts the existing lamin network, thus acting in a dominant-negative manner (35).

We confirmed that the modified cells expressed the lamin constructs at physiological levels by western analysis (Fig. 1B and Supplementary Material, Fig. S2). Moreover,

Downloaded from http://hmg.oxfordjournals.org/ at Cornell University Library on November 14, 2013

Table 1. Human disease-associated LMNA mutations used in this study

Mutation	Disease	Reference
ΔK32	EDMD	(68)
R60G	DCM-CD, DCM-CD + FPLD, DCM-CD + FPLD + CMT2	(62)
L85R	DCM-CD	(62)
N195K	DCM-CD	(62)
E203G	DCM-CD	(62)
E203K	DCM-CD	(77)
E358K	EDMD	(78)
M371K	EDMD	(78)
R386K	EDMD	(78)
R453W	EDMD, EDMD + FPLD, LGMD1B	(78)
R482Q	FPLD	(79)
R482W	FPLD, FPLD + LGMD	(80)
K486N	FPLD	(81)
W520S	EDMD	(78)
R527P	EDMD, EDMD + FPLD, LGMD1B	(82)
T528K	EDMD, LGMD1B	(78)
L530P	EDMD	(82)
ΔNLA	Synthetic dominant-negative construct	(35)

The tested mutations were R60G, L85R, N195K E203K and E203G, causing DCM (62,77); ΔK32, E358K, M371K, R386K, R453W, W520S, R527P, T528K and L530P, found in patients with EDMD (68,78,82); and R482Q, R482W and K486N, identified in patients with FPLD (79–81). In addition, we expressed the engineered dominant-negative construct ΔNLA, which disrupts endogenous lamin organization (35). Note that, although most mutations affect both lamin A and lamin C, we expressed only modified lamin A in MEF cells. EDMD, Emery–Dreifuss muscular dystrophy; LGMD1B, limb–girdle muscular dystrophy type 1B; DCM-CD, dilated cardiomyopathy with conduction defect; CMT2, autosomal recessive Charcot–Marie–Tooth disease; FPLD, familial partial lipodystrophy type Dunnigan (FPLD2). For additional information on these mutations, see also http://www.umd.be/LMNA/.

expression levels of lamin B1 and other nuclear envelope proteins such as emerin and lamin B receptor were not notably altered by ectopic expression of the lamin A variants (Fig. 1B). However, we found a decrease in the expression levels of lamin B2 for some of the mutants, most prominently for R453W, R482Q and L530P. Nuclear strain experiments confirmed that the nuclear stiffness of non- and mock-modified $Lmna^{+/-}$ MEFs has an intermediate value compared with that of $Lmna^{+/+}$ and $Lmna^{-/-}$ cells (19), consistent with the lower levels of lamins A/C in these cells. Ectopic expression of wild-type lamin A in $Lmna^{+/-}$ MEFs completely restored nuclear stiffness to levels of $Lmna^{+/+}$ MEFs (Fig.1C), whereas expression of the dominant negative ΔNLA mutant caused an increase in nuclear deformability in the modified $Lmna^{+/-}$ MEFs, resulting in values comparable to $Lmna^{-/-}$ cells. In contrast, none of the disease-causing lamin mutations resulted in dominant-negative effects on nuclear deformability. Four of the tested lamin A mutants associated with muscular disease, i.e. N195K (DCM), E358K (EDMD), M371K (EDMD) and R386K (EDMD), failed to restore nuclear stiffness and caused nuclear deformations similar to those observed in mock and non-modified $Lmna^{+/-}$ MEFs. These findings imply that these mutant lamins result in a loss of structural function and fail to form a lamina network that can withstand mechanical forces as efficiently as a lamina formed from wild-type lamin. Although these findings implicate increased nuclear deformability in the pathogenesis of myopathic laminopathies, other DCM and EDMD mutations partially or completely restored nuclear stiffness (Fig. 1C), indicating that additional mechanisms may contribute to the disease mechanism. Importantly, all three tested FPLD mutations completely restored nuclear stiffness as efficiently as wild-type lamin A, suggesting that the FPLD mutations have no effect on the structural function of lamin A.

Myopathic lamin A mutations that cause defects in nuclear stability are more soluble

To investigate possible molecular mechanisms for the loss of structural functions in some of the EDMD and DCM mutations, we investigated the intranuclear localization of the various mutants, as increased nucleoplasmic localization could indicate impaired incorporation of mutant proteins into the nuclear lamina. In wild-type cells and in $Lmna^{+/-}$ MEFs expressing wild-type lamin A, lamins A/C were predominantly localized at the nuclear rim (Fig. 2A). In contrast, cells expressing any of the mutations associated with the loss of nuclear stability (i.e. N195K, E358K, M371K and R386K and ΔNLA) had a prominent nucleoplasmic localization of lamins A and C (Fig. 2A). Since lamin A/C-deficient cells have an abnormal distribution of emerin (34), we also assessed expression and localization of emerin in our panel of cells. However, we did not observe any obvious defects in emerin expression (Fig. 1B) or localization (Supplementary Material, Fig. S3). Since the nucleoplasmic pool of lamin A was increased in cells expressing the lamin A variants N195K, E358K, M371K and R386K and the ΔNLA construct, we next quantified the soluble fraction of lamin A in these cells by a sequential protein extraction procedure using mild detergents (36). Cells expressing ΔNLA and the N195K, E358K, M371K and R386K mutants had substantially increased fractions of soluble lamin A compared with wild-type expressing cells (Fig. 2B and C), suggesting that these lamin A mutations fail to correctly incorporate into the nuclear lamina and thereby result in impaired nuclear stability.

Different amino acid substitutions in the same amino acid positions can have distinct effects on lamin structural function

All lamins share a conserved, tripartite organization comprising a central coiled-coil rod domain, as well as non-helical head and tail domains (37,38). The coiled-coil rod is the principal subunit for all structural states, both for extended filaments and for more complex arrays formed from filaments as revealed early on by *in vitro* assembly studies (39) and recently developed further in detail by cryoelectron tomography (40). It is clear from these studies that these coiled coils interact by multiple longitudinal and lateral interactions mediated by the many ionic side chains that are found on the surface of the coiled coil, to form higher order structures. Strikingly, the four mutations that had the most severe effects on

Downloaded from http://hmg.oxfordjournals.org/ at Cornell University Library on November 14, 2013

nuclear structure were localized within, or in the case of R386K just three amino acids after the predicted coiled-coil rod domain of lamin A (41) (Supplementary Material, Fig. S4A). Moreover, the mutated amino acids were located in the outward-facing positions *f* or *g* of the heptad repeat of the coiled-coil dimer (Supplementary Material, Fig. S4B) and were substitutions to the positively charged lysine. On the other hand, substitution of E203, another outward-facing position in the central rod heptad repeat, to the neutral glycine had no effect on the structural function of the protein. Based on these findings, we hypothesized that mutations to lysine in these outward-facing positions might interfere with the higher order assembly of lamin dimers. We therefore tested whether substitutions to small uncharged amino acids (alanine, glycine) could restore normal nuclear stiffness. In the case of E358, both alanine and glycine substitutions rescued nuclear stiffness, supporting our hypothesis. However, in the case of M371, only the glycine substitution restored nuclear stiffness, whereas substitution to alanine resulted in increased nuclear deformability; conversely, in the case of R386, only alanine but not glycine rescued nuclear stiffness (Supplementary Material, Fig. S4C). In addition, we tested whether mutation of amino acid E203 to lysine resulted in increased deformability, i.e. a loss of structural function. Surprisingly, neither lysine nor alanine at position E203 caused nuclei to become more deformable. These data suggest that each individual amino acid position and each substitution can have different effects on structural functions of lamin A and the corresponding nuclear stiffness, consistent with the finding that different amino acid substitutions in the same position can result in different laminopathies (13).

Lamin mutations that cause impaired nuclear stability have disturbed filament and paracrystal assembly *in vitro*

Since our solubility studies suggested that lamin A mutants that have impaired structural function fail to correctly incorporate into the lamina network, we decided to directly assess their assembly into higher order structures. Recombinant human lamin A can be induced to assemble into either paracrystalline structures or filaments *in vitro*, depending on buffer conditions and dialysis procedure (42). We evaluated wild-type lamin A and three lamin mutations that caused the loss of structural function in our nuclear strain assay, namely ΔK32, N195K and E358K mutants (Fig. 1A and C). Although wild-type lamin A formed the expected large structures of laterally organized fibers (paracrystalline arrays), the three lamin A mutants failed to assemble into well-organized structures and instead formed small aggregates lacking the typical 24.5 nm repeat pattern (Fig. 3, top row and Supplementary Material, Fig. S5). Similarly, only wild-type lamin A assembled into regular extended filaments *in vitro* (Fig. 3, bottom row and Supplementary Material, Fig. S5). These results suggest that the loss of structural properties of lamins through distinct mutations associated with more deformable nuclei is caused by impaired assembly interactions of the mutant proteins, consistent with recent reports on *Caenorhabditis elegans* lamin carrying amino acid substitutions that correspond to laminopathic mutations (43,44).

Nuclei of *D. melanogaster* larvae body wall muscle expressing disease-causing Lamin C variants are more deformable

To test whether lamin mutations associated with muscular dystrophy also cause defects in nuclear stability in muscle tissue, we developed a novel experimental assay that enables us to examine nuclear deformability in the intact body wall muscle of *D. melanogaster* third instar larvae subjected to mechanical strain (Fig. 4A and B). *D. melanogaster* possesses genes encoding Lamin C and lamin Dm0, considered to share properties with mammalian A- and B-types, respectively. *D. melanogaster* can serve as a model to study human laminopathies (45–47), and flies and larvae lacking Lamin C show similar defects in nuclear structure as cells from *Lmna*$^{-/-}$ mice and patients with EDMD (47). Muscle-specific expression of *Drosophila* Lamin C possessing mutations modeled after those causing human muscle laminopathies leads to larval locomotion defects, nuclear and cytoplasmic abnormalities and, in some cases, lethality at the pupal stage (46). We assessed nuclear deformability in the body wall muscles of six different *D. melanogaster* strains, expressing wild-type Lamin C, the headless variant of Lamin C lacking the first 42 amino acids (Lamin C ΔN) (47), and the Lamin C variants N210K, R401K, K493W, W557S and L567P, corresponding to the human point mutations N195K, R386K, R453W, W520S and L530P, respectively, which cause DCM (N195K) and EDMD (R386K, R453W, W520S and L530P) in humans. The mutant lamins were expressed using the Gal4/UAS system (48), with the C57 Gal4 driver stock providing the muscle specificity (49). Note that the wild-type and mutant lamins were expressed in an otherwise wild-type genetic background, allowing for tests of dominant-negative function. Body wall muscle expressing the ΔN mutation had misshapen nuclei (Fig. 4B), consistent with previous reports (46). These nuclei also deformed significantly more under applied strain, compared with muscle nuclei expressing wild-type lamin and non-transgenic larvae (Fig. 4C). Similar to our results in MEFs, where only the ΔNLA mutation caused dominant-negative effects on nuclear stiffness, muscle-specific expression of lamin point mutations resulted in substantially milder disturbances in nuclear deformability. Although the differences were not statistically significant compared with the expression of wild-type *Drosophila* Lamin C, we observed a clear trend toward softer nuclei of larvae muscle expressing EDMD mutations (Fig. 4C). This reduced effect on nuclear stiffness in *Drosophila* muscle cells, compared with MEF cells, could be attributed to the fact that in the *Drosophila* system mutations were expressed in a wild-type background of Lamin C expression, whereas in MEF cells mutations were expressed in a *Lmna*$^{+/-}$ background. Importantly, nuclear stiffness of epidermal cells, which did not express the mutant lamins, was indistinguishable between all strains, including larvae with muscle-specific expression of the ΔN mutant (1.248 ± 0.019 for unmodified larvae, 1.239 ± 0.017

Downloaded from http://hmg.oxfordjournals.org/ at Cornell University Library on November 14, 2013

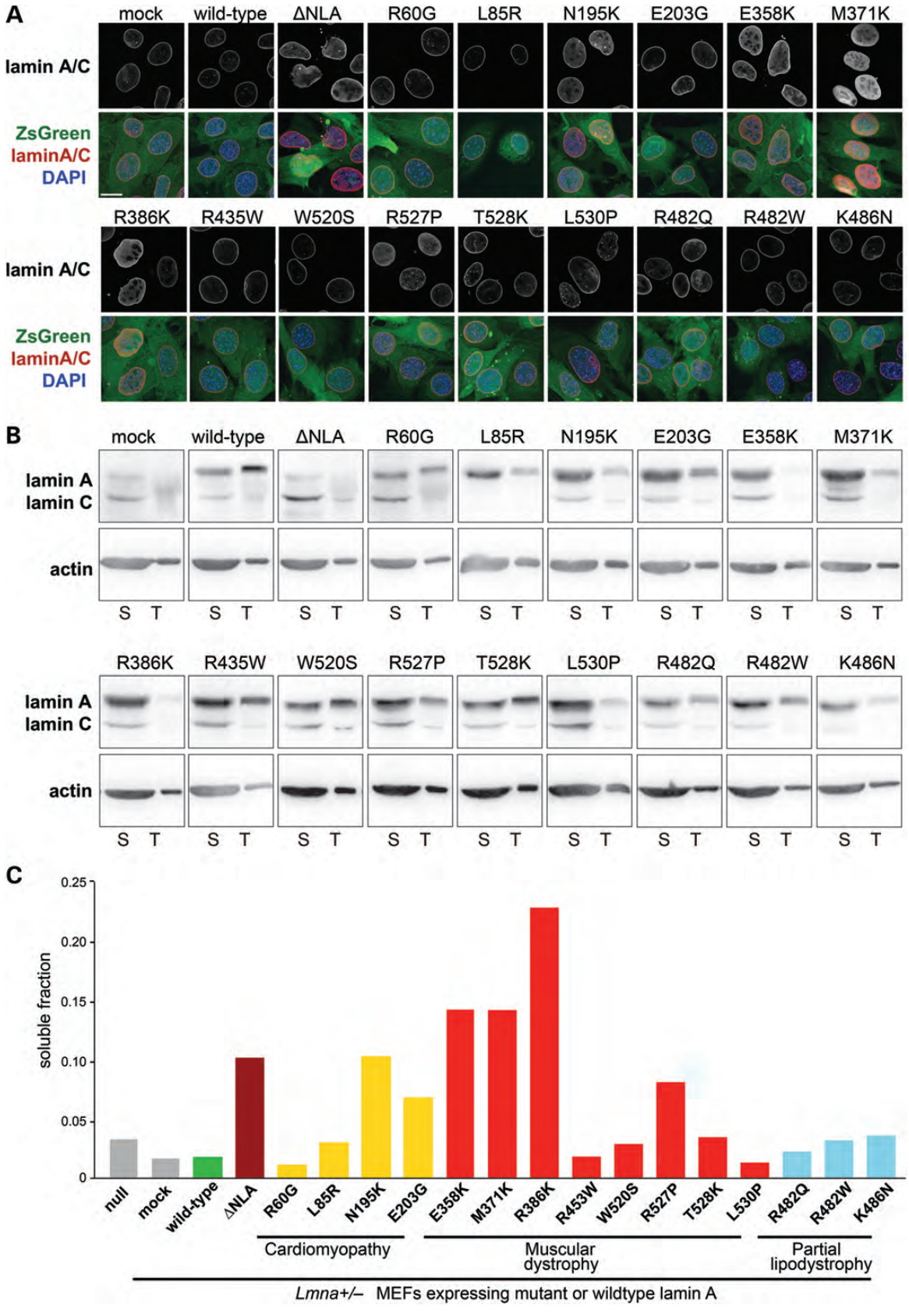

Figure 2. Myopathic lamin A mutations that cause defects in nuclear stability have increased nucleoplasmic distribution and are more soluble. (**A**) Immunofluorescence staining for lamin A/C in *Lmna*$^{+/-}$ fibroblasts stably expressing the empty vector (mock), wild-type lamin A, head-truncated ΔNLA or disease-

Downloaded from http://hmg.oxfordjournals.org/ at Cornell University Library on November 14, 2013

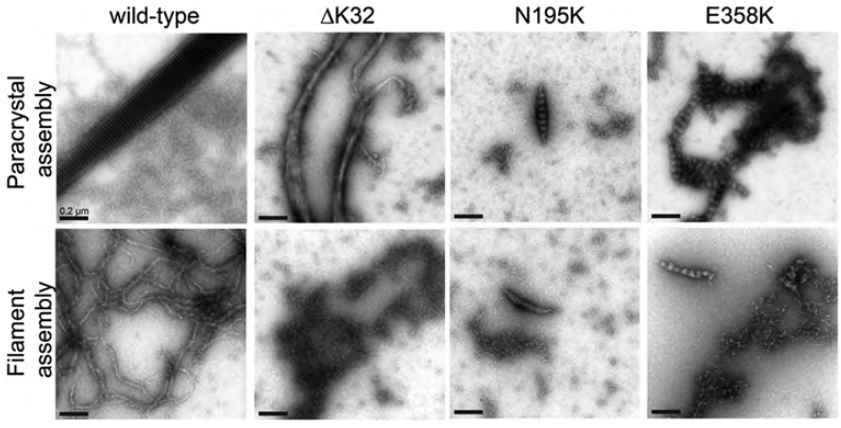

Figure 3. Impaired *in vitro* assembly of myopathic lamin A mutations that alter nuclear mechanical properties. Recombinant human wild-type lamin A ΔC18 (i.e. mature lamin A) as well as the single-amino-acid deletion ΔK32 and the point mutations N195K and E358K were induced to assemble into paracrystalline structures (upper panel) or filaments (lower panel) *in vitro* and imaged by transmission electron microscopy. In contrast to wild-type lamin A, the lamin A variants ΔK32, N195K and E358K failed to assemble into regularly-organized structures and instead formed irregular aggregates. Scale bar: 0.2 μm.

and 1.248 ± 0.023 for wild-type and ΔN-expressing larvae, respectively), confirming that the observed defects in the myonuclei were a direct consequence of the muscle-specific expression of Lamin C mutants.

Laminopathic lamin A mutations disrupt nucleo-cytoskeletal coupling

Our findings that only a subset of the DCM- or EDMD-causing mutations resulted in significantly impaired nuclear stability suggests that additional mechanisms may contribute to the muscular phenotype. One such mechanism could be that lamin mutations disrupt the physical coupling between the nucleus and cytoskeleton, which plays important roles in muscle function. Lamins A/C interact with inner nuclear membrane proteins containing a SUN (Sad1p and Unc-84 homology) domain such as Sun1 and Sun2 (50). Through the SUN domain, these proteins associate across the perinuclear space with the KASH (Klarsicht, Anc-1 and Syne homology) domain of a protein family termed nesprins (51–53) located on the outer nuclear membrane; nesprins in turn connect to cytoskeletal components including actin, microtubules (via dynein) and intermediate filaments (via plectin) (14,54). Lamin mutations could interfere with this nucleo-cytoskeletal connection, and defects in nucleo-cytoskeletal coupling and anchoring have been reported in *Lmna*$^{-/-}$ mice (16) and MEFs (15,55). To directly test the effect of specific lamin mutations on intracellular force transmission between the nucleus and cytoskeleton, we applied a technique recently developed in our laboratory (15), in which we locally apply force to the cytoskeleton while measuring the induced nuclear and cytoskeletal displacements across the cell (Fig. 5A). We performed these measurements on *Lmna*$^{+/-}$ MEFs stably expressing the empty vector (mock), wild-type lamin A or five different laminopathic lamin A mutations: E203G causing DCM; R453W and T528K causing EDMD; and the FPLD mutations R482W and K486N. Importantly, all of these mutations displayed normal nuclear deformability in our nuclear strain assays (Fig. 1C). For comparison, we included *Lmna*$^{+/+}$ MEFs, which serve as control for normal nucleo-cytoskeletal coupling, and *Lmna*$^{+/-}$ MEFs stably expressing a dominant-negative nesprin mutant consisting of the KASH domain of human nesprin 1α (DN KASH) that is sufficient to disrupt nucleo-cytoskeletal coupling by displacing endogenous nesprins into the endoplasmic reticulum (15). *Lmna*$^{+/-}$ MEFs expressing either the empty vector (mock) or DN KASH had significantly impaired force transmission between the nucleus and cytoskeleton, as reflected by smaller nuclear and cytoskeletal displacements in areas away from the force application site (Fig. 5B) compared with *Lmna*$^{+/+}$ MEFs. This indicates that lamin A expression levels from only one functional *Lmna* allele is not sufficient to establish the LINC complexes necessary to provide as strong a coupling between the nucleus and the cytoplasm as in *Lmna*$^{+/+}$ MEFs. Reintroduction of wild-type lamin A was sufficient to completely restore intracellular force transmission in *Lmna*$^{+/-}$ cells to levels comparable with *Lmna*$^{+/+}$ MEFs (Fig. 5B). In contrast, all tested mutations, with the exception

specific lamin A mutations (upper panels) and overlaid with the ZsGreen signal and DAPI chromatin staining (lower panels). Cells expressing the ΔNLA, N195K, E358K, M371K and R386K mutations have increased nucleoplasmic localization of lamin A/C. Scale bar: 20 μm. (**B**) Soluble lamin A protein fraction (S) versus total lamin A and C levels in *Lmna*$^{+/-}$ fibroblasts stably expressing the empty vector (mock), wild-type lamin A, head-truncated ΔNLA or disease-specific lamin A mutations, as detected by western analysis. The soluble fraction contains lamin protein that is not incorporated into the nuclear lamina, and was therefore extracted by treatment of cells with mild detergent. Note that only 1/30 of the total lamin A fraction, compared with the soluble fraction, was loaded on the gel. Similar protein levels were loaded, as reflected by actin staining. Since different amount of cells were loaded onto gels for each cell line, a direct comparison of amounts of soluble or total Lamin A fraction between cell lines is not possible, and it is the ratio between soluble to total protein that is used for the interpretation of the results. Extraction was performed three independent times; one representative panel is shown. (**C**) Quantification of the soluble lamin A fraction of the cells analyzed in (B), indicating that ΔNLA and the disease-specific lamin variants N195K, E358K, M371K and R386K are more soluble than wild-type lamin A and other lamin variants.

Downloaded from http://hmg.oxfordjournals.org/ at Cornell University Library on November 14, 2013

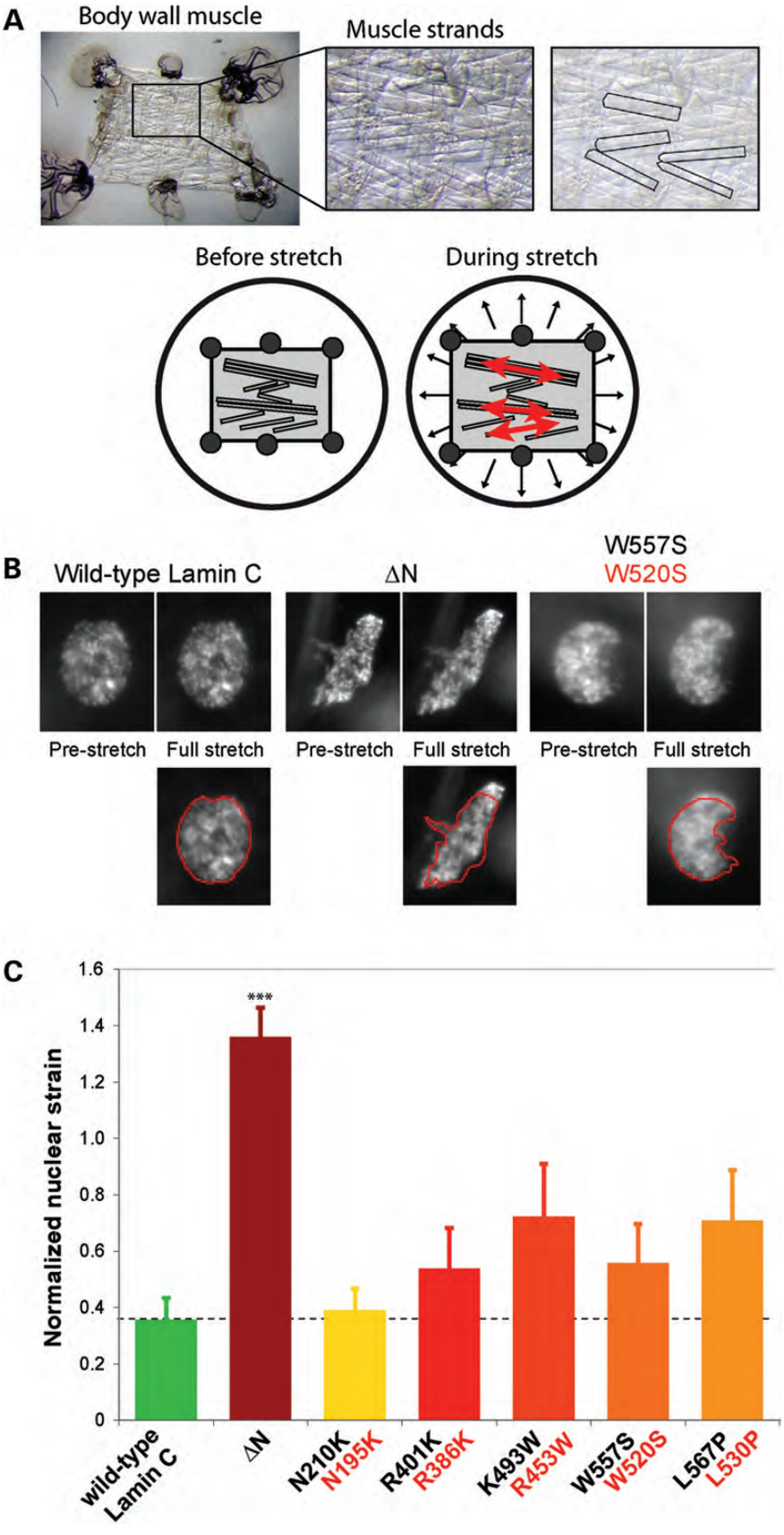

Downloaded from http://hmg.oxfordjournals.org/ at Cornell University Library on November 14, 2013

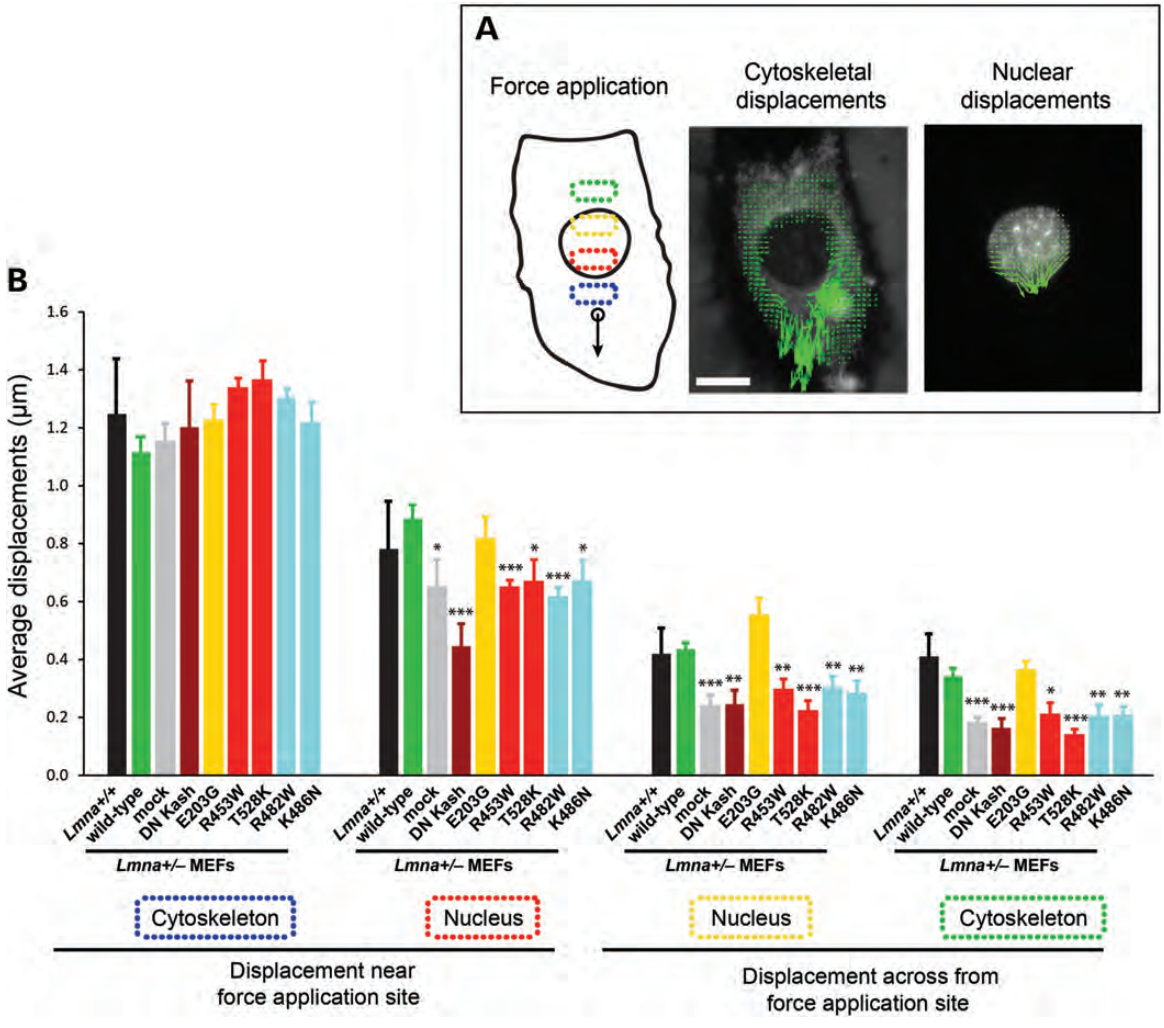

Figure 5. Laminopathic lamin A mutations disrupt force transmission between the nucleus and cytoskeleton. (**A**) Schematic overview of the microneedle manipulation experiments to assess intracellular force transmission between the nucleus and cytoskeleton. A fine microneedle is inserted into the cytoplasm near the nucleus and moved toward the periphery (left panel). Displacement maps of the cytoskeleton (middle panel) and the nucleus (right panel) are plotted by tracking intracellular fluorescent markers; measurements of the average displacements within four defined areas inside the cytoplasm and nucleus (indicated by dotted boxes in the left panel) are used to evaluate the intracellular force transmission between the nucleus and cytoskeleton. Scale bar: 20 μm. (**B**) Average displacements at the indicated regions in $Lmna^{+/+}$ MEFs, and in $Lmna^{+/-}$ fibroblasts stably expressing the empty vector (mock), wild-type lamin A, head-truncated ΔNLA or disease-specific lamin A mutations. The displacements in the first cytoskeletal region were comparable in all cells, illustrating similar strain application with the microneedle. $Lmna^{+/-}$ cells expressing mutant lamins (except for the E203G mutations) and the empty vector had significantly smaller nuclear and cytoskeletal displacements in the three cellular regions observed away from the site of strain application compared with $Lmna^{+/-}$ cells expressing wild-type lamin A or non-modified $Lmna^{+/+}$ cells, indicating reduced intracellular force transmission between the nucleus and cytoskeleton in the mutant cells. $^{*}P < 0.05$; $^{**}P < 0.01$; $^{***}P < 0.001$ versus $Lmna^{+/-}$ MEFs expressing wild-type lamin A.

of the E203G mutant, failed to rescue intracellular force transmission (Fig. 5B), indicating that these mutations interfere with nucleo-cytoskeletal coupling despite having apparently normal incorporation into the nuclear lamina and maintaining normal nuclear stiffness. Surprisingly, these defects were also visible in the two FPLD mutations.

Figure 4. Decreased nuclear stiffness in body wall muscle of *D. melanogaster* larvae expressing Lamin C variants causing EDMD. (**A**) Overview of the experimental approach to observe nuclear deformations in *D. melanogaster* larval filet subjected to strain application. Upper panel: the larval filet, consisting of the body wall muscle, is glued to a transparent silicone membrane (left panel); individual muscle fibers are easily detectable (middle and right panel, with distinct muscle fibers highlighted in the right panel). Lower panel: although biaxial strain is applied to the *Drosophila* larval filet, the tissue strain in the muscle fibers is almost completely uniaxial in the direction of the muscle fiber. (**B**) Change in nuclear shape in pre-stretched and fully stretched muscle strands of larvae expressing wild-type Lamin C (the A-type lamin of *D. melanogaster*), head-truncated ΔN Lamin C or the W557S Lamin C mutation, which corresponds to the human *LMNA* W520S mutation. Muscle cells expressing the ΔN lamin mutation deformed significantly more under applied strain. Images in the lower panel represent nuclei under strain, overlaid with the nuclear contour from the pre-stretch state in red. (**C**) Normalized nuclear stiffness of *D. melanogaster* larvae expressing wild-type *D. melanogaster* Lamin C, head-truncated Lamin C ΔN or Lamin C mutations (labeled in black) that correspond to human EDMD-causing *LMNA* mutations (labeled in red). $^{***}P < 0.001$, compared with muscle nuclei expressing wild-type Lamin C.

Downloaded from http://hmg.oxfordjournals.org/ at Cornell University Library on November 14, 2013

DISCUSSION

The finding that different mutations in the *LMNA* gene cause a variety of human diseases and that many of these mutations result in tissue-specific defects has continued to puzzle researchers for years. Gross alterations in nuclear morphology are often noted as a hallmark of laminopathies (24–29,31), and biopsies from muscular dystrophy and DCM patients have revealed defects in nuclear envelope continuity, loss of compartmentalization and even the presence of mitochondria within the nuclear interior (25,30,56), suggesting physical damage to mechanically fragile nuclei. Nonetheless, it has remained unclear to what extent mechanical defects, i.e. impaired nuclear structure and stability or disruption of nucleo-cytoskeletal connections, contribute to the development of muscular phenotypes observed in many laminopathies.

We performed a comparative study on the effect of a panel of lamin mutations, representing EDMD, DCM and FPLD, on nuclear mechanical properties. We used human patient fibroblasts as well as $Lmna^{+/-}$ MEFs modified to express different disease-causing lamin A mutations. The latter cell line was previously reported to still express a truncated fragment of lamin A (57). In our studies, we found $Lmna^{+/+}$, $Lmna^{+/-}$ and $Lmna^{-/-}$ MEFs to be a valid system to test the effect of laminopathic mutations on nuclear stability: we found that nuclear stiffness shows a dose-dependent increase with the amount of wild-type lamin A, and nuclear deformability increases with loss of its expression (Fig. 1C). Moreover, the reintroduction of wild-lamin A into $Lmna^{+/-}$ MEFs completely restored nuclear stiffness to values comparable with $Lmna^{+/+}$ MEFs. Therefore, the truncated lamin A fragment present in the $Lmna^{+/-}$ and $Lmna^{-/-}$ MEFs had no effect on nuclear deformability.

In our studies on both patient cells and modified $Lmna^{+/-}$ MEFs, we found that all lamin mutants responsible for FPLD had normal nuclear stiffness. In contrast, several mutations associated with EDMD and DCM resulted in a loss of nuclear stability, as evidenced by increased deformation of the nuclei and enhanced sensitivity to mechanical strain. The findings are consistent with previous reports that FPLD mutations, which are often clustered around a small surface region of the lamin Ig-fold, do not affect lamin diffusional mobility (58,59). Of note, we found the most severe defects in EDMD and DCM mutations affecting the N-terminal domain of A-type lamins and specific amino acid substitutions in outward-facing positions of the coiled coil of the central rod, implying that defects in the higher order assembly of lamins are responsible for the loss of structural function. We speculate that distinct myopathic mutations might have effects on the lamina network and nuclear integrity due to impaired assembly into the lamina network. Therefore, a large fraction of these mutant proteins remains nucleoplasmic and more soluble, so that the lamina cannot adequately support nuclear stability. Other mutations might have more subtle effects on assembly or produce minor irregularities in the lamina lattice, which are not easily detectable in our nuclear strain assays. Unlike the nuclear strain experiments, our *in vitro* assembly studies, which revealed severed defects in filament and paracrystal assembly of lamin mutants causing EDMD, were performed in the absence of wild-type lamin A. Although we cannot exclude the possibility that the presence of wild-type lamin A could assist in the formation of more regular-appearing structures comprised of mutant and wild-type lamins (which would likely still be mechanically weaker), previous co-assembly studies with wild-type and mutant desmin found that the mutant protein segregates *in vitro* and *in vivo* (60,61), which would also provide an explanation for the increased solubility of the mutant lamins in our studies (Fig. 2).

We found that different amino acid substitutions at the same amino acid position within the central rod domain can have very distinct effects on nuclear deformability. This observation may at least in part explain why some amino acid substitutions at specific positions are more prevalent among patients with *LMNA* mutations than others. For example, for position E203, both E203K and E203G substitutions have been identified in patients with DCM, whereas substitution to E203A, which had normal structural function in our nuclear strain assay, has never been reported in patients. Similarly, for position E358, the E358K mutation is the only reported amino acid change reported in severe muscular dystrophy, and position R386 has been reported mutated to lysine (K), threonine (T), or methionine (M), but not to glycine (G) or alanine (A). Although this preference for specific amino acid substitutions may simply represent underreporting of disease mutations or the rarity of *LMNA* mutations, it is intriguing to consider the possibility that the fact that some amino acid substitutions have not been reported in patients may indicate that these changes either have no profound effects or are so deleterious that they are lethal during development.

Using muscle-specific expression of myopathic lamin mutants in *D. melanogaster*, we provided the first direct evidence that lamin mutations impair nuclear stability in muscle fibers subjected to mechanical strain. Interestingly, the N210K mutation, which corresponds to the human N195K mutation that causes DCM, had no effect on nuclear stability in the *Drosophila* body wall muscle, which may indicate that lamin mutations can differentially affect nuclear structure and mechanics in skeletal and cardiac muscle. This idea is further supported by the fact that patients carrying the *LMNA* N195K mutation show no clinical symptoms typical for muscular dystrophy, and skeletal muscle biopsies exhibit no pathology (62).

Although our findings strongly support a role for impaired nuclear mechanics in the development of muscular phenotypes in laminopathy patients, it is important to note that only four of the 12 EDMD and DCM mutations caused severe defects in nuclear stability, whereas other mutations displayed normal nuclear stiffness in our assays and yet cause EDMD or DCM in humans. For cases in which no obvious defect in nuclear stability was observed, we cannot exclude the possibility that abnormalities are masked by impaired nucleo-cytoskeletal coupling. However, considering the strong correlation between nuclear deformation (Fig. 1C) and solubility of mutant lamins (Fig. 2C), it seems likely that our measurements reflect specific differences in structural function of different lamin mutations. This idea is supported by prior observations using C2C12 myoblasts that demonstrated diffuse, nucleoplasmic localization in transfected cells for the same four mutations we found to be defective in providing nuclear stability (63). For cases where we did not observe negative effects on nuclear stiffness, we favor

Downloaded from http://hmg.oxfordjournals.org/ at Cornell University Library on November 14, 2013

the explanation that additional factors must contribute to the development of muscular disease, specifically a disruption of nucleo-cytoskeletal connections. In support of this hypothesis, we observed defects in intracellular force transmission (Fig. 5B). Our findings are consistent with a recent report in which laminopathic mutations associated with DCM and EDMD caused impaired nuclear movement in MEFs, which was attributed to defects in the attachment of cytoskeletal actin cables to the nuclear lamina via nesprin-2 giant/Sun2 complexes termed transmembrane actin-associated nuclear lines (55).

One potential limitation of the current studies is that we investigated mutations in lamin A only, whereas most human mutations affect both lamins A and C. However, we found that the expression of lamin A was sufficient to completely restore nuclear stiffness in *Lmna*$^{+/-}$ MEFs, suggesting some redundancy between these two isoforms, which is consistent with the lack of phenotype in mice lacking either lamin A or C (64–66). In addition, we obtained similar results in *Drosophila* muscle fibers which express only a single A-type lamin.

Taken together, our findings demonstrate the complexity of lamin mutations and their effect on nuclear structure and stability in muscle diseases. Many, but not all, mutations associated with EDMD and DCM are characterized by defects in structural function, resulting in more deformable and more fragile nuclei, which could render cells more sensitive to mechanical stress. In addition, all tested EDMD mutations disrupted nucleo-cytoskeletal coupling, which could further impair muscle function, for example, by failure of myonuclei to anchor at neuromuscular junctions (16). In addition to these mechanical aspects, it is likely that lamin mutations can interfere with a broad range of other cellular processes requiring lamins, including replication, gene expression, DNA repair, proliferation and stem-cell differentiation (10,21). In this scenario, different lamin mutations may specifically impact one or more of these functions, thus explaining the broad spectrum of human diseases caused by the diverse *LMNA* mutations.

MATERIALS AND METHODS

Cell lines

Lmna$^{+/+}$, *Lmna*$^{+/-}$ and *Lmna*$^{-/-}$ MEFs were cultured in D10 medium (DMEM supplemented with 10% fetal bovine serum, 4 mM L-glutamine, 50 U/ml penicillin and 50 μg/ml streptomycin). 293GPG cells (67) were cultured in D10 supplemented with 1 μg/ml tetracycline, 2 μg/ml puromycin and 300 μg/ml G418. Human patient fibroblasts (68) were kindly provided by Howard Worman (Columbia University, New York, NY, USA) and maintained in D10 containing 5 μg/ml Plasmocin™ (InvivoGen) for prophylactic treatment against mycoplasma contamination.

Plasmids

cDNAs of wild-type and point-mutated human prelamin A, as well as the ΔNLA lamin variant lacking the first 33 amino acids, were kindly provided by Howard Worman [Columbia University, New York, NY, USA (63)]. The point-mutated cDNAs used in this study cause amino acid substitutions as shown in Table 1. Lamin variants were either amplified by PCR and ligated into pRetroX-IRES-ZsGreen1 using *Not*I and *Bam*HI restriction sites, or subcloned from a shuttle vector as described previously (69). Mutagenesis of the codons of amino acids E203, E358, M371 and R386 to either glycine or alanine was performed by amplifying human prelamin A in two fragments and inducing codon changes over the respective primers. After PCR, the two fragments were ligated together via an introduced restriction site that does not change the primary sequence of the prelamin A protein (introducing *Bsp*DI at amino acid positions 195–196: 583–588acaggc→atcgat results in N195N, G196G; introducing *Eco*RV at amino acid positions 364 and 365: 1090–1095gacatc→gatatc results in D364D, I365I; or introducing *Xho*I at amino acid positions 380 and 381: 1138–1142ttggag→ctcgag results in L380L, E381E). As control, primers with the same introduced restriction sites but without amino acid change in positions E203, E358, M371 and R386 were used to amplify the two prelamin A fragments that were ligated together. Ligated full-length prelamin A variants were ligated into pRetroX-IRES-ZsGreen1 using *Not*I and *Bam*HI restriction sites. The dominant-negative nesprin KASH (DN KASH) plasmid was described previously (15). Constructs encoding the mutant forms of *Drosophila* Lamin C were generated using the QuikChange II Site-Directed Mutagenesis Kit. The primers contain nucleotide substitutions that result in single-amino-acid substitutions within Lamin C. The mutated Lamin C sequences were cloned into the *P*-element transformation vector pUAST (70) and used to generate transgenic stocks (45). For all mutagenesis procedures, introduced mutations were confirmed by sequencing.

Retroviral infection and cell sorting

Lmna$^{+/-}$ MEFs were modified by retroviral infection. 293GPG cells were transfected with pRetroX-IRES-ZsGreen1 vectors containing lamin A variants, using Lipofectamine™ 2000 (Invitrogen). Starting 6 h after transfection, cells were maintained in D10 without tetracycline, puromycin and G418. For 6 subsequent days, cell medium was collected and replaced. This medium containing assembled virus was filtered through 0.45 μm pores, supplemented with 8 μg/μl Polybrene and added to *Lmna*$^{+/-}$ MEFs for 24 h. At 5–10 days after retroviral infection, positive cells were sorted for the bicistronically expressed ZsGreen, which allowed us to finely control expression levels of the ectopically expressed lamins translated from the same bicistronic mRNA. Cell sorting was performed on a BD FACSARIA Special Order 11 color sorter, using a 488 nm laser to excite ZsGreen1 and with a sort pressure of 70 psi.

Protein extraction

Preparation of total cell extracts containing 3×10^5 cells per microliters was performed as previously described by resuspending pelleted cells in Laemmli sample buffer (LSB, 10% glycerol, 3% SDS, 62.5 mM Tris–HCl, 50 mM DTT and 0.05% bromphenol blue) and subsequent boiling for 5 min (71). Extraction of the soluble lamin A/C fraction of modified and unmodified *Lmna*$^{+/-}$ MEFs was performed following a

Downloaded from http://hmg.oxfordjournals.org/ at Cornell University Library on November 14, 2013

modified protocol for differential protein extraction (36). Confluent cells were washed with phosphate-buffered saline (PBS), trypsinized and resuspended in 1.2 ml of growth medium. An amount of 33 μl of the cell suspension was immediately boiled with 267 μl of LSB ('total cell fraction'). Another 1 ml of aliquot ('soluble lamin fraction') of the cell suspension was transferred into a new tube; cells were briefly spun down and resuspended in 200 μl of lysis buffer containing 0.5× PBS, 50 mM MOPS (pH 7.0), 10 mM $MgCl_2$, 1 mM EGTA, 1% NP40, protease inhibitor (SIGMAFAST™ Protease Inhibitor, Sigma-Aldrich) and 0.75% saturated PMSF in ethanol. Extraction with 1% NP40 detergent was previously shown to release the soluble lamin A/C fraction but not lamina-associated A-type lamins (36). Extraction was performed at room temperature for 5 min; cell remnants were spun down, and 150 μl of the supernatant were boiled with 75 μl of 3× LSB. Extraction was performed three independent times. Notably, owing to slight changes in experimental conditions for each isolation, e.g. cell density, buffer composition, vortexing or extraction timing, the absolute results of the soluble lamin fractions varied between individual experiments, even though the relative difference between cell lines within each experiment were very similar.

Immunofluorescence analysis

Immunofluorescence analysis was performed as previously described (71). In brief, cells were plated on sterile coverslips and grown overnight, briefly washed with PBS, fixed in 4% formaldehyde (pH 7.4) and permeabilized with 0.5% Triton X-100 in PBS. Fixed cells were incubated either with mouse anti-lamin A/C antibody [LaZ (72)] or with guinea pig anti-emerin antibody [Em-N-term (73)], diluted 1:2 and 1:300, respectively, in PBS containing 10% normal donkey serum (Jackson ImmunoResearch). Cells were washed and incubated with secondary antibodies: Cy3-coupled donkey anti-mouse or donkey anti-guinea pig IgG, diluted 1:500 in PBS containing 10% normal donkey serum. Cells were then incubated in 2 μg/ml Hoechst 33342 and embedded in Eukitt quick-hardening mounting medium (Fluka). Confocal laser scanning microscopy was performed on a TCS-SP II microscope (Leica Microsystems). Images were acquired with a 63.0× oil-immersion objective (NA 1.40) with a 1 airy unit pinhole.

Western analysis

Western analysis of modified and unmodified $Lmna^{+/-}$ MEFs was performed as previously described (71). Polyvinylidene difluoride membranes were incubated with the following antibodies diluted in PBS containing 0.5% Tween-20 and 5% milk powder: mouse anti-lamin A/C antibody (LaZ) at 1:5 dilution, goat anti-lamin A/C antibody (N-18, Santa Cruz #sc-6215) at 1:500 dilution, goat anti-lamin B1 antibody (M-20, Santa Cruz #sc-6217) at 1:500 dilution, mouse anti-lamin B2 antibody (X223, Progen #65147C) at 1:5 dilution, guinea pig anti-emerin antibody (Em-N-term) at 1:2000 dilution and rabbit anti-actin antibody (Sigma-Aldrich, #20–33) at 1:5000 dilution. Membranes were washed in PBS containing 0.5% Tween-20 and incubated with secondary antibodies: peroxidase-coupled donkey anti-guinea pig, donkey anti-rabbit, donkey anti-goat or donkey anti-mouse IgG (Jackson ImmunoReseach) diluted 1:5000 in PBS containing 0.5% Tween-20 and 5% milk powder. Enhanced luminescence reaction was performed and membranes were exposed to X-ray films.

Drosophila stocks

Generation of transgenic stocks was performed as previously described (45). Stocks expressing wild-type and mutant lamins under the control of a UAS element were crossed to the C57 Gal4 driver stock (49) and the resulting larval progeny were analyzed for muscle defects (45). The lamin stocks encode wild-type Lamin C, headless Lamin C (lacking the first 42 amino acids, Lamin C ΔN) or the mutations N210K, R401K, K493W, W557S and L567P (corresponding to human mutations N195K, R386K, R453W, W520S and L530P, respectively) (46,47,74). *Drosophila* stocks were maintained on standard corn meal media at room temperature; the Gal4/UAS crosses were performed at 25°C.

Nuclear strain analysis and microneedle manipulation assay of cultured cells

Nuclear strain analysis and microneedle manipulation of patient fibroblasts and $Lmna^{+/-}$ MEFs, as well as data analysis, were performed as described previously (32,75).

Nuclear strain analysis in muscle tissue

For nuclear strain analysis of *D. melanogaster* muscle tissue, third instar larvae were placed in a drop of cold low-potassium buffer containing 108 mM NaCl, 5 mM KCl, 2 mM $CaCl_2$, 8 mM $MgCl_2$, 1 mM NaH_2PO_4, 4 mM $NaHCO_3$, 10 mM sucrose, 5 mM trehalose, 5 mM HEPES and 100 μg/ml Hoechst 33342 nuclear stain on a glass slide. Subsequently, the head and tail were removed and the body wall muscle was opened with a horizontal incision down the length of the longitudinal axis to remove the organs. The body wall muscle filet was then transferred onto an elastic silicone membrane clamped into the strain dish and covered with 15 ml of high-potassium buffer containing 108 mM NaCl, 35 mM KCl, 1 mM EDTA, 8 mM $MgCl_2$, 1 mM NaH_2PO_4, 4 mM $NaHCO_3$, 10 mM sucrose, 5 mM trehalose, 5 mM HEPES and 10 μg/ml Hoechst 33342. To securely attach the muscle filet in the open position to the center of the silicone membrane, a small amount of histoacryl blue adhesive (Tissue Seal, LLC) was applied to the four corners and to two to four additional points along the periphery of the muscle filet and then affixed to the silicone membrane. The muscle filets were then subjected to biaxial strain application as described previously for adherent cells (32,75), with minor modifications. To facilitate imaging of muscle fibers, the muscle filet was pre-stretched by applying low-level biaxial strain to the silicon membrane, resulting in taut but only lightly strained muscle fibers. Fluorescence images of 1–3 muscle fibers, containing up to 15 myonuclei, were acquired at this position. Subsequently, the silicone membrane was further stretched, resulting in larger tissue strain and induced nuclear deformations. Importantly, although the

Downloaded from http://hmg.oxfordjournals.org/ at Cornell University Library on November 14, 2013

applied membrane strain is biaxial, due to the muscle physiology and attachment, the tissue strain in the muscle fibers is almost completely uniaxial in the direction of the muscle fiber. The same myonuclei were then imaged in this strained condition. To calculate tissue strain, changes in the internuclear distance within a single muscle strand were calculated using a custom-written MATLAB program. Nuclear deformations were then quantified as previously described (32,75).

In vitro lamin assembly

Recombinant human lamin A ΔC18 ('mature' lamin A) as well as the single-amino-acid deletion ΔK32 and the point mutations N195K and E358K were expressed using the pET24 system. A clone coding for lamin A ΔK32 was generously provided by Gisele Bonne (Inserm U582 – Institut de Myologie, Paris, France) and subcloned into pET24a. Induction with 1 mM IPTG was done for 3 h at 37°C (42). Inclusion bodies were isolated as described previously (76). For *in vitro* paracrystal assembly, lamin protein stored in 8 M urea at a concentration of 0.5 mg/ml was dialyzed into 10 mM Tris–HCl (pH 7.4), 300 mM NaCl, 2 mM EDTA and 1 mM DTT overnight at 4°C to obtain soluble lamin complexes. Lamins were briefly centrifuged in a benchtop centrifuge at full speed for 15 min to remove all protein at higher assembly states. Lamin proteins were diluted to 0.1 mg/ml and further dialyzed in the same buffer, but with stepwise reduction of salt concentration from 300 to 50 mM NaCl. Each dialysis step was performed for 20 min at 37°C. For *in vitro* filament assembly, lamin protein in 8 M urea at a concentration of 0.2 mg/ml was dialyzed into 25 mM Tris (pH 8), 250 mM NaCl and 1 mM DTT for 1 h at 37°C to obtain lamin dimers, then dialyzed into 25 mM MES, pH 6.5, 250 mM NaCl and 1 mM DTT for 50 min at 37°C. Assembled filaments, fixed with 0.1% glutaraldehyde, and paracrystals were then applied to glow-discharged, carbon-coated copper electron microscopy grids and analyzed in a Philips 410 transmission electron microscope (FEI). Images were taken with a CCD camera (Bioscan 792, Gatan).

Statistical data analysis

All measurements were performed at least three independent times. All data are expressed as mean ± standard error of the mean. Statistical analyses were performed with PRISM 3.0 (GraphPad Software, Inc.). Data were analyzed by a two-tailed Student *t*-test (for comparison between two groups) or one-way ANOVA with post-test for comparison of several groups. A two-tailed *P*-value of ≤ 0.05 was considered significant, with the symbols '*' for $P \leq 0.05$, '**' for $P \leq 0.01$ and '***' for $P \leq 0.001$.

SUPPLEMENTARY MATERIAL

Supplementary Material is available at *HMG* online.

ACKNOWLEDGEMENTS

Imaging was performed with the support of the Center for Microscopy and Image Analysis, University of Zurich. We thank Dr Colin Stewart for providing $Lmna^{+/+}$, $Lmna^{+/-}$ and $Lmna^{-/-}$ cell lines; Dr Howard Worman for providing plasmids and patient fibroblast cell lines; and Dr Richard C. Mulligan for providing us with the 293GPG cells. We further thank Dr Ohad Medalia and Dr Sergei Strelkov for support and advice.

Conflict of Interest statement. None declared.

FUNDING

This work was supported by National Institutes of Health awards (grant numbers R01 NS059348, R01 HL082792) to J.L.; a postdoctoral fellowship from the American Heart Association to D.E.J. (AHA award 09POST2320042); a grant from the NIH/National Institutes of Health (grant number AR0600012) to L.L.W. and by postdoctoral fellowships of the American Heart Association (10POST3920014) and the Association Francaise contre les Myopathies (18336000) to G.D.

REFERENCES

1. Stewart, C.L., Roux, K.J. and Burke, B. (2007) Blurring the boundary: the nuclear envelope extends its reach. *Science*, **318**, 1408–1412.
2. Dwyer, N. and Blobel, G. (1976) A modified procedure for the isolation of a pore complex-lamina fraction from rat liver nuclei. *J. Cell Biol.*, **70**, 581–591.
3. Goldman, A.E., Maul, G., Steinert, P.M., Yang, H.Y. and Goldman, R.D. (1986) Keratin-like proteins that coisolate with intermediate filaments of BHK-21 cells are nuclear lamins. *Proc. Natl Acad. Sci. USA*, **83**, 3839–3843.
4. McKeon, F.D., Kirschner, M.W. and Caput, D. (1986) Homologies in both primary and secondary structure between nuclear envelope and intermediate filament proteins. *Nature*, **319**, 463–468.
5. Herrmann, H., Bar, H., Kreplak, L., Strelkov, S.V. and Aebi, U. (2007) Intermediate filaments: from cell architecture to nanomechanics. *Nat. Rev. Mol. Cell Biol.*, **8**, 562–573.
6. Parry, D.A. (2005) Microdissection of the sequence and structure of intermediate filament chains. *Adv. Protein Chem.*, **70**, 113–142.
7. Lin, F. and Worman, H.J. (1993) Structural organization of the human gene encoding nuclear lamin A and nuclear lamin C. *J. Biol. Chem.*, **268**, 16321–16326.
8. Peter, M., Kitten, G.T., Lehner, C.F., Vorburger, K., Bailer, S.M., Maridor, G. and Nigg, E.A. (1989) Cloning and sequencing of cDNA clones encoding chicken lamins A and B1 and comparison of the primary structures of vertebrate A- and B-type lamins. *J. Mol. Biol.*, **208**, 393–404.
9. Vorburger, K., Kitten, G.T. and Nigg, E.A. (1989) Modification of nuclear lamin proteins by a mevalonic acid derivative occurs in reticulocyte lysates and requires the cysteine residue of the C-terminal CXXM motif. *EMBO J.*, **8**, 4007–4013.
10. Dechat, T., Adam, S.A., Taimen, P., Shimi, T. and Goldman, R.D. (2010) Nuclear lamins. *Cold Spring Harb. Perspect. Biol.*, **2**, a000547.
11. Worman, H.J. (2012) Nuclear lamins and laminopathies. *J. Pathol.*, **226**, 316–325.
12. Pereira, S., Bourgeois, P., Navarro, C., Esteves-Vieira, V., Cau, P., De Sandre-Giovannoli, A. and Levy, N. (2008) HGPS and related premature aging disorders: from genomic identification to the first therapeutic approaches. *Mech. Ageing Dev.*, **129**, 449–459.
13. Bertrand, A.T., Chikhaoui, K., Yaou, R.B. and Bonne, G. (2011) Clinical and genetic heterogeneity in laminopathies. *Biochem. Soc. Trans.*, **39**, 1687–1692.

Downloaded from http://hmg.oxfordjournals.org/ at Cornell University Library on November 14, 2013

14. Crisp, M., Liu, Q., Roux, K., Rattner, J.B., Shanahan, C., Burke, B., Stahl, P.D. and Hodzic, D. (2006) Coupling of the nucleus and cytoplasm: role of the LINC complex. *J. Cell Biol.*, **172**, 41–53.
15. Lombardi, M.L., Jaalouk, D.E., Shanahan, C.M., Burke, B., Roux, K.J. and Lammerding, J. (2011) The interaction between nesprins and sun proteins at the nuclear envelope is critical for force transmission between the nucleus and cytoskeleton. *J. Biol. Chem.*, **286**, 26743–26753.
16. Mejat, A., Decostre, V., Li, J., Renou, L., Kesari, A., Hantai, D., Stewart, C.L., Xiao, X., Hoffman, E., Bonne, G. *et al.* (2009) Lamin A/C-mediated neuromuscular junction defects in Emery-Dreifuss muscular dystrophy. *J. Cell Biol.*, **184**, 31–44.
17. Burke, B. and Stewart, C.L. (2002) Life at the edge: the nuclear envelope and human disease. *Nat. Rev. Mol. Cell Biol.*, **3**, 575–585.
18. Houben, F., Ramaekers, F.C., Snoeckx, L.H. and Broers, J.L. (2007) Role of nuclear lamina-cytoskeleton interactions in the maintenance of cellular strength. *Biochim. Biophys. Acta*, **1773**, 675–686.
19. Lammerding, J., Schulze, P.C., Takahashi, T., Kozlov, S., Sullivan, T., Kamm, R.D., Stewart, C.L. and Lee, R.T. (2004) Lamin A/C deficiency causes defective nuclear mechanics and mechanotransduction. *J. Clin. Invest.*, **113**, 370–378.
20. Muchir, A., Pavlidis, P., Decostre, V., Herron, A.J., Arimura, T., Bonne, G. and Worman, H.J. (2007) Activation of MAPK pathways links LMNA mutations to cardiomyopathy in Emery-Dreifuss muscular dystrophy. *J. Clin. Invest.*, **117**, 1282–1293.
21. Scaffidi, P. and Misteli, T. (2008) Lamin A-dependent misregulation of adult stem cells associated with accelerated ageing. *Nat. Cell Biol.*, **10**, 452–459.
22. Broers, J.L., Peeters, E.A., Kuijpers, H.J., Endert, J., Bouten, C.V., Oomens, C.W., Baaijens, F.P. and Ramaekers, F.C. (2004) Decreased mechanical stiffness in LMNA-/- cells is caused by defective nucleo-cytoskeletal integrity: implications for the development of laminopathies. *Hum. Mol. Genet.*, **13**, 2567–2580.
23. Lammerding, J., Fong, L.G., Ji, J.Y., Reue, K., Stewart, C.L., Young, S.G. and Lee, R.T. (2006) Lamins A and C but not lamin B1 regulate nuclear mechanics. *J. Biol. Chem.*, **281**, 25768–25780.
24. Arbustini, E.A., Pasotti, M., Pilotto, A., Repetto, A., Grasso, M. and Diegoli, M. (2005) Gene symbol: CMD1A. Disease: dilated cardiomyopathy associated with conduction system disease. *Hum. Genet.*, **117**, 295.
25. Ben Yaou, R., Gueneau, L., Demay, L., Stora, S., Chikhaoui, K., Richard, P. and Bonne, G. (2006) Heart involvement in lamin A/C related diseases. *Arch. Mal. Coeur Vaiss*, **99**, 848–855.
26. Decostre, V., Ben Yaou, R. and Bonne, G. (2005) Laminopathies affecting skeletal and cardiac muscles: clinical and pathophysiological aspects. *Acta. Myol.*, **24**, 104–109.
27. Filesi, I., Gullotta, F., Lattanzi, G., D'Apice, M.R., Capanni, C., Nardone, A.M., Columbaro, M., Scarano, G., Mattioli, E., Sabatelli, P. *et al.* (2005) Alterations of nuclear envelope and chromatin organization in mandibuloacral dysplasia, a rare form of laminopathy. *Physiol. Genomics*, **23**, 150–158.
28. Goldman, R.D., Shumaker, D.K., Erdos, M.R., Eriksson, M., Goldman, A.E., Gordon, L.B., Gruenbaum, Y., Khuon, S., Mendez, M., Varga, R. *et al.* (2004) Accumulation of mutant lamin A causes progressive changes in nuclear architecture in Hutchinson-Gilford progeria syndrome. *Proc. Natl Acad. Sci. USA*, **101**, 8963–8968.
29. Wang, Y., Herron, A.J. and Worman, H.J. (2006) Pathology and nuclear abnormalities in hearts of transgenic mice expressing M371K lamin A encoded by an LMNA mutation causing Emery-Dreifuss muscular dystrophy. *Hum. Mol. Genet.*, **15**, 2479–2489.
30. Park, Y.E., Hayashi, Y.K., Goto, K., Komaki, H., Hayashi, Y., Inuzuka, T., Noguchi, S., Nonaka, I. and Nishino, I. (2009) Nuclear changes in skeletal muscle extend to satellite cells in autosomal dominant Emery-Dreifuss muscular dystrophy/limb-girdle muscular dystrophy 1B. *Neuromuscul. Disord.*, **19**, 29–36.
31. Fidzianska, A. and Hausmanowa-Petrusewicz, I. (2003) Architectural abnormalities in muscle nuclei. Ultrastructural differences between X-linked and autosomal dominant forms of EDMD. *J. Neurol. Sci.*, **210**, 47–51.
32. Lammerding, J. and Lee, R.T. (2009) Mechanical properties of interphase nuclei probed by cellular strain application. *Methods. Mol. Biol.*, **464**, 13–26.
33. Cupesi, M., Yoshioka, J., Gannon, J., Kudinova, A., Stewart, C.L. and Lammerding, J. (2010) Attenuated hypertrophic response to pressure overload in a lamin A/C haploinsufficiency mouse. *J. Mol. Cell Cardiol.*, **48**, 1290–1297.
34. Sullivan, T., Escalante-Alcalde, D., Bhatt, H., Anver, M., Bhat, N., Nagashima, K., Stewart, C.L. and Burke, B. (1999) Loss of A-type lamin expression compromises nuclear envelope integrity leading to muscular dystrophy. *J. Cell Biol.*, **147**, 913–920.
35. Spann, T.P., Moir, R.D., Goldman, A.E., Stick, R. and Goldman, R.D. (1997) Disruption of nuclear lamin organization alters the distribution of replication factors and inhibits DNA synthesis. *J. Cell Biol.*, **136**, 1201–1212.
36. Kolb, T., Maass, K., Hergt, M., Aebi, U. and Herrmann, H. (2011) Lamin A and lamin C form homodimers and coexist in higher complex forms both in the nucleoplasmic fraction and in the lamina of cultured human cells. *Nucleus*, **2**, 425–433.
37. Herrmann, H., Strelkov, S.V., Burkhard, P. and Aebi, U. (2009) Intermediate filaments: primary determinants of cell architecture and plasticity. *J. Clin. Invest.*, **119**, 1772–1783.
38. Parry, D.A., Strelkov, S.V., Burkhard, P., Aebi, U. and Herrmann, H. (2007) Towards a molecular description of intermediate filament structure and assembly. *Exp. Cell Res.*, **313**, 2204–2216.
39. Aebi, U., Cohn, J., Buhle, L. and Gerace, L. (1986) The nuclear lamina is a meshwork of intermediate-type filaments. *Nature*, **323**, 560–564.
40. Ben-Harush, K., Wiesel, N., Frenkiel-Krispin, D., Moeller, D., Soreq, E., Aebi, U., Herrmann, H., Gruenbaum, Y. and Medalia, O. (2009) The supramolecular organization of the *C. elegans* nuclear lamin filament. *J. Mol. Biol.*, **386**, 1392–1402.
41. Strelkov, S.V., Schumacher, J., Burkhard, P., Aebi, U. and Herrmann, H. (2004) Crystal structure of the human lamin A coil 2B dimer: implications for the head-to-tail association of nuclear lamins. *J. Mol. Biol.*, **343**, 1067–1080.
42. Foeger, N., Wiesel, N., Lotsch, D., Mucke, N., Kreplak, L., Aebi, U., Gruenbaum, Y. and Herrmann, H. (2006) Solubility properties and specific assembly pathways of the B-type lamin from *Caenorhabditis elegans*. *J. Struct. Biol.*, **155**, 340–350.
43. Bank, E.M., Ben-Harush, K., Feinstein, N., Medalia, O. and Gruenbaum, Y. (2012) Structural and physiological phenotypes of disease-linked lamin mutations in *C. elegans*. *J. Struct. Biol.*, **177**, 106–112.
44. Bank, E.M., Ben-Harush, K., Wiesel-Motiuk, N., Barkan, R., Feinstein, N., Lotan, O., Medalia, O. and Gruenbaum, Y. (2011) A laminopathic mutation disrupting lamin filament assembly causes disease-like phenotypes in *Caenorhabditis elegans*. *Mol. Biol. Cell*, **22**, 2716–2728.
45. Dialynas, G., Flannery, K.M., Zirbel, L.N., Nagy, P.L., Mathews, K.D., Moore, S.A. and Wallrath, L.L. (2012) LMNA variants cause cytoplasmic distribution of nuclear pore proteins in *Drosophila* and human muscle. *Hum. Mol. Genet.*, **21**, 1544–1556.
46. Dialynas, G., Speese, S., Budnik, V., Geyer, P.K. and Wallrath, L.L. (2010) The role of *Drosophila* Lamin C in muscle function and gene expression. *Development*, **137**, 3067–3077.
47. Schulze, S.R., Curio-Penny, B., Speese, S., Dialynas, G., Cryderman, D.E., McDonough, C.W., Nalbant, D., Petersen, M., Budnik, V., Geyer, P.K. *et al.* (2009) A comparative study of *Drosophila* and human A-type lamins. *PLoS One*, **4**, e7564.
48. Duffy, J.B. (2002) GAL4 system in *Drosophila*: a fly geneticist's Swiss army knife. *Genesis*, **34**, 1–15.
49. Koh, Y.H., Popova, E., Thomas, U., Griffith, L.C. and Budnik, V. (1999) Regulation of DLG localization at synapses by CaMKII-dependent phosphorylation. *Cell*, **98**, 353–363.
50. Haque, F., Mazzeo, D., Patel, J.T., Smallwood, D.T., Ellis, J.A., Shanahan, C.M. and Shackleton, S. (2010) Mammalian SUN protein interaction networks at the inner nuclear membrane and their role in laminopathy disease processes. *J. Biol. Chem.*, **285**, 3487–3498.
51. Roux, K.J., Crisp, M.L., Liu, Q., Kim, D., Kozlov, S., Stewart, C.L. and Burke, B. (2009) Nesprin 4 is an outer nuclear membrane protein that can induce kinesin-mediated cell polarization. *Proc. Natl Acad. Sci. USA*, **106**, 2194–2199.
52. Wilhelmsen, K., Litjens, S.H., Kuikman, I., Tshimbalanga, N., Janssen, H., van den Bout, I., Raymond, K. and Sonnenberg, A. (2005) Nesprin-3, a novel outer nuclear membrane protein, associates with the cytoskeletal linker protein plectin. *J. Cell Biol.*, **171**, 799–810.
53. Zhang, Q., Skepper, J.N., Yang, F., Davies, J.D., Hegyi, L., Roberts, R.G., Weissberg, P.L., Ellis, J.A. and Shanahan, C.M. (2001) Nesprins: a novel family of spectrin-repeat-containing proteins that localize to the nuclear membrane in multiple tissues. *J. Cell Sci.*, **114**, 4485–4498.

Downloaded from http://hmg.oxfordjournals.org/ at Cornell University Library on November 14, 2013

54. Mejat, A. and Misteli, T. (2010) LINC complexes in health and disease. *Nucleus*, **1**, 40–52.
55. Folker, E.S., Ostlund, C., Luxton, G.W., Worman, H.J. and Gundersen, G.G. (2011) Lamin A variants that cause striated muscle disease are defective in anchoring transmembrane actin-associated nuclear lines for nuclear movement. *Proc. Natl Acad. Sci. USA*, **108**, 131–136.
56. Fidzianska, A., Walczak, E., Glinka, Z. and Religa, G. (2008) Nuclear architecture remodelling in cardiomyocytes with lamin A deficiency. *Folia Neuropathol.*, **46**, 196–203.
57. Jahn, D., Schramm, S., Schnolzer, M., Heilmann, C.J., de Koster, C.G., Schutz, W., Benavente, R. and Alsheimer, M. (2012) A truncated lamin A in the Lmna-/- mouse line: implications for the understanding of laminopathies. *Nucleus*, **3**, 463–474.
58. Gilchrist, S., Gilbert, N., Perry, P., Ostlund, C., Worman, H.J. and Bickmore, W.A. (2004) Altered protein dynamics of disease-associated lamin A mutants. *BMC Cell Biol.*, **5**, 46.
59. Broers, J.L., Kuijpers, H.J., Ostlund, C., Worman, H.J., Endert, J. and Ramaekers, F.C. (2005) Both lamin A and lamin C mutations cause lamina instability as well as loss of internal nuclear lamin organization. *Exp. Cell Res.*, **304**, 582–592.
60. Bar, H., Kostareva, A., Sjoberg, G., Sejersen, T., Katus, H.A. and Herrmann, H. (2006) Forced expression of desmin and desmin mutants in cultured cells: impact of myopathic missense mutations in the central coiled-coil domain on network formation. *Exp. Cell Res.*, **312**, 1554–1565.
61. Bar, H., Mucke, N., Kostareva, A., Sjoberg, G., Aebi, U. and Herrmann, H. (2005) Severe muscle disease-causing desmin mutations interfere with *in vitro* filament assembly at distinct stages. *Proc. Natl Acad. Sci. USA*, **102**, 15099–15104.
62. Fatkin, D., MacRae, C., Sasaki, T., Wolff, M.R., Porcu, M., Frenneaux, M., Atherton, J., Vidaillet, H.J. Jr., Spudich, S., De Girolami, U. *et al.* (1999) Missense mutations in the rod domain of the lamin A/C gene as causes of dilated cardiomyopathy and conduction-system disease. *N. Engl. J. Med.*, **341**, 1715–1724.
63. Ostlund, C., Bonne, G., Schwartz, K. and Worman, H.J. (2001) Properties of lamin A mutants found in Emery-Dreifuss muscular dystrophy, cardiomyopathy and Dunnigan-type partial lipodystrophy. *J. Cell Sci.*, **114**, 4435–4445.
64. Fong, L.G., Ng, J.K., Lammerding, J., Vickers, T.A., Meta, M., Cote, N., Gavino, B., Qiao, X., Chang, S.Y., Young, S.R. *et al.* (2006) Prelamin A and lamin A appear to be dispensable in the nuclear lamina. *J. Clin. Invest.*, **116**, 743–752.
65. Davies, B.S., Barnes, R.H. II, Tu, Y., Ren, S., Andres, D.A., Spielmann, H.P., Lammerding, J., Wang, Y., Young, S.G. and Fong, L.G. (2010) An accumulation of non-farnesylated prelamin A causes cardiomyopathy but not progeria. *Hum. Mol. Genet.*, **19**, 2682–2694.
66. Coffinier, C., Jung, H.J., Li, Z., Nobumori, C., Yun, U.J., Farber, E.A., Davies, B.S., Weinstein, M.M., Yang, S.H., Lammerding, J. *et al.* (2010) Direct synthesis of lamin A, bypassing prelamin a processing, causes misshapen nuclei in fibroblasts but no detectable pathology in mice. *J. Biol. Chem.*, **285**, 20818–20826.
67. Ory, D.S., Neugeboren, B.A. and Mulligan, R.C. (1996) A stable human-derived packaging cell line for production of high titer retrovirus/vesicular stomatitis virus G pseudotypes. *Proc. Natl Acad. Sci. USA*, **93**, 11400–11406.
68. Muchir, A., Medioni, J., Laluc, M., Massart, C., Arimura, T., van der Kooi, A.J., Desguerre, I., Mayer, M., Ferrer, X., Briault, S. *et al.* (2004) Nuclear envelope alterations in fibroblasts from patients with muscular dystrophy, cardiomyopathy, and partial lipodystrophy carrying lamin A/C gene mutations. *Muscle Nerve*, **30**, 444–450.
69. Rowat, A.C., Jaalouk, D.E., Zwerger, M., Ung, W.L., Eydelnant, I.A., Olins, D., Olins, A., Herrmann, H., Weitz, D.A. and Lammerding, J. (2013) Nuclear envelope composition determines the ability of neutrophil-type cells to passage through micron-scale constrictions. *J. Biol. Chem.*, doi: 10.1074/jbc.M112.441535. http://www.ncbi.nlm.nih.gov/pubmed/23355469 (25 January 2013, date last accessed).
70. Brand, A.H. and Perrimon, N. (1993) Targeted gene expression as a means of altering cell fates and generating dominant phenotypes. *Development*, **118**, 401–415.
71. Zwerger, M., Kolb, T., Richter, K., Karakesisoglou, I. and Herrmann, H. (2010) Induction of a massive endoplasmic reticulum and perinuclear space expansion by expression of lamin B receptor mutants and the related sterol reductases TM7SF2 and DHCR7. *Mol. Biol. Cell*, **21**, 354–368.
72. Geiger, S.K., Bar, H., Ehlermann, P., Walde, S., Rutschow, D., Zeller, R., Ivandic, B.T., Zentgraf, H., Katus, H.A., Herrmann, H. *et al.* (2008) Incomplete nonsense-mediated decay of mutant lamin A/C mRNA provokes dilated cardiomyopathy and ventricular tachycardia. *J. Mol. Med. (Berl.)*, **86**, 281–289.
73. Dreger, C.K., Konig, A.R., Spring, H., Lichter, P. and Herrmann, H. (2002) Investigation of nuclear architecture with a domain-presenting expression system. *J. Struct. Biol.*, **140**, 100–115.
74. Schulze, S.R., Curio-Penny, B., Li, Y., Imani, R.A., Rydberg, L., Geyer, P.K. and Wallrath, L.L. (2005) Molecular genetic analysis of the nested *Drosophila melanogaster* lamin C gene. *Genetics*, **171**, 185–196.
75. Lombardi, M.L. and Lammerding, J. (2011) Keeping the LINC: the importance of nucleocytoskeletal coupling in intracellular force transmission and cellular function. *Biochem. Soc. Trans.*, **39**, 1729–1734.
76. Herrmann, H., Kreplak, L. and Aebi, U. (2004) Isolation, characterization, and *in vitro* assembly of intermediate filaments. *Methods Cell Biol.*, **78**, 3–24.
77. Jakobs, P.M., Hanson, E.L., Crispell, K.A., Toy, W., Keegan, H., Schilling, K., Icenogle, T.B., Litt, M. and Hershberger, R.E. (2001) Novel lamin A/C mutations in two families with dilated cardiomyopathy and conduction system disease. *J. Card. Fail.*, **7**, 249–256.
78. Bonne, G., Mercuri, E., Muchir, A., Urtizberea, A., Becane, H.M., Recan, D., Merlini, L., Wehnert, M., Boor, R., Reuner, U. *et al.* (2000) Clinical and molecular genetic spectrum of autosomal dominant Emery-Dreifuss muscular dystrophy due to mutations of the lamin A/C gene. *Ann. Neurol.*, **48**, 170–180.
79. Cao, H. and Hegele, R.A. (2000) Nuclear lamin A/C R482Q mutation in Canadian kindreds with Dunnigan-type familial partial lipodystrophy. *Hum. Mol. Genet.*, **9**, 109–112.
80. Vigouroux, C., Magre, J., Vantyghem, M.C., Bourut, C., Lascols, O., Shackleton, S., Lloyd, D.J., Guerci, B., Padova, G., Valensi, P. *et al.* (2000) Lamin A/C gene: sex-determined expression of mutations in Dunnigan-type familial partial lipodystrophy and absence of coding mutations in congenital and acquired generalized lipoatrophy. *Diabetes*, **49**, 1958–1962.
81. Shackleton, S., Lloyd, D.J., Jackson, S.N., Evans, R., Niermeijer, M.F., Singh, B.M., Schmidt, H., Brabant, G., Kumar, S., Durrington, P.N. *et al.* (2000) LMNA, encoding lamin A/C, is mutated in partial lipodystrophy. *Nat. Genet.*, **24**, 153–156.
82. Bonne, G., Di Barletta, M.R., Varnous, S., Becane, H.M., Hammouda, E.H., Merlini, L., Muntoni, F., Greenberg, C.R., Gary, F., Urtizberea, J.A. *et al.* (1999) Mutations in the gene encoding lamin A/C cause autosomal dominant Emery-Dreifuss muscular dystrophy. *Nat. Genet.*, **21**, 285–288.

Downloaded from http://hmg.oxfordjournals.org/ at Cornell University Library on November 14, 2013

Assays to Measure Nuclear Mechanics in Interphase Cells

Philipp Isermann,[1,2] Patricia M. Davidson,[1,2] Josiah D. Sliz,[1,2] and Jan Lammerding[1]

[1]Cornell University, Ithaca, New York
[2]These authors contributed equally to this work.

ABSTRACT

The nucleus is the characteristic hallmark of all eukaryotic cells. The physical properties of the nucleus reflect important biological characteristics, such as chromatin organization or nuclear envelope composition; they can also directly affect cellular function, e.g., when cells pass through narrow constrictions, where the stiff nucleus may present a limiting factor. We present two complementary techniques to probe the mechanical properties of the nucleus. In the first, nuclear stiffness relative to the surrounding cytoskeleton is inferred from induced nuclear deformations during strain application to cells on an elastic substrate. In the second approach, nuclear deformability is deduced from the transit time through a perfusion-based microfabricated device with constrictions smaller than the size of the nucleus. These complementary methods, which can be applied to measure nuclear stiffness in large numbers of living adherent or suspended cells, can help identify important changes in nuclear mechanics associated with disease or development. *Curr. Protoc. Cell Biol.* 56:22.16.1-22.16.21. © 2012 by John Wiley & Sons, Inc.

Keywords: nucleus • microfluidics • cell/nuclear mechanics • deformation

INTRODUCTION

The mechanical properties of the nucleus have recently gained increasing interest, as it is now emerging that changes in nuclear structure and mechanics are associated with a variety of human diseases and also occur during normal differentiation and development (Zwerger et al., 2011). The nucleus often occupies a large fraction of the cell volume and houses the genomic DNA. It is enclosed by the nuclear envelope, consisting of two lipid bilayers, the outer and inner nuclear membranes, and an underlying dense protein meshwork, the nuclear lamina. The nuclear lamina is composed of lamin proteins and connected to the inner nuclear membrane via nucleus-specific transmembrane proteins such as emerin, lamin B receptor (LBR), and SUN proteins (Holaska, 2008). Importantly, the nucleus is physically connected to the surrounding cytoskeleton via nesprins and SUN proteins at the nuclear envelope, enabling continuous force transmission between the extracellular matrix and the nuclear interior (Lombardi and Lammerding, 2011). The mechanical behavior of the nucleus is primarily determined by contributions from the nuclear lamina and the nuclear interior. The lamina deforms elastically and can stretch significantly under stress (Dahl et al., 2004). The nuclear interior, consisting of chromatin and chromatin-associated proteins, has characteristics of a viscoelastic medium (Rowat et al., 2008). In most normal cells, the nucleus is significantly stiffer than the surrounding cytoplasm. As such, the mechanical properties of the nucleus often govern the overall mechanical behavior of cells during large cell deformations. Nuclear deformability may even constitute a limiting factor in the cell's ability to migrate through narrow constrictions, e.g., during cancer cell metastasis or white blood cell migration through tissues (Friedl et al., 2010). Furthermore, mutations in nuclear envelope proteins, such as lamins, cause a large number of human diseases (Simon and Wilson 2011), including muscular

Current Protocols in Cell Biology 22.16.1-22.16.21, September 2012
Published online September 2012 in Wiley Online Library (wileyonlinelibrary.com).
DOI: 10.1002/0471143030.cb2216s56
Copyright © 2012 John Wiley & Sons, Inc.

dystrophy and dilated cardiomyopathy, and it has been suggested that increased nuclear fragility could contribute to the often muscle-specific disease phenotypes. Modifications in nuclear envelope composition during development or differentiation are also associated with changes in nuclear mechanics (Pajerowski et al., 2007). Therefore, characterizing the mechanical properties of the cell nucleus is an important factor in understanding the function and behavior of normal and diseased cells.

Here, we present two independent and complementary approaches to measure nuclear mechanics. In the first, adherent cells are subjected to substrate strain, and nuclear stiffness is inferred from the induced nuclear deformations. In the second approach, suspended cells are perfused through microfluidic channels with constrictions smaller than the size of the nucleus. The transit time through the constrictions is indicative of nuclear stiffness. The best choice of which technique to use (or to use both) will depend on the cells under investigation and the specific aims of the study.

STRATEGIC PLANNING

When performing a large number of experiments, it is helpful to automate parts of the image acquisition and the image analysis. A protocol for the use with a motorized stage that makes it easier to revisit previously recorded fields of view is included. For the image analysis, we have developed several MATLAB scripts to compute nuclear and membrane strains. These scripts are available from the authors upon request.

To ensure that all cells have a similar size, shape, and orientation, contact printing can be used to deposit extracellular matrix molecules in only precisely defined areas.

The current protocol uses a one-step strain application, and cells cannot be imaged during the strain application process. Motorized strain devices can help alleviate this problem, although changes in focal position and membrane displacement can impose further challenges.

BASIC PROTOCOL 1

NUCLEAR DEFORMATION DURING APPLIED SUBSTRATE STRAIN

Observing induced nuclear deformation resulting from stretching adherent cells can provide important information on the mechanical properties of the nucleus and nucleo-cytoskeletal force transmission. In the assay described in this protocol, the cell is stretched by applying uniform strain to the cell's substrate. The associated forces are transmitted across the focal adhesions through the cytoskeleton and the nuclear envelope to the nuclear interior. Previous studies indicate that the resulting nuclear strain is closely correlated to the applied substrate strain of the substrate (Caille et al., 1998; Lammerding et al., 2004). Importantly, since the nucleus is normally significantly stiffer than the surrounding cytoskeleton, the induced nuclear strain is typically only a fraction of the applied membrane strain, and the cytoskeleton absorbs most of the applied strain. Hence, the ratio of the induced nuclear strain to the applied membrane strain can give a reliable measurement of the nuclear stiffness relative to the surrounding cytoskeleton. Low nuclear strain values correspond to a stiff nucleus (or soft cytoskeleton), whereas larger nuclear strain values indicate softer, more deformable nuclei. In these experiments, the substrate strain can be applied bi-axially or uniaxially, mimicking physiological conditions. For example, cells in the lung and bladder are typically exposed to bi-axial strain, whereas muscle cells are predominantly stretched in only one direction, along the muscle fiber. In our experience, we found that uniaxial strain application is often preferable for the substrate strain experiments, since many cells can tolerate uniaxial strain application better than bi-axial strain (presumably because it requires a smaller increase in total plasma membrane area), so that higher strains can be applied, which allows for better quantification of the induced nuclear deformations.

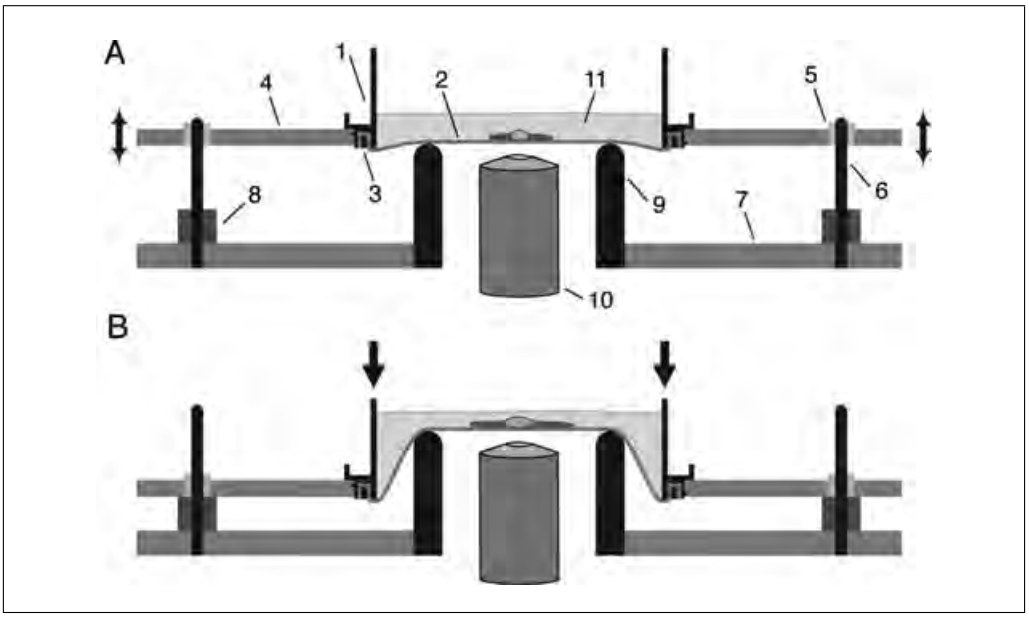

Figure 22.16.1 Overview of the strain device: (**1**) Strain dish with the mounted silicone membrane (**2**). The membrane is held in place by a plastic O-ring (**3**). The strain dish is inserted into the dish holder plate (**4**), which contains four nylon sliders (**5**) to slide up and down on vertical pins (**6**) fixed in the base plate (**7**). The vertical moving range, and thereby the maximum applied membrane strain, are limited by nylon spacers (**8**). The membrane is stretched over the stationary Teflon-impregnated delrin platen (**9**). The platen contains a central opening wide enough to fit an objective (**10**) through it. The dish should contain enough imaging medium (**11**) that during stretch the membrane does not dry out. (**A**) Device in un-stretched condition as required for pre- and post-stretch images. (**B**) Device in fill-stretch condition, by application of weight to the strain device, illustrated by the arrows pointing down. The membrane stretch is limited by the nylon spacers (8).

The microscope-mounted strain device described in this protocol is a custom-designed system (Fig. 22.16.1). Such a device can be built in a basic machine shop at a reasonable cost. Alternatively, one can use a commercially available system (see Materials for suggestions). However, many of the available devices have the limitation that they use thick silicone membranes, which can reduce image quality and resolution. The custom-built strain device described in the following protocol consists of a strain dish with an elastic silicone membrane at the bottom on which cells are cultured and a platform that is mounted on an inverted microscope. The bottom rim of the strain dish has an outer thread to fix the strain dish in the holder plate. The silicone membrane is secured to the strain dish with a plastic O-ring, which tightly fits into the groove of the strain dish from the bottom side.

The membrane is stretched by applying a weight to the top of the strain dish, pushing it down over a stationary platen in the base plate. This results in a uniform bi-axial strain field in the center of the silicone membrane. Vertical metal pins in the base plate help to guide the strain dish in the holding plate and keep it aligned parallel to the base plate and objective. The maximum applied strain can be adjusted by limiting the vertical displacement of the strain dish and holding plate by placing nylon spacers between the base plate and the holding plate. The strain dish can be easily modified for uniaxial strain application by applying two parallel strips of Scotch tape to the membrane (see Fig. 22.16.2). Since the silicone membrane cannot deform where the Scotch tape is applied, the area between the two strips of tape is subjected to uniform uniaxial strain.

The cells are stained with a cell permeable blue fluorescent DNA dye (Hoechst 33342), which allows high-resolution imaging of nuclear shape. Phase contrast and fluorescence

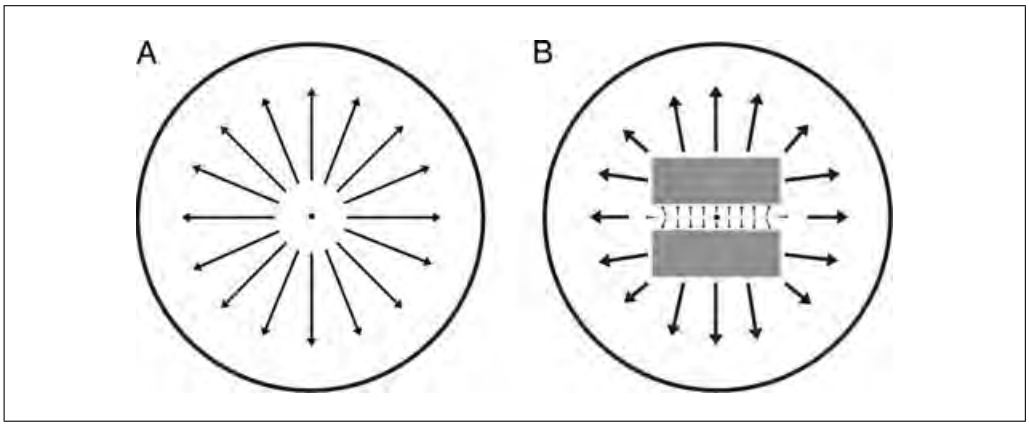

Figure 22.16.2 Overview of the applied membrane strain. View from the top or bottom of the strain dish during strain application. (**A**) Membrane with central landmark. Note the uniform radial (bi-axial) strain field. (**B**) Membrane with central landmark and two parallel Scotch tape stripes (in gray) next to the landmark, one on each side of the landmark. The Scotch tape, which locally restricts the deformation of the silicone membrane, results in a uniaxial strain field between the stripes.

images of several membrane sections are imaged before, during, and after strain application. Marking the center of the strain dish with a fine-tip marker on the bottom of the silicone membrane can aid in locating (and re-locating) specific membrane sections for the repeated imaging, as the central dot serves as a landmark, and the positions relative to this landmark remain relatively constant during strain application.

Image analysis is typically performed off-line following the strain experiments. The applied membrane strain is calculated by comparing phase-contrast images of the silicone membrane between prestrain and full-strain images; nuclear strain is calculated by comparing fluorescence images of the cell nucleus. Comparison between prestrain and post-strain phase-contrast images of the cells can serve to identify cells that became damaged or detached during the strain application and that should be excluded from the analysis.

Materials

Deionized water to rinse assembled strain dishes

70% ethanol

Phosphate-buffered saline (PBS) or Hank's Balanced Salt Solution (HBSS), both Ca/Mg-ion-free

Fibronectin or other suitable extracellular matrix proteins to coat silicone membrane

Appropriate cell culture medium, e.g., Dulbecco's modified Eagle medium (DMEM) supplemented with fetal bovine serum (FBS) and penicillin/streptomycin

Trypsin/EDTA

Hoechst 33342

HEPES buffered, phenol red-free imaging medium: e.g., Dulbecco's modified Eagle medium (DMEM) without phenol red and with HEPES

Chemically inert, silicone-impermeable grease (e.g., Braycote804; Castrol)

Custom-built strain device consisting of microscope-mounted base plate, dish holding plate, and components for strain dish (Fig. 22.16.1); alternatively, one can use commercially available systems (e.g., from Flexcell International Corporation, the Cell Stretcher by Electron Microscopy Sciences, or the STREX instruments from B-Bridge International)

Silicone membrane: 0.005-in.-thick silicone sheeting in 12 × 12-in. sheets (Gloss/Gloss nonreinforced silicone sheeting; Specialty Manufacturing)
Scissors
Kimwipes or other tissues
Ethanol prep pad: 1.1 × 2.6-in.
Autoclavable bags
Autoclave
10-cm disposable plastic dishes, sterile
Fine-tip black permanent marker suitable to mark silicone membrane
Scotch tape (19-mm width)
4°C incubator
Centrifuge
Hemacytometer
37°C cell culture incubator
Microscope
Inverted epifluorescence microscope equipped for fluorescence and phase-contrast image acquisition with light sensitive CCD camera
Filter sets for DAPI/Hoechst 33342
60× non-immersion phase-contrast objective with long working distance
Weight plate (~5 lb) to place on strain dish for strain application (Fig. 22.16.1)
Image acquisition software
Linear-encoded motorized stage (optional)
Image analysis software: e.g., ImageJ, Adobe Photoshop or MATLAB (Mathworks)

NOTE: DIC objectives can be used as an alternative for phase contrast; however, in our experience, DIC illumination is more sensitive to deviations from the ideal Koehler illumination that can occur with custom-build strain devices, resulting in reduced image quality that can make it difficult to analyze the transmitted light images.

NOTE: We have also successfully used (water) immersion objectives for the strain experiments; however, care must be taken that the silicone membrane is not accidentally stretched over the objective, particularly when applying strain, as this could cause additional local strain in the substrate. When using immersion objectives, it is best to lower the objective when applying the weight to the strain dish and the refocusing once full membrane strain is reached.

Prepare the strain dishes

1. Prior to assembling the strain dish, clean all components, including the O-ring, with water and soap, wipe with 70% ethanol, rinse thoroughly with tap water, then deionized water, and air dry the components.

2. Mount the silicone membrane on the clean strain dish using the plastic O-ring. We typically place a 3 × 3-in. piece of silicone membrane over the plastic O-ring lying on a clean surface and press the strain dish from the top over the plastic O-ring with the membrane. The O-ring is held in place in the groove of the strain dish together with the membrane. Cut excess membrane with scissors as close to the strain dish as possible so that the excess membrane cannot get into the outer thread of the strain dish when mounted into the holding plate.

   After placing the membrane on top of the O-ring, ensure that the membrane is wrinkle free, which would cause leakages during cell culture or strain-experiments.

3. Clean the top (inner) surface of the membrane by wiping with a Kimwipe soaked in 70% ethanol in a circular motion from the center to the periphery of the dish, ending by wiping the dish walls in the inside of the dish. If necessary, clean the outside of the silicone membrane.

4. Repeat the previous cleaning step with a sterile ethanol prep pad.
5. Rinse the device under running deionized water and let it air dry.
6. Place the dishes in autoclavable bags and autoclave using the dry cycle for glass and plastic.
7. Once dishes are sterilized and have cooled down to room temperature, open the autoclave bag inside a sterile biosafety cabinet and place each strain dish in an inverted 10-cm sterile disposable plastic dish.
8. Invert the dish, so that the bottom of the silicone membrane faces up. Use a fine-tip black marker to draw a small dot at the center of the silicone membrane, which will serve as the landmark to re-locate cells during and after strain application.
9. For uniaxial strain experiments, place two parallel pieces of Scotch tape (~20 mm × 19 mm) centered around the black dot, approximately 5-mm apart.
10. Turn over the strain device to the upright position, so that the inside of the silicone membrane faces up and cover the strain dish with a sterile disposable petri dish.
11. Pipet 10 ml of 2 μg/ml fibronectin in sterile PBS into the strain dish; gently swirl to ensure that the entire membrane is covered.
12. Incubate overnight at 4°C. Alternatively, incubate for 2 hr at 37°C

    Ensure that the surface is completely covered with the coating solution.
13. Aspirate the fibronectin solution and rinse the membrane once with sterile PBS. Fill the dishes with 10 ml of appropriate cell culture medium and place in the incubator to prewarm.

    When handled outside the biosafety cabinet, strain dishes should always be kept inside an inverted sterile 10-cm disposable plastic petri dish to minimize risk of contamination.

Plate cells for the experiments

In our experiments, we have successfully used mouse embryo fibroblasts, human skin fibroblasts, breast epithelial cells, and mouse myoblasts and myotubes for the strain experiments. The conditions below were optimized for mouse embryo fibroblasts. Other cell types may require some adjustments. For fibroblasts, reseed cells every two to three days at 60% to 80% cell confluency in cell culture flask (e.g., 75-cm^2 flask). Avoid growing cells to total confluency.

14. Remove the culture medium and rinse cells once with sterile PBS or HBSS without calcium and magnesium for 1 min at room temperature.
15. Detach the cells with trypsin/EDTA solution for 5 min at 37°C.

    We typically use 1 ml for a 75-cm^2 flask.
16. Add 2 to 5 ml of culture medium, containing 10% fetal bovine serum, to the trypsin/EDTA suspension to inactivate the trypsin. Gently mix by pipetting up and down to breakup cell clusters and achieve a single-cell suspension.

    For a 75-cm^2 flask, we add 4 ml medium.
17. Centrifuge the cell suspension for 5 min at 230 × *g*, 4°C, and remove the supernatant.
18. Resuspend the cell pellet in 5 ml cell culture medium and count cell density with a hemacytometer.

19. Seed the cells in the prepared strain dishes to achieve a desired cell confluency of ~20% to 30% within 1 to 2 days. The cell density should be high enough to contain several cells per field of view while at the same time low enough to minimize cell-cell contacts.

20. Maintain cells overnight or longer in cell culture incubator to achieve sufficient cell attachment before using the strain dish for experiments.

Prepare the cultured cells for stretch experiment

21. Add Hoechst 33342 directly to the strain dish with cell culture medium to a final concentration of 1.5 μg/ml; gently swirl to mix and incubate for 15 min at 37°C in a cell culture incubator.

    The final concentration of Hoechst 33342 may be optimized for each cell type to achieve bright nuclear fluorescence labeling while avoiding cytotoxic effects.

22. Replace Hoechst-containing medium with 15 ml phenol red-free imaging medium containing HEPES.

Set up the microscope-mounted strain device

23. Remove the strain dish from the incubator. Gently apply a thin layer of Braycote grease along the periphery of the bottom of the silicone membrane with a gloved finger.

    Make sure to keep the center of the dish free of any grease, as this could interfere with the imaging process.

24. Carefully screw the strain dish into the dish holder plate, making sure not to spill any medium.

25. Position the strain device base plate on the microscope stage. Insert appropriate spacers onto the guidance pins of the base plate. Switch the microscope to a high-power long working distance objective. We typically use a 60× objective, but have also successfully conducted experiments with a 40× water immersion objective.

    Depending on the design of the strain device, you may require an objective extension tube (e.g., from Thor Labs) to account for the altered imaging plane.

26. Carefully position the holding plate with strain dish onto the base plate and slowly lower it until the silicone membrane rests on the central platen.

27. Adjust the microscope stage position so that the landmark dot on the silicone membrane is centered over the objective. The system is now ready for image acquisition.

Image and perform strain application

28. In phase contrast mode, locate the landmark dot at the bottom of the silicone membrane and acquire an image of the reference point for later identification.

29. Focus on the cells plated on the silicone membrane and identify a field of view with one to five healthy looking, well-spread cells with the nucleus located in the cell center. Acquire a phase contrast and a fluorescence image. For the phase-contrast image, focus on the cell boundary and the silicone membrane; for the fluorescence image, focus on the center cross-section of the fluorescently labeled nucleus.

    Make sure to remember the location of the field of view relative to the reference landmark dot.

30. Move the field of view along an imaginary line perpendicular to the intended strain direction (in the case of uniaxial strain application), as the relative positions along this line will not change during strain application. Take note of the relative position

of the field of view relative to the landmark dot so that the same cells can be found again.

Leave the phase-contrast images open in the acquisition program to help identify the same fields of view later. Acquire ten to fifteen pictures of different areas. This prestrain acquisition phase should take no more than 5 to 10 min.

31. Carefully place the weight plate on top of the strain dish to apply membrane strain. Wait ~1 min for viscoelastic effects to dissipate.

32. Focus on the bottom of the silicone membrane and search for the landmark spot. Comparison with the previously acquired images will aid in this task. Acquire full-strain image of reference dot.

33. Focus on cells on the silicone membrane. Re-locate cells acquired during prestrain imaging, taking images in phase contrast and fluorescence for each field of view, making sure to match the focal positions of the prestrain images. Use the images of the first set of image pairs to find the same field of view and to adjust the fine focus.

    Do not exceed more than 15 min of full strain application to prevent cytoskeletal remodeling and other cellular adjustments to the strain application.

34. Carefully remove the weight plate. If necessary, gently lift up the strain dish, until it loosely rests on the silicone membrane on the platen, matching the position during prestrain imaging. Wait for 1 to 2 min for the cells and membrane to relax.

35. Acquire final set of image pairs (post-strain) following the procedure above. Use the previously acquired prestrain images to help find the same cells again and to match the focal position.

36. Remove the strain dish from the microscope and repeat the process with the next strain dish.

    The entire imaging procedure should take less than 30 min.

Protocol variation: Simple acquisition protocol with motorized stage

37. In phase contrast mode, find the landmark dot on the bottom of the silicone membrane.

38. Acquire an image of the landmark dot to make it easier to identify the same spot during and after strain application.

39. Set the stage position to zero at this location; all other recorded positions will be relative to this location.

40. Focus on the cells above (or slightly to the side) of the landmark dot. Acquire phase contrast and fluorescence images for the first field of view as described in step 29.

41. Move the stage in the direction perpendicular to the intended uniaxial strain direction and find the next field of view with suitable cells. Acquire pictures in phase contrast and the DAPI/Hoechst channel as described above. Store the stage position of each field of view in the image acquisition program.

42. Repeat the above step for six to ten additional fields of views. The entire process should take less than 10 min.

43. Apply the substrate strain as described in step 31. Wait for 1 to 2 min for viscoelastic effects to dissipate. During that time, locate the landmark dot and focus on the same spot on the membrane. Use the reference image acquired in step 38 for orientation.

44. Reset the stage coordinates to zero in the acquisition program.

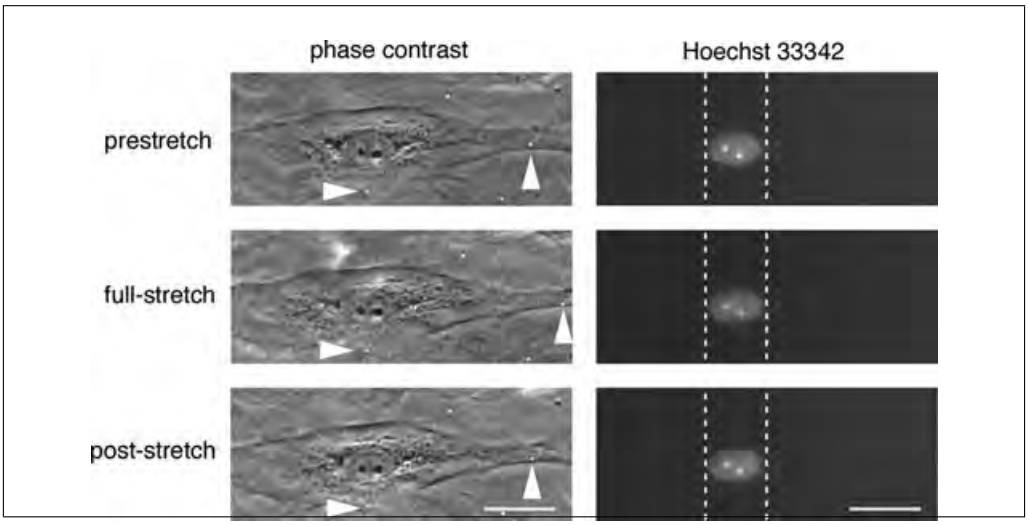

Figure 22.16.3 Phase-contrast and Hoechst fluorescence images of a cell before, during, and after uniaxial strain application. The top row shows the cell before strain application. The center row shows the cell during full strain application (≈20% strain in the *x*-direction). The arrow heads in the phase-contrast images indicate how much the speckles on the membrane move during the strain application. The Hoechst images illustrate the induced nuclear deformation during stretch; the dashed line indicates the maximal extension during full strain application. The bottom row of images depicts the cell after strain application. The membrane has returned to the prestretched condition and the cell did not retract, since it has the same shape as in the prestretched image. Scale bar: 25 μm.

45. Use the motorized stage and the stored (relative) stage positions to revisit the previously acquired fields of view. If necessary, manually adjust the focus and stage position to closely match the original view. Again, take phase and fluorescence images as described in step 29. Proceed with the other fields of view in the list of recorded stage positions.

    Do not exceed 10 min of strain application.

46. Carefully remove the weight from the strain dish as described in step 34 and wait 1 to 2 min for viscoelastic effects to dissipate. During this time, bring the landmark dot into the field of view.

47. With the landmark dot closely matching the previously acquired field of view (see step 38), re-zero the stage coordinates. Acquire the same set of image pairs for each position as described above.

Analyze the image with ImageJ or Photoshop

A typical set of images acquired in matching fields of view is shown in Figure 22.16.3. The cell was imaged in phase contrast and fluorescence (Hoechst 33342) mode in pre-, full-, and post-stretched conditions. The uniaxial strain application is clearly visible by the displacement of distinct speckles on the silicone membrane in the phase-contrast field and by elongation of the nucleus in the strain direction in the fluorescence images.

48. Calculate the applied membrane strain by measuring the distances between matching image features on the membrane in image pairs acquired before and during strain application. Compare image pairs acquired before and after strain application to confirm that the membrane relaxed back to the prestretched shape and cells did not become damaged or detached. Exclude cells with obvious differences in morphology from further analysis.

    In our experience, the silicone membranes usually contain sufficient intrinsic speckles and other distinguishable features that can be used for the membrane strain computation. It is

important to use only features firmly attached to the membrane (and not floating particles) and located outside the cells. It is best to use several pairs of features to make sure that the computed results are consistent. The entire process can be further optimized with image processing algorithms implemented in MATLAB or similar programs. For uniaxial strain application, the pairs of speckles should be located along the strain direction, as displacements in the perpendicular direction should be minimal.

49. Calculate the induced nuclear strain by comparing the length of the nucleus measured before, during, and after strain application in corresponding image-sets. Alternatively, pictures can be overlapped in Photoshop and the prestretched image adjusted by free transformation and stretching to the full-stretched image. Repeat this process for each cell in the field of view.

    For mouse cells, the bright condensed heterochromatin spots (chromocenters) can be used to align the images of the nuclei, or to measure intranuclear distances.

    Note that we here define strain as the relative increase in size, e.g., the change in length divided by the initial (unstrained) length.

50. Repeat the above steps for the image sets acquired at additional positions.

    The membrane strain should be fairly uniform between different fields of view and can be averaged to compute the mean membrane strain.

51. Calculate the normalized nuclear strain for each cell by dividing the induced nuclear strain by the applied membrane strain.

$$\text{normalized nuclear strain} = \frac{\text{nuclear strain}}{\text{applied membrane strain}}$$

BASIC PROTOCOL 2

ASSESSING NUCLEAR DEFORMABILITY WITH A MICROFLUIDIC PERFUSION DEVICE

The mechanical properties of viscoelastic objects, such as nuclei and cells, can be determined by observing their dynamic deformation under stress. A commonly used method to probe nuclear mechanics is micropipet aspiration, in which the stiffness of the nucleus is determined by gently aspirating the nucleus into a micropipet with a tip diameter smaller than the size of the nucleus (typically a few microns) and quantifying the time-dependent deformation into the pipet opening (Dahl et al., 2004). The stiffer the nucleus is, the longer it will take to (partially) aspirate it into the narrow opening of the pipet. The approach presented here is based on a similar principle. Intact cells or isolated nuclei are perfused with a constant pressure gradient through microfluidic channels containing precisely defined constrictions narrower than the size of the nuclei. Since the nucleus is significantly stiffer than the surrounding cytoskeleton, nuclear deformability will largely determine the transit time through the narrow constrictions. While cells with highly deformable nuclei can rapidly pass through the constrictions, cells with stiffer nuclei will take longer or even be unable to transit through the constrictions altogether. A major advantage of this device over the aforementioned techniques is that hundreds of nuclei can be probed within a few minutes because of the rapid cell throughput and the many channels that can be imaged in parallel.

These perfusion devices are made of polydimethylsiloxane (PDMS) by soft lithography. In a first step carried out in a cleanroom facility, a silicon wafer spin-coated with photoresist is exposed to UV light through an optical mask containing the desired channel layout and subsequently developed. Thereafter, in a well-equipped laboratory, a PDMS replica is cast from the master and bonded to a glass slide to create a microfluidic device. Cells are then perfused through the device, and their ability to pass through narrow channels is assessed as a measure of nuclear mechanics.

Materials

SU-8 2010 photoresist (Microchem)
SU-8 Developer (1-Methoxy-2-propyl acetate, Microchem)
Isopropanol
Nitrogen
Anti-stiction coating: e.g., (tridecafluoro-1,1,2,2-tetrahydrooctyl)trichlorosilane, a fluorinated silane (also known as FOTS)
Sylgard 184 silicone elastomer base
Sylgard 184 silicone elastomer curing agent
0.2 M HCl
70% ethanol
Deionized water
Bovine serum albumin (BSA; see recipe)
Phosphate-buffered saline (PBS; see recipe)
Pluronic I-127 (optional)
Cells for analysis (1 ml cell suspension in PBS with BSA at a density of 3×10^6 cells/ml)
Trypsin
Cell culture medium appropriate for the cell type studied [e.g., Dulbecco's modified Eagle medium (DMEM) with 10% fetal bovine serum (FBS)]
Cytochalasin D (optional)
10% bleach in water (optional)

Microfabrication facility with the following tools: mask generator, contact aligner, molecular vapor deposition and spin coater
CAD software (e.g., AutoCAD, L-edit)
4-in. silicon wafers
Oven
Hot plate
150-mm (diameter) plastic petri dishes
Premium vacuum pump, 115 V (Harrick Plasma)
Desiccator
Packing tape
Utility knife
Cutting mat
0.75-mm (diameter) Uni-Core hole-puncher (Harris)
Glass coverslips (22 × 50 mm, thickness 1.5)
Glass slides (27 × 75 × 1.0–mm)
Compressed air tank with 5% CO_2
Expanded plasma cleaner, 115 V (Harrick Plasma)
0.2-μm (pore size) syringe filter
5-ml syringes
0.015-in. i.d., 1/32-in. o. d. pre-cut natural PEEK tubing for microfluidics (Ing)
Forceps (rounded tip)
Cell culture incubator
Hemacytometer
Centrifuge
40-μm (pore size) cell strainer
High-speed microscope camera, 60 frames per second or higher: e.g., PIKE F-032 1/3" CCD FireWire.B Monochrome Camera with up to 208 frames per second (Edmund Optics)
Inverted microscope with camera mount
Image acquisition software
Image Analysis software (ImageJ)

15- and 50-ml Falcon tubes
Pressurized cap for 15-ml Falcon tubes for microfluidics (World Precision Instruments, FLUIWELL-1C-15ML)
Two stage brass analytical pressure regulator, 0 to 25 psi (Airgas)
5/16-in. (i.d.) PVC tubing, 40’ length
0.05-in. (i.d.) PVC tubing, 2’ length

Design and microfabricate the device

1. Design a mask for your device using CAD software (see Fig. 22.16.4). The device consists of an inlet channel (item 1 in Fig. 22.16.4), into which a hole is punched to allow for the connection of tubing, followed by a filter (item 2 in Fig. 22.16.4) with a minimum width of 15 μm to prevent the passage of aggregated cells and dust, followed by a series of bifurcations that end with several parallel constriction channels (item 6 in Fig. 22.16.4). The constriction channels consist of a sequence of constrictions narrower than the cell nucleus. In our devices, these constrictions are 3-, 5-, or 8-μm wide. Narrower constrictions are used for smaller or more deformable cells (e.g., neutrophils), while larger constrictions are suitable for fibroblasts or other larger cells. Two wider bypass channels are included in the device. These channels serve to maintain an approximately constant perfusion rate (and pressure drop across the constriction channels) in case some of the constriction channels become blocked

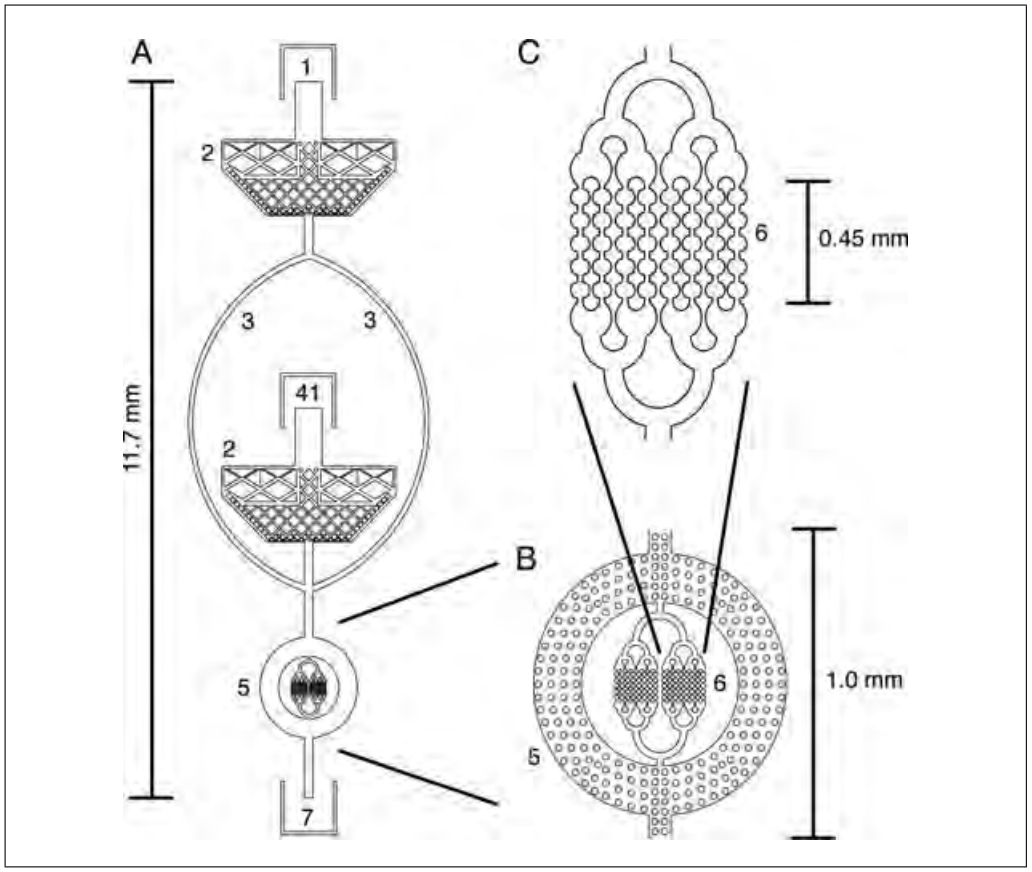

Figure 22.16.4 Perfusion device design. (**A**) Overview of the entire device, with the pillars needed to support the PDMS ceiling removed for viewing purposes. (**B**) Close-up of device constrictions and bypass channels with pillars to reveal additional details. (**C**) Further close-up view of the constrictions channels. (**1**) Flushing inlet, to clear blocked constriction channels. (**2**) Filter to eliminate large dust particulates and cell aggregates. (**3**) Flushing channels. (**4**) Inlet for cell suspension. (**5**) Bypass channels to maintain constant pressure in constriction channels. (**6**) Constriction channels or microchannels. (**7**) Device outlet.

with cells or debris. If the device is set up with a constant pressure perfusion, rather than constant flow rate, as in our setup, these bypass channels are not necessary. The device also contains an extra inlet that can be used to flush the channels with PBS if the constriction channels get clogged. Features are also integrated into the design around the inlet to serve as guides while punching holes.

For an instructional video describing the fabrication process, see video 1 at http://www.currentprotocols.com/protocol/cb2216.

It is critical that an aspect ratio (channel width:channel height) of no more than 4:1 is maintained for any features in the channels to prevent the PDMS ceiling from collapsing into the channels. Thus, for a channel height of 8 μm, the channel width should not exceed 32 μm.

2. Write the mask design created in step 1 onto a 5-in. mask in the microfabrication facility using a mask writer.

   Several companies also offer custom-produced high resolution masks for a reasonable price (e.g., Fineline Imaging).

3. Bake 4-in. silicon wafers at 200°C for at least 20 min and allow the wafers to cool for a few minutes. Pour enough SU-8 2010 on the wafer centered on the spin coater to cover half the diameter of the wafer, then spin the wafer at 500 rpm for 10 sec (with 100 rpm/second acceleration), and then 3000 rpm for 30 sec (with 300 rpm/second acceleration).

   If another type of photoresist is used, follow the manufacturer's spin-coating recommendations to obtain a 10-μm-thick layer of photoresist.

4. Allow the SU-8 photoresist to relax at room temperature for 10 min.

5. To remove any remaining solvent, bake the wafers on a hot plate at 60°C for 10 min, allowing the hot plate to ramp up from room temperature with the wafers placed on it.

   Take care not to exceed the temperature.

6. Expose the photoresist-coated wafers in a contact aligner with a dose of 250 mJ/cm^2. The exact exposure time will depend on the specifications of the instrument. Allow the resist to relax for 1 hr post-exposure.

   The exposure dose used here is double the manufacturer's recommended dose, as we have found that higher doses improve binding of the SU-8 features to the silicon wafer and reduce the appearance of cracks without any ill-effects on the structures. However, this may not be the case for all designs.

7. Post-bake the photoresist coated wafers for 3.5 min at 90°C. Allow the wafers to cool down on the hot plate, which has been switched off to ensure a slow cool-down.

   The structures in the resist should now be visible to the naked eye.

8. Submerge the wafer in SU-8 developer for 5 to 10 min at room temperature, then rinse the wafer thoroughly with isopropanol and dry with a stream of nitrogen.

   If a white precipitate appears upon rinsing with isopropanol, the SU-8 has not been completely dissolved and the wafer should be rinsed with SU-8 developer and then placed in a dish with fresh SU-8 developer, since precipitate in the developer will result in white streaks on the wafer.

9. Hard bake the wafer for 30 min at 200°C.

10. Coat the wafer with an anti-stiction coating, such as (tridecafluoro-1,1,2,2-tetrahydrooctyl)trichlorosilane, a fluorinated silane (also known as FOTS).

    This coating helps prevent PDMS from becoming permanently stuck to the wafer.

Mold the PDMS and assemble the microfluidic device

11. Place the wafer in a 150-mm (diameter) plastic petri dish, with the photoresist features facing up. Combine ~6 g curing agent and 54 g silicone elastomer base of the Sylgard 184 kit in a disposable container (10% solution by weight). Mix vigorously for a few minutes and then degas the solution under vacuum in a desiccator for 10 to 30 min to remove air bubbles. Pour the degassed solution on top of the wafer; the PDMS layer should be 3- to 5-mm thick to ensure that inlet and outlet tubing can be properly connected to the final device. Place the dish with the wafer and PDMS solution in the oven at 65°C for 2 hr to cure PDMS.

    Optionally, once the solution has been poured on top of the wafer, it can be placed under vacuum as well, although this step is usually not necessary. Degassing can also be performed by pouring the solution into a Falcon tube and centrifuging it.

12. Slowly peel off the cured PDMS from the wafer. Tape a piece of packing tape to a laboratory bench (adhesive side up) and then place the side of the PDMS that was in contact with the wafer onto the packing tape to minimize dust accumulation on the PDMS.

13. Cut devices out of the PDMS on a cutting mat with a utility knife, while the packing tape is still adhered to the PDMS. Punch inlet and outlet holes in each device at the designated areas using a 0.75-mm diameter Uni-Core hole-puncher.

14. Clean glass coverslips or glass slides by placing them in a 0.1 M HCl solution for at least 10 min. Rinse the glass slides with ~20 ml deionized water, followed by ~10 ml ethanol, and then 20 ml water again. Dry under a stream of compressed air.

    Only dry glass slides close to the time they are going to be used, to minimize the possibility of dust particles.

    Glass slides in the HCl solution will quickly sink to the bottom of their container. Ensure that there is solution in between the pieces of glass and the container by swirling the solution occasionally. Prevent oil in the compressed air system from being sprayed on glass slides by connecting a filter in series with the tubing leading from the compressed air source.

15. Immediately prior to plasma treatment, remove the tape from the devices.

16. Place a piece of glass slide and PDMS, with microstructure side up, side by side in the plasma cleaner. Treat with plasma for 5 min at the highest setting (200 W). Release the vacuum, remove the glass slide and PDMS from the plasma chamber, and immediately bring the two into contact with each other, pressing both parts firmly together. Place the device on a 95°C hot plate for 10 min, and then allow to cool for 10 min at room temperature.

    Check if the device has adhered properly by gently trying to peel the PDMS off from the glass slide; if the PDMS becomes detached, then there is a bonding problem. To mediate bonding problems, eliminate sources of dust and oil. For example, wipe down the inside of the plasma cleaner and keep the door closed when not in use. Additionally, gloves are often coated with a surfactant to prevent them from sticking to each other in their packaging; wash gloves thoroughly with 70% ethanol to remove this coating.

Fill and prime the microfluidic device

17. Prepare ~10 ml of 20 mg/ml bovine serum albumin (BSA) suspended in phosphate-buffered saline (PBS). Filter the solution in a laminar flow hood (biosafety cabinet) using a 0.2-μm syringe filter to sterilize it.

    The BSA does not dissolve quickly; stir in order to more efficiently suspend the solute. An alternative to the BSA solution is a solution of 0.2% I-127 Pluronic in PBS.

18. Passivate each device with 20 mg/ml BSA in PBS solution to prevent cells from adhering to the channel walls as follows:

    a. Using a clean sterile 5-ml syringe, aspirate 1 ml of the sterile filtered BSA solution.

    b. Connect 0.015-in. (i.d.) PEEK tubing to the syringe using a pair of forceps and then insert tubing into the device inlet.

    c. Firmly press on the syringe plunger until the solution can be seen coming out of the other holes of the device.

    d. Continue injecting solution until air bubbles stop appearing in the liquid coming out of the device. Do not remove tubing from the inlet. The device should not contain any air bubbles.

    The extent to which the device has been filled can be examined under a standard bright-field microscope at low magnification. Bubbles generally form near constriction points and appear lighter in color than the channels that are filled with solution. Continue injecting BSA solution until all bubbles have disappeared.

19. Inject additional solution using the syringe every 5 to 10 min in order to refresh solution in the device channels and to prevent the inlets and outlet from drying out. Leave the solution in the device for ~ 30 min to ensure proper BSA coating.

    BSA adsorbs onto the surfaces in the microfluidic device, making them less adherent to cells and preventing excessive clogging of the channels.

Prepare the cell lines

20. While priming the microfluidic devices, prepare cell lines to be examined.

    Each experiment requires at least 1 ml cell suspension, with a cell density of ~3×10^6 cells/ml. Typically, a confluent 75-cm^2 cell culture flask is more than sufficient to provide the required number of cells.

21. Rinse the plated cells with ~10 ml PBS and then detach the cells with 1 ml trypsin solution for 5 min at 37°C. Once the cells are detached, deactivate the trypsin with 4 ml medium containing serum.

22. Count the cells using a hemacytometer.

23. Centrifuge the cells for 4 min at 223 × *g*, 25°C, and resuspend them in 20 mg/ml BSA in PBS solution at a density of 3×10^6 cells/ml.

    Make sure to repeatedly pipet the cell suspension up and down to break up any cell clumps and to obtain a single-cell suspension, as cell clusters can clog the microfluidic channels.

24. Remove any remaining cell clusters by passing the cell suspension through a cell strainer with a 40-μm pore size attached to a 50-ml Falcon tube.

25. Assess cell size. Pipet ~30 μl cell suspension from each sample onto a glass slide and cover with a coverslip. Acquire four to five images with a 10× objective in bright-field mode, so that 100 to 300 cells are imaged. Use an image analysis program (e.g., ImageJ) to determine the cell size (i.e., cross-sectional area) distribution for each population.

    To avoid any confounding factors, such as difference in cell size, it is important to only compare samples with similar cell size distributions. Image cells immediately after pipetting on the glass slide, before the cells have attached and spread.

26. If one wants to minimize the effect of cytoskeletal stiffness or is interested in the effect of the (actin) cytoskeleton on cell transit times, one could treat cells with cytochalasin D. This will depolarize the actin cytoskeleton and the results obtained will be independent of cytoskeleton stiffness.

Perfuse the cells

27. Transfer 1 to 2 ml cell suspension into a 15-ml Falcon tube. Attach the tube to a pressure cap for 15-ml tubes.

    The pressure cap seals and pressurizes the Falcon tube with the cell suspension.

    A constant flow rate device, e.g., a syringe pump, can also be used to perfuse cells through the microfluidic device. However, if there is significant clogging of the device due to dust particles or cell aggregates, this will result in an increased flow rate in channels that are not blocked. A constant pressure apparatus will maintain a constant flow rate in all channels, even when some of them become blocked.

28. Insert the PEEK tubing into the pressure cap so that the tubing inlet is submerged in the cell suspension near the bottom of the Falcon tube.

    Cells tend to accumulate in clumps at the very bottom of the Falcon tube. The cell suspension reservoir should be gently agitated every 5 min to keep cells in suspension.

29. Attach the manometer to a gas tank using PVC tubing. Use the two-stage regulator on the gas tank to set the pressure in the Falcon tube to ~10 psi. Once the cell suspension has filled the tubing and starts flowing out the end, connect the tubing to the inlet of the microfluidic device (see Fig. 22.16.5). At the same time, connect a 5-ml syringe with the 20 mg/ml BSA in PBS solution to a small length of tubing

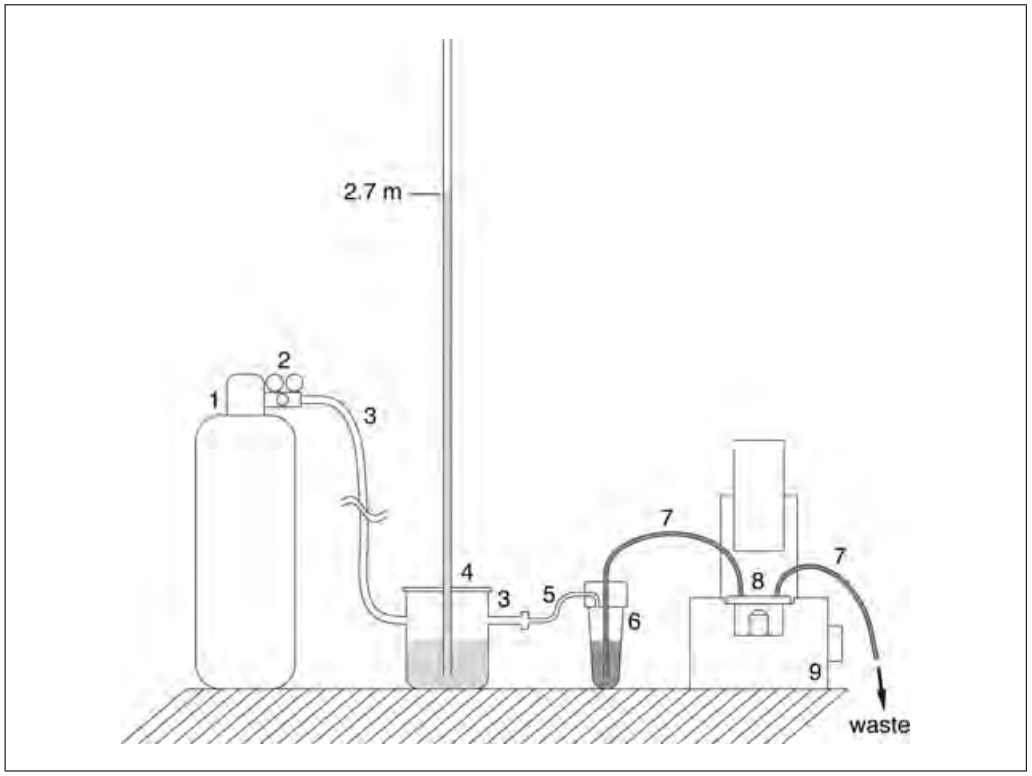

Figure 22.16.5 Experimental setup of perfusion device. (**1**) Pressurized air tank (5% CO_2) with (**2**) two-stage pressure regulator to control perfusion pressure. (**3**) PVC tubing with 5/16-in. i.d. The tubing may be 40' in length or longer, depending on the distance between the tank and microscope. (**4**) Manometer or other device for measuring pressure just before the tubing enters cell suspension reservoir. (**5**) PVC tubing with 0.05-in. i.d. This tubing only needs to be a few feet in length, as its primary purpose is to provide the correct-sized connection to the pressurized cap on the cell suspension reservoir. (**6**) Cell suspension reservoir—composed of a 15-ml Falcon tube with a pressurized cap with sealed opening for tubing. (**7**) PEEK tubing with 0.015-in. i.d.. (**8**) Perfusion-based microfluidic device, see Figure 22.16.4 for details. (**9**) Inverted bright-field microscope with 10× objective and high-speed camera.

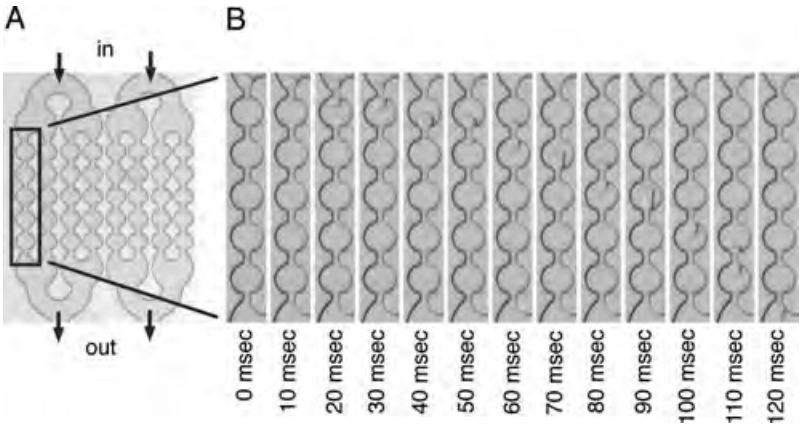

Figure 22.16.6 (**A**) Image of eight parallel constriction channels in bright-field mode. Constrictions are 8 μm in width. Cells are perfused from the top and exit the channels at the bottom as indicated by the arrows. (**B**) Time-series of a mouse embryonic fibroblast cell passing through a channel with 5-μm-wide constriction at a pressure of 10 psi, acquired at 100 frames per second. The limiting step for the cell to travel through the channels is the deformation time to pass the first constriction. Subsequent constrictions are traversed substantially faster.

(approximately 1 ft) and connect the tubing to the inlet of the flushing channel. The syringe can be used to flush clogged channels, if necessary.

30. Mount the perfusion device on a microscope with video-capture capabilities. Set the microscope to bright-field mode and locate constriction channels of the device. Orient the device and camera so that parallel constriction channels can be simultaneously monitored.

    Note microchannels that have become blocked by cells and other debris—it is normal for several channels to become blocked during an experiment. As long as a few constriction channels remain open during the observation period, devices can be used for experiments.

31. Preview device using the camera and image acquisition software (see Fig. 22.16.6). Set the rate of frame capture between 50 fps and 100 fps, depending on the speed that the cells traverse the constrictions. As an approximate guideline, the minimum transit duration should be 2 to 5 frames.

32. Wait for the pressure in the device to equilibrate before acquiring the first video. This may take up to 10 min.

    The length of tubing leading from the compressed air tank to the cell suspension reservoir is compliant and can store energy via elastic deformation. Therefore, the pressure gradient will be transient whenever there is a perturbation to the system, including when the pressure is initially turned on and the reading at the tank may not be representative of the pressure elsewhere in the system. This transient pressure can most accurately be monitored by taking pressure measurements near the cell suspension reservoir over time and waiting for the pressure to level off. See Troubleshooting for construction of a manometer to alleviate these inconsistencies.

33. Acquire several videos of 60 to 90 sec duration. Flush channels in between videos as necessary; when cells become lodged in the microchannels, firmly press the plunger of the syringe connected to the flushing channel to remove debris. Wait several minutes for the pressure to equilibrate again before acquiring another video sequence.

34. After finishing perfusion of one cell line, the next cell line should be perfused through a separate microfluidic device using the same protocol.

The pressure regulator should be adjusted based on manometer readings to ensure uniform pressure for all experiments. Additionally, new or sterilized tubing should be used for each cell line. The new tubing should be the same length as in the previous experiment.

Tubing may be cleaned and sterilized by perfusing 10% bleach through the tubing. After 5 min, perfuse deionized water through each tubing length to remove bleach residue.

Analyze the data

35. Measure the time that it takes for each cell to travel through the first constriction of the microfluidic device and the time needed to travel through the entire length of a constriction channel with an image analysis program such as ImageJ. Either of these two transit times may be used for analysis.

    Cells usually take the longest amount of time to pass through the first constriction, as the initial deformation occurs here. Cells keep their general deformed shape as they pass through subsequent constrictions and, therefore, often travel through these constrictions much faster.

36. Sum the number of frames needed for each cell to pass through the constriction channels, or first constriction, and convert this to a total cell transit time based on the frame rate.

    This step can be done manually in an image analysis software program like ImageJ. Cell tracking can also be automated to quickly analyze large data sets, as described previously (Rosenbluth et al., 2008).

37. Visually verify each transit event in the video sequence. Make sure to include only valid events in the final analysis. Cells should enter the constriction channels one at a time and traverse the entire channel before another cell enters the channel. Cells often pause and deform at each constriction, with the longest pause and largest change in conformation occurring at the first constriction. Examples of invalid events that should be excluded from analysis include: multiple cells traversing one constriction channel at the same time, cell conglomerates clogging a constriction channel, large dust particles, which may be mistaken as cells, or broken-up pieces of cells flowing through the channels.

    Expect between 20 and 300 cells, in total, traversing the constriction channels per one minute of video.

38. Compare the distribution of transit times between different cell populations using appropriate statistical tests.

REAGENTS AND SOLUTIONS

Use deionized, distilled water in all recipes and protocol steps. For common stock solutions, see ***APPENDIX 2A****; for suppliers, see* ***SUPPLIERS APPENDIX****.*

Bovine serum albumin (BSA) solution

Add 200 mg BSA powder to a 50-ml Falcon tube and add phosphate-buffered saline (PBS; see recipe) to obtain a final volume of 10 ml. Mix vigorously until BSA is fully dissolved. Sterilize by passing solution through a 0.2-μm syringe filter. BSA powder should be stored at 4°C. The 20 mg/ml solution of BSA in PBS should be stored up to 1 month at 4°C.

Dulbecco's PBS

Dissolve the following in 1 liter of deionized water:
0.2 g potassium chloride (KCl)
0.2 g potassium phosphate monobasic (KH_2PO_4)
8 g sodium chloride (NaCl)

continued

2.16 g sodium phosphate dibasic ($Na_2HPO_4 \cdot 7H_2O$)
Check pH and adjust to 7.4, if necessary, using 1M NaOH or 1M HCl
Autoclave solution to sterilize
Store up to 6 months at room temperature
Alternatively, commercial solutions without calcium or magnesium can be used.

COMMENTARY

Background Information

Several techniques have been developed to probe the mechanical properties of nuclei (see Lammerding et al., 2007; Rowat et al., 2008 for recent reviews). These include single-cell-based techniques, such as atomic force microscopy on living cells, micropipet aspiration of suspended cells, and microneedle manipulation, in which the deformation of the nucleus is observed when strain is locally applied to the part of the cell, as well as global techniques, such as cell compression, in which the deformation of a cell sandwiched between two plates is observed. Some of these techniques can be applied to isolated nuclei, which has the advantage of probing the nucleus directly without the confounding influence of the cytoskeleton. However, nuclear isolation can damage the nucleus and may also alter the mechanical properties of the nucleus, e.g., by osmotic swelling (Dahl et al., 2004).

In the techniques presented here, measurements can be carried out on many cells over a short period of time. In the case of the cell stretching experiment, the number of cells that can be probed is limited to the number of cells that can be observed in the field of view and imaged in the relative short time of stretching (less than 10 min). When acquiring cells from several nearby fields of view, this corresponds to circa ten to fifteen cells per experiment. In the perfusion technique, hundreds of cells can be observed in a matter of minutes. This latter technique can also be used with isolated nuclei or in the presence of cytoskeletal-disrupting drugs to reduce the effect of the cytoskeleton on the perfusion time.

Critical Parameters and Troubleshooting

Basic Protocol 1: Stretching

It is essential to thoroughly clean the strain dishes before plating cells. Our experience shows that this is one of the most critical steps in the experimental procedure and the most common reason cells fail to grow on the silicone membrane. Another important parameter is cell density. We found that a critical cell density is necessary to achieve viable cells after plating. We recommend conducting pilot studies on the membranes with increasing cell densities to find an optimal setting that ensures high cell viability while minimizing cell-cell contacts.

The maximal membrane strain that can be applied without causing cell damage may vary between different cell types, as some cells can tolerate more membrane strain than others. This parameter should be optimized before performing experiments. We found that for fibroblasts, 5% biaxial or 20% uniaxial strains are generally well tolerated by most cells.

The choice of extracellular matrix type and concentration may be adjusted to achieve maximal cell adhesion for the experiments. Note that cells that are spread very thin may be more sensitive to strain application.

We have successfully acquired additional color channels during the experiments (typically only before strain application), e.g., to identify cells expressing specific GFP- or mCherry-fusion proteins or that have been genetically modified.

Basic Protocol 2: Perfusion

Many factors need to be taken into consideration in the device design, including the size of the constrictions, which will depend on the size of the cells or nuclei that will be perfused, and additional features such as filters for larger particles, flushing channels, and inlets for localized chemical perfusion. One additional aspect that needs to be considered in the design is appropriately sizing structures to avoid collapse of wide channels. This can be achieved by including support pillars in the design located within the channels without blocking the flow. We found that an aspect ratio, i.e., the ratio of channel width to its height, of 4:1 prevents PDMS collapse in most applications. In the case of a device with channels 10-μm tall, this means that the distance between the outer edges of two pillars in a single row should be no more than 40-μm apart.

Poor bonding of PDMS to glass slides will invariably lead to leaky devices. The most likely causes of poor bonding, in our experience, are dirtied bonding surfaces and inadvertently eliminating the plasma treatment by contacting plasma treated surfaces with gloves or tweezers. To troubleshoot this problem,

ensure that all work surfaces are clean and dust-free before beginning work. Placing a piece of packing tape on the microstructured side of the PDMS can also help eliminate dust contamination. Tweezers, gloves, hands, and any other material that may be in close contact with the PDMS or glass slide should be thoroughly washed with soapy water and ethanol.

It is essential for data analysis that the cell populations being analyzed are similar in size. Populations with larger cells will have longer average transit times. To ensure the validity of data, confirm that the populations are similar in size by measuring the area of non-adhered cells on a glass slide. Take four to five images of each glass slide using the 10× objective of a bright-field microscope, then compare the cell size distributions of the different cell populations.

Another key to obtaining consistent data is to ensure that the applied perfusion pressure in each device is uniform between experiments. The pressure reading at the inlet to the device might not always match the pressure reading at the air tank, due to the elastic tubing and compressible air. To monitor the pressure in the device more closely, pressure readings should be conducted near the inlet of the device. For example, the pressure can be monitored by connecting a pressure gauge to the tubing or by constructing a simple manometer (see Fig. 22.16.5).

A manometer is a simple and inexpensive way to accurately track the pressure just before the cell suspension reservoir. A manometer can be constructed by connecting a 500-ml bottle to the tubing system close to the device inlet. Connect tubing coming from the compressed air tank to one side of the bottle and connect another length of tubing to the other side, which will lead to the device inlet. Connect a final piece of tubing to the bottle that will be submerged in the manometer fluid. Use a saturated sugar aqueous solution to increase the density of the fluid in the manometer to ∼1.3 g/ml and add food coloring to increase fluid visibility. The increased density will result in a lower fluid height in the manometer upon pressurization of the system. For a pressure of 5 psi, the sugar solution height will be ∼2.7 meters, or 8.9 feet, as opposed to 3.5 meter, or 11.5 feet, for water alone. Wait for the fluid height to equilibrate to help ensure that there is little difference in pressure between experiments.

If alternative channel heights are desired, the microfabrication protocol will need to be modified. The manufacturer's recommendations for spin-coating speeds and accelerations appropriate for the height desired should be followed as a starting point. The wafer processing will also need to be modified; the baking times and exposure times will increase or decrease if the desired structures are taller or shorter. The protocol may need troubleshooting to obtain structures that are well-adhered and not cracked. Parameters to modify include the wafer cleaning procedure, the wafer dehydration procedure, the post-spinning, post-exposing and post-baking relaxation times of the resist, and the baking temperatures and times.

Anticipated Results

Basic Protocol 1

The normalized nuclear strain reflects the nuclear stiffness relative to the cytoskeletal stiffness. Typical values for nuclear strain are 0.1 for mouse embryo fibroblasts for uniaxial strain application (20% strain) and 0.05 to 0.1 for human skin fibroblasts for similar levels of uniaxial strain. Normalized nuclear strain values of 0.3 and higher indicate extremely deformable nuclei, e.g., in lamin A/C–deficient cells. Occasionally, we observe single cells with nuclear strain values as high a 1, but this is quite rare. Nuclear strain values of 0 correspond to extremely stiff nuclei that do not show any nuclear deformation under strain. Negative nuclear strain values mean that the nucleus contracted during strain application and often indicate cells that became damaged or detached during strain application.

Since the normalized nuclear strain reports nuclear stiffness relative to the cytoskeletal stiffness, it is important to evaluate cells' potential changes in cytoskeletal structure and mechanics when comparing results from different cell lines. This can be done by magnetic bead microrheology (Lammerding et al., 2004) and complemented by immunofluorescence analysis of cytoskeletal filaments.

Basic Protocol 2

For cells passing through narrow constrictions with a diameter smaller than the size of the nucleus, the deformation of the large and relatively stiff nucleus presents the rate-limiting step in the transit process. Thus, cells with stiffer, less deformable nuclei will take longer to pass through the narrow constrictions than cells with more pliable nuclei. When perfusing mouse embryo fibroblasts through 5-μm wide constrictions, we typically observe transit times between 20 to 200 msec, with some cells taking as long as a few seconds to

pass the constrictions. In addition to comparing the mean transit times, it can also be helpful to plot a histogram of the transit times for each cell line, as such a histogram can reveal the fraction of cells that become (transiently) stuck in the narrow constrictions. Lastly, performing additional experiments with perfusion devices with constrictions larger than the nuclear size can serve as an important control, as differences in nuclear mechanics between populations should have no effect on transit times with these settings.

Time Considerations

Basic Protocol 1

- Assembling strain devices: 2 hr
- Culturing cells: 3 days
- Stretching cells: 1 hr per dish

Basic Protocol 2

- Microfabrication: 1 day
- Microfluidic device fabrication: 3 hr
- Perfusion experiment: 2 hr

Acknowledgment (optional)

This work was supported by funding from the National Institutes of Health (NIH) [awards R01 NS059348 and R01 HL082792], the Department of Defense Breast Cancer Research Program (BC102152), and the Progeria Research Foundation.

Literature Cited

Caille, N., Tardy, Y., and Meister, J.J. 1998. Assessment of strain field in endothelial cells subjected to uniaxial deformation of their substrate. *Ann. Biomed. Eng.* 26:409-416.

Dahl, K.N., Kahn, S.M., Wilson, K.L., and Discher, D.E. 2004. The nuclear envelope lamina network has elasticity and a compressibility limit suggestive of a molecular shock absorber. *J. Cell Sci.* 117:4779-4786.

Friedl, P., Wolf, K., and Lammerding, J. 2010. Nuclear mechanics during cell migration. *Curr. Opin. Cell Biol.* 23:55-64.

Holaska, J.M. 2008. Emerin and the nuclear lamina in muscle and cardiac disease. *Circ. Res.* 103:16-23.

Lammerding, J., Schulze, P.C., Takahashi, T., Kozlov, S., Sullivan, T., Kamm, R.D., Stewart, C.L., and Lee, R.T. 2004. Lamin A/C deficiency causes defective nuclear mechanics and mechanotransduction. *J. Clin. Invest.* 113:370-378.

Lammerding, J., Dahl, K.N., Discher, D.E., and Kamm, R.D. 2007. Nuclear mechanics and methods. *Methods Cell Biol.* 83:269-294.

Lombardi, M.L. and Lammerding, J. 2011. Keeping the LINC: The importance of nucleocytoskeletal coupling in intracellular force transmission and cellular function. *Biochem. Soc. Trans.* 39:1729-1734.

Lombardi, M.L., Zwerger, M., and Lammerding, J. 2011. Biophysical assays to probe the mechanical properties of the interphase cell nucleus: Substrate strain application and microneedle manipulation. *J. Vis. Exp.* 55:e3087.

Pajerowski, J.D., Dahl, K.N., Zhong, F.L., Sammak, P.J., and Discher, D.E. 2007. Physical plasticity of the nucleus in stem cell differentiation. *Proc. Natl. Acad. Sci. U.S.A.* 104:15619-15624.

Rosenbluth, M.J., Lam, W.A., and Fletcher, D.A. 2008. Analyzing cell mechanics in hematologic diseases with microfluidic biophysical flow cytometry. *Lab. Chip* 8:1062-1070.

Rowat, A.C., Lammerding, J., Herrmann, H., and Aebi, U. 2008. Towards an integrated understanding of the structure and mechanics of the cell nucleus. *BioEssays* 30:226-236.

Simon, D.N. and Wilson, K.L. 2011. The nucleoskeleton as a genome-associated dynamic "network of networks". *Nat. Rev. Mol. Cell Biol.* 12:695-708.

Zwerger, M., Ho, C.Y., and Lammerding, J. 2011. Nuclear mechanics in disease. *Annu. Rev. Biomed. Eng.* 13:397-428.

Key Reference

Basic Protocol 1

Caille et al., 1998. See above.

This article characterizes the effect of substrate strain application on nuclear and cytoskeletal deformations.

Lammerding et al., 2004. See above.

This article provides an example of the application of the nuclear strain assay to compare the mechanical stiffness of nucleus in lamin A/C-deficient and wild-type fibroblasts.

Basic Protocol 2

Huang, Y., Agrawal, B., Sun, D., Kuo, J.S., and Williams, J.C. 2011. Microfluidics-based devices: New tools for studying cancer and cancer stem cell migration. *Biomicrofluidics* 5:13412.

This review provides an overview of the microfabrication process involved in the fabrication of microfluidic devices and the current applications of microfluidics.

Rosenbluth et al., 2008. See above.

This article presents a microfluidic device similar to the produced in this protocol and provides an example for its application.

Whitesides, G.M., Ostuni, E., Takayama, S., Jiang, X., and Ingber, D.E. 2001. Soft lithography in biology and biochemistry. *Annu. Rev. Biomed. Eng.* 3:335-373.

This review presents an overview of soft lithography techniques.

Internet Resources

http://www.jove.com/details.php?id=3087

This is a JoVE article: Biophysical Assays to Probe the Mechanical Properties of the Interphase Cell Nucleus: Substrate Strain Application and Microneedle Manipulation (Lombardi et al., 2011).